



HAL
open science

Solvent-induced assembly of patchy silica nanoparticles : towards new colloidal molecules

Weiya Li

► **To cite this version:**

Weiya Li. Solvent-induced assembly of patchy silica nanoparticles : towards new colloidal molecules. Material chemistry. Université de Bordeaux, 2019. English. NNT : 2019BORD0127 . tel-03298895

HAL Id: tel-03298895

<https://theses.hal.science/tel-03298895>

Submitted on 25 Jul 2021

HAL is a multi-disciplinary open access archive for the deposit and dissemination of scientific research documents, whether they are published or not. The documents may come from teaching and research institutions in France or abroad, or from public or private research centers.

L'archive ouverte pluridisciplinaire **HAL**, est destinée au dépôt et à la diffusion de documents scientifiques de niveau recherche, publiés ou non, émanant des établissements d'enseignement et de recherche français ou étrangers, des laboratoires publics ou privés.

THÈSE PRÉSENTÉE
POUR OBTENIR LE GRADE DE
DOCTEUR DE
L'UNIVERSITÉ DE BORDEAUX

ÉCOLE DOCTORALE DES SCIENCES CHIMIQUES
SPÉCIALITÉ : PHYSICO-CHIMIE DE LA MATIÈRE CONDENSÉE

Par Weiya LI

Solvent-induced assembly of patchy silica nanoparticles
Towards new colloidal molecules

Sous la direction de : Etienne DUGUET et Serge RAVAINÉ

Soutenue le : 24 Juillet 2019

Membres du jury :

Mme KRAFT, Daniela
Mme GERARDIN, Corine
M. GROSCHEL, André
M. MAGLIONE, Mario

Professeure, Université de Leiden
Directrice de recherche, CNRS-Montpellier
Professeur, Université de Duisburg-Essen
Directeur de recherche, CNRS-Bordeaux

Rapporteuse
Rapporteuse, Présid.
Examinateur
Examinateur

Acknowledgements

I have never thought about how my PhD study will be before starting the ENLARgER project (# ANR-15-CE09-010). It was tough and would have been tougher without the help from all the guys around me. Before finishing my PhD Study, I would express my sincere appreciation to everyone who helped me a lot not only in scientific research but also in my personal life.

Firstly, I would like to thank my supervisor, Professor Etienne Duguet, for offering me the great opportunity to continue my PhD research in this wonderful group (G5, ICMCB). There is no suitable advisor in this world for my PhD study but you. I appreciate your advice in the experiment design, the workload on the thesis, paper revision and the excellent discussion that we had. Your broad knowledge of polymer and soft matter impressed me, and the rigorous working attitude will affect me not only in the scientific field but also in my routine life. The perfect barbecue in your house every summer will be carved in my memory forever. Thanks for all your concern in the last 4 years and hope you have a good academic output every year.

Many thanks should be given to my co-supervisor, Serge Ravaine, in CRPP. I enjoyed working with you through my PhD project, especially in the part of chaining from two-patch silica and the preparation of honeycomb-like sheet through Langmuir technique. Your deep insight into physical chemistry helped me a lot in the experiment design and discussion. The correction on my thesis deserved many thanks.

I would like to thank the members involved in the project ENLARgER, Luc Belloni, Antoine Thill, Jean-Paul Chapel, Jérôme Majimel, Rémi Mérindol, Pierre-Etienne Rouet and Hervé Palis, for your fantastic suggestions in the regular discussion. The China Scholarship Council (CSC) would be thanked for the 4-years scholarship.

The sincere thanks will be transferred to the thesis jury members, Corine Gerardin, Daniela Kraft, André Gröschel, Serge Ravaine and Etienne Duguet for your kind attendance to my defence and the valuable advice of my thesis content. The absence of Mario Maglione was a pity, but your questions inspired me a lot on the future work of our projects.

The great thanks will be expressed to the TEM technician in CRPP, Isabelle Ly and Sandra Nada. I cannot finish my project smoothly without your help in maintaining the TEM at a good state all the time. Nicolas Penin, the most sportive guy in ICMCB, helped me calcinating the particles whenever I need. I appreciate your greeting every morning as a good start of the new day.

The perfect teammate in my group gave me countless help during my study and research in the last 4 years. I will cherish all the useful discussions and working collaboration with the permanent staff, including Marie-Hélène Delville, Mona Tréguer-Delapierre, Graziella Goglio, Stéphane Mornet and Glenna Drisko. Lydia Roudier, the chef in preparing cakes, thanks for your nice lemon cake and I will never forget its unique taste. My colleagues and close friends, Dr Véronique Many, Elham Yammine, Yasmine Ziouni, thanks a lot for the research inspiration, daily life sharing and the French teaching, even if sometimes I tried to persuade you the authentic way of speaking French. The great working atmosphere should be ascribed to, Maxime Bronchy, Alexandre Guyonnet, Clément Vecco-Garda, and other former PhD students. Hope all of you have a bright future. My wonderful roommate, Gonzalez Juan, thanks for the happiness that you brought to me in the last two years.

Several Chinese friends that I met 4 years ago, like Ye Xiao, Jianqiao Jiang, Yuxin Ma, Xiaozhou Ma. It was you who helped me adapt to this new environment as soon as I arrived in France. This four years with you will be the irreplaceable duration in my life. Thanks all of you. I would like to thank Qingguo Bai, Junjie Hao and Fenghuan Zhao for the tasty food and the perfect party organisation. It is unbelievable to witness the born of Wenzheng Bai (daughter of Qingguo) and Nano (daughter of Fenghuan) during my PhD study. Hope everything goes well for you and your family. To these Chinese friends, I cannot even find the appropriate word to express my gratitude.

Finally, I would thank my great family members. My parents (李矫西和赵相珍), they even do not understand what the PhD stands for while supporting me with the selfless love. My brother (李威), who will finish his bachelor in one year. Thanks for staying with our parents in China in my absence. You should trust the strength of education and go further to reach your dream. The deepest love would be said to my friend, soulmate, previous colleague, classmate and wife, Dr Yan Liu (刘艳). I was proud to witness your growth in every minute. Thanks for accompanying me in the last 5 years even with a 3-year long-distance relationship. Thank you, my forever love.

Li Weiya

Pessac,

31, July, 2019

Résumé

Le terme « molécules colloïdales » (CMs) décrit des agrégats, constitués de quelques particules généralement sphériques, imitant la forme de molécules conventionnelles dans leur modèle dit compact, c'est-à-dire où les atomes sont représentés par des sphères dont le rayon est proportionnel au rayon atomique. Les particules constitutives sont alors appelées « atomes colloïdaux ». La synthèse de nouvelles CMs a suscité beaucoup d'attention au cours des deux dernières décennies à la fois pour des motivations purement académiques, mais aussi dans l'objectif de créer des briques de construction complexes susceptibles de conduire à des matériaux originaux après assemblage. Le 1^{er} enjeu est de trouver un moyen d'encoder la valence de la particule, c'est-à-dire sa capacité à engager des « liaisons » avec un nombre prédéfini d'autres particules dans des directions, elles aussi, prédéfinies. Le 2nd enjeu est de trouver la force motrice qui va assurer, si possible de manière pérenne, la robustesse de la « liaison » entre les particules.

Depuis quelques années à l'université de Bordeaux, nous mettons en œuvre un nouveau paradigme qui consiste à (1) fabriquer des CMs sous la forme de nanoparticules (NPs) multipodiques constituées d'un cœur de silice et de podes de polystyrène (PS) par polymérisation en émulsion du styrène en présence de germes de silice et (2) les déconstruire pour obtenir des particules à patchs où la valence des multipodes précurseurs reste encodée sous la forme de résidus de quelques chaînes de PS greffées. Les travaux menés dans le cadre de cette thèse ont consisté à utiliser le caractère hydrophobe et collant du PS lorsqu'il est dispersé dans un mélange d'un bon et d'un mauvais solvant.

Le chapitre 1 décrit l'état de l'art de la synthèse des CMs, la synthèse des particules à patchs et l'assemblage de ces dernières. Pour les assemblages 2-D et 3-D, l'analyse a été menée essentiellement sur la base d'études de simulation. Cette étude bibliographique nous a appris que la démarche proposée est originale, que les assemblages robustes de NPs ne sont pas si courants et que les contraintes en termes de monodispersité en taille et en valence des particules à patchs, d'une part, et de réversibilité des « liaisons » pour autocorriger les éventuelles erreurs d'empilement, d'autre part, augmentent avec la dimension des assemblages visés.

Le chapitre 2 est consacré à la synthèse de NPs de silice à un patch et leur assemblage sous la forme de clusters (assemblages 0-D). Pour cette étude, nous avons utilisé une voie de synthèse décrite dans la littérature qui permet de contrôler la morphologie en haltère dissymétrique silice/PS par des étapes de polymérisation en émulsion incluant des processus de gonflement et de séparation de phases, suivie d'une étape de dépôt de silice régiosélectif. Le

rapport de tailles patch/particule a été facilement contrôlé via le volume de monomère utilisé pour l'étape de gonflement (Fig. 1a). L'assemblage de ces NPs de silice à un patch a été réalisé dans des mélanges binaires éthanol/DMF (Fig. 1b). Nous avons pu identifier un régime « collant » pour des fractions volumiques de DMF dans la gamme 30-50 % conduisant à des clusters avec un nombre d'agrégation maximal de 4. Cette valeur monte au-delà de 30 lorsqu'une étape de centrifugation est ajoutée après celle d'incubation. L'influence de différents paramètres ont été étudiés : la concentration en NPs, la durée d'incubation et le rapport de tailles patch/particule. Les résultats liés à la variation de ce dernier paramètre se sont avérés contre-intuitifs : pour des valeurs faibles, nous avons bien observé une augmentation du nombre d'agrégation moyen, mais lorsque le rapport de tailles patch/particule a dépassé la valeur de 0,62, le nombre d'agrégation moyen a chuté. Nous avons proposé une explication liée à un manque de robustesse de la « liaison » entre les particules assurée par l'enchevêtrement des chaînes de PS et nous l'avons confirmée par des mesures de masses molaires par chromatographie d'exclusion stérique. La stratégie a été étendue pour obtenir des clusters à base d'or au prix de légères modifications du mode opératoire d'assemblage (Fig. 2).

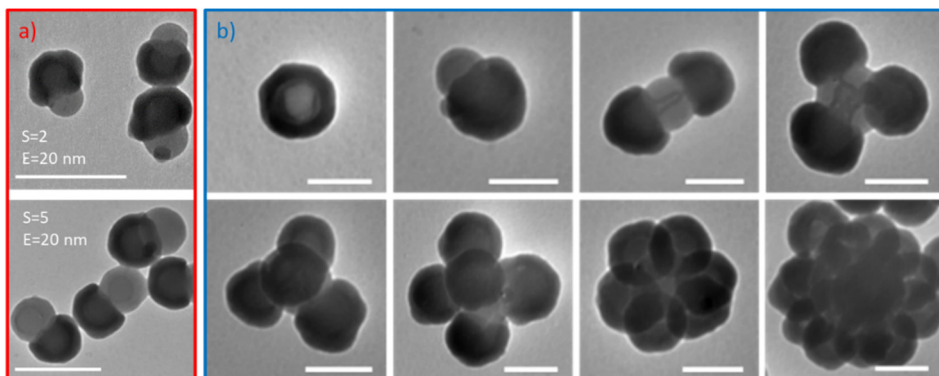


Fig. 1 Images représentatives de microscopie électronique en transmission de a) NPs de silice à un patch de PS avec différents rapports de tailles patch/particule obtenues en variant le taux de gonflement S pour une épaisseur E de silice (Barres d'échelle: 200 nm) et b) clusters résultant de l'assemblage de ces NPs dans un mélange éthanol/DMF après une étape finale de centrifugation à 12,000 g pendant 10 min (Barres d'échelle: 100 nm).

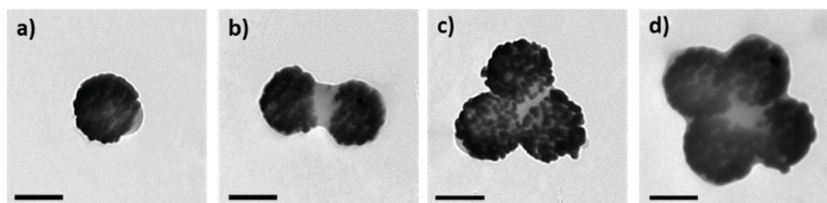


Fig. 2 Images représentatives de microscopie électronique en transmission d'haltères dissymétriques silice/PS où la silice a été recouverte d'une coque plus ou moins continue d'or (a) et de clusters résultant de leurs assemblages dans un mélange éthanol/DMF avec des nombres d'agrégation de 2 (b), 3 (c) et 4 (d). Barres d'échelle : 100 nm.

Le chapitre 3 décrit nos efforts pour obtenir des chaînes (assemblages 1-D) à partir de NPs de silice à deux patchs. Celles-ci ont été préparées à partir de la recette de polymérisation en émulsion ensemencée mise au point à l'université de Bordeaux. Nous avons utilisé des germes de silice de 55 nm. Les bipodes silice/PS ont été obtenus avec une pureté morphologique de 97 %, les impuretés étant des monopodes ou des tripodes. Les cœurs de silice ont été regrossis jusqu'à 155 ou 190 nm de façon régiosélective selon une recette de type Stöber (Fig. 3 haut). Puis les chaînes de PS non-greffées ont été éliminées par lavage au THF (Fig. 3 bas).

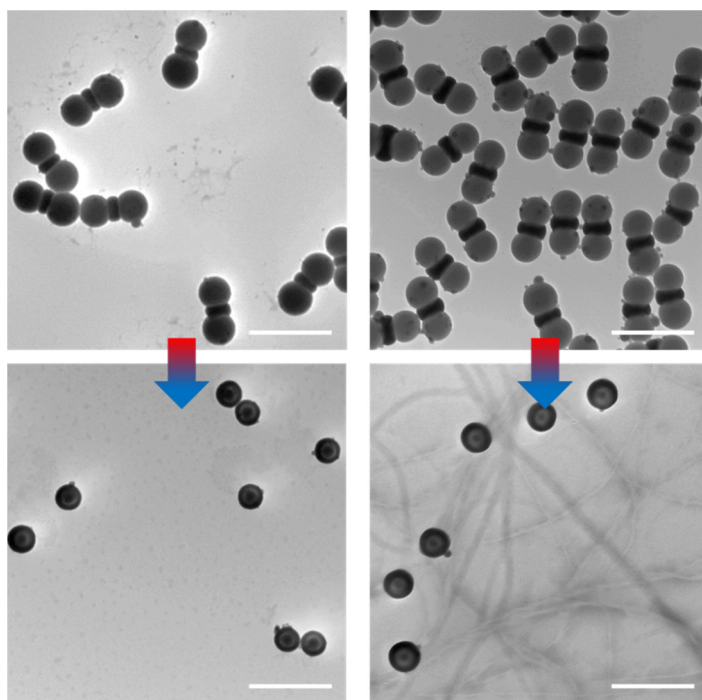


Fig. 3 Images représentatives de microscopie électronique en transmission de bipodes silice/PS où le cœur de silice a été regrossi jusqu'à 155 nm (gauche) ou 190 nm (droite) et ceci avant (haut) ou après lavage au THF (bas). Barres d'échelle : 500 nm.

L'assemblage des NPs de silice à deux patchs a été conduit dans un mélange THF/eau 70/30 en ajoutant une certaine quantité de chlorure de sodium (NaCl). Nous avons fait varier la concentration en NaCl, le rapport volumique THF/eau, la durée d'incubation, la concentration en NPs et le rapport de tailles patch/particule. Les expériences d'assemblage se sont avérées plus reproductibles lorsque le rapport de tailles patch/particule est plus faible (cœurs de silice de 190 nm par rapport à ceux de 155 nm). L'étude cinétique de la croissance des chaînes a mis en évidence un mécanisme de type polymérisation par étapes, limité au bout d'environ 2 h par un processus contrôlé par la diffusion (Fig. 4a). La longueur moyenne des chaînes est de 6 μm correspondant à un degré de polymérisation d'environ 60 (Fig. 4b). Des stratégies pour imiter des homopolymères, des copolymères statistiques, des copolymères séquencés à blocs et des polymères ramifiés ont été mises en œuvre, en utilisant comme briques de base des NPs à un

patch, des NPs à deux patchs avec des tailles ou des fonctions de surface différentes et/ou des NPs à trois patchs.

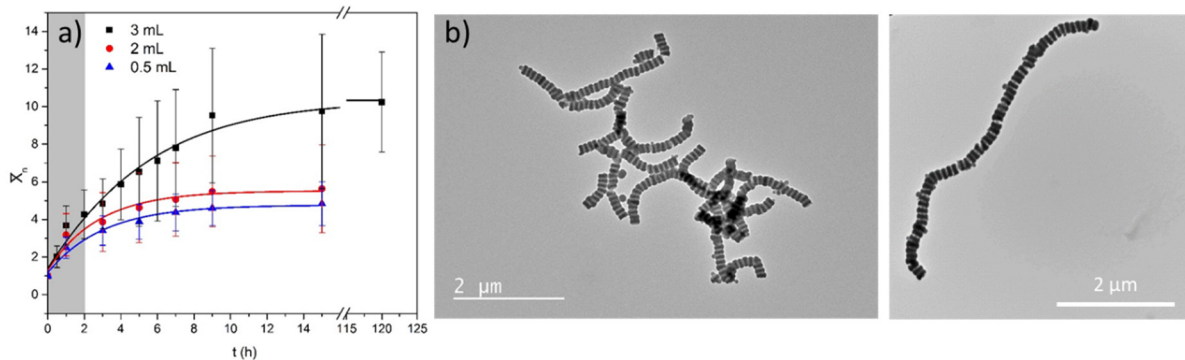


Fig. 4 a) Evolution avec le temps du degré de polymérisation moyen des chaînes obtenues dans un mélange THF/eau en fonction de la concentration en NPs de silice à deux patchs. b) Images représentatives de microscopie électronique en transmission de chaînes obtenues dans les conditions les plus favorables à leur croissance.

Le chapitre 4 décrit la synthèse de NPs de silice à 3 patchs et les résultats d'expériences préliminaires d'assemblage pour obtenir une structure 2-D en nid d'abeille. Les NPs de silice à trois patchs ont été obtenues par la même voie de synthèse que celles à deux patchs avec un rendement morphologique de 75 % (Fig. 5). Pour les assembler dans des structures 2-D en nid d'abeille, nous avons utilisé la technique de Langmuir en épandant sur l'eau une dispersion des NPs dans le chloroforme et nous avons étudié l'influence de différents paramètres expérimentaux : nombre de cycles de lavage au THF, taille et concentration des NPs et vitesse de compression (Fig. 6). Une étape de recuit sous vapeur de THF a été mise en œuvre, ce qui a permis de renforcer mécaniquement l'assemblage, mais sans effet significatif sur la compacité du film qui reste à améliorer.

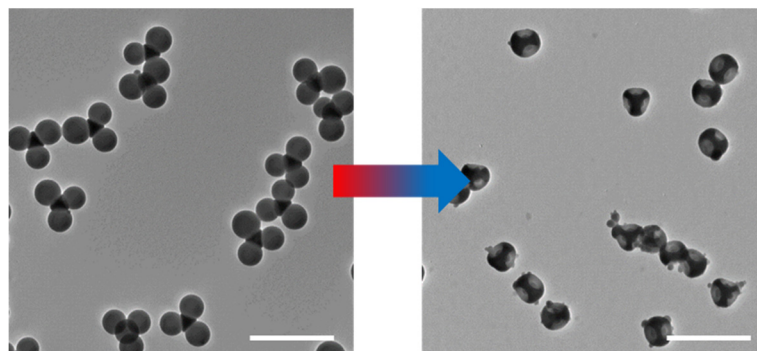


Fig. 5 Images représentatives de microscopie électronique en transmission de tripodes silice/PS avant (à gauche) et après lavage au THF (à droite). Barres d'échelle : 500 nm.

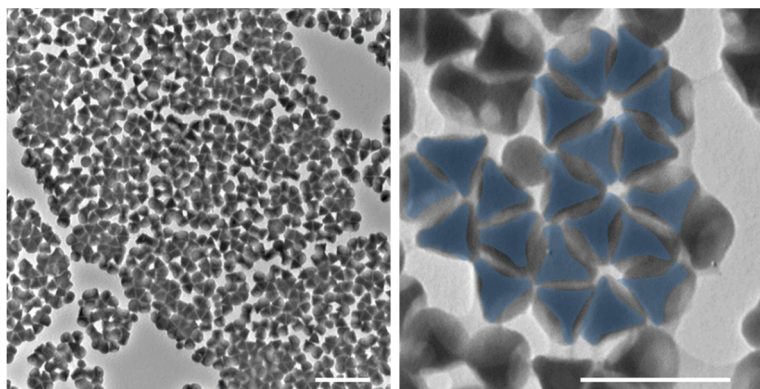


Fig. 6 Images représentatives de microscopie électronique en transmission de l'assemblage 2-D de NPs de silice à trois patches à la surface d'une cuve de Langmuir et après transfert sur un substrat solide. L'amorce d'un réseau en nid d'abeille a été mis en évidence en coloriant en bleu les particules de silice impliquées. Barres d'échelle : 500 nm.

Summary

This study deals with the assembly of patchy particles to get new materials. The state-of-the-art allowed us to select and implement an original strategy whose driving force is the solvent-induced assembly, *i.e.* based on the stickiness of polystyrene (PS) macromolecules when they are subjected to a mixture of good and bad solvents. We investigated the assembly into clusters, chains or monolayers of one-patch, two-patch or three-patch silica nanoparticles (NPs), respectively, the patches being PS macromolecules grafted at specific positions on their surface.

One-patch silica NPs with controllable patch-to-particle size ratio were successfully synthesised through phase separation and site-specific silica coating. Their assembly was performed in DMF/ethanol binary mixtures. The effect of the solvent quality, centrifugation force, particle concentration, incubation time and patch-to-particle size ratio was investigated and discussed. The strategy was spread to obtain gold-coated clusters.

The two-patch silica NPs were prepared through a seed-growth emulsion polymerisation of styrene and the patch-to-particle size ratio was adjusted through the extent of the silica core regrowth. The chaining of the NPs was efficiently achieved in the THF/NaCl aqueous solution mixtures by varying the NaCl concentration, solvent quality, incubation time, NPs concentration and patch-to-particle size ratio. We showed that the kinetics of the chaining process is characteristic of a reaction-controlled step-growth polymerisation. Strategies to mimic homopolymers, random copolymers, block copolymers and branched polymers were implemented by using one-patch NPs, two-patch NPs with different sizes/surface chemical functions and/or three-patch NPs as building units.

The three-patch silica NPs were obtained through the same synthetic pathway than two-patch ones. For assembling them in honeycomb-like 2-D structures, we used the Langmuir technique and we studied the influence of different experimental parameters. THF vapour annealing was implemented to mechanically reinforce the assembly but without significative effect on the packing ratio.

Keywords: patchy particles, silica, polystyrene, assembly, clusters, chains, monolayers, emulsion polymerisation.

Table of Contents

General introduction	1
References	5
Chapter 1 Colloidal assemblies from patchy particles: state-of-the-art	7
1.1 Colloidal molecules	9
1.1.1 Colloidal molecules through controlled clustering routes	9
1.1.2 Colloidal molecules through controlled phase separation phenomena	14
1.1.3 Colloidal molecules through controlled surface nucleation and growth	16
1.2 Colloidal molecules vs patchy colloids	18
1.3 Synthesis of patchy particles	19
1.3.1 Strategies specific to a particular number of patches	20
1.3.1.1 One-patch particles	20
1.3.1.2 Two-patch particles	21
1.3.1.3 Six-patch particles	22
1.3.1.4 Twelve-patch particles.....	23
1.3.2 Versatile strategies.....	23
1.3.2.1 Template-free methods	23
1.3.2.2 Derivatisation of preformed colloidal molecules	24
1.3.2.3 Phase separation and reshaping	27
1.4 Assembly of patchy particles into hierarchical structures	29
1.4.1 Zero-dimension assemblies	29
1.4.1.1 Directed assembly of satellite particles around one multipatch particle	29
1.4.1.2 Controlled aggregation of one-patch particles	32
1.4.2 One-dimension assemblies	33
1.4.2.1 From polymer-tethered metal nanorods	33
1.4.2.2 From particles with two concave or convex patches.....	35
1.4.2.3 From multicomponent macromolecular micelles	35
1.4.3 Two-dimension assemblies.....	37
1.4.4 Three-dimension assemblies.....	39
1.5 Strategies implemented in this work	40
1.6 References	41
Chapter 2 Solvent-induced assembly of one-patch silica nanoparticles into clusters .	51
2.1 Introduction	53
2.2 Methods and materials.....	54
2.2.1 Materials	54
2.2.2 Polystyrene seeds synthesis by emulsion polymerisation	55
2.2.3 Surface crosslinking of the polystyrene seeds.....	55

2.2.4	Changing polystyrene seeds into dumbbell-like nanoparticles through styrene swelling and polymerisation	55
2.2.5	Derivatisation into silica/polystyrene dumbbells by site-specific coating with silica	56
2.2.6	Synthesis of gold seeds	56
2.2.7	Site-specific gold grafting on the silica lobe of the silica/PS dumbbells	56
2.2.8	Seeded growth of gold on the silica lobe of the silica/PS dumbbells	56
2.2.9	Solvent-driven assembly of the silica/PS dumbbells	57
2.2.10	Sort clusters through density gradient centrifugation	57
2.2.11	Characterisation	57
2.3	Results and discussion	58
2.3.1	Fabrication of the silica/PS dumbbells as one-patch silica nanoparticles	58
2.3.2	Solvent-induced assembly of the one-patch silica nanoparticles into clusters	65
2.3.2.1	Effect of the solvent quality and centrifugation force	65
2.3.2.2	Effect of the particle concentration	68
2.3.2.3	Effect of the incubation time	69
2.3.2.4	Effect of the patch-to-particle size ratio	70
2.3.2.5	Tentative sorting of clusters through density gradient centrifugation	74
2.3.3	Spread of the strategy to gold-coated clusters	75
2.3.3.1	Decoration of the silica lobe of the silica/PS dumbbells with tiny gold particles	76
2.3.3.2	Investigation of Route #1	77
2.3.3.3	Investigation of Route #2	78
2.4	Conclusion	79
2.5	References	80
	Chapter 3 Solvent-induced chaining of two-patch silica nanoparticles.....	83
3.1	Introduction	85
3.2	Materials and methods	86
3.2.1	Materials	86
3.2.2	Silica seed synthesis by sol-gel chemistry and surface functionalisation.....	87
3.2.3	Synthesis of silica/polystyrene bipods by seed-growth emulsion polymerisation .	88
3.2.4	Derivatisation into S2PS NPs	88
3.2.5	Assembly of two-patch silica nanoparticles into chains	89
3.2.6	Formation of gold-modified chains	90
3.2.7	Characterisation	90
3.3	Results and discussion	91
3.3.1	Synthesis of the patchy silica nanoparticles	91
3.3.1.1	Synthesis of the 55-nm silica seeds	91

3.3.1.2	Synthesis of silica/polystyrene bipods by seed-growth emulsion polymerisation	92
3.3.1.3	Derivatization into patchy silica nanoparticles.....	94
3.3.2	Tentative chaining of the patchy silica nanoparticles in ethanol/DMF mixtures ...	96
3.3.3	Derivatisation into slim two-patch silica nanoparticles.....	96
3.3.4	Chaining of the 155-nm slim two-patch silica nanoparticles in salted water/THF mixtures	97
3.3.4.1	Influence of the salt concentration	99
3.3.4.2	Influence of the incubation time.....	100
3.3.4.3	Influence of the solvent quality	101
3.3.4.4	Optimising the TEM image quality	102
3.3.4.5	Influence of the S2PS nanoparticles concentration.....	103
3.3.4.6	Towards gold-modified chains	104
3.3.5	Chaining of the 190-nm slim two-patch silica nanoparticles in salted water/THF mixtures	105
3.3.5.1	Kinetics study	106
3.3.5.2	Mimicking the formation of colloidal random copolymers	110
3.3.5.3	Mimicking the formation of block copolymers.....	112
3.3.5.4	Using one-patch silica nanoparticles as chain stoppers.....	114
3.3.5.5	Using three-patch silica nanoparticles to induce the formation of branched polymers	115
3.4	Conclusion.....	116
3.5	References	117
Chapter 4 Tentative assembly of three-patch silica nanoparticles into honeycomb sheets.....		119
4.1.	Introduction	121
4.2	Materials and methods.....	122
4.2.1	Materials	122
4.2.2	Silica seed synthesis by sol-gel chemistry and surface functionalisation	122
4.2.3	Synthesis of silica/polystyrene tripods by seed-growth emulsion polymerisation	123
4.2.4	Derivatisation into three-patch silica nanoparticles.....	123
4.2.5	Assembly of three-patch silica nanoparticles into honeycomb-like structure	124
4.2.5.1	Assembly in bulk solution	124
4.2.5.2	Assembly assisted by Langmuir technique	124
4.2.5.3	THF solvent vapour annealing	125
4.2.6	Characterisation	125
4.3	Results and discussion.....	126
4.3.1	Synthesis of three-patch silica nanoparticles.....	126
4.3.2	Assembly of three-patch silica nanoparticles in bulk solution.....	129

4.3.3 Assembly of three-patch silica nanoparticles by the Langmuir technique	130
4.3.4 Effect of an extra stage of solvent vapour annealing.....	134
4.4 Conclusion	135
4.5 References	136
General conclusion and perspectives	139
1 Achievements	141
2 Perspectives	142
3 References.....	144

List of abbreviations

	Colloidal atoms
CCs	Colloidal crystals
CMs	Colloidal molecules
SDS	Sodium dodecyl sulphate
NP 30	Polyethylene glycol nonylphenyl ether
NaPS	Sodium persulphate
MMS	Methacryloxymethyltrimethoxysilane
VBS	4-vinylbenzenesulfonate
TEOS	Tetraethoxysilane
APTES	(3-aminopropyl)triethoxysilane
AIBN	2,2'-Azobis(2-methylpropionitrile)
DMF	Dimethylformamide
PS	Polystyrene
MPS	Methacryloxypropyltrimethoxysilane
THF	Tetrahydrofuran
THPC	Tetrakis(hydroxymethyl)phosphonium chloride
MPTMS	(3-mercaptopropyl)trimethoxysilane
S2PS	Slim two-patch silica
RT	Room temperature
NPs	Nanoparticles
fcc	Face-centred cubic
hcp	Hexagonal-close packed
\bar{X}_n	Number-average polymerisation degree
\bar{X}_w	Weight-average polymerisation degree

PDI	Polydispersity index
\bar{D}_n	Number-average diameter
\bar{M}_n	Number-average molecular weight
\bar{M}_w	Weight-average molecular weight
TEM	Transmission electron microscopy
SEM	Scanning electron microscopy
FTIR	Fourier-transform infrared spectroscopy
SEC	Size-exclusion chromatography

General introduction

Over the last few decades, particles have served as hard sphere models for atoms, and they are often called **colloidal atoms** (CAs) within this context.¹ This analogy has turned out to be the most rewarding and the origin of several major developments. For instance, self-assembly of size-monodisperse isotropic CAs in aqueous dispersions helped to clarify crystallisation and phase transition mechanisms.²⁻⁴ Thanks to their mesoscopic size, CAs can indeed be studied in detail at the single-particle level and their dynamics are slowed down sharply in comparison with atomic systems, such that the formation of a crystal nucleus can be followed in detail. The crystallisation of CAs in **colloidal crystals** (CCs) is an entropy-driven process in which configurational entropy and free volume entropy at low and high concentrations, respectively dominate. Concentrating the dispersions allows the disorder-to-order transition; *fcc* and *hcp* structures are thermodynamically favoured, as they gain more free volume entropy than other packing symmetries. Nevertheless, it requires a long time because of the slow relaxation of large CAs and the high viscosity of concentrated suspensions. So **metal crystals** and crystallisation are quite easily mimicked from CAs self-assembly, especially for evidencing the formation of defects such as vacancies, macroscopic cracks, polycrystalline domains, and stacking faults.

Mimicking **ionic crystals**, *i.e.* crystals made of cations and anions, was also achieved through the self-assembly of binary mixtures of CAs.⁵ For instance, mixing oppositely surface-charged and differently-sized CAs and tuning the coulombic attraction through the nature and length of the capping agents enable the fabrication of binary CCs with AB, AB₂, AB₃, AB₄, AB₅, AB₆ and AB₁₃ symmetries, providing a mesoscale embodiment of NaCl, AlB₂, MgZn₂, CaB₆, NaZn₁₃, *etc.* crystals.⁶

Up to now, **covalent crystals**, *i.e.* crystals made of pure covalent bonds such as diamond, Si, Ge, SiC crystals, have remained unmimickable at the colloidal scale, because their assembly necessitates highly directional interactions between CAs. Indeed, the diamond structure, with a packing factor of 0.34 against 0.74 for *fcc* and *hcp*, is based on tetrahedral arrangements, *i.e.* fourfold coordination, of atoms displaying a fourfold valence (sp^3 orbital hybridisation of carbon atoms). So there is a huge interest in giving CAs predetermined “instructions” for directional assembly by decorating their surface with “sticky patches” or topological discontinuities such as “dimples” for locking the neighbouring spherical CAs, as numerically demonstrated.^{7,8} These two different types of patches have recently been conceptualised as enthalpic or entropic patches, respectively.⁹

The molecular world is also essentially based on covalent bonding and entirely built from atoms displaying valences of 1 (non-directional), 2 (sp), 3 (sp^2), 4 (sp^3) and, to a lesser extent, 5 (sp^3d) and 6 (sp^3d^2). It was also naturally proposed as a source of inspiration for designing colloidal analogues of simple molecules.¹⁰ Such **colloidal molecules** (CMs) are defined as robust discrete clusters of CAs. Those made of one central CA and satellite CAs may be prepared in various ways from polymer, metal, or metal oxide from the nano- to the microscale.¹¹ Nevertheless, only a very few routes allow a fine tuning of the morphology, good yield and large amounts (at least at the gram scale). Among them, the route developed at the University of Bordeaux, and based on the emulsion polymerisation of styrene in the presence of silica seeds, remains one of the most promising.^{12–14} It leads to copious amounts of regular multipod-like silica/polystyrene with morphology yields over 80% allowing to mimic simple molecules, *e.g.* HCl, BeCl₂, BF₃ or CH₄ (Fig. 1).

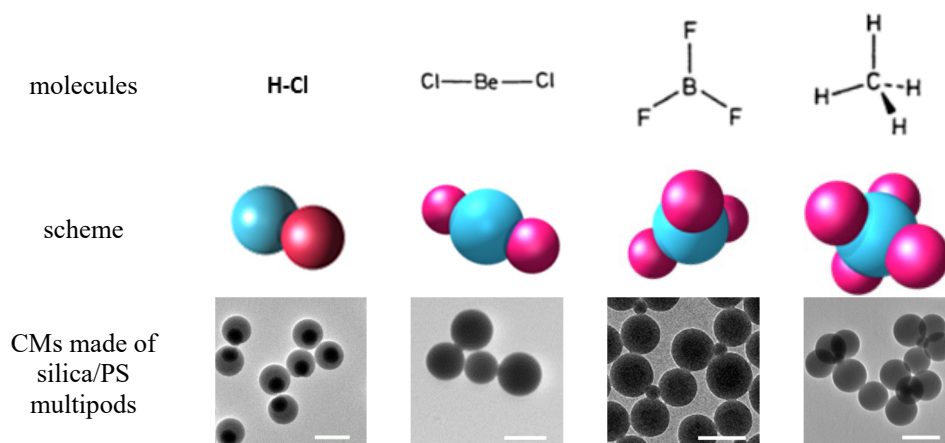


Fig. 1 Representative silica/PS multipods mimicking simple molecules. Scale bars: 200 nm.

The new paradigm underlying the present study consisted in considering that the deconstruction of CMs mimicking HCl, BeCl₂, BF₃ and CH₄ could be the most efficient way to fabricate valence-endowed patchy or dimpled CAs with a valence of 1, 2, 3 and 4, respectively (Fig. 2). In this context, the silica/polystyrene CMs are of particular interest because the silica core can be easily regrown using the polystyrene satellite ones as colloidal masks which become dimples after their subsequent dissolution in conventional solvents.¹⁵ In this way, the number and positions of the dimples, *i.e.* patches, correspond to those of the initial polystyrene nodules, taking advantage of the high symmetry of the multipod-like precursors. Moreover, both the surface of the silica particles and the polystyrene macromolecules at the bottom of the dimples can be regioselectively functionalised, thereby leading to particles with potentially both enthalpic and entropic patchiness.¹⁶

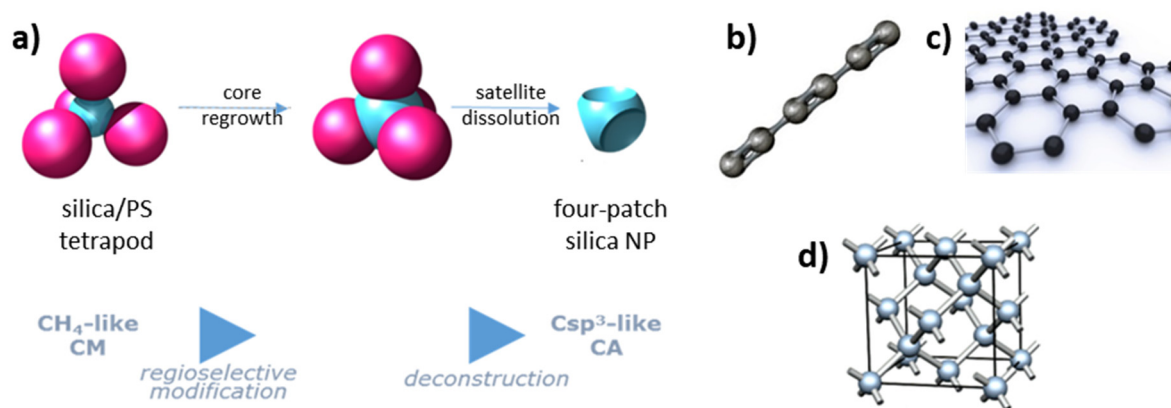


Fig. 2 a) Scheme showing the deconstruction of CMs to get valence-endowed CAs (tetrapod as an example) and possible targeted assemblies corresponding to full bonding: b) carbyne-like colloidal macromolecule from two-patch CAs, c) graphene-like CC from three-patch CAs and d) diamond-like CC from four-patch CAs.

Therefore, the main goal of the present study was to develop strategies to attach these powerful valence-endowed CAs to get not only new CMs but also assemblies of higher dimensions that could mimic carbyne chains, graphene sheets or diamond crystals. We focused on hydrophobic interactions and, in that sense, this work is complementary to that of Pierre-Etienne Rouet,¹⁷ who investigated in parallel covalent and supramolecular routes.^{18,19}

The manuscript is organised in four independent chapters. The first chapter is dedicated to the state-of-the-art in order to get comprehensive views of the fabrication of CMs and patchy particles, and of the use of the latter to get assemblies of increasing dimensions. In the conclusion part, the strategy of the present study is justified and refined. The three following chapters describe our experimental efforts to get clusters, chains (*i.e.* carbyne-like) and honeycomb structures (*i.e.* graphene-like) from one-patch, two-patch and three-patch silica nanoparticles, respectively. The general conclusion is the opportunity for an objective summary of our achievements and a prospective discussion about the expected issues for reaching assemblies of higher dimensions, *e.g.* diamond-like structures.

References

1. Duguet, É., Hubert, C., Chomette, C., Perro, A. & Ravaine, S. Patchy colloidal particles for programmed self-assembly. *Comptes Rendus Chim.* **19**, 173–182 (2016).
2. Anderson, V. J. & Lekkerkerker, H. N. W. Insights into phase transition kinetics from colloid science. *Nature* **416**, 811–815 (2002).
3. Gasser, U. Crystallization in three- and two-dimensional colloidal suspensions. *J. Phys. Condens. Matter* **21**, 203101-203124 (2009).
4. Palberg, T. Crystallization kinetics of colloidal model suspensions: recent achievements and new perspectives. *J. Phys. Condens. Matter* **26**, 333101-333122 (2014).

5. Zhang, H., Edwards, E. W., Wang, D. & Möhwald, H. Directing the self-assembly of nanocrystals beyond colloidal crystallization. *Phys. Chem. Chem. Phys.* **8**, 3288–3299 (2006).
6. Shevchenko, E. V., Talapin, D. V., Murray, C. B. & O'Brien, S. Structural characterization of self-assembled multifunctional binary nanoparticle superlattices. *J. Am. Chem. Soc.* **128**, 3620–3637 (2006).
7. Zhang, Z., Keys, A. S., Chen, T. & Glotzer, S. C. Structures through molecular mimicry. *Nat. Mater.* **21**, 409–413 (2005).
8. Smallenburg, F. & Sciortino, F. Liquids more stable than crystals in particles with limited valence and flexible bonds. *Nat. Phys.* **9**, 554–558 (2013).
9. van Anders, G., Ahmed, N. K., Smith, R., Engel, M. & Glotzer, S. C. Entropically patchy particles: engineering valence through shape entropy. *ACS Nano* **8**, 931–940 (2014).
10. Van Blaaderen, A. Colloidal molecules and beyond. *Science*. **301**, 470–471 (2003).
11. Duguet, E., Désert, A., Perro, A. & Ravaine, S. Design and elaboration of colloidal molecules: an overview. *Chem. Soc. Rev.* **40**, 941–960 (2011).
12. Perro, A., Duguet, E., Lambert, O., Taveau, J.-C., Bourgeat-Lami, E. & Ravaine, S. A chemical synthetic route towards “colloidal molecules”. *Angew. Chemie Int. Ed.* **48**, 361–365 (2009).
13. Désert, A., Chaduc, I., Fouilloux, S., Taveau, J.-C., Lambert, O., Lansalot, M., Bourgeat-Lami, E., Thill, A., Spalla, O., Ravaine, S. & Duguet, E. High-yield preparation of polystyrene/silica clusters of controlled morphology. *Polym. Chem.* **3**, 1130–1132 (2012).
14. Désert, A., Morele, J., Taveau, J.-C., Lambert, O., Lansalot, M., Bourgeat-Lami, E., Thill, A., Spalla, O., Belloni, L., Ravaine, S. & Duguet, E. Multipod-like silica/polystyrene clusters. *Nanoscale* **8**, 5454–5469 (2016).
15. Désert, A., Hubert, C., Fu, Z., Moulet, L., Majimel, J., Barboteau, P., Thill, A., Lansalot, M., Bourgeat-Lami, E., Duguet, E. & Ravaine, S. Synthesis and site-specific functionalization of tetravalent, hexavalent, and dodecavalent silica particles. *Angew. Chemie Int. Ed.* **52**, 11068–11072 (2013).
16. Hubert, C., Chomette, C., Désert, A., Sun, M., Treguer-Delapierre, M., Mornet, S., Perro, A., Duguet, E. & Ravaine, S. Synthesis of multivalent silica nanoparticles combining both enthalpic and entropic patchiness. *Faraday Discuss.* **181**, 139–46 (2015).
17. Rouet, P.-E. PhD thesis Univ. Bordeaux. (2018).
18. Rouet, P.-E., Chomette, C., Adumeau, L., Duguet, E. & Ravaine, S. Colloidal chemistry with patchy silica nanoparticles. *Beilstein J. Nanotechnol.* **9**, 2989–2998 (2018).
19. Rouet, P.-E., Chomette, C., Duguet, E. & Ravaine, S. colloidal molecules from valence-endowed nanoparticles by covalent chemistry. *Angew. Chemie Int. Ed.* **57**, 15754–15757 (2018).

Chapter 1

Colloidal assemblies from patchy particles:

state-of-the-art

1.1 Colloidal molecules

The concept of colloidal molecules (CMs) was first evoked by van Blaaderen in 2003 for describing non-spherical colloids stemming from the aggregation of a small number of particles.¹ This perspective paper was in particular inspired by the pioneering work of Pine and co-workers.² The latest developments of CMs were published and presented in several reviews.³⁻⁹

Among them, Duguet *et al.* reported in 2011 an exhaustive critical review of the diverse synthesis routes for creating robust clusters of spherical particles which could mimic the space-filling models of exact simple molecules.⁴ They proposed a classification of CMs using and extending the well-known formalism of Gillespie derived from the Valence Shell Electron Pair Repulsion (VSEPR) model (Fig. 1). These routes concern either the controlled clustering of preformed colloids or strategies starting from a single particle which is decorated by satellite ones by taking advantage of controlled phase separation or nucleation and growth phenomena. These routes were compared from the viewpoint of the accessible shapes, their tunability and scalability (Table 1).

Herein, we only describe the major examples interrelated to this work, enriched with more recent ones.

1.1.1 Colloidal molecules through controlled clustering routes

These routes start from preformed isotropic colloids whose clustering is assisted by depletion interaction, capillary condensation, van der Waals forces, electrostatic interactions, coalescence, chemical bonding, or 2-D and 3-D geometrical confinement. We deliberately omitted those using Janus-like or patchy colloids that are described in the 1.4.1 section.

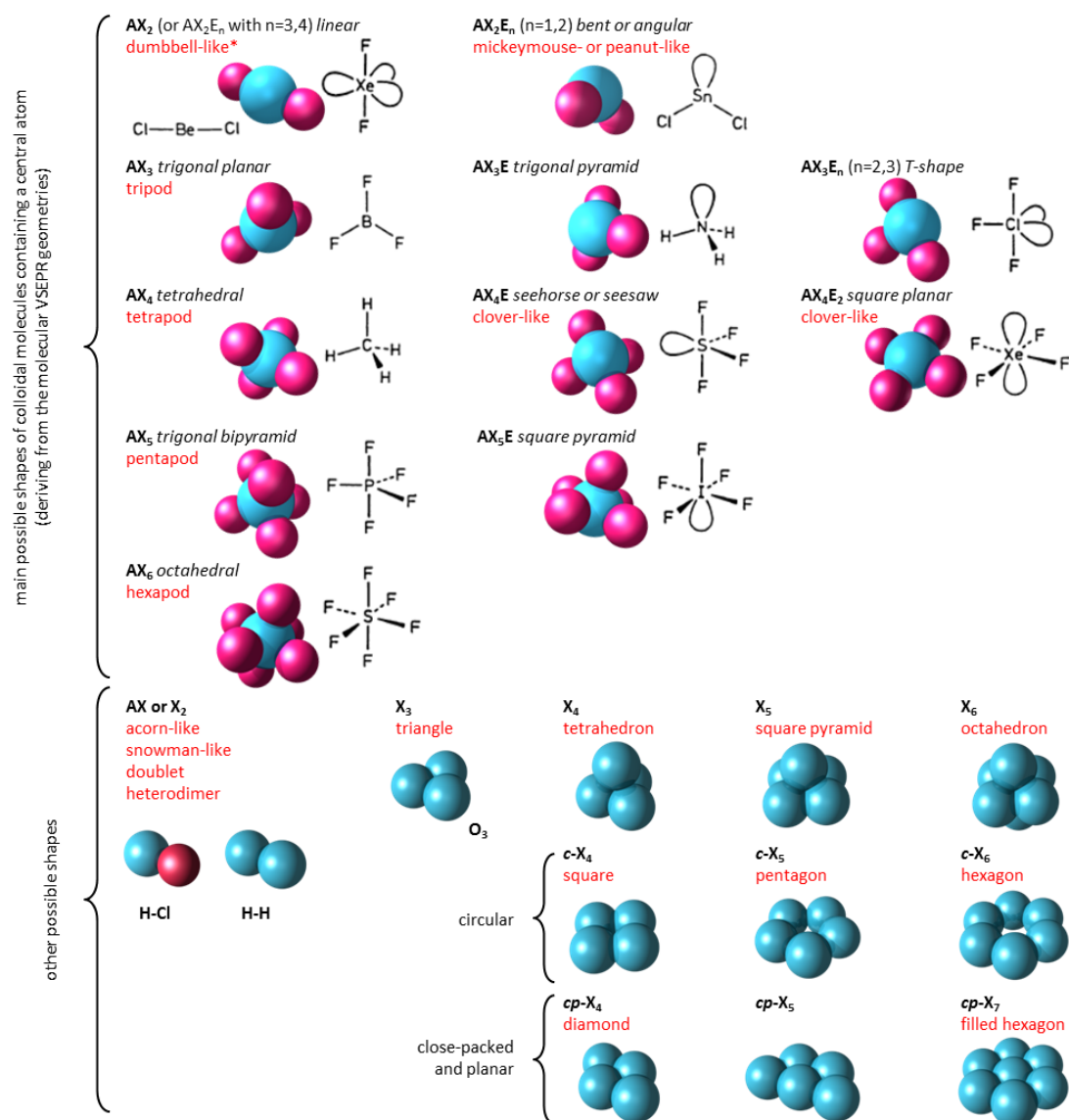


Fig. 1 Proposition of classification for CMs based on spheres and mimicking space-filling models of simple molecules (respective atomic radii are not systematically guaranteed). The usual terms found in the literature for describing such clusters are written in red. * According to authors, the dumbbell analogy was also sometimes assigned to AX or X₂ morphologies.⁴

Table 1 Comparison of the different synthetic routes investigated for the synthesis of CMs mimicking the space-filling models of simple true molecules.⁴

	Controlled clustering assisted by				Controlled phase separation				Controlled surface nucleation and growth										
	Capillary condensation	Depletion	van der Waals forces	Electrostatic interactions	Structural forces	External fields	Coalescence	Chemical bonding (except DNA)	Chemical bonding (DNA)	2-D geometrical confinement	3-D geometrical confinement	From core-shell inorganic particles	Induced by solvent evaporation (polymer)	In seeded emulsion polymerisation	In seeded dispersion polymerisation	Inorganic epitaxial growth	Competitive ligand coordination	Emulsion polymerisation	Dispersion polymerisation
Size domain	•	•	•	•	•	•	•	•	•	•	•	•	•	•	•	•	•	•	•
100–999 μm																			
10–99 μm	•	•	•	•	•	•	•	•	•	•	•	•	•	•	•	•	•	•	•
1–9 μm	•	•	•	•	•	•	•	•	•	•	•	•	•	•	•	•	•	•	•
100–999 nm	•	•	•	•	•	•	•	•	•	•	•	•	•	•	•	•	•	•	•
10–99 nm	•	•	•	•	•	•	•	•	•	•	•	•	•	•	•	•	•	•	•
1–9 nm	•	•	•	•	•	•	•	•	•	•	•	•	•	•	•	•	•	•	•
Main accessible shapes																			
AX ₂							•	•	•	•	•	•	•	•	•	•	•	•	•
AX ₂ E _n							•	•	•	•	•	•	•	•	•	•	•	•	•
AX ₃							•	•	•	•	•	•	•	•	•	•	•	•	•
AX ₃ E _n							•	•	•	•	•	•	•	•	•	•	•	•	•
AX ₄							•	•	•	•	•	•	•	•	•	•	•	•	•
AX ₄ E _n							•	•	•	•	•	•	•	•	•	•	•	•	•
AX ₅							•	•	•	•	•	•	•	•	•	•	•	•	•
AX ₅ E							•	•	•	•	•	•	•	•	•	•	•	•	•
AX ₆							•	•	•	•	•	•	•	•	•	•	•	•	•
AX/AX ₂							•	•	•	•	•	•	•	•	•	•	•	•	•
X ₃							•	•	•	•	•	•	•	•	•	•	•	•	•
X ₄							•	•	•	•	•	•	•	•	•	•	•	•	•
c-X ₄							•	•	•	•	•	•	•	•	•	•	•	•	•
cp-X ₄							•	•	•	•	•	•	•	•	•	•	•	•	•
X ₅							•	•	•	•	•	•	•	•	•	•	•	•	•
c-X ₅							•	•	•	•	•	•	•	•	•	•	•	•	•
cp-X ₅							•	•	•	•	•	•	•	•	•	•	•	•	•
X ₆							•	•	•	•	•	•	•	•	•	•	•	•	•
c-X ₆							•	•	•	•	•	•	•	•	•	•	•	•	•
cp-X ₇							•	•	•	•	•	•	•	•	•	•	•	•	•
Accurate control of																			
Relative size																			
Chemical composition																			
Robustness																			
Bond angle																			
Morphology																			
yield																			
Scalability																			

^a ○ demonstrated; • possible.

Among these achievements, the work of Manoharan, Pine and co-workers is of particular interest about confinement within oil-in-water emulsion droplets containing polymer or silica microspheres and produced by a homogeniser.^{10,11} The subsequent controlled removal of the liquid from the droplets generates compressive forces that draw the particles together. When the spheres touch one another on the surface of the droplets, removing more liquid causes the droplet to deform and generate capillary forces which collapse the particles into a cluster (Fig. 2).² The structures of these clusters include familiar polyhedra such as tetrahedron (X_4) and octahedron (X_6), and ones that are more unusual. The selection of a unique packing arises almost entirely from geometrical constraints during the drying.¹² Nevertheless, the size polydispersity of the initial emulsion droplet led to complex mixtures of different clusters that were finally sorted by density gradient centrifugation. In order to narrow the size distribution of the droplets, the emulsification stage was improved by shearing a polydisperse premix emulsion between two concentric cylinders and larger amounts of colloidal silica clusters with a linear, triangular and tetrahedral morphology were obtained.¹³ Later, Monte Carlo simulations allowed a full description of the dynamics correlated to experiments.¹⁴

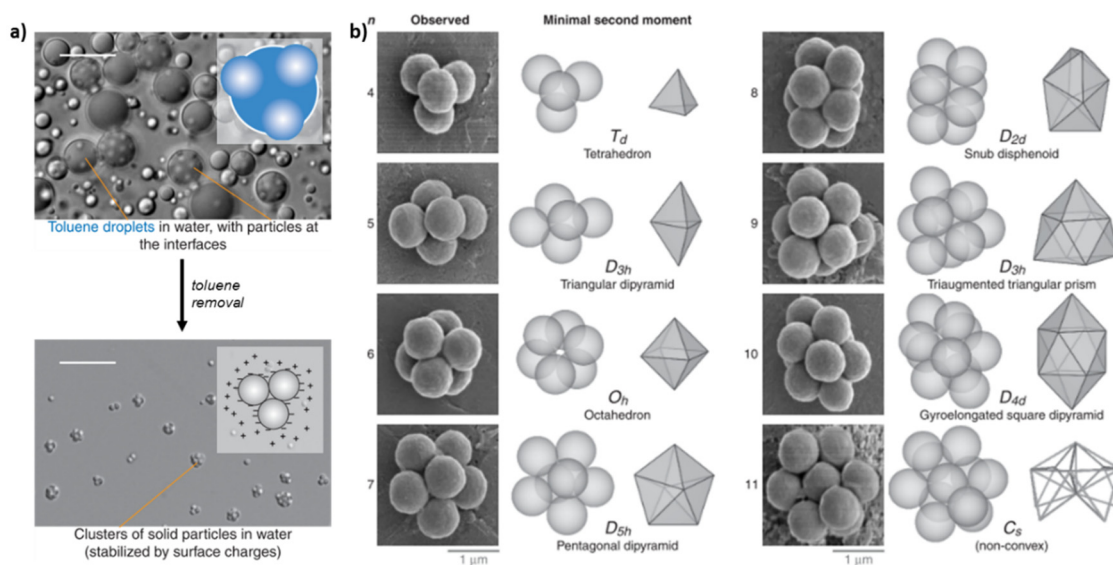


Fig. 2 Clustering of polystyrene microparticles through their confinement within a liquid droplet: a) optical micrographs and diagrams (insets) of the packing process and b) SEM images and geometry of the obtained CMs.² Scale bars in a) and b) are $10\ \mu\text{m}$ and $1\ \mu\text{m}$, respectively.

Clustering can also result from the single protrusion emerging from the surface of crosslinked polymer microparticles when they are swollen with monomer and temperature is raised. In this way, Kraft *et al.* showed that delaying the polymerisation of the protrusions on PS NPs previously coated with vinyl acetate leads to coalescence of the droplets upon collision, thereby creating easily CMs that can be solidified upon polymerisation (Fig. 3).¹⁵ AX to AX₉

morphologies were obtained after solidification of the merged protrusions giving rise to the central CA. They were obtained as mixtures of different CMs types, but these were easily sorted by gradient density centrifugation. Interestingly, the swelling liquid can be an apolar solvent allowing to reconfigure any aggregate of PS spheres thanks to a diffusion-limited aggregation process. The swollen effect lowers the van der Waals forces and lubricates the contact area between the spheres, thereby yielding regular CMs (AX_n with n from 1 to 5) through minimisation of the interfacial energy. For AX_6 , octahedra coexist with polytetrahedra, which is strongly preferred over the minimal second-moment arrangement. The patch arrangement is uniform and random when the number of assembling particles is lower and more than 5, respectively. The final morphology can be tuned by varying the swelling ratio, swelling solvent, surfactant concentration, and swelling time.

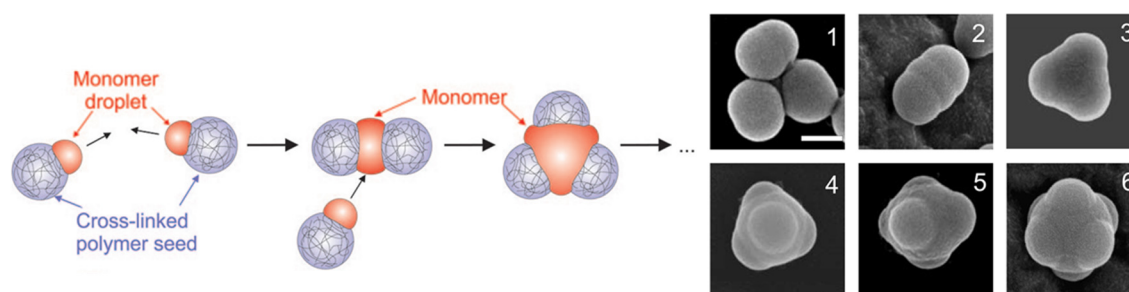


Fig. 3 Schematic representation of merging of liquid protrusions yielding CMs and SEM images of CMs from AX to AX_6 types.¹⁵ Scale bars: 200 nm.

More recently, Zhang and co-workers reported an original strategy leading exclusively to AX_{12} CMs from soft poly(N-isopropylacrylamide) (PNIPAM) microgel submicron spheres.¹⁶ When *fcc*- or *hcp*-like colloidal crystals (CCs) are prepared from a 40:1 mixture of PNIPAM microspheres with surface thiol groups and surface vinyl groups, the latter are statistically in close contact with 12 microspheres bearing thiol groups. Under UV-light irradiation, the thiol-end reaction allows to bind covalently the 13 microspheres, which are recovered as independent clusters after the destruction of the CCs. Nevertheless, by-product CMs with a higher number of microspheres were found in the same batch as well when two vinyl-PNIPAM microgels were entrapped too closely, *i.e.* with less than two separating thiol-PNIPAM microgels. Nevertheless, they were easily separated by density gradient centrifugation. The same strategy was extended to AX_4 , AX_5 and AX_6 CMs using vinyl-PNIPAM microspheres smaller than the thiol-PNIPAM ones in order to accommodate them in the interstitial sites of different close-packed lattices.¹⁷

According to a similar clustering strategy in confined 3-D environments, Tabelaing and co-workers reported a strategy to get CMs (X_n with $n = 3$ to 6) in microfluidic channels.¹⁸ Close-

packed planar CMs obtained under depletion conditions in a 2-D cell were studied by Manoharan and co-workers,¹⁹ while Grzybowski and coll. used 2-D virtual magnetic moulds.²⁰ Lastly, using alternating-current electric fields applied perpendicularly to the 2-D substrate supporting isotropic microparticles, Wu and coll. generated anisotropic interactions between them leading to quasi-planar clusters with aggregation number as high as 9.²¹

1.1.2 Colloidal molecules through controlled phase separation phenomena

The more impressive achievements were obtained through seeded emulsion polymerisation. Emulsion polymerisation is a heterophase process of great industrial importance leading to stable colloidal dispersions of polymer particles in water, called “latex”.²² Generally the polymer particles have final diameters in the range of 0.05-1 μm . One of the critical features of emulsion polymerisation is the ability to control particle morphology, *e.g.* formation of core-shell particles and other equilibrium morphologies by successive additions of different monomers, *i.e.* seeded growth polymerisation. In particular, snowman-like morphologies can be obtained as the consequence of a phase separation phenomenon. The anisotropy was arisen from the immiscibility of the second stage polymer in crosslinked polymer networks, leading to the formation of a protrusion on one side of the seed latex particle. Overall, the phase separation process is favoured by increasing either the monomer/polymer swelling ratio, the seed crosslink density, the seed size, the temperature or the crosslinker concentration in the mixture of swelling monomers, *etc.* In some situations, when the seed polymer is more polar than the second stage polymer, *e.g.* poly(methyl methacrylate) (PMMA) and poly(*n*-butyl acrylate-*co*-styrene), and when the T_g of the second stage polymer is less than the polymerisation temperature, several protrusions can be simultaneously obtained, but without control of their number, size and positions on the central seed latex.²³

This seeded emulsion polymerisation route was revisited recently in order to prepare more complex latex microparticles combining polymers of different chemical compositions and/or more sophisticated shapes.²⁴⁻²⁶ Indeed, snowman-like colloids were designed by combining styrene, MMA, butyl methacrylate, *etc.* eventually copolymerised with a functional monomer, *e.g.* to make one of the nodules hydrophilic and therefore the whole colloid amphiphilic.²⁴ Concerning shape variations, crosslinking density gradients were used to overcome the effect of surface tension and provide reproducible directionality to phase separations. Starting from snowman-like particles, *i.e.* dimers, whose both polystyrene (PS) nodules were crosslinked at controlled densities, Weitz and coll. obtained linear (AX_2) or triangular (X_3) trimers.²⁵ Indeed, the third nodules are capable of growing linearly from the less crosslinked nodules or in a

perpendicular direction when the crosslinking densities of both nodules are similar (Fig. 4). Diamond particles ($c\text{-X}_4$) are made similarly to the triangle particles at the expense of using a 20% excess of crosslinker. Combining three swelling/polymerisation stages, Dufresne and co-workers fabricated CMs successfully with the symmetry of water molecules (AX_2E_2).²⁶ Interestingly, the bond angle can also be tuned from about 80 to 140° , vs 104.5° within the true water molecule, by varying the swelling ratio in the final step.

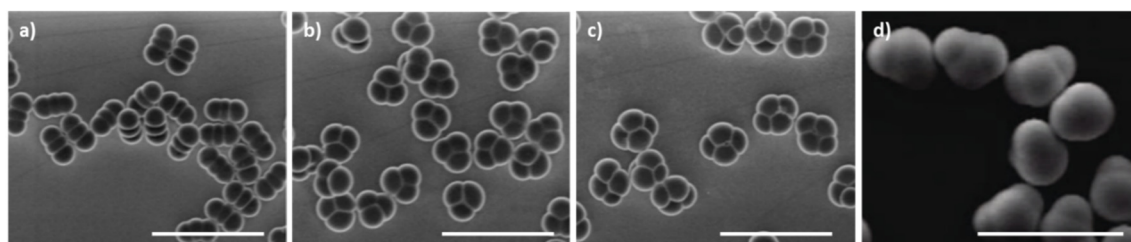


Fig. 4 SEM images of a) AX_2 dumbbell-like, b) X_3 triangle-like and c) $cp\text{-X}_4$ diamond-like²⁵ and d) AX_2E_2 water-like²⁶ latex CMs obtained through phase separation in seeded growth emulsion polymerisation. Scale bars: $20\ \mu\text{m}$.

More recently, Peng and coll. reported that AX_2 CMs can be obtained in one stage from a conventional spherical $3\text{-}\mu\text{m}$ latex seed made of crosslinked PMMA.²⁷ They showed by real-time optical microscopy that a large number of small droplets of swelling monomers form simultaneously on the surface of the seeds, and then fuse until two protrusions remaining on the opposite sides (Fig. 5a left). Stirring not only accelerates the swelling process but also induces the coalescence of the liquid protrusions from different seeds leading to CMs with AX_2E_2 , AX_3E and even acetylene-like morphologies (Fig. 5b). The subsequent polymerisation makes the structures permanent (Fig. 5a right and 5c).

Lastly, more advanced AX_3E and AX_2E_2 CMs made of PS for the central latex particle and poly(4-vinylpyridine) (P4VP) for the satellites were reported by Wang and coll.²⁸ Accordingly to the pioneering studies, the phase separation occurs simultaneously to the polymerisation of the swelling monomer and not before as shown in the just above work.

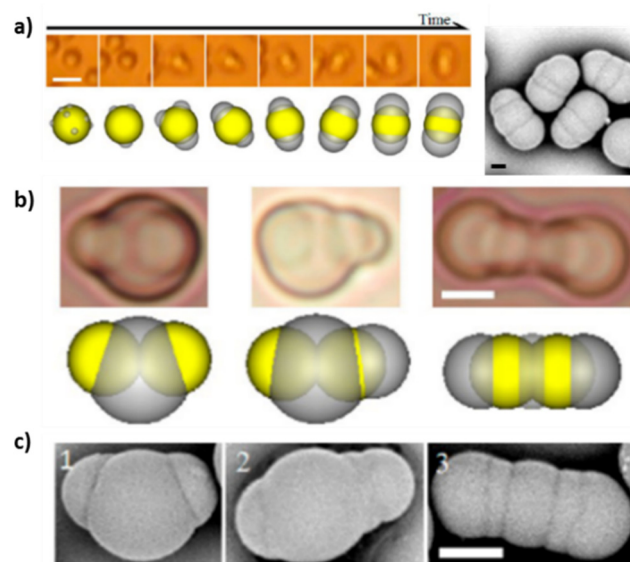


Fig. 5 PMMA-based CMs obtained through monomer-swelling of the seeds and subsequent polymerisation: a) snapshots of the swelling and protrusion fusion as observed by real-time microscopy (left) and SEM image of the as-obtained AX_2 CMs after polymerisation (right); b) optical microscopy images and corresponding schemes of the swollen structures after coalescence of the liquid protrusion between two seeds bearing two protrusions; c) SEM images of the corresponding CMs as obtained after polymerisation.²⁷ Scale bars in a) and b) are $5\ \mu\text{m}$ and $3\ \mu\text{m}$, respectively.

1.1.3 Colloidal molecules through controlled surface nucleation and growth

This synthesis pathway leads essentially to AX_n -type CMs and consists in the controlled nucleation and growth of the satellite colloids onto the surface of the central one, which plays the role of a preformed seed. Contrarily to the previous section, the seed cannot be swollen by the monomer, because this is generally an inorganic nanoparticle. Seeded growth emulsion polymerisation is well-suited to get hybrid CMs in size range of few hundreds of nanometres while dispersion polymerisation leads to larger CMs but generally with less good control of the morphologies.⁴

Our group reported an efficient recipe where a controlled number of PS latex nodules grow onto the surface of silica seed particles.^{29,30,31} The surface of these silica seeds needs to be previously treated by compatibilisers, *e.g.* methacryloxyalkyltrimethoxysilane in low surface density, in order to create reactive (co)polymerisable loci promoting the surface capture of the growing PS macromolecules and therefore the nucleation of the latex particles. In the range of 0.1-1 molecules per nm^2 , we showed that the higher the silane surface density, the more encapsulating the PS nodules. Original cryo-electron tomography experiments allowed to follow-up the nucleation and growth of the PS nodules.³² Early samples showed the presence of numerous small PS nodules bound to silica seeds in a random distribution. As far as the

polymerisation is running, the number of PS nodules per silica seed decreases, leading to morphologies imposed by the satellite steric repulsion, *i.e.* by the satellite-to-seed size ratio. This ratio can be tuned through experimental parameters such as the seed concentration, seed diameter, monomer concentration, and fraction of the sodium dodecylsulphate (SDS) introduced as co-surfactant as a complement to the main surfactant which is the polyethylene glycol nonylphenyl ether. A model was proposed to help understand the mechanism of the nodules growth³³ and predict the optimal recipe parameters for a targeted morphology.³⁴ This comprehensive study allowed to produce an extensive range of CMs and to reach morphology yields higher than 80% in particular for the CMs deriving from Platonic solids, *e.g.* AX₄, AX₆ and AX₁₂, which correspond to tetrahedra, octahedra and icosahedra, respectively. AX₃, AX₈ and AX₉ CMs were also obtained. AX and AX₂ morphologies were achieved when the surface density and hydrophobicity was adjusted, *i.e.* replacing methacryloxymethyltrimethoxysilane (MMS) by methacryloxypropyltrimethoxysilane (MPS) (Fig. 6a).³⁵

A recent study showed that quite similar CMs are achievable when using a different mechanism combining nitroxide-mediated polymerisation and induced self-assembly of amphiphilic block copolymers, but the morphology yields were not determined.³⁶

Lastly, the AXY triphasic CMs with a silica core, one PS nodule and one PMMA nodule were obtained through a two-stage protocol, where a PS nodule was conventionally created in a first step.³⁷ To forbid the polymerisation of the MMA molecules possibly swelling the PS nodule and promote successfully the nucleation of the MMA nodule on the other seed side, the silica surface was previously treated by a cationic initiator, namely 2,2'-azobis(N,N'-dimethylene isobutyramidine) dihydrochloride (Fig. 6b).

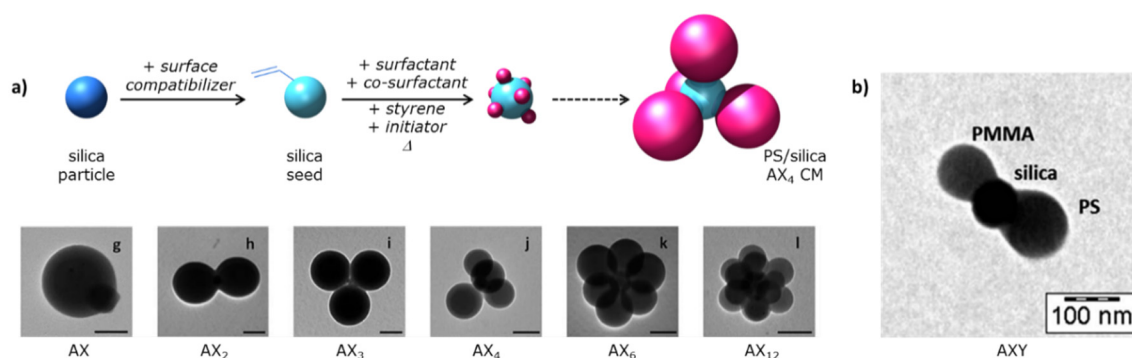


Fig. 6 a) silica/PS AX_n-type CMs obtained through seeded growth emulsion polymerisation of styrene in the presence of MMS-modified silica seeds: synthesis scheme and TEM images of the as-obtained CMs,³⁵ b) TEM image of the AXY-type CM made from a silica seed with one PS nodule and one PMMA nodule.³⁷ Scale bars: 100 nm.

1.2 Colloidal molecules vs patchy colloids

When van Blaaderen introduced the concept of CMs, he took into account not only that spherical colloids can be treated as if they were atoms, but also that molecules form more complex materials than atoms do. However, 16 years later, it must be admitted that there are very few examples of CMs assembly to obtain complex materials such as colloidal crystals. The probably most exciting result was recently reported by Pine and co-workers and consisted in co-assembling 780-nm PS spheres with X_4 CMs made of four 650-nm PS spheres.³⁸ Each type of building blocks is previously made fluorescent and surface modified with complementary ss-DNA strands, which creates a temperature-dependent attractive interaction between the CMs and the spheres. Helped by weak depletion conditions, crystallisation occurs successfully when decreasing very slowly the temperature near the aggregation temperature leading, as expected from simulations, to colloidal isomorphs of the $MgCu_2$ Laves phase, *i.e.* a diamond lattice that interpenetrates a pyrochlore lattice (Fig. 7).

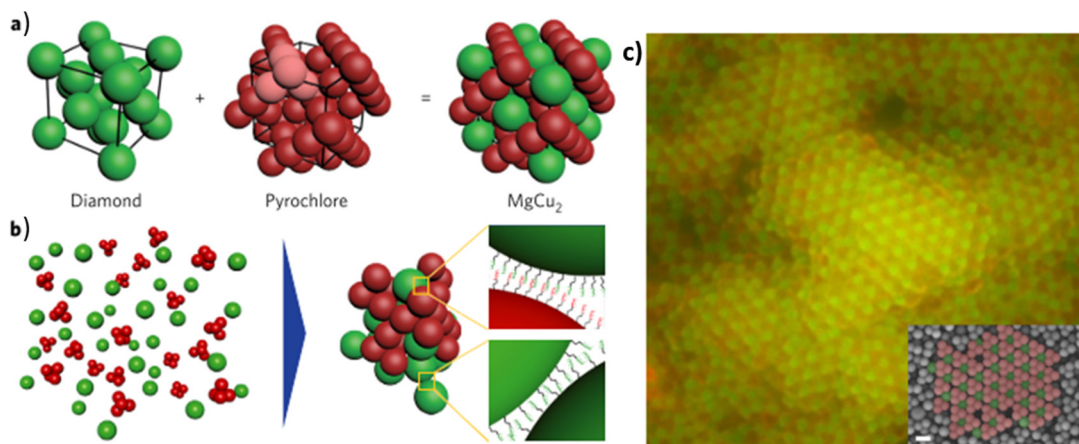


Fig. 7 a) the $MgCu_2$ superlattice made up of two sublattices, diamond in green and pyrochlore in red; b) the mixture of PS spheres (in green) and X_4 CMs (in red) expected to interact through complementary surface ss-DNA strands; c) Fluorescence microscope image of system-spanning crystals with the $MgCu_2$ structure formed after slow cooling through the melting temperature (the field of view is $50 \mu\text{m} \times 50 \mu\text{m}$). Inset: an electron microscope photograph of a section of the $MgCu_2$ crystal whose different building blocks is evidenced with false colours.³⁸ Scale bar: $1 \mu\text{m}$.

Nevertheless, another concept has made its way in the meantime: that is the concept of patchy particles.^{39–41} These are patterned particles with chemical or topological surface discontinuities which are expected to promote assembly in a limited number of specific directions. These predetermined instructions for directional assembly can be related to the atomic concept of valence extended here at the colloidal scale. That is why patchy particles are also sometimes called patchy colloidal atoms or valence-endowed colloidal atoms. When the patch is

“chemically sticky”, it is called enthalpic patch. When it corresponds to topological patterning, *e.g.* surface dimples, allowing for locking another particle with a complementary shape in depletion conditions, this is called entropic patchiness.

Both concepts of CMs and patchy colloids are closely related: firstly, because some types of CMs can be the precursors of patchy particles; secondly, because patchy particles can be original building blocks for new CMs, among other assembly types.

The concept of patchy particles can also be seen as an extension of that of Janus-like particles. In the field of science, the particle consisting of two faces with different properties is called as Janus particle by de Gennes⁴², which is quite close to the connotation of Yin-Yang (阴-阳) in Chinese philosophy illustrating the interconnection between the seemingly opposite and/or contrary forces in the natural world. These Janus particles have various applications, such as giant surfactant^{43,44}, micromotors⁴⁵, *etc.* If one hemisphere is attracting while the second one is repulsing, Janus-like particles can be seen as one-patch particles. Patchy particles, *i.e.* particles with at least two patches, are less easy to be fabricated all the more so as the variability can concern not only the patch size and the interaction type but also the number, shape and relative position of the patches (Fig. 8a).⁴⁶ Moreover, the perspective of enthalpic and/or entropic patchiness leads to consider also the flat, concave or convex shape of the patches (Fig. 8b).

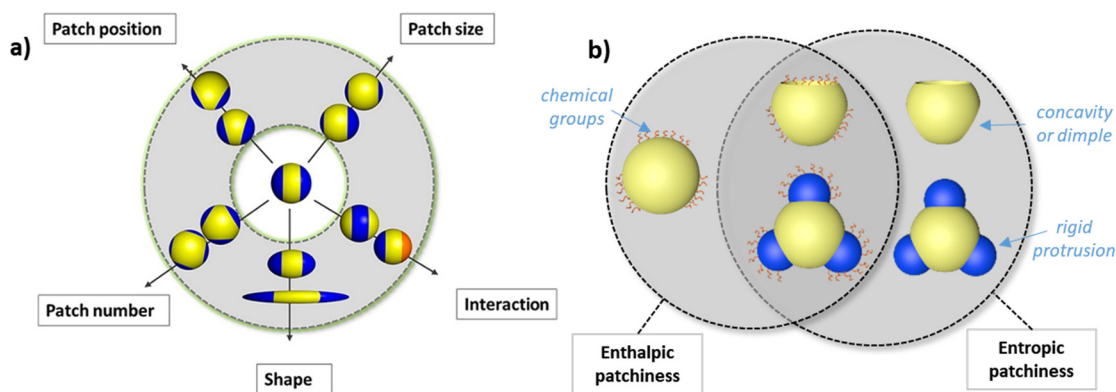


Fig. 8 Schematic showing a) the various parameters to be tuned for controlling the assembly capability of patchy particles⁴⁶ and b) the differences and interrelations between enthalpic and entropic patchiness.

1.3 Synthesis of patchy particles

Several techniques have been investigated and optimised to fabricate patchy particles. Among them, some are specific to a particular number of patches, while others are more versatile. This state-of-the-art is restricted to the synthesis routes leading efficiently to the creation of a maximum number of twelve patches regularly arranged all around the particle, describing

repulsion figures similar to those of the VSEPR model. In other words, the raspberry-like structures have deliberately been omitted.

1.3.1 Strategies specific to a particular number of patches

1.3.1.1 One-patch particles

As previously mentioned, one-patch particles can be seen as Janus-like particles whose one of both hemispheres is or could be made attractive or sticky. Their synthesis was intensively investigated these last three decades and reviewed many times.^{47–52} It would be too long to present here the numerous synthesis pathways that allow breaking the symmetry of isotropic colloids. We focus on those which can also be combined with other techniques to get a higher number of patches and/or which are interrelated to the strategies adopted in this work.

Briefly, particles to be made dissymmetric are partially trapped into or contacted on a flat/curved interface and the exposed side is regioselectively functionalized to create the patch. When the substrate is solid and the reagents are gaseous, the particles must be previously spread densely on the solid surface through spin coating⁵³, evaporation⁵⁴, *etc.* Pawar *et al.* developed the glancing angle deposition (GLAD) method to partially coat with a metal or metal oxide a close-packed monolayer of particles, whose neighbouring particles and the substrate serve as protecting masks.⁵⁵ The position, shape and coverage extent of the patch can be controlled by the orientation angle α of the layer and the deposition angle Θ (Fig. 9).

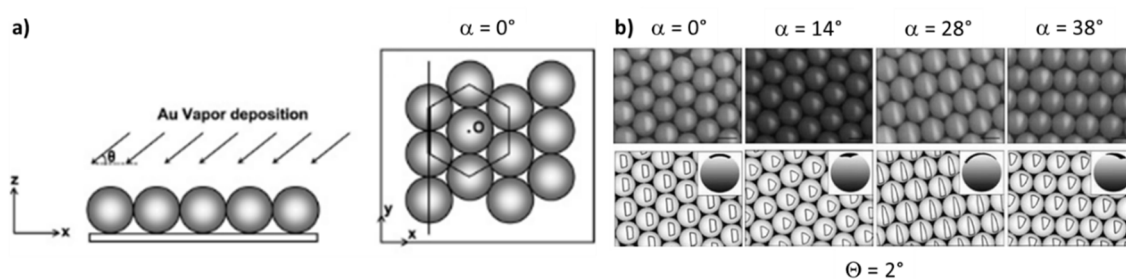


Fig. 9 Glancing angle deposition (GLAD) technique: a) schematic describing the process and evidencing both angular parameters and b) top row: SEM images of gold patches on 2.4- μm PS particles prepared by tuning the incidence angle and monolayer orientation, and bottom row: numerical simulation of patches at given angles.⁵⁵ Scale bars: 2 μm .

The dissymmetrisation interface can also be solid-liquid such as wax-in-water emulsions, as reported by Granick and coll.⁵⁶ The Pickering emulsion is achieved by the stabilisation of the particles within the temperature range of the liquid wax. After solidification of the wax droplets, the exposed surface is regioselectively functionalised^{57,58} or partially etched to form shape-

anisotropic particles.⁵⁹ The wax Pickering strategy allows tuning the patch extent through the control of the trapping degree of the particle into the wax phase by playing with the ionic strength, pH value, *etc.*

Concerning the preparation of one-dimple polymer particles, Yi and coll. reported an efficient route based on a phase separation phenomenon occurring during a temperature-controlled swelling-deswelling process.⁶⁰ The conventional PS latex particles are firstly swollen by decane, which is partially soluble in water-ethanol medium from 60°C; then the phase separation happens when decreasing the temperature (Fig. 10). The following removal of surfactant and the evaporation of the oil phase lead to particles with one hydrophobic dimple while the rest of the surface remains hydrophilic due to the presence of the surfactant.

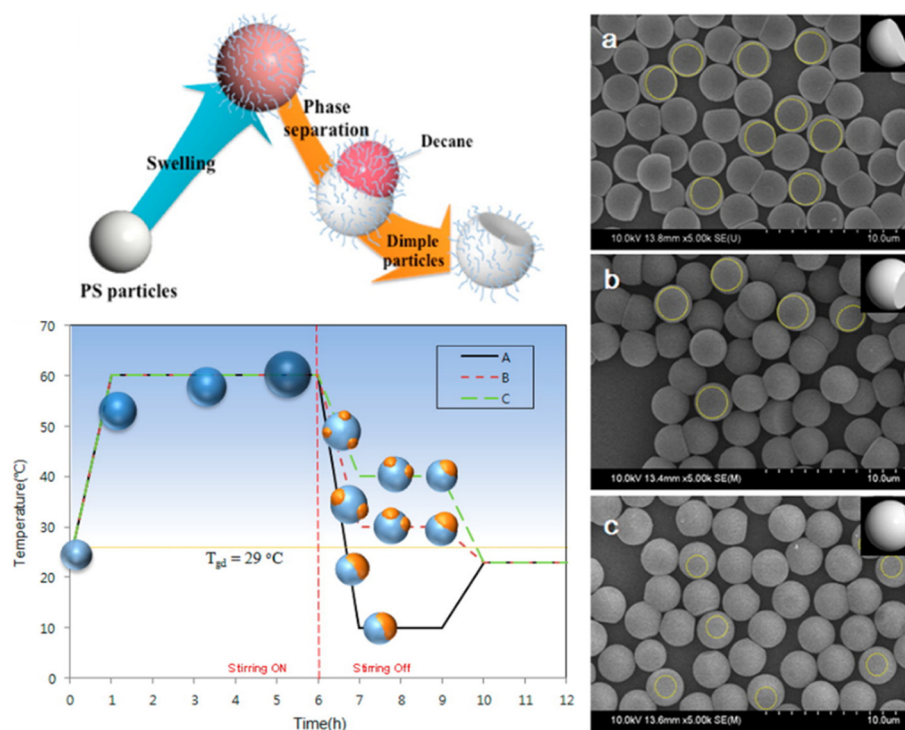


Fig. 10 Temperature-controlled swelling-deswelling process. Left: schematic describing the heating-cooling path which can be programmed (A-C) to obtain different particle morphologies. Right SEM images of 3- μm PS particles with dimples which were swollen at 60°C and cooled down to a) 10, b) 30, and c) 40°C in a water-ethanol mixture (40/60).⁶⁰ Cavities are indicated by a yellow dotted line.

1.3.1.2 Two-patch particles

The creation of two patches oppositely positioned on an isotropic spherical particle necessitates two stages. The GLAD method can be used twice if a particle stamping technique is employed using a polydimethylsiloxane stamp to invert the close-packed particle monolayer making the patches from the first vapour deposition facing down (Fig. 11).⁶¹ The accuracy of the stamping technique lies in efficiently inverting the monolayer and was evaluated by comparing the

experimentally observed patch geometries of the two-pole patchy particles to the mathematically predicted ones. The patch complexity can also be increased by tuning the template orientation and the beam incident angle simultaneously.⁶²

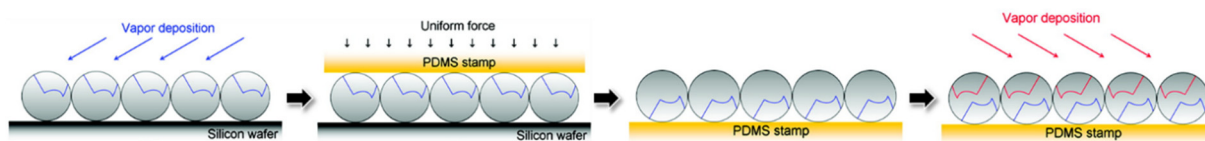


Fig. 11 Cross-sectional schematic of the GLAD and particle stamping techniques to get two-pole patchy particles.⁶¹

Lastly, crystalline particles present the advantage of exposing facets of different atomic densities and different affinities for adsorbing or reacting molecules accordingly. Kumacheva and co-workers took advantage of the presence of $\{111\}$ facets specifically at both ends of gold nanorods to create two opposite patches.⁶³ Cetyltrimethylammonium bromide (CTAB) is well-known to be an efficient structuring agent for gold nanorods through the seeded growth method considering the larger affinity of CTAB to the $\{110\}$ facet on the body part.⁶⁴ Then, at the ends of the nanorod, CTAB can be more easily shifted from the $\{111\}$ facets for instance by thiol-ended PS macromolecules leading to two hydrophobic patches capable of chaining the nanorods.⁶³

1.3.1.3 Six-patch particles

In the same vein, Yi and co-workers created successfully six silica patches from the six faces of hematite nanocubes.⁶⁵ In their presence, water droplets nucleate on the surface of hematite by phase separation in pentanol. By adjusting the water concentration, six droplets can form on each face of the hematite cube. When tetraethoxysilane (TEOS) is then added, it gradually diffuses into the water droplets through the oil phase. Within the droplets, hydrolysis and condensation of the precursors take place, leading to the formation of silica rods. In order to get flat silica patches, a small amount (1%) of hydrophobic glycidoxypropyl trimethoxysilane (GPTMS) is added in the precursor to reduce the contact angle of water droplets on silica. TEOS is consumed at the initial stage forming a small neck, and then GPTMS is consumed to form large plates (Fig. 12).

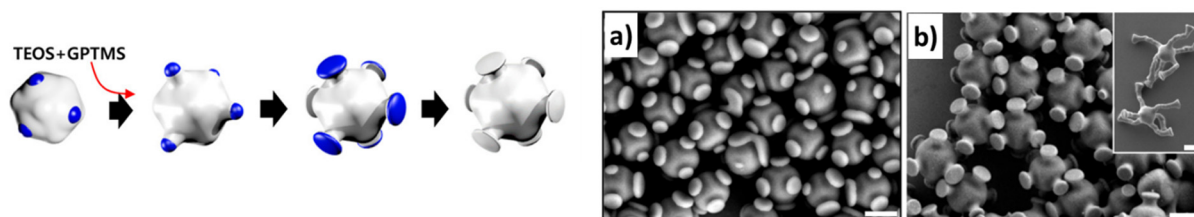


Fig. 12 Left: schematic illustration of the formation of six silica patches on hematite cubes in pentanol. The blue dots represent the water droplets. Right: SEM images of the as-obtained six-patch particles from hematite cubes (edge length: 950 nm) at a) 5°C and b) 10°C. Inset shows longer tack-like patches grown at room temperature.⁶⁵ Scale bars: 1 μm .

1.3.1.4 Twelve-patch particles

Twelve corresponds to the coordination number of spherical size-monodisperse particles in close-packed CCs. According to a strategy similar to the 3-D geometrical confinement in CCs (*cf.* 1.1.1 section), Zhao and co-workers prepared opals from 415-nm silica spheres and annealed them at 750°C in order to allow connections between adjacent spheres.⁶⁶ Subsequently, the CC was immersed in a solution containing MPS to functionalize the exposed surface of the particles. Washing and redispersion yielded individual particles, whose surface was patterned by MPS (the connection areas were not modified by MPS). To reveal the patchiness, the authors used them as seeds in a subsequent regrowth of silica. Silica was successfully condensed only on the unmodified areas giving rise to twelve silica protrusions whose diameter can be controlled by the connection size, *i.e.* the annealing time. Nevertheless, a fraction of the particles had a silica nodule number different from twelve: not only those which were not fully coordinated because located on the surface or edges of the CCs, but also those inside the CCs that were not fully coordinated for size-polydispersity reasons, *i.e.* too large distance between some particles to achieve the connections. More recently, Bae *et al.* developed a similar strategy but used octadecyltrichlorosilane self-assembly monolayer preferentially to MPS for growing titania patches.⁶⁷ They compared ultrasonic and conventional agitation during patch growth, and they found that enhanced mass transfer is the key to controlled, homogeneous transport of the molecular precursors in a solvent onto the nanoparticles.

1.3.2 Versatile strategies

1.3.2.1 Template-free methods

Taylor Klupp and co-workers reported a one-pot approach to patchy particles based on the heterogeneous nucleation of silver onto the bare surface of calcined silica followed by surface diffusion dominated growth.⁶⁸ The method was extended to the formation of gold patches onto

cationic PS nanospheres using ascorbic acid to reduce the auric ion.⁶⁹ Among several other experimental parameters, pH value and ascorbic acid concentration appeared to be critical parameters to control the patch morphology and number (Fig. 13). Nevertheless, this technique is far to allow fine control of the size and position of the patches.

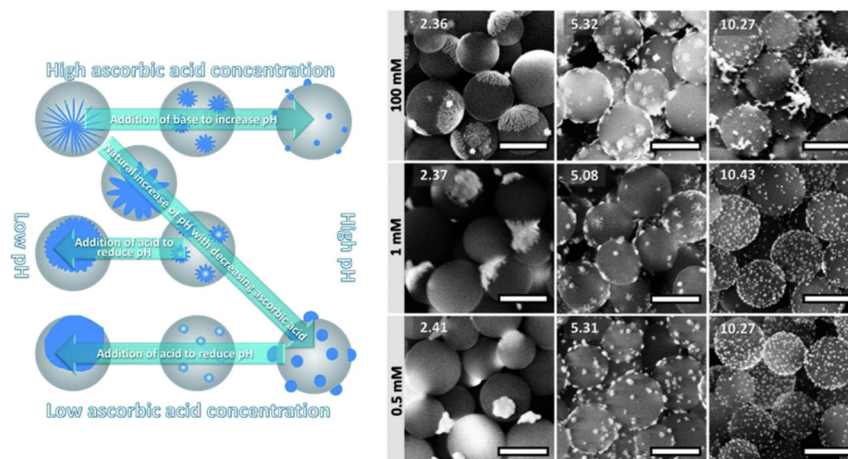


Fig. 13 Left: schematic representation of the influence of reaction parameters on the patch morphology and number obtained by heterogeneous nucleation. Right: corresponding SEM images of patchy particles obtained by mixing the same amount of cationic PS nanospheres with different concentrations of ascorbic acid (horizontal rows), adjusting the pH to the value shown on the image label, followed by addition of the same amount of chloroauric acid.⁶⁹ Scale bars: 250 nm.

Bon and coll. reported that when using polymer nanogels as stabilisers in emulsion polymerisation of styrene, surface segregation of the nanogels yielded to the formation of patches whose number and size can be tuned by controlling the initial number of nanogels, ionic strength and pH value (Fig. 14).⁷⁰ Once again, the control of the relative positions of the patches was not demonstrated.

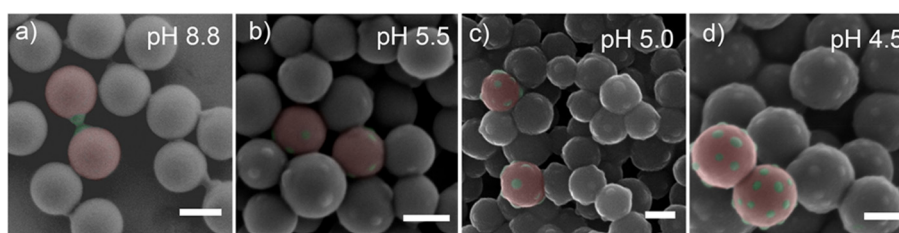


Fig. 14 False coloured SEM images of PS latex particles obtained by emulsion polymerisation stabilised by nanogels showing that the number of patches made of nanogels aggregates depends on the pH value prior to polymerisation.⁷⁰ Scale bars: 100 nm.

1.3.2.2 Derivatisation of preformed colloidal molecules

As previously discussed, CMs and patchy particles are quite close concepts. In particular, CMs whose satellites particles are naturally sticky or could be made sticky under external stimuli

such as temperature, solvent, *etc.* can also be considered as patchy particles. However, CMs are more often potential precursors of patchy particles subject to some chemical modifications.

In this way, the micron sized CMs obtained by Pine and coll. through confinement in liquid droplets were derivatised in two types of patchy particles. Patchy particles with DNA functionalised patches were obtained from CMs made of amidinated PS microspheres.⁷¹ They were swollen by styrene in order to let emerging amidine patches. After styrene polymerisation, biotin was regioselectively grafted on the patches, prior to the anchoring of biotinised DNA oligomers via a biotin-streptavidin-biotin linkage (Fig. 15 left). Particles with concave patches, *i.e.* dimples, were created differently from silica CMs, partial encapsulation in MPS which was then polymerised before silica etching with fluorhydric acid (Fig. 15 right).⁷² These strategies were successfully implemented to a quite large series of CMs. A mixed strategy combining PS CMs and MPS also allowed to get particles with concave or convex features on demand.⁷³ The design is based on the solvent-induced shifting of the patch shape. The initial concave patchy particles were synthesised in a water suspension by a swelling-induced buckling process. Upon exposure to different solvents, the patches were tuned reversibly to be either concave or convex.

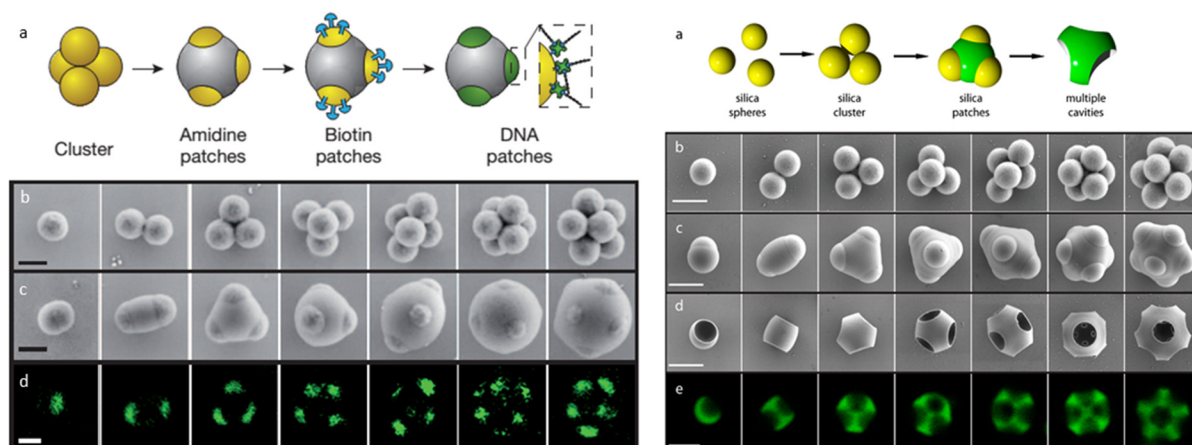


Fig. 15 Left: Fabrication of DNA-based patchy PS particles. a) Synthesis route. SEM images of amidinated, b) PS CMs and c) patchy particles after encapsulation. d) Confocal fluorescent images of the latter.⁷¹ Scale bars: 500 nm. Right: Fabrication of dimpled particles. a) Synthesis route. Electron micrographs of b) silica CMs, c) silica-TPM patchy particles, and d) multicavity particles. e) Confocal fluorescent images of fluorescently labelled multicavity particles.⁷² Scale bars: 1 μm .

An even more innovative strategy was carried out by Sacanna and coll., who envisioned and implemented the concept of colloidal fusion.⁷⁴ Using coordination dynamics and wetting forces, it consists in parking PS particles on a liquid core droplet made of curable silicone oil to get hybrid liquid-solid clusters that evolve on the addition of a plasticiser to spherical particles with liquid surface patches capable of forming curable bonds with neighbouring particles (Fig. 16).

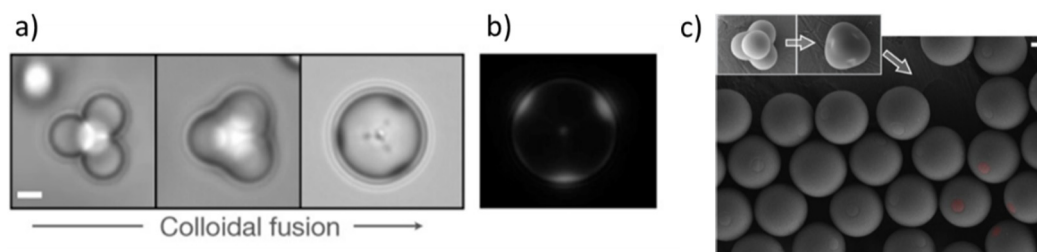


Fig. 16 Colloidal fusion: a) bright-field time-lapse images showing the deformation of a tetrahedral liquid-core colloidal cluster after the addition of the plasticiser; b) fluorescence microscopy image at the final time point; c) SEM image of polymerised patchy particles (some patches are false-coloured). The insets show SEM images of deformed clusters with increasing degrees of plasticisation.⁷⁴ Scale bars: 1 μm .

The silica/PS CMs obtained in our group by controlled surface nucleation and growth were also successfully converted into silica colloids combining entropic and enthalpic patchiness.^{35,75} Those were easily obtained by first regrowing the silica core and then removing the PS nodules by simple dissolution (Fig. 17). The as-created dimples not only present the same features than those of the template satellites in term of number, size and position, but also they bear anchored PS macromolecules at the bottom of the dimples originating from the copolymerisation of some growing PS chains with the surface grafted MPS compatibiliser. These macromolecules make the dimples naturally sticky via hydrophobic interactions, but they can also be derivatised to developed ionic interactions or covalent bonding.

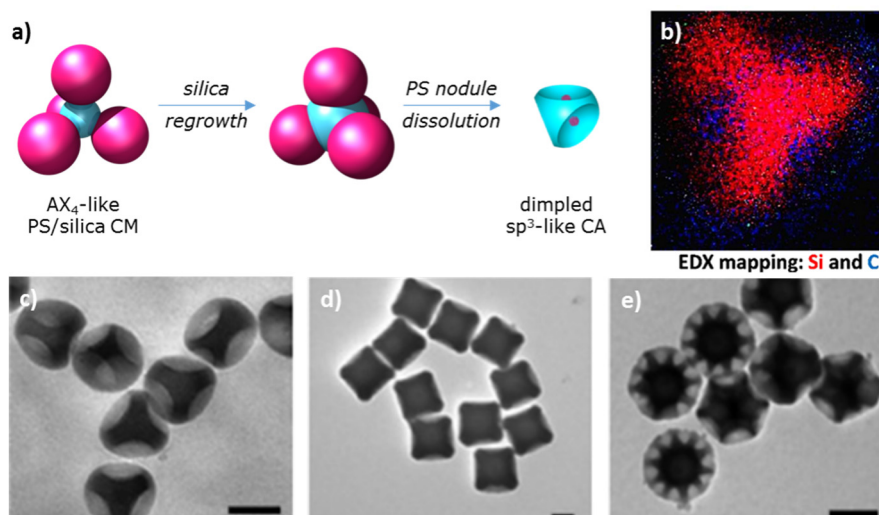


Fig. 17 Conversion of silica/PS CMs into silica particles with patches simultaneously enthalpic and entropic: a) synthesis route; b) STEM-EDX mapping evidencing the presence of PS residue at the bottom of the dimples; TEM images of patchy silica particles so-obtained from silica/PS CMs with c) four, d) six and e) twelve PS nodules.⁷⁵ Scale bars: 100 nm.

1.3.2.3 Phase separation and reshaping

We discussed in the 1.1.2 section how controlled phase separation phenomena could be exploited to generate protrusions in the course of emulsion polymerisation seeded with polymer latex particles. This method was also used by Wang and coll. to fabricate dimpled particles by controlling the adding speed of crosslinker at different stages (Fig. 18).⁷⁶ The formation of mono- or multi-cavities is attributed to the single- or multi-location of polydivinylbenzene (PDVB) at the latex surface. Specifically, DVB added at slow speed prefers to locate at one place and induces the single cavity after phase separation to reduce Gibbs interfacial free energy, as the network of PDVB is more rigid than the core seed. However, multi-cavity particles can be fabricated alternatively if DVB is fast added. Nevertheless, it was not demonstrated that the number of cavities could be finely tuned through this strategy.

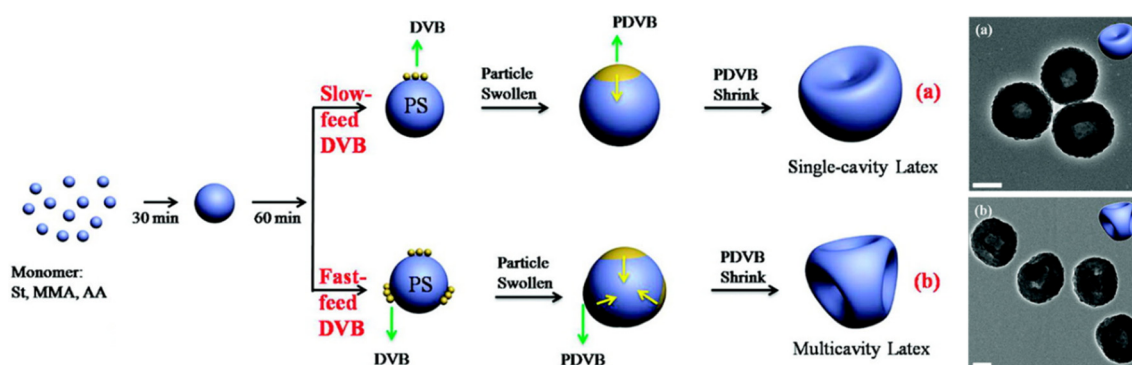


Fig. 18 Schematic representation of the preparation of dimpled latex particles and corresponding TEM images showing that the number of cavities depends on the a) slow and b) fast charging mode.⁷⁶ Scale bars: 200 nm.

In seeded growth emulsion polymerisation, the protrusions or concavities endowing the patchy character are controlled by phase separation phenomena, which yields to complex entanglements of linear and crosslinked homopolymers and copolymers. Nevertheless, patchy particles at lower scales can be achieved through the reverse way, *i.e.* the high precision synthesis of block copolymers and their controlled phase separation by solvent evaporation induced assembly within emulsion droplets (3-D confinement) or through selective solvent swelling.

In a first example, the most accessible typical system, *i.e.* with two blocks usually illustrated by PS and P4VP, is initially dissolved in a good solvent for both blocks, such as chloroform, and the solution was subsequently emulsified in the bad solvent for PS (water) to obtain the patchy particles after evaporating the chloroform. In this way, Yang and coll. obtained Janus nanoparticles and showed that their aspect ratio is controlled by the P4VP fraction.⁷⁷ This method is robust without the requisites of narrow molecular weight distribution and a specific

range of block fraction of the copolymers. The same authors,⁷⁸ simultaneously to Kim and co-workers,⁷⁹ showed that the strategy could be extended for the synthesis of PS nanoparticles with up to nine P4VP patches by increasing the volume of the emulsion droplet, *i.e.* the volume of the particle (Fig. 19 left). For a given particle volume, the morphology can then be precisely tuned by modulating the interfacial interaction at the particle/water interface using a mixture of two different surfactants.⁷⁹

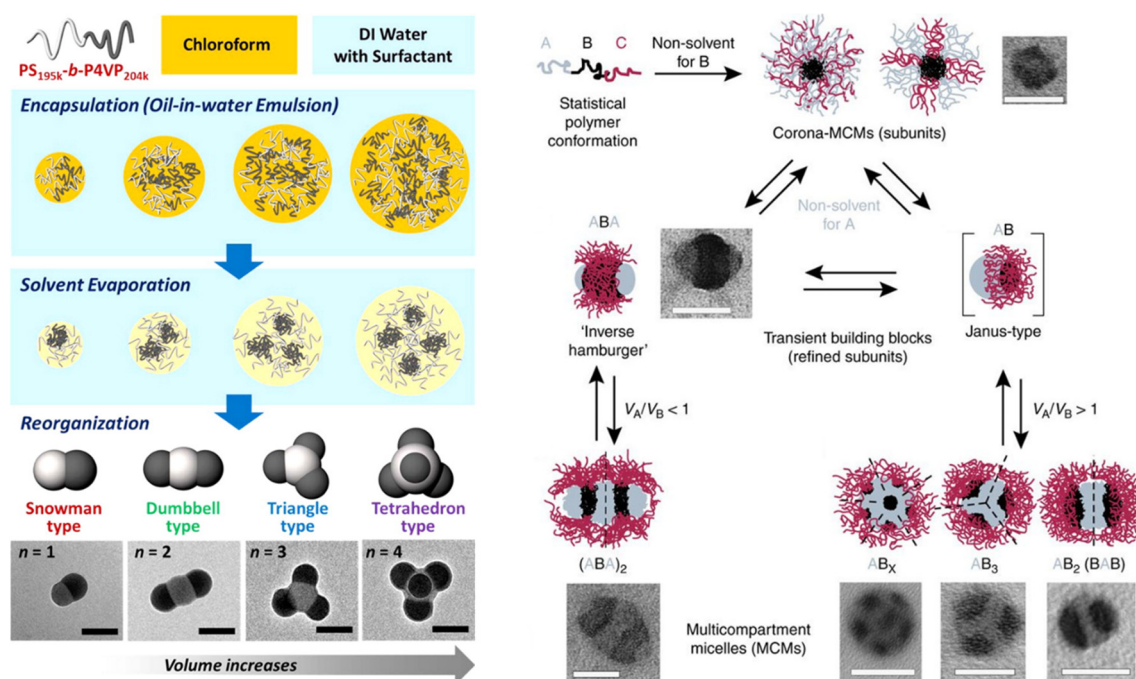


Fig. 19 Left: Schematic illustration of the fabrication of soft patchy particles of PS-*b*-P4VP through oil-in-water emulsion evidencing the influence of the volume of the particles on the patch number.⁷⁹ Scale bars in the TEM images: 100 nm. Right: Schematic illustration of the synthesis pathway of multicompartment micelles from triblock copolymers and corresponding TEM images after OsO₄-staining (PS grey, PB black and PMMA not visible due to e-beam degradation).⁸⁰ Scale bars: 50 nm.

The second example concerns well-defined triblock copolymers that do not need confinement conditions to yield to multicomponent patchy nanoparticles.⁸⁰ Gröschel *et al.* simply played with selective solvent and non-solvent for each block (Fig. 19 right). The morphology of the as-obtained particles depends on the volume of each unit and the solvent introducing sequence with unprecedented structural control via the intermediate pre-assembly of subunits. This directed self-assembly leads to a stepwise reduction of the degree of conformational freedom and dynamics and avoids undesirable kinetic obstacles during the structure build-up.

1.4 Assembly of patchy particles into hierarchical structures

The assembly of patchy particles is expected to yield well-defined structures and especially more open frameworks than isotropic particles do. Nevertheless, the interrelationship between the number of patches and the number of established bonds is not as simple as in the atomic world as demonstrated thanks to the huge amount of simulation studies which have described these last two decades the diversity of the possible structures.⁸¹ The patch-to-particle size ratio is one of the critical parameters. Roughly, the larger the patch, the higher the number of establishable bonds, especially as the patch number is low. That is why one-patch particles are often multivalent, leading to large clusters or chains, and two-patch particles can be not only chained but also arranged in 2-D structures such as kagome-like lattices.

The aim of this section consists of describing the assemblies that have been experimentally achieved. We focus on the physicochemical and chemical driving forces, *e.g.* depletion forces, hydrophobic/solvophobic interactions, DNA hybridisation, covalent or supramolecular coupling, meaning that we deliberately omitted the assembly strategies using external fields, such as electric⁸² or magnetic⁸³ fields. For a comprehensive survey of the simulation studies, there exist several review papers.⁸⁴⁻⁸⁶

1.4.1 Zero-dimension assemblies

These are clusters obtained through the assembly of one central multipatch particle combined to satellite particles generally to reach new CMs. However, there are also many examples of clusters obtained in an entirely controlled way from the self-assembly of one-patch particles.

1.4.1.1 Directed assembly of satellite particles around one multipatch particle

Depletion forces

The depletion attraction force was firstly introduced by Asakura and Oosawa through a simple conceptual experiment.⁸⁷ This consists of adding to the liquid dispersion of the particles some depletant agents, which can be smaller particles or macromolecules whose main feature is the lack of interaction with the colloids. When the distance between two colloidal particles is less than the diameter of a depletant, the jointed region is occupied by the pure solvent. So, the osmotic pressure induces the elimination of the pure solvent to the outside region with additives, thereby forming the attraction between the two colloids and forcing their closure. Already exploited for the formation of CCs,⁸⁸ the depletion technique has been recently extended to fabricate clusters from microparticles.

Depletion attraction is indeed particularly efficient when the particle shapes are complementary, as evidenced through the lock-and-key principle proposed by Pine and co-workers.^{60,89,90} They used silica microparticles with a well-defined number of concavities (*cf.* Fig. 15 right) combined to conventional spheres whose diameter fits that of the dimples, in the presence of poly(ethylene oxide) ($\bar{M}_w = 600,000$ g/mol) as depletant.⁹⁰ AX, AX₂, AX₃, AX₄, and AX₅ CMs were stoichiometrically achieved when shifting the monovalent lock to multivalent ones (Fig. 20).

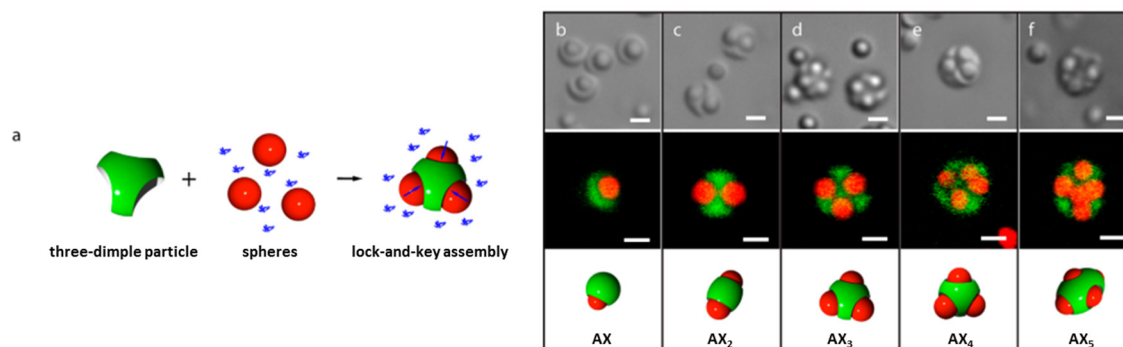


Fig. 20 Lock-and-key assemblies. a) Schematic illustration showing a three-patch particle with three assembled spheres using depletion interaction. The depletant (blue coil) causes osmotic pressure (arrows) between adjacent colloids, which is maximised when a sphere assembles into a cavity. b-f) Bright field micrographs (top panel), confocal micrographs (middle panel), and cartoons (bottom panel) showing multivalent lock particles with b) one, c) two, d) three, e) four, and f) five cavities binding to red fluorescent spheres stoichiometrically.⁹⁰ Scale bars: 1 μm .

DNA hybridisation

DNA interaction was utilised for the assembly of particles bearing patches made of complementary strands. A typical example was reported by Pine and co-workers from the patchy particles described in Fig. 15 left.⁷¹ They obtained new CMs from AX to AX₄ morphology (Fig. 21). Thanks to a high patch-to-particle size ratio, they also observed *cis* and *trans* configurations and CMs, which could mimic ethylene molecules if both carbon atoms are considered embedded in the single oblong colloid.

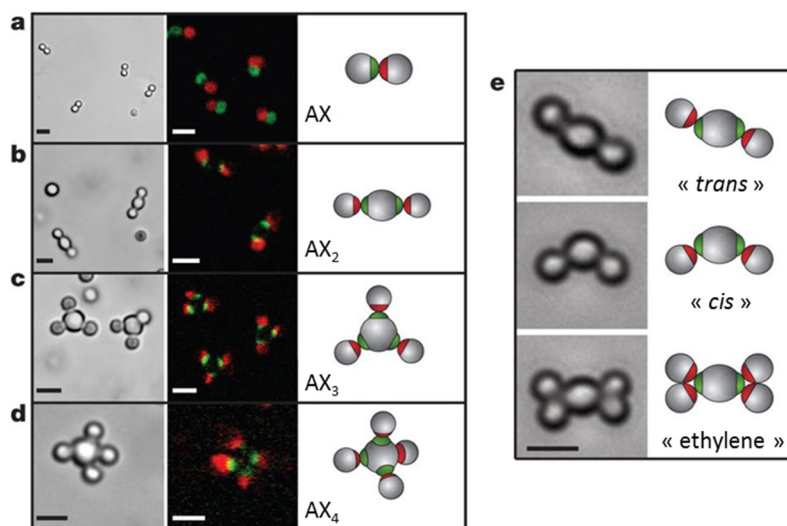


Fig. 21 Specific directional bonding between PS microparticles with DNA patches observed with optical microscopes. a–e) Bright-field (left panels), confocal fluorescent (middle panels), and schematic images (right panels) show CMs self-assembled from patchy particles through DNA hybridisation. a) Complementary green and red monovalent particles form dumbbell-shaped AX-type molecules. Supra-colloidal molecules AX_2 , AX_3 and AX_4 are formed by mixing red monovalent with green divalent b), trivalent c) and tetravalent d) particles. e) When particles with larger patches are used, cis-trans-like isomers can form. Introducing more monovalent particles leads to ethylene-like colloidal molecules. Images are bright-field (left panels) and schematic (right panels).⁷¹ Scale bars: 2 μm .

Covalent bonding

Our group successfully obtained silica CMs from the dimpled particles fabricated according to the pathway summarised in Fig. 17. The strategy consists of derivatising the anchored PS macromolecules at the bottom of the dimples to make them first chloromethylated, second aminated.⁹¹ Then, they are incubated in DMF with an excess of silica NPs whose surface ester groups are activated in order to lock the spheres within the dimples via amide bonds. TEM pictures show that most of the dimples are indeed occupied by the satellite particles in a robust way making separation by centrifugation possible. When the size of the satellite is well adapted, the number of satellites corresponds to the number of patches meaning that in such systems the valence can be controlled simply through the patch number. Different CMs were obtained from di-, tri- and tetravalent particles (Fig. 22 left) and the diversity was also increased when two types of silica satellites were simultaneously employed (Fig. 22 right).⁹² Chiral molecules were observed randomly when using four differently-sized satellites.⁹¹

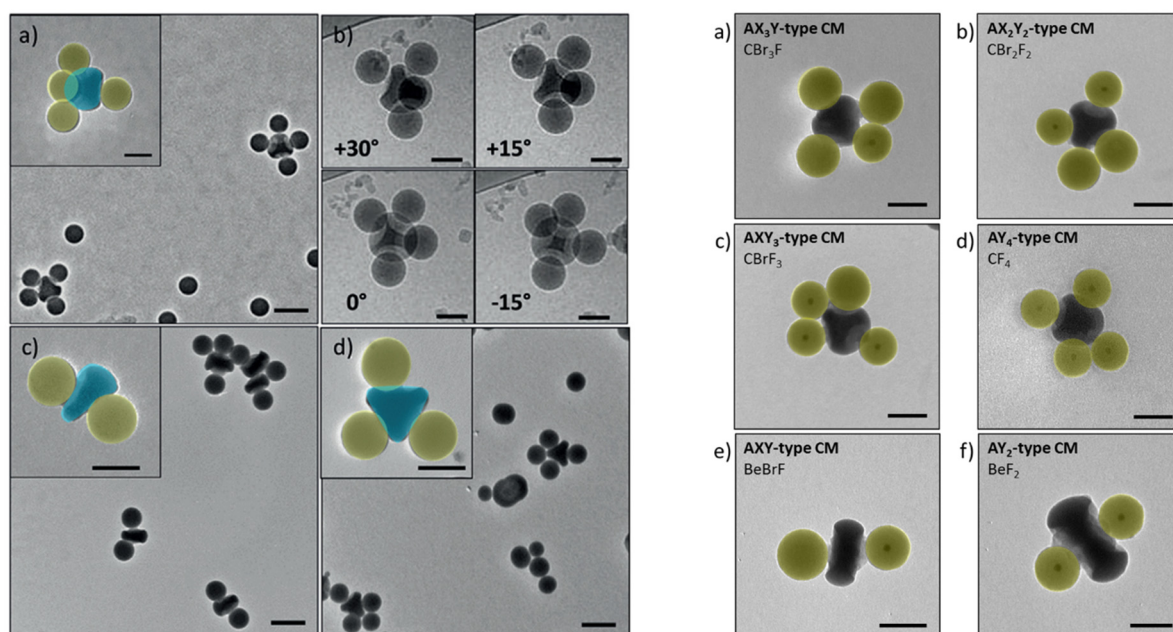


Fig. 22 Silica CMs obtained by directional covalent bonding from dimpled CAs. Left: TEM (a) and cryo-TEM (b) images of the CMs obtained from mixing 100-nm NPs with four-dimple CAs in a 4/4 ratio. TEM images of CMs obtained from mixing 100 nm NPs with two-dimple CAs in a 2/2 ratio (c) and three-dimple CAs in a 3/3 ratio (d). Scale bars: 200 nm and 100 nm for the inserts.⁹¹ Right: TEM images of the CMs obtained from mixing NPs with four aminated dimples with 100-nm silica NPs and 90 nm core-shell nanoparticles in ratios of (a) 4/3/1, (b) 4/2/2, (c) 4/1/3 and (d) 4/0/4 where the bold figures represent the number of dimples of the central CAs. TEM images of the CMs obtained from mixing particles with two aminated dimples with 100 nm silica nanospheres and 90 nm core-shell nanoparticles in ratios of (e) 2/1/1 and (f) 2/0/2 ratio.⁹² Scale bars: 100 nm.

1.4.1.2 Controlled aggregation of one-patch particles

There exist several reported works dedicated to the self-aggregation of one-patch, *i.e.* Janus-like, particles in the range of 50 nm to 200 μm (Table 2) and the field was recently reviewed.^{51,52,93} The authors generally obtained complex mixtures of fragile clusters prohibiting any purification attempt. This relative instability is due to the too low or reversible attractive forces between the patchy particles. As far as we know, their strengthening by a chemical or physicochemical process was not reported.

Table 2: Some examples of clusters obtained from one-patch particles.

One-patch particles	Driving force for assembly	Aggregation number N	Ref.
1- μm carboxylate-coated PS spheres then half-coated with gold treated with (11-mercaptoundecyl)ammonium chloride	Electrostatic attraction	2-12	94
1- μm carboxylate-modified PS spheres half-coated with gold treated with alkanethiol	Solvophobic effect helped with electrostatic screening	2-9	95
1- μm sulphate PS spheres half-coated with gold treated with alkanethiol	Hydrophobic attraction and electrostatic repulsion	2-7	96
4- μm snowman-like PS particles with smooth body and rough head	Roughness-controlled depletion attraction	2-12	97
3- μm gold half-coated silica spheres	At tipping points of thermally-switched wetting	4-~20	98
4- μm iron oxide half-coated latex spheres	Lipid-induced capillary bridging	2-5	99
120-nm organosilica sphere with one 44-nm gold head	van der Waals force and electrostatic force	2-3	100
50-nm silica sphere with one 45-nm gold head coated with alkanethiol	Solvophobic effect	4-7	101
200- μm hydrophilic poly(ethylene glycol) diacrylate sphere with 160- μm ethoxylated trimethylolpropane triacrylate head	Drying of Pickering-like water droplets	2-8	102

1.4.2 One-dimension assemblies

Chaining of particles, often described as colloidal polymerisation, is a field of intense research that was recently reviewed several times.^{103–105} In the restricted fields of inorganic particles, Pyun and co-workers identified three main strategies based on assembly directed by dipoles, *e.g.* electrostatic or magnetic, by surface lattice fringes or by surface organic ligands providing electrostatic, covalent or non-covalent linkages, *e.g.* oligonucleotide. In this last scheme, there exist few studies employing patchy particles for programming a one-direction growth.¹⁰⁵ We describe some of them below by emphasising those using two-patch particles, *i.e.* omitting those employing one-patch particles which generally give rise to helical chains or double-line chains.¹⁰⁶

1.4.2.1 From polymer-tethered metal nanorods

The main achievements in this area concern the chaining of metal nanorods.¹⁰⁴ As previously discussed, gold nanorods can be considered as two-patch NPs because of the different reactivity of their heads compared to the body part. Murphy and co-workers were among the first ones to observe that the density of CTAB ligands is lower at the tips of the gold nanorods making possible to site-specifically bind biotin disulfide and therefore link the NPs end-to-end by

adding streptavidin.¹⁰⁷ Kumacheva and co-workers enhanced the patchiness of CTAB-coated gold nanorods by the functionalization of their tips with thiol-terminated polystyrene ligands, which enabled the formation of linear and cyclic colloidal polymers when dispersed and deposited onto substrates from selective solvent systems.⁶³ The driving force to assemble hydrophobic NPs derives from the solvation free energy reduction between the isolated particles and their assembly.¹⁰⁸ Based on this principle, hydrophobic patches become attractive in binary solvent mixtures with different polarities to decrease the free volume energy.¹⁰⁹ In this way, the authors succeeded in the self-assembly of the PS-tethered gold nanorods by using mixtures of one good solvent, *e.g.* THF or DMF, and one bad solvent for PS, *e.g.* water or ethanol (Fig 23).^{63,110} Degrees of polymerisation (DP) of up to 50 were observed by TEM for linear chains of nanorods end-functionalized with PS ligands ($\bar{M}_n = 30,000$ g/mol) and cast from DMF/water dispersions.¹¹¹ Copolymer-like assemblies were also achieved when mixing gold and palladium nanorods.¹¹² The colloidal polymerisation was shown to follow step-growth polymerisation models, and this was the first quantification attempt using classical polymerisation approaches.¹¹⁰ They also developed the concept of colloidal chain stoppers for controlling DP by using snowman-like particles made of an iron oxide body and gold head subjected to a two-step ligand exchange to cap them with dopamine-terminated polyethylene glycol and thiol-terminated PS macromolecules, respectively.¹¹³ Lastly, the authors reported that in the presence of salts, the major driving force for self-assembly is a decrease in solubility of the polystyrene ligands rather than a screening of the electrostatic repulsion.¹¹⁴ Photo-crosslinking of poly(styrene-co-isoprene) end-functionalized gold nanorods was also demonstrated as a useful means to covalently fix the bond angles in the chains.¹¹⁵

Alternatively, gold nanorods functionalised at both ends with thiol-terminated PNIPAM ($\bar{M}_n = 13,000$ g/mol) ligands were also demonstrated to undergo (photo)thermally triggered self-assembly to form linear and branched colloidal polymers.¹¹⁶ The NPs were heated above the lower critical solution temperature (LCST) of PNIPAM to induce colloidal polymer formation with an average DP of 11. Similar chaining was observed when the LCST was reached upon illumination at a wavelength near the longitudinal plasmon band of the nanorods.

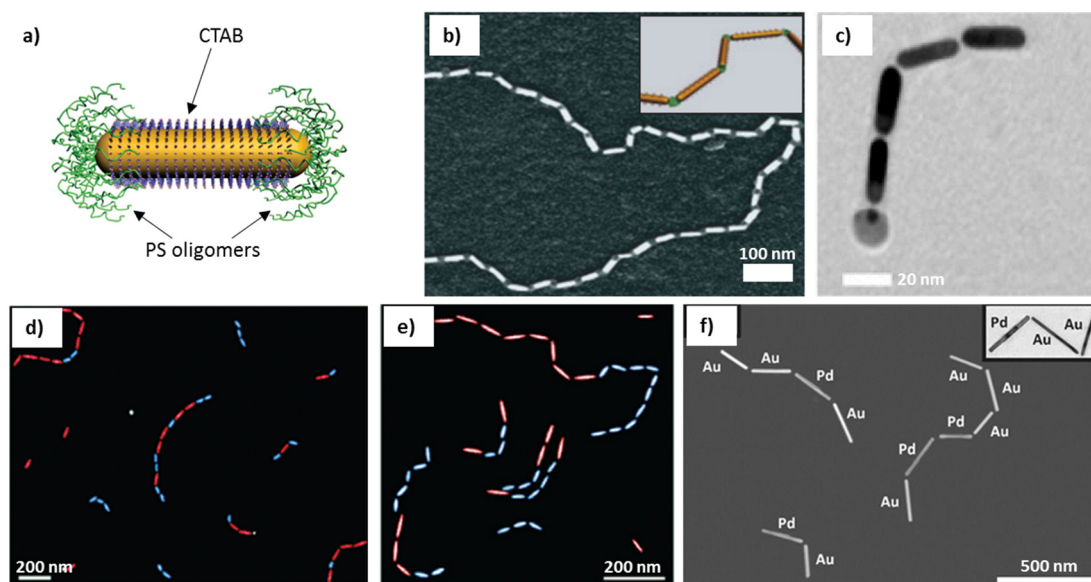


Fig. 23 a) schematic representation of gold nanorods where CTAB ligands at the tips have been replaced by thiol-terminated PS chains; TEM images of b) a long chain after end-to-end assembly, c) a chain terminated by a chain stopper, d) random copolymers and e) block-copolymers from nanorods of two different lengths, and f) random copolymers from gold and palladium nanorods.^{63,112,113}

1.4.2.2 From particles with two concave or convex patches

According to the lock-and-key concept, Pine and co-workers subjected organosilica microspheres bearing one dimple to depletion conditions and observed their stacking when the diameter of the dimples fits that of the other hemisphere.⁸⁹ The absence of irreversible chemical bonds between the building blocks allows these ball-in-socket joints to move freely and confers high flexibility to the colloidal macromolecules. Similar results were obtained by Tigges and Walther by using cone-shaped microparticles fabricated by direct 3-D laser writing which consists in crosslinking a resin through two-photon lithography.¹¹⁷

Pine and coll. also obtained short chains from two-patch organosilica microparticles and DNA hybridisation.⁷¹ With the same microparticles, the idea was extended to reversible supramolecular coupling by metal coordination,¹¹⁸ host-guest pairing cucurbit[7]uril and viologen motifs not only light-mediated,¹¹⁹ but also redox-mediated.¹²⁰ Nevertheless, DP generally remained below 12 and branches due to the simultaneous interaction of three patches were frequently observed.

1.4.2.3 From multicomponent macromolecular micelles

The ABC triblock NPs prepared by Gröschel *et al.* (*cf.* Fig. 19 right) were successfully employed to get long and highly regular chains thanks to selective solvents.¹²¹ Briefly they showed that SDM tri-block copolymers made of polystyrene-*block*-poly(3-

butenyl(dodecyl)sulphane)-*block*-poly(methyl methacrylate) where $V_s/V_D < 1$ are changed first into core-corona colloids where the S blocks create two opposite patches in the presence of a non-solvent of the central blocks, and second into linear chains once the solvent quality has been reduced to a critical threshold for the S patches (Fig. 24a). The authors prepared hybrid materials by selectively encapsulating 10-nm magnetite NPs within the D segments of $SD^M S$ at the first stage (Fig. 24b) and extended this approach to design multiblock co-assemblies by combining two divalent units, *i.e.* $SD^M S$ and $SB^M S$ where B is a polybutadiene block (Fig. 24c). They also got many other complex morphologies.¹²¹

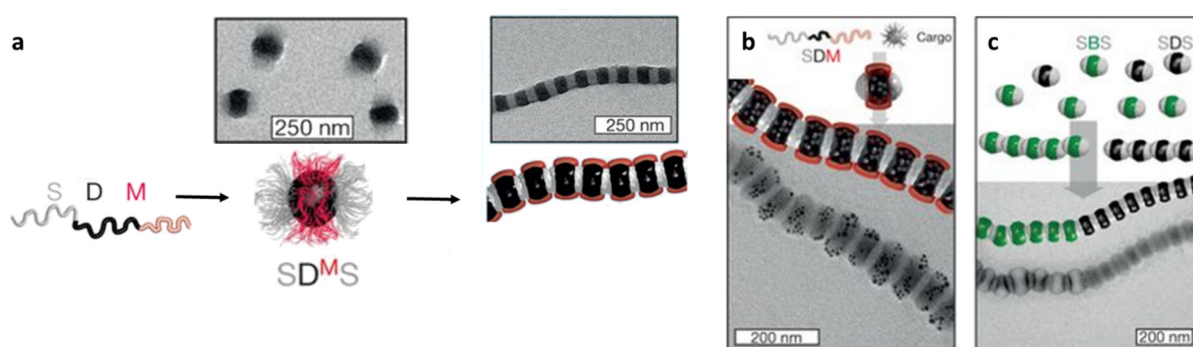


Fig. 24 Hierarchical assembly of triblock copolymers in selective solvents: a) schematic representation of the two-stage process and corresponding TEM images, b) hybrid co-assemblies with 10-nm magnetite NPs selectively loaded within the D segment, and c) linear multiblock co-assembly composed of $[SD^M S]_m/[SB^M S]_n$ sequences (M corona omitted for clarity).¹²¹

In the same vein, Sohn and coll. reported recently the preparation and polymerisation of two-patch micelles obtained from PS-P4VP macromolecules after crosslinking of the P4VP core with 1,4-dibromobutane (Fig. 25a) and dispersion in DMF - a good solvent for P4VP but a bad solvent for PS - rearranging the PS corona into two separate patches (Fig. 25b).¹²² Then, the polymerisation is triggered by adding water (Fig. 25c). The possibility to reach block or random copolymers was demonstrated using two differently-sized micelles, *i.e.* with different block lengths (Fig. 25d-e) or micelles labelled with two types of quantum dots (Fig. 25f-i).¹²³ Lastly, branching and crosslinking were introduced in a controlled way by employing three-patch micelles generated when the PS-to-P4VP volume ratio was increased.¹²⁴

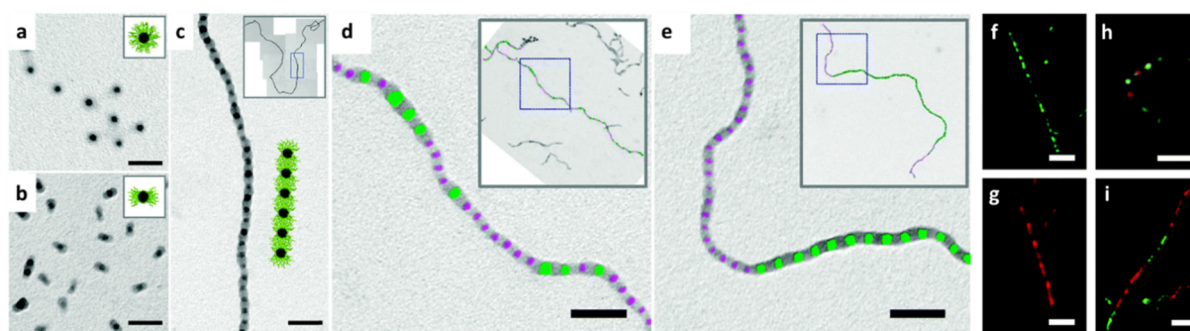


Fig. 25 Polymerisation of patchy micelles: TEM images of a) spherical micelles of PS(51)-P4VP(18); b) two-patch micelles obtained after DMF addition, c) colloidal macromolecules obtained after water addition, d) random and e) block copolymer chains obtained from PS(51)-P4VP(18) and PS(25)-P4VP(7) micelles (false colours for clarity),¹²² and structured illumination microscopy (SIM) images of homopolymers from micelles bearing f) green and g) red quantum dots, h) random copolymers and i) block copolymers from the same fluorescent micelles.¹²³ Scale bars for TEM and SIM images are 100 nm and 1 μm , respectively.

1.4.3 Two-dimension assemblies

The well-known 2-D kagome structure reported by Granick and co-workers eight years ago was obtained from microparticles bearing only two patches which were sufficiently large to interact each with two others,¹²⁵ as demonstrated *in silico* by Romano et Sciortino (Fig. 26).^{126,127} They showed that self-assembly occurs when the strength of the interaction between patches (depicted in red) is large enough to overcome the random forces arising from the thermal jiggling of the particles. In this case, they crystallise into a kagome lattice or a closed-packed triangular lattice at higher density. Experimentally, the two-patch microparticles, improperly called triblock Janus particles, were made up of an electrically charged band in-between two hydrophobic caps of the proper size and fabricated by the double metal deposition and intermediary particle stamping techniques. After sedimentation, a salt solution allowed to shield the repulsion force and slowly induced the self-assembly.

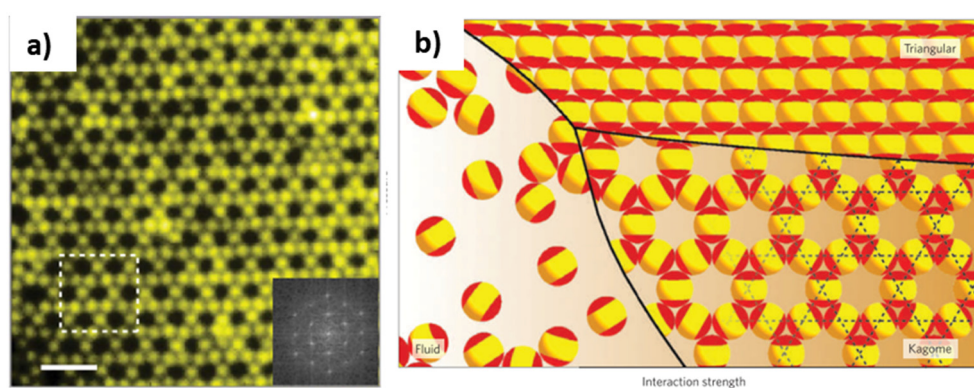


Fig. 26 2-D kagome structure obtained by two-patch microparticles self-assembly: a) fluorescence image of the obtained structure¹²⁵ and b) snapshot of the forming assembly obtained by simulation¹²⁷. Scale bar: 4 μm .

As far as we know, there is no concrete example of colloidal monolayer made of three-patch particles and only Monte-Carlo simulations were reported.^{127–132} Doppelbauer *et al.* investigated in a two-dimensional system the self-assembly scenario of particles with three attractive patches.¹²⁸ They identified two minimum energy configurations: at low pressure, honeycomb structure where all patches are saturated via bonds, and at high pressure, a 2-D hexagonal structure where the cores of the particles are close-packed. The number of bonds that the particles can form via the patches plays a minor role in the energetic considerations (Fig. 27a). Sciortino and co-workers identified at low T three different fully bonded structures: a collection of independent honeycomb-like planes, a crystal consisting of inter-penetrating honeycomb-like planes and a fully bonded *fcc* structure if the patches are wide enough (Fig. 27b).¹²⁹

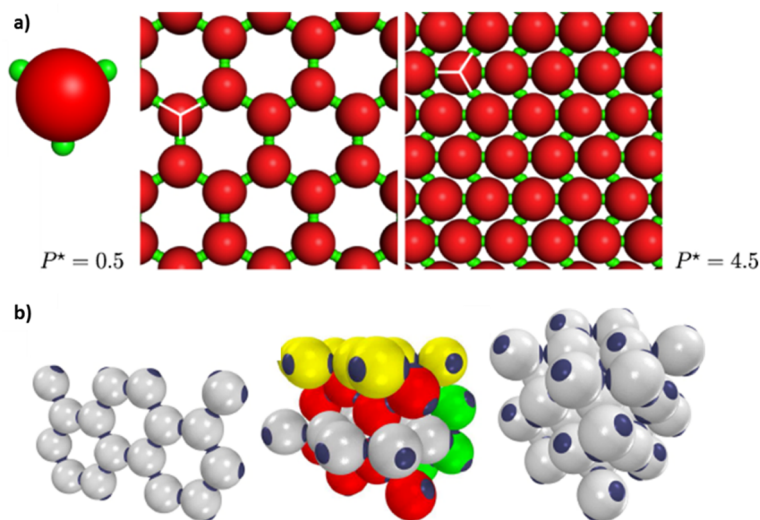


Fig. 27 Simulation of assemblies from three-patch particles: a) two minimum energy configurations depending on pressure when constrained in a two-dimensional system,¹²⁸ and b) schematic representation of the crystals examined in a three-dimensional system, *i.e.* independent honeycomb-like planes, a crystal consisting of inter-penetrating honeycomb-like planes and a fully bonded *fcc* structure. For better visualisation of the structure, particles in the 2nd phase are coloured according to the plane they belong to.¹²⁹

Noya *et al.* confirmed the existence of the honeycomb lattice at moderately low temperature and pressure, whereas the system would form a close-packed triangular lattice at high temperature and pressure.¹³¹ When the half-opening angle of the patches is lower than 10° , the fluid transforms upon increasing the pressure into a rather exotic phase, *i.e.* honeycomb lattice whose voids are filled continuously with additional particles that remain, on average, unbound and capable of free rotation (Fig. 28 top). At moderately low temperature, the fluid transforms into a nearly empty honeycomb lattice, whereas at high temperature it transforms directly into the almost filled lattice. Interestingly, for particles with big patches (with a half opening angle

of 20°), the honeycomb-like and triangular lattices are separated by a liquid phase that remains stable down to fairly low temperatures (Fig. 28 bottom). Less surprisingly, only particles with big patches exhibit an equilibrium gas-liquid separation.

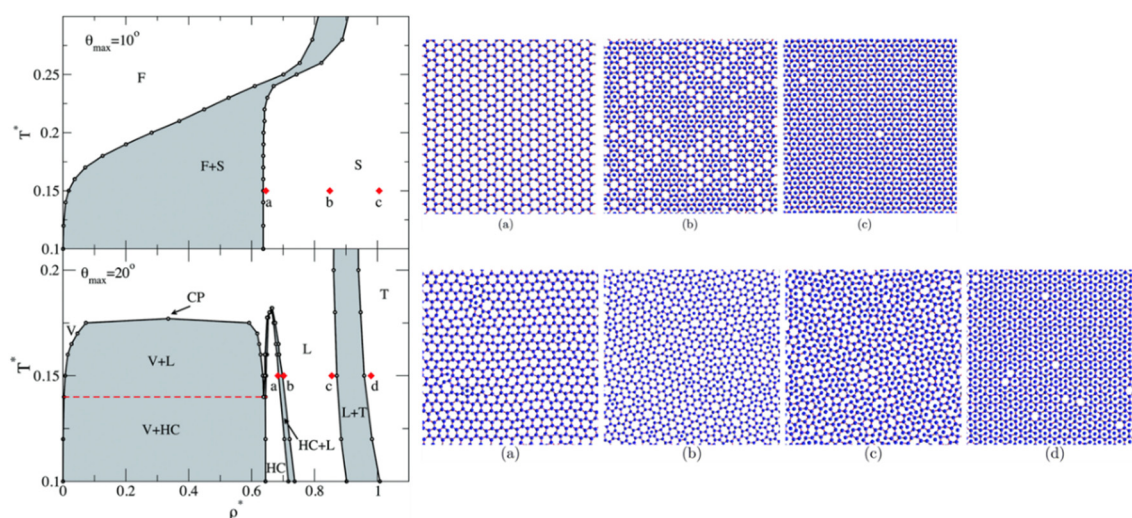


Fig. 28 Simulation of assemblies from three-patch particles: T - ρ phase diagram of three-patch particles with small patches (top panel) and big patches (bottom panel). Regions of coexistence of two phases are shown in grey. For particles with small patches, there are only two stable phases, namely, the fluid (F) and the solid (S). For particles with big patches, besides the vapour (V) and the liquid (L), there are two stable solid phases, namely, the honeycomb (HC) and the triangular (T) solids. The horizontal dotted red line marks the location of a triple point at which the vapour, the liquid and honeycomb solids coexist. The critical point (CP) is also labelled. Red diamonds indicate the state points corresponding to the configurations depicted in the right.¹³¹

More recently, Sun and co-workers developed for dynamics simulations a model specific to soft patchy particles,¹³⁰ and Torquato and co-workers generalized inverse techniques to design experimentally realizable spherical colloidal particles with optimized “patchy” anisotropic interactions for a wide class of targeted low-coordinated two-dimensional crystal structures, e.g. square, honeycomb, kagome, and parallelogrammic crystals, that are defect-free.¹³²

1.4.4 Three-dimension assemblies

Patchy particles were originally invented by Glotzer and co-workers in 2005 to solve the problem of the *in silico* crystallisation of diamond structures.¹³³ They indeed envisioned particles with four sticky patches in a tetrahedral arrangement and showed that the diamond structure from the disordered state could be obtained (Fig. 29). From this time, many complementary papers were published because photonic crystals based on a diamond structure are expected to present a full photonic band gap. The phase diagram of tetrahedral patchy particles was found to be indeed very rich, with several re-entrant coexistence lines. It appears that the self-assembly of tetrahedral patchy particles into a diamond-like crystal might not be

so straightforward. Crystallisation to the diamond structure is greatly favoured when a seed crystal is introduced.¹³³ Lastly, Glotzer and co-workers recently introduced the notion of entropically patchy particles and showed how specific self-assembled structures could be specifically targeted by engineering directional entropic forces through the systematic alteration of particle shape.¹³⁴ They demonstrated that tetrahedrally faceted spheres, *i.e.* with four concave patches, crystallise to a diamond lattice when the amount of faceting exceeds a certain value.

However, as far as we know, there is no concrete realisation of diamond-like CCs using four-patch particles. Some artifices were used to reach the goal without patchy particles, such as the guidance of tetrahedral DNA origami, in which gold NPs were entrapped.¹³⁵

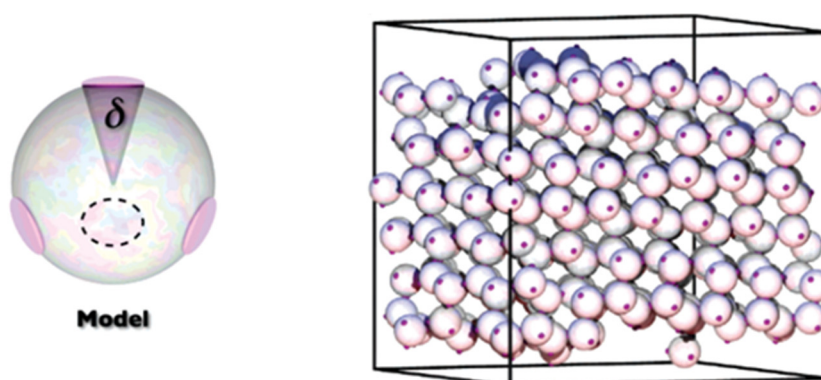


Fig. 29 The original model of patchy particle and its assembly into the diamond-like structure through simulation.¹³³

1.5 Strategies implemented in this work

We learnt from the state-of-the-art that:

- i) depletion attraction is an effective driving force for the assembly of microparticles reversibly by merely removing the depletant agent. Therefore, the fabrication of robust assemblies would necessitate an extra chemical consolidation step.
- ii) the higher the dimension of the expected assembly, the higher demanding the purity of the patchy particles in terms of the geometry and size and the higher the degree of reversibility needed to self-heal the stacking errors.
- iii) as been evidenced by the good match between computer simulations and the concrete assembly into clusters, chains and even kagome structures, we can expect that the simulated honeycomb and diamond-like structures are genuinely achievable.

Four years ago, we envisaged valorising our silica/PS multipods as valence-endowed colloidal atoms and investigating their self-assembly to mimic the conventional (macro-)molecules as robust colloids. Pursuing this inspiration and the preliminary work of Céline Hubert¹³⁶ about

the solvent-induced assembly of PS nodules, the following strategy in three stages of increasing complexity was implemented.

In Chapter 2, we report our first efforts for understanding and controlling the stickiness of the PS patches by studying the assembly of one-patch silica particles. However, our conventional recipe to obtain the silica/PS monopod (Fig. 6g) was rapidly abandoned because of the excessive dimension of the PS patch. Silica/PS dumbbells with varying PS nodule size were successfully synthesised and assembled into clusters in binary solvent mixtures. The effect of solvent quality, centrifugation force, particle concentration, incubation time and the patch-to-particle size ratio was studied. The strategy was spread to gold-coated clusters as well.

In Chapter 3, we present how to chain efficiently the two-patch silica particles through a similar driving force and the growth kinetics/mechanisms. Strategies to mimic homopolymers, random copolymers, block copolymers and branched polymers were successfully implemented.

In Chapter 4, we firstly describe the recipe optimisation to obtain high-yield three-patch silica particles. Our efforts for crystallising them into honeycomb-like structure at the air-water interface on the Langmuir trough are reported.

1.6 References

1. van Blaaderen, A. Colloidal molecules and beyond. *Science*. **301**, 470–471 (2003).
2. Manoharan, V. N. Dense packing and symmetry in small clusters of microspheres. *Science*. **301**, 483–487 (2003).
3. Li, F., Josephson, D. P. & Stein, A. Colloidal assembly: the road from particles to colloidal molecules and crystals. *Angew. Chemie Int. Ed.* **50**, 360–388 (2011).
4. Duguet, E., Désert, A., Perro, A. & Ravaine, S. Design and elaboration of colloidal molecules: an overview. *Chem. Soc. Rev.* **40**, 941 (2011).
5. Sacanna, S., Pine, D. J. & Yi, G.-R. Engineering shape: the novel geometries of colloidal self-assembly. *Soft Matter* **9**, 8096 (2013).
6. Plüsch, C. S. & Wittemann, A. Shape-tailored polymer colloids on the road to become structural motifs for hierarchically organized materials. *Macromol. Rapid Commun.* **34**, 1798–1814 (2013).
7. Morphew, D. & Chakrabarti, D. Clusters of anisotropic colloidal particles: from colloidal molecules to supracolloidal structures. *Curr. Opin. Colloid Interface Sci.* **30**, 70–80 (2017).
8. Elacqua, E., Zheng, X., Shillingford, C., Liu, M. & Weck, M. Molecular recognition in the colloidal world. *Acc. Chem. Res.* **50**, 2756–2766 (2017).
9. Yu, B., Cong, H., Peng, Q., Gu, C., Tang, Q., Xu, X., Tian, C. & Zhai, F. Current status and future developments in preparation and application of nonspherical polymer

- particles. *Adv. Colloid Interface Sci.* **256**, 126–151 (2018).
10. Cho, Y.-S., Yi, G.-R., Kim, S.-H., Pine, D. J. & Yang, S.-M. Colloidal clusters of microspheres from water-in-oil emulsions. *Chem. Mater.* **17**, 5006–5013 (2005).
 11. Manoharan, V. N. Colloidal spheres confined by liquid droplets: geometry, physics, and physical chemistry. *Solid State Commun.* **139**, 557–561 (2006).
 12. Lauga, E. & Brenner, M. P. Evaporation-driven assembly of colloidal particles. *Phys. Rev. Lett.* **93**, 238301 (2004).
 13. Zerrouki, D., Rotenberg, B., Abramson, S., Baudry, J., Goubault, C., Leal-Calderon, F., Pine, D. J. & Bibette, J. Preparation of doublet, triangular, and tetrahedral colloidal clusters by controlled emulsification. *Langmuir* **22**, 57–62 (2006).
 14. Schwarz, I., Fortini, A., Wagner, C. S., Wittemann, A. & Schmidt, M. Monte Carlo computer simulations and electron microscopy of colloidal cluster formation via emulsion droplet evaporation. *J. Chem. Phys.* **135**, 244501 (2011).
 15. Kraft, D. J., Vlug, W. S., van Kats, C. M., van Blaaderen, A., Imhof, A. & Kegel, W. K. Self-assembly of colloids with liquid protrusions. *J. Am. Chem. Soc.* **131**, 1182–1186 (2009).
 16. Yuan, Q., Gu, J., Zhao, Y., Yao, L., Guan, Y. & Zhang, Y. Synthesis of a colloidal molecule from soft microgel spheres. *ACS Macro Lett.* **5**, 565–568 (2016).
 17. Yao, L., Li, Q., Guan, Y., Zhu, X. X. & Zhang, Y. Tetrahedral, octahedral, and triangular dipyrnidal microgel clusters with thermosensitivity fabricated from binary colloidal crystals template and thiol–ene reaction. *ACS Macro Lett.* **7**, 80–84 (2018).
 18. Shen, B., Ricouvier, J., Malloggi, F. & Tabeling, P. Designing colloidal molecules with microfluidics. *Adv. Sci.* **3**, 1–7 (2015).
 19. Perry, R. W. & Manoharan, V. N. Segregation of ‘isotope’ particles within colloidal molecules. *Soft Matter* **12**, 2868–2876 (2016).
 20. Demirörs, A. F., Pillai, P. P., Kowalczyk, B. & Grzybowski, B. A. Colloidal assembly directed by virtual magnetic moulds. *Nature* **503**, 99–103 (2013).
 21. Ma, F., Wu, D. T. & Wu, N. Formation of colloidal molecules induced by alternating-current electric fields. *J. Am. Chem. Soc.* **135**, 7839–7842 (2013).
 22. Asua, J. M. Emulsion polymerization: from fundamental mechanisms to process developments. *J. Polym. Sci. Part A Polym. Chem.* **42**, 1025–1041 (2004).
 23. Stubbs, J. M. & Sundberg, D. C. The dynamics of morphology development in multiphase latex particles. *Prog. Org. Coatings* **61**, 156–165 (2008).
 24. Kim, J. W., Larsen, R. J. & Weitz, D. A. Synthesis of nonspherical colloidal particles with anisotropic properties. *J. Am. Chem. Soc.* **128**, 14374–14377 (2006).
 25. Kim, J. W., Larsen, R. J. & Weitz, D. A. Uniform nonspherical colloidal particles with tunable shapes. *Adv. Mater.* **19**, 2005–2009 (2007).
 26. Park, J. G., Forster, J. D. & Dufresne, E. R. Synthesis of colloidal particles with the symmetry of water molecules. *Langmuir* **25**, 8903–8906 (2009).
 27. Peng, B., van Blaaderen, A. & Imhof, A. Direct observation of the formation of liquid protrusions on polymer colloids and their coalescence. *ACS Appl. Mater. Interfaces* **5**,

- 4277–4284 (2013).
28. Yang, M., Wang, G. & Ma, H. An efficient approach for production of polystyrene/poly(4-vinylpyridine) particles with various morphologies based on dynamic control. *Chem. Commun.* **47**, 911–913 (2011).
 29. Désert, A., Chaduc, I., Fouilloux, S., Taveau, J.-C., Lambert, O., Lansalot, M., Bourgeat-Lami, E., Thill, A., Spalla, O., Ravaine, S. & Duguet, E. High-yield preparation of polystyrene/silica clusters of controlled morphology. *Polym. Chem.* **3**, 1130–1132 (2012).
 30. Perro, A., Reculosa, S., Pereira, F., Delville, M.-H., Mingotaud, C., Duguet, E., Bourgeat-Lami, E. & Ravaine, S. Towards large amounts of Janus nanoparticles through a protection–deprotection route. *Chem. Commun.* 5542–5543 (2005).
 31. Perro, A., Duguet, E., Lambert, O., Taveau, J.-C., Bourgeat-Lami, E. & Ravaine, S. A chemical synthetic route towards “colloidal molecules”. *Angew. Chemie Int. Ed.* **48**, 361–365 (2009).
 32. Taveau, J.-C., Nguyen, D., Perro, A., Ravaine, S., Duguet, E. & Lambert, O. New insights into the nucleation and growth of ps nodules on silicananoparticles by 3d cryo-electron tomography. *Soft Matter* **4**, 311–315 (2008).
 33. Thill, A., Désert, A., Fouilloux, S., Taveau, J.-C., Lambert, O., Lansalot, M., Bourgeat-Lami, E., Spalla, O., Belloni, L., Ravaine, S. & Duguet, E. Spheres growing on a sphere: a model to predict the morphology yields of colloidal molecules obtained through a heterogeneous nucleation route. *Langmuir* **28**, 11575–11583 (2012).
 34. Désert, A., Morele, J., Taveau, J.-C., Lambert, O., Lansalot, M., Bourgeat-Lami, E., Thill, A., Spalla, O., Belloni, L., Ravaine, S. & Duguet, E. Multipod-like silica/polystyrene clusters. *Nanoscale* **8**, 5454–5469 (2016).
 35. Hubert, C., Chomette, C., Désert, A., Sun, M., Treguer-Delapierre, M., Mornet, S., Perro, A., Duguet, E. & Ravaine, S. Synthesis of multivalent silica nanoparticles combining both enthalpic and entropic patchiness. *Faraday Discuss.* **181**, 139–46 (2015).
 36. Qiao, X. G., Dugas, P.-Y., Charleux, B., Lansalot, M. & Bourgeat-Lami, E. Synthesis of multipod-like silica/polymer latex particles via nitroxide-mediated polymerization-induced self-assembly of amphiphilic block copolymers. *Macromolecules* **48**, 545–556 (2015).
 37. Chaduc, I., Parvole, J., Duguet, E., Ravaine, S., Lansalot, M. & Bourgeat-Lami, E. Synthesis of HCN-like poly(methyl methacrylate)/polystyrene/silica colloidal molecules. *Polym. Chem.* **3**, 3232–3234 (2012).
 38. Ducrot, É., He, M., Yi, G.-R. & Pine, D. J. Colloidal alloys with preassembled clusters and spheres. *Nat. Mater.* **16**, 652–657 (2017).
 39. Pawar, A. B. & Kretzschmar, I. Fabrication, assembly, and application of patchy particles. *Macromol. Rapid Commun.* **31**, 150–168 (2010).
 40. Rezvantalab, H. & Shojaei-Zadeh, S. Designing patchy particles for optimum interfacial activity. *Phys. Chem. Chem. Phys.* **16**, 8283–8293 (2014).
 41. Ravaine, S. & Duguet, E. Synthesis and assembly of patchy particles: recent progress and future prospects. *Curr. Opin. Colloid Interface Sci.* **30**, 45–53 (2017).

42. De Gennes, P.-G. soft matter (Nobel lecture). *Angew. Chemie Int. Ed. English* **31**, 842–845 (1992).
43. Binks, B. P. Particles as surfactants—similarities and differences. *Curr. Opin. Colloid Interface Sci.* **7**, 21–41 (2002).
44. Passas-Lagos, E. & Schüth, F. Amphiphilic Pickering emulsifiers based on mushroom-type Janus particles. *Langmuir* **31**, 7749–7757 (2015).
45. Longbottom, B. W. & Bon, S. A. F. Improving the engine power of a catalytic Janus-sphere micromotor by roughening its surface. *Sci. Rep.* **8**, 1–10 (2018).
46. Chen, Q., Yan, J., Zhang, J., Bae, S. C. & Granick, S. Janus and multiblock colloidal particles. *Langmuir* **28**, 13555–13561 (2012).
47. Perro, A., Reculosa, S., Ravaine, S., Bourgeat-Lami, E. & Duguet, E. Design and synthesis of Janus micro- and nanoparticles. *J. Mater. Chem.* **15**, 3745–3760 (2005).
48. Du, J. & O'Reilly, R. K. Anisotropic particles with patchy, multicompartiment and Janus architectures: preparation and application. *Chem. Soc. Rev.* **40**, 2402–2416 (2011).
49. Lattuada, M. & Hatton, T. A. Synthesis, properties and applications of Janus nanoparticles. *Nano Today* **6**, 286–308 (2011).
50. Hu, J., Zhou, S., Sun, Y., Fang, X. & Wu, L. Fabrication, properties and applications of Janus particles. *Chem. Soc. Rev.* **41**, 4356–4378 (2012).
51. Walther, A. & Müller, A. H. E. Janus particles: synthesis, self-assembly, physical properties, and applications. *Chem. Rev.* **113**, 5194–5261 (2013).
52. Zhang, J., Grzybowski, B. A. & Granick, S. Janus particle synthesis, assembly, and application. *Langmuir* **33**, 6964–6977 (2017).
53. Ogi, T., Modesto-Lopez, L. B., Iskandar, F. & Okuyama, K. Fabrication of a large area monolayer of silica particles on a sapphire substrate by a spin coating method. *Colloids Surfaces A Physicochem. Eng. Asp.* **297**, 71–78 (2007).
54. Xie, Y., Guo, S., Guo, C., He, M., Chen, D., Ji, Y., Chen, Z., Wu, X., Liu, Q. & Xie, S. Controllable two-stage droplet evaporation method and its nanoparticle self-assembly mechanism. *Langmuir* **29**, 6232–6241 (2013).
55. Pawar, A. B. & Kretzschmar, I. Patchy particles by glancing angle deposition. *Langmuir* **24**, 355–358 (2008).
56. Jiang, S., Schultz, M. J., Chen, Q., Moore, J. S. & Granick, S. Solvent-free synthesis of Janus colloidal particles. *Langmuir* **24**, 10073–10077 (2008).
57. Perro, A., Meunier, F., Schmitt, V. & Ravaine, S. Production of large quantities of 'Janus' nanoparticles using wax-in-water emulsions. *Colloids Surfaces A Physicochem. Eng. Asp.* **332**, 57–62 (2009).
58. Huang, C. & Shen, X. Janus molecularly imprinted polymer particles. *Chem. Commun.* **50**, 2646–2649 (2014).
59. Liu, B., Zhang, C., Liu, J., Qu, X. & Yang, Z. Janus non-spherical colloids by asymmetric wet-etching. *Chem. Commun.* 3871–3873 (2009).
60. Kim, S. H., Hollingsworth, A. D., Sacanna, S., Chang, S. J., Lee, G., Pine, D. J. & Yi, G. R. Synthesis and assembly of colloidal particles with sticky dimples. *J. Am. Chem.*

- Soc.* **134**, 16115–16118 (2012).
61. Pawar, A. B. & Kretzschmar, I. Multifunctional patchy particles by glancing angle deposition. *Langmuir* **25**, 9057–9063 (2009).
 62. He, Z. & Kretzschmar, I. Template-assisted glancing angle deposition: approach to single and multipatch patchy particles with controlled patch shape. *Langmuir* **29**, 15755–15761 (2013).
 63. Nie, Z., Fava, D., Kumacheva, E., Zou, S., Walker, G. C. & Rubinstein, M. Self-assembly of metal-polymer analogues of amphiphilic triblock copolymers. *Nat. Mater.* **6**, 609–614 (2007).
 64. Nikoobakht, B. & El-Sayed, M. A. Preparation and growth mechanism of gold nanorods (NRs) using seed-mediated growth method. *Chem. Mater.* **15**, 1957–1962 (2003).
 65. Kim, J. H., Hwang, H. J., Oh, J. S., Sacanna, S. & Yi, G. R. Monodisperse magnetic silica hexapods. *J. Am. Chem. Soc.* **140**, 9230–9235 (2018).
 66. Wang, L., Xia, L., Li, G., Ravaine, S. & Zhao, X. S. Patterning the surface of colloidal microspheres and fabrication of nonspherical particles. *Angew. Chemie - Int. Ed.* **47**, 4725–4728 (2008).
 67. Bae, C., Kim, H., Montero Moreno, J. M., Yi, G.-R. & Shin, H. Toward coordinated colloids: site-selective growth of titania on patchy silica particles. *Sci. Rep.* **5**, 9339 (2015).
 68. Bao, H., Peukert, W. & Taylor, R. N. K. One-pot colloidal synthesis of plasmonic patchy particles. *Adv. Mater.* **23**, 2644–2649 (2011).
 69. Bao, H., Bihl, T., Smith, A.-S. & Klupp Taylor, R. N. Facile colloidal coating of polystyrene nanospheres with tunable gold dendritic patches. *Nanoscale* **6**, 3954–3966 (2014).
 70. Lotierzo, A., Longbottom, B. W., Lee, W. H. & Bon, S. A. F. Synthesis of Janus and patchy particles using nanogels as stabilizers in emulsion polymerization. *ACS Nano* **13**, 399–407 (2019).
 71. Wang, Y., Wang, Y., Breed, D. R., Manoharan, V. N., Feng, L., Hollingsworth, A. D., Weck, M. & Pine, D. J. Colloids with valence and specific directional bonding. *Nature* **490**, 51–55 (2012).
 72. Wang, Y., Wang, Y., Zheng, X., Yi, G.-R., Sacanna, S., Pine, D. J. & Weck, M. Three-dimensional lock and key colloids. *J. Am. Chem. Soc.* **136**, 6866–6869 (2014).
 73. Zheng, X., Liu, M., He, M., Pine, D. J. & Weck, M. Shape-shifting patchy particles. *Angew. Chemie Int. Ed.* **56**, 5507–5511 (2017).
 74. Gong, Z., Hueckel, T., Yi, G.-R. & Sacanna, S. Patchy particles made by colloidal fusion. *Nature* **550**, 234–238 (2017).
 75. Désert, A., Hubert, C., Fu, Z., Moulet, L., Majimel, J., Barboteau, P., Thill, A., Lansalot, M., Bourgeat-Lami, E., Duguet, E. & Ravaine, S. Synthesis and site-specific functionalization of tetravalent, hexavalent, and dodecavalent silica particles. *Angew. Chemie Int. Ed.* **52**, 11068–11072 (2013).
 76. Huang, Y., Wang, J., Zhou, J., Xu, L., Li, Z., Zhang, Y., Wang, J., Song, Y. & Jiang, L. Controllable synthesis of latex particles with multicavity structures. *Macromolecules* **44**, 2404–2409 (2011).

77. Deng, R., Li, H., Zhu, J., Li, B., Liang, F., Jia, F., Qu, X. & Yang, Z. Janus nanoparticles of block copolymers by emulsion solvent evaporation induced assembly. *Macromolecules* **49**, 1362–1368 (2016).
78. Deng, R., Li, H., Liang, F., Zhu, J., Li, B., Xie, X. & Yang, Z. Soft colloidal molecules with tunable geometry by 3d confined assembly of block copolymers. *Macromolecules* **48**, 5855–5860 (2015).
79. Ku, K. H., Kim, Y., Yi, G.-R., Jung, Y. S. & Kim, B. J. Soft patchy particles of block copolymers from interface-engineered emulsions. *ACS Nano* **9**, 11333–11341 (2015).
80. Gröschel, A. H., Schacher, F. H., Schmalz, H., Borisov, O. V., Zhulina, E. B., Walther, A. & Müller, A. H. E. Precise hierarchical self-assembly of multicompartment micelles. *Nat. Commun.* **3**, 710 (2012).
81. Bianchi, E., Blaak, R. & Likos, C. N. Patchy colloids: state of the art and perspectives. *Phys. Chem. Chem. Phys.* **13**, 6397–6410 (2011).
82. Gangwal, S., Pawar, A., Kretzschmar, I. & Velev, O. D. Programmed assembly of metallodielectric patchy particles in external ac electric fields. *Soft Matter* **6**, 1413–1418 (2010).
83. Sacanna, S., Rossi, L. & Pine, D. J. Magnetic click colloidal assembly. *J. Am. Chem. Soc.* **134**, 6112–6115 (2012).
84. Teixeira, P. I. C. & Tavares, J. M. Phase behaviour of pure and mixed patchy colloids — theory and simulation. *Curr. Opin. Colloid Interface Sci.* **30**, 16–24 (2017).
85. Avendaño, C. & Escobedo, F. A. Packing, entropic patchiness, and self-assembly of non-convex colloidal particles: a simulation perspective. *Curr. Opin. Colloid Interface Sci.* **30**, 62–69 (2017).
86. Rovigatti, L., Russo, J. & Romano, F. How to simulate patchy particles. *Eur. Phys. J. E* **41**, 59–71 (2018).
87. Asakura, S. & Oosawa, F. On interaction between two bodies immersed in a solution of macromolecules. *J. Chem. Phys.* **22**, 1255–1256 (1954).
88. Dinsmore, A. D., Yodh, A. G. & Pine, D. J. Phase diagrams of nearly-hard-sphere binary colloids. *Phys. Rev. E* **52**, 4045–4057 (1995).
89. Sacanna, S., Irvine, W. T. M., Chaikin, P. M. & Pine, D. J. Lock and key colloids. *Nature* **464**, 575–578 (2010).
90. Wang, Y., Wang, Y., Zheng, X., Yi, G., Sacanna, S., Pine, D. J. & Weck, M. Three-dimensional lock and key colloids. 2–5 (2014).
91. Rouet, P.-E., Chomette, C., Duguet, E. & Ravaine, S. Colloidal molecules from valence-endowed nanoparticles by covalent chemistry. *Angew. Chemie Int. Ed.* **57**, 15754–15757 (2018).
92. Rouet, P.-E., Chomette, C., Adumeau, L., Duguet, E. & Ravaine, S. Colloidal chemistry with patchy silica nanoparticles. *Beilstein J. Nanotechnol.* **9**, 2989–2998 (2018).
93. Zhang, J., Luijten, E. & Granick, S. Toward design rules of directional Janus colloidal assembly. *Annu. Rev. Phys. Chem.* **66**, 581–600 (2015).
94. Liang, H., Cacciuto, A., Luijter, E. & Granick, S. Clusters of charged Janus spheres.

- Nano Lett.* **6**, 2510–2514 (2006).
95. Hong, L., Cacciuto, A., Luijten, E. & Granick, S. Clusters of amphiphilic colloidal spheres. *Langmuir* **24**, 621–625 (2008).
 96. Chen, Q., Whitmer, J. K., Jiang, S., Bae, S. C., Luijten, E. & Granick, S. Supracolloidal reaction kinetics of Janus spheres. *Science*. **331**, 199–202 (2011).
 97. Kraft, D. J., Ni, R., Smallenburg, F., Hermes, M., Yoon, K., Weitz, D. A., van Blaaderen, A., Groenewold, J., Dijkstra, M. & Kegel, W. K. From the cover: surface roughness directed self-assembly of patchy particles into colloidal micelles. *Proc. Natl. Acad. Sci.* **109**, 10787–10792 (2012).
 98. Yu, C., Zhang, J. & Granick, S. Selective Janus particle assembly at tipping points of thermally-switched wetting. *Angew. Chemie Int. Ed.* **53**, 4364–4367 (2014).
 99. Bharti, B., Rutkowski, D., Han, K., Kumar, A. U., Hall, C. K. & Velev, O. D. Capillary bridging as a tool for assembling discrete clusters of patchy particles. *J. Am. Chem. Soc.* **138**, 14948–14953 (2016).
 100. Hu, H., Ji, F., Xu, Y., Yu, J., Liu, Q., Chen, L., Chen, Q., Wen, P., Lifshitz, Y., Wang, Y., Zhang, Q. & Lee, S. T. Reversible and precise self-assembly of Janus metal-organosilica nanoparticles through a linker-free approach. *ACS Nano* **10**, 7323–7330 (2016).
 101. Castro, N., Constantin, D., Davidson, P. & Abécassis, B. Solution self-assembly of plasmonic Janus nanoparticles. *Soft Matter* **12**, 9666–9673 (2016).
 102. Ge, X.-H., Geng, Y.-H., Chen, J. & Xu, J.-H. Smart amphiphilic Janus microparticles: one-step synthesis and self-assembly. *ChemPhysChem* **19**, 2009–2013 (2018).
 103. Velev, O. D. & Gupta, S. Materials fabricated by micro- and nanoparticle assembly - the challenging path from science to engineering. *Adv. Mater.* **21**, 1897–1905 (2009).
 104. Liu, K., Zhao, N. & Kumacheva, E. Self-assembly of inorganic nanorods. *Chem. Soc. Rev.* **40**, 656–671 (2011).
 105. Hill, L. J., Pinna, N., Char, K. & Pyun, J. Colloidal polymers from inorganic nanoparticle monomers. *Prog. Polym. Sci.* **40**, 85–120 (2015).
 106. Wang, H., Chen, L., Shen, X., Zhu, L., He, J. & Chen, H. Unconventional chain-growth mode in the assembly of colloidal gold nanoparticles. *Angew. Chemie Int. Ed.* **51**, 8021–8025 (2012).
 107. Caswell, K. K., Wilson, J. N., Bunz, U. H. F. & Murphy, C. J. Preferential end-to-end assembly of gold nanorods by biotin-streptavidin connectors. *J. Am. Chem. Soc.* **125**, 13914–13915 (2003).
 108. Chandler, D. Interfaces and the driving force of hydrophobic assembly. *Nature* **437**, 640–647 (2005).
 109. Kim, J., Choi, C. H., Yeom, S. J., Eom, N., Kang, K. K. & Lee, C. S. Directed assembly of Janus cylinders by controlling the solvent polarity. *Langmuir* **33**, 7503–7511 (2017).
 110. Liu, K., Nie, Z., Zhao, N., Li, W., Rubinstein, M. & Kumacheva, E. Step-growth polymerization of inorganic nanoparticles. *Science*. **329**, 197–200 (2010).
 111. Nie, Z., Fava, D., Rubinstein, M. & Kumacheva, E. “Supramolecular” assembly of gold

- nanorods end-terminated with polymer “pom-poms”: effect of pom-pom structure on the association modes. *J. Am. Chem. Soc.* **130**, 3683–3689 (2008).
112. Liu, K., Lukach, A., Sugikawa, K., Chung, S., Vickery, J., Therien-Aubin, H., Yang, B., Rubinstein, M. & Kumacheva, E. Copolymerization of metal nanoparticles: a route to colloidal plasmonic copolymers. *Angew. Chemie Int. Ed.* **53**, 2648–2653 (2014).
 113. Klinkova, A., Therien-Aubin, H., Choueiri, R. M., Rubinstein, M. & Kumacheva, E. Colloidal analogs of molecular chain stoppers. *Proc. Natl. Acad. Sci.* **110**, 18775–18779 (2013).
 114. Liu, K., Resetco, C. & Kumacheva, E. Salt-mediated kinetics of the self-assembly of gold nanorods end-tethered with polymer ligands. *Nanoscale* **4**, 6574–6580 (2012).
 115. Lukach, A., Liu, K., Therien-Aubin, H. & Kumacheva, E. Controlling the degree of polymerization, bond lengths, and bond angles of plasmonic polymers. *J. Am. Chem. Soc.* **134**, 18853–18859 (2012).
 116. Fava, D., Winnik, M. A. & Kumacheva, E. Photothermally-triggered self-assembly of gold nanorods. *Chem. Commun.* 2571–2573 (2009).
 117. Tigges, T. & Walther, A. Hierarchical self-assembly of 3d-printed lock-and-key colloids through shape recognition. *Angew. Chemie Int. Ed.* **55**, 11261–11265 (2016).
 118. Wang, Y., Hollingsworth, A. D., Yang, S. K., Patel, S., Pine, D. J. & Weck, M. Patchy particle self-assembly via metal coordination. *J. Am. Chem. Soc.* **135**, 14064–14067 (2013).
 119. Elacqua, E., Zheng, X. & Weck, M. Light-mediated reversible assembly of polymeric colloids. *ACS Macro Lett.* **6**, 1060–1065 (2017).
 120. Benyettou, F., Zheng, X., Elacqua, E., Wang, Y., Dalvand, P., Asfari, Z., Olsen, J.-C., Han, D. S., Saleh, N., Elhabiri, M., Weck, M. & Trabolsi, A. Redox-responsive viologen-mediated self-assembly of cb[7]-modified patchy particles. *Langmuir* **32**, 7144–7150 (2016).
 121. Gröschel, A. H., Walther, A., Löbbling, T. I., Schacher, F. H., Schmalz, H. & Müller, A. H. E. Guided hierarchical co-assembly of soft patchy nanoparticles. *Nature* **503**, 247–251 (2013).
 122. Kim, J.-H., Kwon, W. J. & Sohn, B.-H. Supracolloidal polymer chains of diblock copolymer micelles. *Chem. Commun.* **51**, 3324–3327 (2015).
 123. Kim, K., Jang, S., Jeon, J., Kang, D. & Sohn, B. H. Fluorescent supracolloidal chains of patchy micelles of diblock copolymers functionalized with fluorophores. *Langmuir* **34**, 4634–4639 (2018).
 124. Lee, S., Jang, S., Kim, K., Jeon, J., Kim, S. S. & Sohn, B. H. Branched and crosslinked supracolloidal chains with diblock copolymer micelles having three well-defined patches. *Chem. Commun.* **52**, 9430–9433 (2016).
 125. Chen, Q., Bae, S. C. & Granick, S. Directed self-assembly of a colloidal kagome lattice. *Nature* **469**, 381–384 (2011).
 126. Romano, F. & Sciortino, F. Two dimensional assembly of triblock Janus particles into crystal phases in the two bond per patch limit. *Soft Matter* **7**, 5799–5804 (2011).
 127. Romano, F. & Sciortino, F. Patchy from the bottom up. *Nat. Mater.* **10**, 171–173 (2011).

128. Doppelbauer, G., Bianchi, E. & Kahl, G. Self-assembly scenarios of patchy colloidal particles in two dimensions. *J. Phys. Condens. Matter* **22**, 104105 (2010).
129. Romano, F., Sanz, E., Tartaglia, P. & Sciortino, F. Phase diagram of trivalent and pentavalent patchy particles. *J. Phys. Condens. Matter* **24**, 064113 (2012).
130. Li, Z.-W., Zhu, Y.-L., Lu, Z.-Y. & Sun, Z.-Y. A versatile model for soft patchy particles with various patch arrangements. *Soft Matter* **12**, 741–749 (2016).
131. Noya, E. G., Almarza, N. G. & Lomba, E. Assembly of trivalent particles under confinement: from an exotic solid phase to a liquid phase at low temperature. *Soft Matter* **13**, 3221–3229 (2017).
132. Chen, D., Zhang, G. & Torquato, S. Inverse design of colloidal crystals via optimized patchy interactions. *J. Phys. Chem. B* **122**, 8462–8468 (2018).
133. Zhang, Z., Keys, A. S., Chen, T. & Glotzer, S. C. Structures through molecular mimicry. *Science* **210**, 409–413 (2005).
134. Van Anders, G., Ahmed, N. K., Smith, R., Engel, M. & Glotzer, S. C. Entropically patchy particles: engineering valence through shape entropy. *ACS Nano* **8**, 931–940 (2014).
135. Liu, W., Tagawa, M., Xin, H. L., Wang, T., Emamy, H., Li, H., Yager, K. G., Starr, F. W., Tkachenko, A. V. & Gang, O. Diamond family of nanoparticle superlattices. *Science* **351**, 582–586 (2016).
136. Hubert, C. PhD thesis Univ. Bordeaux (2016).

Chapter 2

Solvent-induced assembly of one-patch silica nanoparticles into clusters

2.1 Introduction

In recent decades, the efforts of chemists combined with ever more efficient characterisation techniques have made it possible to develop more and more complex solid colloids. In particular, the anisotropy of shape and/or chemical composition is particularly sought after because it makes it possible to program assembly capabilities into structures of larger dimensions. Thus Janus particles¹⁻³ and more recently patchy particles⁴⁻⁶ have attracted significant attention as potential building blocks on both simulation and experimental aspects.

Among Janus particles, asymmetric dumbbells and snowman-like colloids are of special interest if (i) one of both lobes is hard and potentially repulsive and the other one is attractive, and (ii) they self-assemble into clusters with small aggregation numbers N , often called colloidal molecules (CMs). Some previous studies showed that this strategy may be used with colloids of few tens of nanometers,^{7,8} few hundreds of nanometers,⁹ few micrometers¹⁰⁻¹⁴ or few hundreds of micrometres.¹⁵ Nevertheless, the clusters were obtained thanks to solvophobic interactions,^{8,11,12} electrostatic attraction,^{7,10} or roughness-controlled depletion forces,¹³ or lipid-induced capillary bridging,¹⁴ which are weak and can be made reversible.

To get robust clusters, it may be envisioned that the attractive lobe should be sticky and possibly capable of merging with similar ones. Kraft *et al.* reported an original pathway where the sticky lobe is a monomer protrusion ready to coalesce before solidification by polymerisation.⁹ These protrusions are spontaneously formed when cross-linked polystyrene particles are made hydrophilic by surface modification with vinyl acetate, dispersed in water, swollen with styrene and heated at 80 °C. The final clusters with N from 2 to 9 are more precisely described as spherical hydrophilic particles with a defined number of hydrophobic polystyrene patches. Xu and co-workers exploited the drying of Pickering-like water droplets made from 200- μm hydrophilic poly(ethylene glycol) diacrylate sphere with 160- μm ethoxylated trimethylolpropane tri-acrylate head.¹⁵

We report here another strategy using silica/polystyrene dumbbells whose polystyrene lobe is made sticky and ready to coalesce when the dispersion medium is a suitable mixture of a good and a bad solvent. This leads to multipod-like clusters made of one polystyrene core and a defined number of silica satellites. Moreover, this is the reverse morphology of highly symmetrical multipods that we have already reported considering that polystyrene and silica switch their roles.^{16,17}

For this study, we did not use the silica/PS monopods that we know how to prepare according to the seeded growth emulsion polymerisation process, because the PS patch would be larger than the silica NP (Fig. 6g in Chapter 1).¹⁸ We prepared them according to a protocol previously reported by Guignard and Lattuada¹⁹ (Fig. 1) and assembled them by making their PS lobe sticky through incubation in mixtures of good and bad solvent for PS. We especially studied several experimental parameters such as the solvent quality, effect of an additional centrifugation stage after incubation, NPs concentration, incubation time, and patch-to-particle size ratio. We also extended this facile method to the fabrication of gold-coated silica clusters. The NPs and clusters morphology, as well as the proportion of every species, was essentially estimated from transmission electron microscopy (TEM) images.

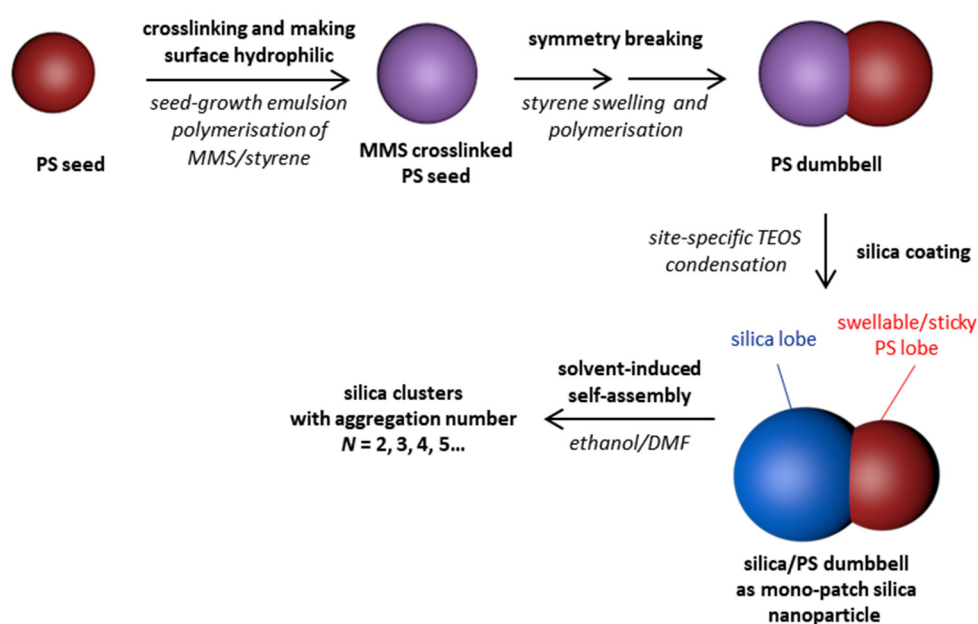


Fig. 1 Scheme summarising the one-patch silica NPs preparation and their assembly into clusters

2.2 Methods and materials

2.2.1 Materials

Styrene (99.5%, with c.a. 50 ppm 4-tert-butylcatechol as stabiliser), sodium dodecyl sulphate (SDS, 99%), 4-vinylbenzenesulfonate (VBS, $\geq 90\%$), tetraethoxysilane (TEOS, $\geq 99\%$), dimethylformamide (DMF, $\geq 99\%$), sodium persulphate (NaPS, $\geq 99\%$), (3-aminopropyl)triethoxysilane (APTES, 99%), hydroxylamine hydrochloride ($\text{NH}_2\text{OH}\cdot\text{HCl}$, 98%), gold chloride hydrate (HAuCl_4 , 99.999%), potassium carbonate (K_2CO_3) and tetrakis(hydroxymethyl)phosphonium chloride solution (THPC, 80% in water), sucrose (grade puriss.) and sodium hydroxide ($\geq 98.5\%$, microprills) were purchased from Sigma-Aldrich.

Methacryloxymethyltrimethoxysilane (MMS, 95%) was provided by ABCR, Germany. Ammonium hydroxide (NH₄OH, 28-30% in water) was purchased from JT. Baker and ethanol (99%) was provided by Atlantic Labo. 2,2'-Azobis(2-methylpropionitrile) (AIBN, 98%) was received from ACROS ORGANICS. Deionised water with a resistivity of 18.2 MΩ·cm at 25°C was obtained from a Milli-Q system (Millipore). All chemicals were used without further purification.

2.2.2 Polystyrene seeds synthesis by emulsion polymerisation

One g SDS was dissolved in 83.75 mL water in a 250-mL three-neck flask under 400 rpm agitation and degassed by nitrogen for 40 min. 20 g styrene were added with one-shot afterwards and the mixture was stirred for another 40 min. Subsequently, the pre-emulsified solution was heated to 75 °C and 10 mL water containing 0.1 g NaPS initiator were injected dropwise within 10 min through the syringe pump. The reaction was kept for 12 h and the white emulsion was collected and used as obtained in the next step.

2.2.3 Surface crosslinking of the polystyrene seeds

The dispersion of PS seeds was diluted to about 90 g/L with water before carrying out the following experiments. We mixed 50 mL of the diluted seed dispersion, 84 mL water and monomer solution into a three-neck flask and stirred at 300 rpm for 40 min. The monomer solution contained styrene (80% vol./vol.), MMS (20% vol./vol.) and AIBN (3% wt./vol.). The used volume of this solution was equal to the volume of PS particle in the dispersion. The solution mixture was degassed by nitrogen reflux for 40 min under 300 rpm stirring. The polymerisation process was initiated by increasing temperature to 75°C and completed after 12 h. The dispersion of the as-crosslinked PS seeds was used as obtained for the next step.

2.2.4 Changing polystyrene seeds into dumbbell-like nanoparticles through styrene swelling and polymerisation

The concentration of the crosslinked seeds was adjusted to around 60 g/L. We mixed 20 mL of this dispersion with 40 mL water and a certain amount of VBS (0.8% wt./vol. to the total volume of styrene) in a 250-mL three-neck flask. The mixture was degassed by nitrogen for 30 min under 400 rpm stirring. A specific volume of styrene with AIBN (3% wt./vol. to monomer volume) was added in order to reach the targeted value of the swelling ratio, *i.e.* styrene-to-seed volume ratio. When the swelling time was elapsed, the temperature was increased to 75 °C afterwards to trigger the initiator decomposition and styrene polymerisation. The reaction was

lasted for 12 h to maximise the monomer-to-polymer conversion. The dumbbell-like PS NPs were used in the next step as obtained.

2.2.5 Derivatisation into silica/polystyrene dumbbells by site-specific coating with silica

The crosslinked hydrophilic lobe of the PS dumbbells was coated with silica by regioselective condensation of TEOS following a protocol adapted from the conventional Stöber method.²⁰ Typically, 10 mL of the PS dumbbells dispersion was dispersed in 67 mL ethanol, and 5.1 mL of ammonia was added under 400-rpm stirring. Lastly, 7.2 mL ethanol/TEOS mixture (vol./vol. 1/1) were injected with a syringe pump at the rate of 0.5 mL/h to avoid homogeneous nucleation of silica NPs. The silica/PS dumbbells were washed by 3 centrifugation/redispersion cycles (12,000 g; 10 min) before redispersion in 85 mL ethanol. The final concentration was estimated to $1.12 \cdot 10^{16}$ NPs/L.

2.2.6 Synthesis of gold seeds

THPC-stabilised gold seeds were obtained by following a protocol of Duff and co-workers.²¹ Typically, 227.5 mL water, 7.5 mL NaOH (0.2 M) and 2.5 mL THPC (120 μ L in 10 mL water) were mixed under moderate stirring for 15 min. Subsequently, 10 mL of HAuCl₄ (25 mM) was quickly injected into the mixture by one-shot under vigorous stirring (more than 600 rpm). The solution turned from pale yellow to brown in few seconds indicating the formation of gold NPs. Then it was aged at 4 °C for at least 3 days before using.

2.2.7 Site-specific gold grafting on the silica lobe of the silica/PS dumbbells

APTES was used to modify the silica surface (50 molecules/nm²) under moderate stirring at RT overnight and the dumbbells were washed by 2 centrifugation/redispersion cycles (12,000 g; 10 min) before redispersion in 1 mL ethanol. Five mL of the gold seeds dispersion was added and the mixture was roller-mixed at 60 rpm for 6 h. The gold-adsorbed silica/PS dumbbells were washed by 3 centrifugation/redispersion cycles (12,000 g; 10 min; 6 mL) before redispersion into 1 mL ethanol.

2.2.8 Seeded growth of gold on the silica lobe of the silica/PS dumbbells

The same protocol inspired from an already published recipe²² was applied to regrow the gold seeds adsorbed on the silica lobes before or after silica/PS dumbbells assembly. First, two stock solutions were prepared. The solution #1 was made by dissolving NH₂OH·HCl (130 mg) in

water (1 L) and the other one (solution #2) was fabricated by dissolving K_2CO_3 (130 mg) in an aqueous $HAuCl_4$ solution (1 L, 0.375 mM), which should be aged at 4 °C for 1 day before using. The gold-decorated silica/PS dumbbells dispersion (0.1 mL) was mixed with 10 mL water and 10 mL solution #2, followed by dropwise addition of 5 mL solution #1 at the rate of 10 mL/h under vigorous stirring. The final as-modified NPs were washed by 3 centrifugation/redispersion cycles (12,000 g; 10 min) before redispersion into 0.1 mL ethanol. This protocol was repeated to obtain iteratively the targeted thickness of the gold coating.

2.2.9 Solvent-driven assembly of the silica/PS dumbbells

The self-assembly experiments were routinely performed into 1.5 mL Eppendorf® tubes and the sum of the DMF and ethanol volumes were systematically equal to 1 mL. For instance, we mixed the previous ethanol dispersion of silica/PS dumbbells (47 μ L), DMF (300 μ L) and ethanol (653 μ L) by vortexing for 30 s. The Eppendorf® tubes were put on a roller-mixer at 60 rpm for 20 min or 20 h at RT to induce the assembly process. For TEM analysis, a drop was directly collected from the dispersion and let to evaporate on the TEM grid. Alternatively, the dispersion might be centrifuged at 12,000 g for 10 min and the pellet redispersed into ethanol after removal of the supernatant prior to the TEM grid preparation.

2.2.10 Sort clusters through density gradient centrifugation

A gradient maker (BioComp Gradient Master™ 108) was used to prepare at 4°C a 5-20 wt./vol. % linear gradient of sucrose in water. Five hundred μ L of the cluster suspension (prepared from 2.2.9) were carefully loaded on top of 12 mL of gradient before centrifuging with a TH-641 swinging-bucket rotor (Thermo Fisher Scientific) for 20 min at 8,000 g and 4°C. A BioComp Piston Gradient Fractionator™ was used to pull out individual bands from the sample. The fractions were purified by several centrifugation-redispersion cycles (8,000 g; 4 min) in water.

2.2.11 Characterisation

FTIR scans were performed on Shimadzu FTIR spectrophotometer IRAffinity-1S with MIRacle 10 single reflection ATR accessory. Every sample was previously dried overnight under air at 70°C.

TEM images were obtained on Hitachi H600 or JEOL 1400 microscopes operating at 75 kV or 120 kV, respectively. Typically, the particles possibly diluted with ethanol were dropped directly on carbon-coated copper film (300 mesh) and ethanol was let to evaporate at RT.

Statistics from image analysis were performed over at least 300 nano-objects for the seeds, 500 for the dumbbells and 250 for their assemblies. The size polydispersity index (*PDI*) was calculated according to the following equation:

$$PDI = \frac{\bar{D}_w}{\bar{D}_n} = \frac{\sum n_i \sum n_i d_i^4}{\sum n_i d_i \sum n_i d_i^3}$$

Polymer molar masses were determined by size-exclusion chromatography (SEC) using DMF and lithium bromide (LiBr, 1g/L) as the eluent on an Ultimate 3000 system from Thermo Fisher Scientific equipped differential refractive index detector from Wyatt technology. Macromolecules (5 mg/mL) were separated on Shodex Asahipak gel columns (GF-1G 7B, 7.5*50 mm; GF-310, 7.5*300 mm and GF-510, 7.5*300 mm) at a flow rate of 0.5 mL/min at 50°C. EasiVial kit of polystyrene from Agilent was used as the standard for calibration (\bar{M}_n from 162 to 364 000 g/mol).

2.3 Results and discussion

2.3.1 Fabrication of the silica/PS dumbbells as one-patch silica nanoparticles

The multistep preparation of the silica/PS dumbbells was inspired from the protocol of Guignard and Lattuada.¹⁹ This started from conventional PS latex NPs and evolved to the specific dumbbell-like morphology through surface crosslinking, monomer swelling, phase separation during polymerisation, and TEOS regioselective condensation.

PS seeds were prepared through emulsion polymerisation of styrene initiated by $\text{Na}_2\text{S}_2\text{O}_8$ and stabilised by SDS. The monomer-to-polymer conversion determined by the dry-extract method was 97%. The analysis of the TEM images showed an average size of $\bar{D}_n = 59$ nm with a quite high PDI of 1.08 (Fig. 2). This large size distribution is generally observed for latex particles smaller than 80 nm using SDS as emulsifier while could be optimised in the presence of a zwitterionic surfactant.²³

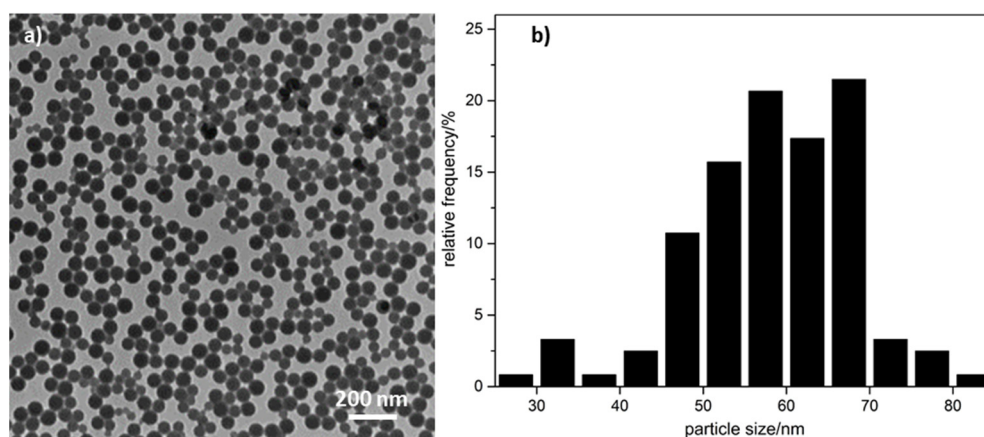


Fig.2 a) Representative TEM image of the PS seeds and b) histogram of their size distribution.

The PS seeds surface was simultaneously crosslinked and made more hydrophilic through encapsulation in a shell of *in-situ* synthesised poly(styrene-*co*-MMS). The MMS-to-styrene molar ratio for this seeded growth polymerisation was 20/80, the total volume of monomer was equivalent to the volume of the PS seeds and AIBN was used as the initiator. After 12 h, the monomer-to-polymer conversion was 94%. TEM analysis showed that the spherical morphology of the initial seeds was preserved and that their diameter increased from 59 to 71 nm and the PDI from 1.08 to 1.10 (Fig. 3). This volume increase of 84% was in very good agreement with the expected value of 85%.* The concentration of silicon atoms within the crosslinked shell was too low for evidencing the core-shell morphology on the TEM images. FTIR spectroscopy allowed us to characterise the chemical composition of the shell (Fig. 4). Comparing the spectra before and after crosslinking showed the appearance of specific bands at 1100 cm^{-1} and 1720 cm^{-1} which were ascribed to Si-O-C/Si-O-Si and C=O vibrations of the MMS monomer units, respectively. Moreover, the absence of bands in the 1637 cm^{-1} range, assigned to the C=C bond, indicates that the MMS monomer was essentially attached to the macromolecules through the copolymerisation scheme. Nevertheless, the presence of the Si-O-Si band is the proof that a fraction of the methoxy groups reacted together and therefore served as crosslinking points. Because of the tricky task of detecting Si-OH vibrations on the IR spectrum, the hydrophilic character of crosslinked seeds was more easily evidenced by dispersing the NPs in a mixture of water and hexane, shaking vigorously and checking that the crosslinked ones were more readily found in the aqueous phase while they were essentially located in the hexane phase before crosslinking (Fig. 5).

* considering the weight-averaged diameters of the seeds before and after crosslinking, the monomer-to-polymer conversion of 94%, the density of styrene and MMS of 0.91 and 1.07, respectively, and assuming that the density of poly(styrene-*co*-MMS) more or less crosslinked and hydrolyzed is close to that of PS (1.04).

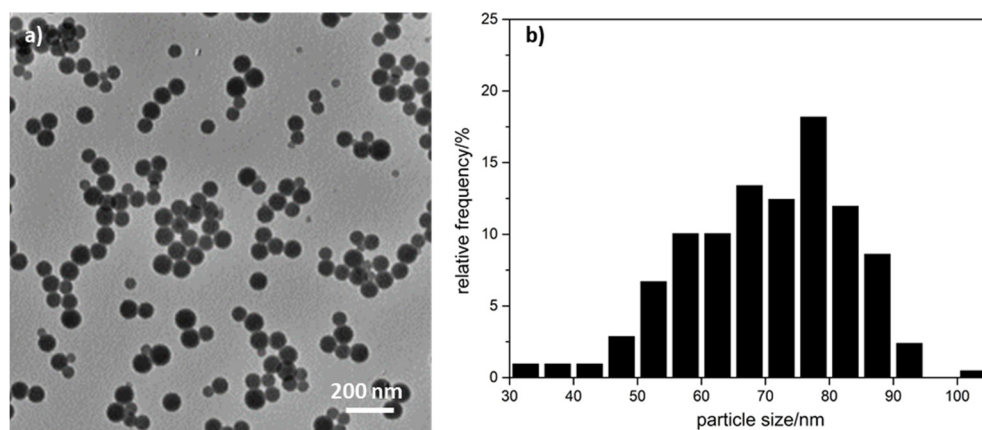


Fig. 3 a) Representative TEM image of the MMS-crosslinked PS seeds and b) histogram of their size distribution.

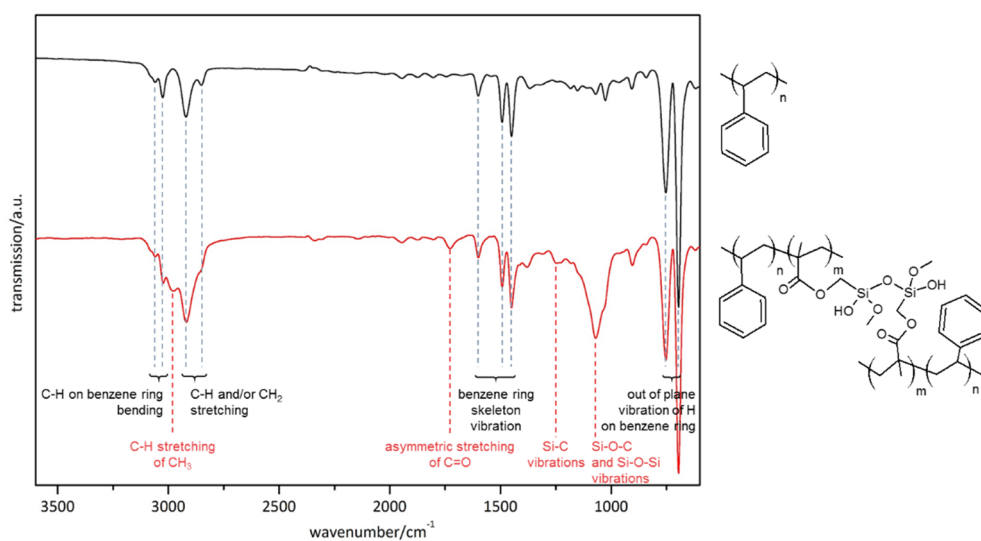


Fig. 4 FTIR spectra of the PS seeds before (black) and after (red) crosslinking through the MMS monomer units.

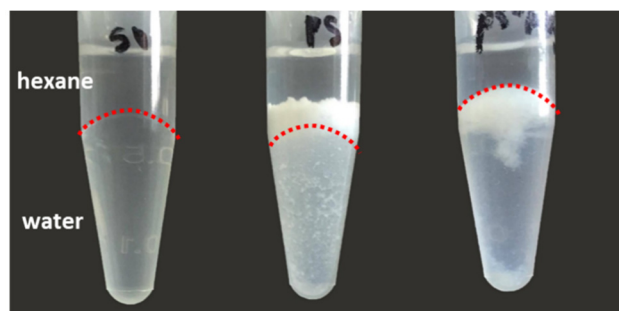


Fig. 5 Dispersion state of the PS seeds in hexane/water mixtures before (middle) and after (right) MMS crosslinking after removal of the residual SDS surfactant by several centrifugation/redispersion cycles in water.

The symmetry breaking of the PS seeds to get the PS dumbbells was performed by swelling the seeds with styrene, then increasing the temperature and triggering the polymerisation. The heating procedure afterwards caused the phase separation driven by elastic stress, and the wetting angle between the new PS lobe and the PS seed is determined by the surface hydrophilicity of the latter. It shall be mentioned that this stage is a surfactant-free emulsion

polymerisation with VBS as a comonomer introduced in very low amount before the styrene swelling. The sulphate groups present in the VBS-styrene copolymer tend to position at the surface of the particles and act as a stabiliser in the same way as surfactant molecules.¹⁹ Two parameters were varied: the swelling ratio S , *i.e.* the styrene-to-seed volume ratio, and the swelling time. A reference experiment was carried out with $S = 2$. First, we observed that the swelling time of 1 h reported by Guignard and Lattuada was underestimated. We checked that even after 2 h small spherical PS particles were generated through a homogeneous nucleation phenomenon, meaning that a fraction of the styrene was not within the seeds (Fig. 6a). Nevertheless, a swelling time of 3 h was enough to avoid this phenomenon and get exclusively PS dumbbells (Fig. 6b) with a morphology yield of about 97%.[†] The presence of the smallest dumbbells was due to the size polydispersity of the initial PS seeds.

Size measurements were performed over 60 PS dumbbells from the TEM images by considering that both lobes are intersecting spheres. This allowed us to determine that, after symmetry breaking, the average diameter of the crosslinked seed increased from 71 to 75 nm, the average diameter of the PS protrusion was 68 nm and its centre was at the average distance $d = 43$ nm from the seed centre. We calculated the average total volume of the PS dumbbells and the average volume of the PS protrusions thanks to the following equations:

- volume of the PS dumbbell = volume of the sphere inscribing the hydrophilic lobe + volume of the sphere inscribing the PS protrusion – volume of the sphere intersection

$$= \frac{4\pi R_h^3}{3} + \frac{4\pi R_p^3}{3} - \frac{\pi}{12d} (R_h + R_p - d)^2 (d^2 + 2R_p d - 3R_p^2 + 2R_h d + 6R_h R_p - 3R_h^2)$$

- volume of the PS protrusion = volume of the sphere inscribing the PS protrusion – volume of the sphere intersection

$$= \frac{4\pi R_p^3}{3} - \frac{\pi}{12d} (R_h + R_p - d)^2 (d^2 + 2R_p d - 3R_p^2 + 2R_h d + 6R_h R_p - 3R_h^2)$$

where R_h is the radius of the hydrophilic lobe originating from the MMS-crosslinked seed and R_p is the radius of the PS protrusion, *i.e.* PS lobe. We found the average values of 352,000 nm³ and 127,000 nm³ for the PS dumbbell and PS protrusion, respectively. With regard to the average volume of the initial crosslinked seeds (71 nm, *i.e.* 187,000 nm³), the average volume increase after the symmetry breaking was 88%. This is quite far from the expected value of

[†] the side-products were seeds with a too small PS protrusion with regard to the expected dumbbell-like morphology.

163%.[‡] We have no solid assumption to explain this discrepancy, but it may be noted that Guignard and Lattuada experienced the same phenomenon since they reported that “a swelling ratio equal to three or four to one was optimum to get dumbbells having two lobes of about the same size”.¹⁹ Nevertheless, they mentioned neither the value of their monomer-to-polymer conversion, nor the accurate dimensions of their dumbbells.

We checked that varying the swelling ratio from 0.5 to 5 allows varying the protrusion-to-seed size ratio (without a rigorous control as explained just above) leading to a dumbbell-like morphology when the protrusion diameter was close to that of the seed ($S = 2$), snowman-like ones when $S < 2$ and reverse snowman-like ones when $S > 2$ (Fig. 7). Even if some discrepancies were observed between the expected and obtained protrusion size, it was possible to draw a sizing chart allowing selecting the right value of S to obtained protrusions of a specific diameter (Fig. 8).

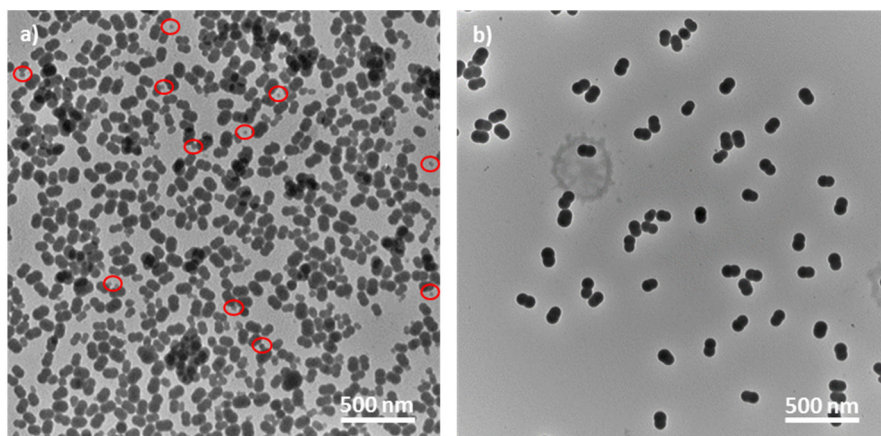


Fig. 6 Representative TEM images of the PS dumbbells obtained after a swelling time of a) 2 h and b) 3 h. Red circles highlight PS particles generated from a homogeneous nucleation phenomenon.

[‡] considering the monomer-to-polymer conversion of 93%, the density of styrene and PS of 0.91 and 1.04, respectively, and the swelling ratio, *i.e.* styrene-to-seed volume ratio, of 2.

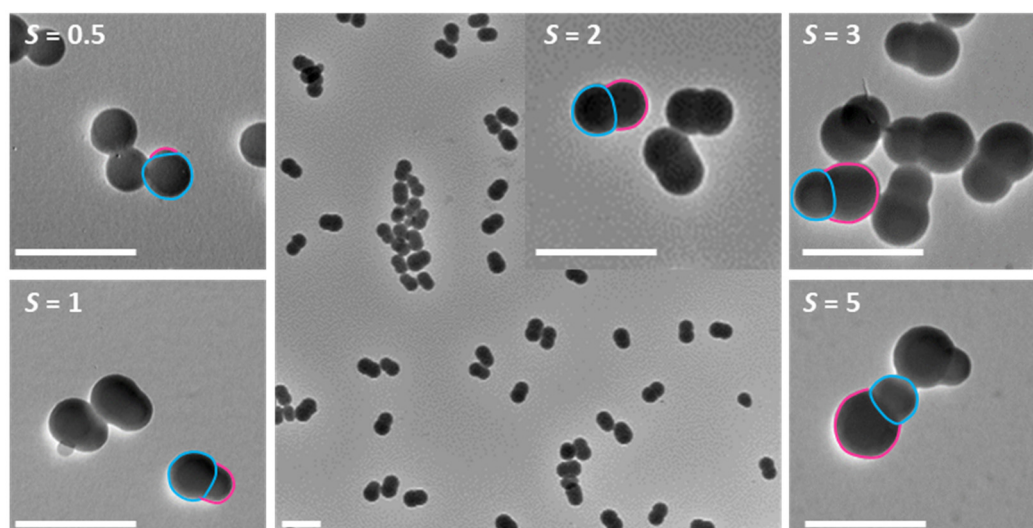


Fig. 7 Representative TEM images of the PS snowman-like (left), dumbbell-like (middle), and reverse snowman-like (right) NPs obtained from crosslinked PS seeds ($\bar{D}_n = 71$ nm) using different swelling ratios S and a swelling time of 3 h; the blue and pink circles delineate the seed and newly formed PS protrusion, respectively. Scale bars: 200 nm

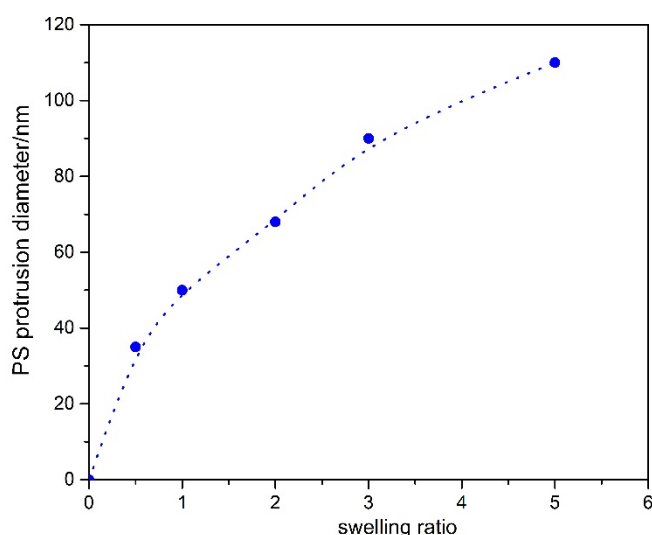


Fig. 8 Sizing chart of the PS protrusion as a function of the styrene-swelling ratio (established for 71-nm PS seeds).

Lastly, the hydrophilic lobe of the PS dumbbells was site-specifically coated with silica. This task was made easier thanks to the presence of the MMS monomer units of the crosslinked shell providing not only hydrophilicity but also “vitrophilicity”, *i.e.* capability to condense with the alkoxy silane groups of the silica precursors. We used TEOS and conventional Stöber conditions (hydro alcoholic reacting medium and NH_4OH as catalyst). To avoid homogeneous nucleation of silica, the TEOS solution was added at a slow rate. The TEM image of Fig. 9a confirms the site-specific condensation of TEOS leading to silica/PS dumbbells with a strong contrast between both lobes, where only the hydrophilic lobe was enlarged. The silica layer thickness was found to be $E = 20$ nm, but it may be easily varied by playing with the TEOS amount (See

Fig. 9c where E was extended to 35 nm). The presence of the silica coating was also evidenced by a destructive test where we calcined the dumbbells in a furnace under air at 600°C for 6 h (Fig. 9b). It shows that the PS component was completely removed and the silica lobes became silica nanobowls with a regular thickness as previously reported.¹⁹

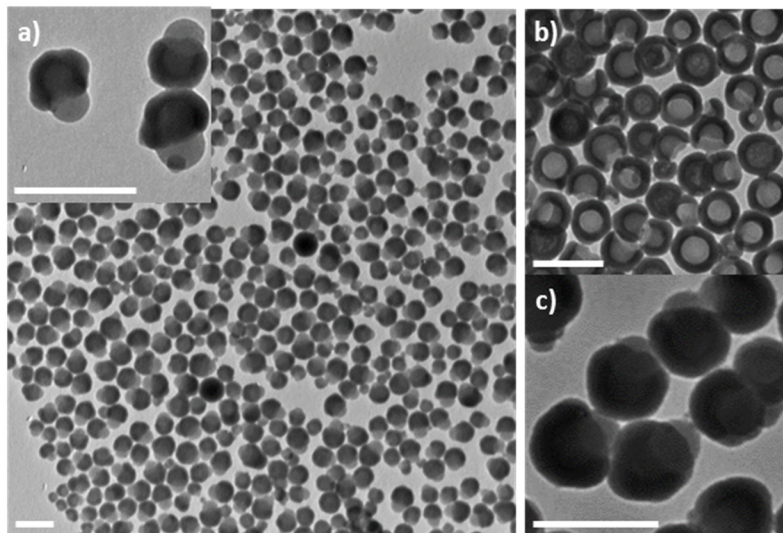


Fig. 9 Representative TEM images of the silica/PS dumbbells from PS dumbbells obtained with a swelling ratio $S = 2$ a) before and b) after calcination with a silica thickness $E = 20$ nm (Batch #3) and c) before calcination with a silica thickness $E = 35$ nm (Batch #4). Scale bars: 200 nm.

The morphology features of the silica/PS dumbbells, *i.e.* one-patch silica NPs, synthesised for this study are summarised in Table 1.

Table 1 Morphological features of the one-patch silica NPs prepared for this study.

Swelling ratio S	Silica thickness E (nm)	Silica lobe diameter D (nm)	PS protrusion diameter D_p (nm)	Patch-to-particle size ratio D_p/D	Batch number
0.5	20	110	35	0.32	#1
1	20	110	50	0.45	#2
2	20	110	68	0.62	#3
2	35	140	68	0.49	#4
3	20	110	90	0.82	#5
5	20	110	110	1.00	#6

2.3.2 Solvent-induced assembly of the one-patch silica nanoparticles into clusters

The silica/PS dumbbells were assembled into clusters in the mixtures of good/bad solvent for PS. We studied different experimental parameters, including solvent quality, use of a final centrifugation stage, NPs concentration, incubation time, and patch-to-particle size ratio.

2.3.2.1 Effect of the solvent quality and centrifugation force

This series of experiments was carried out with the Batch #3 where the silica/PS dumbbells ($S = 2$; $E = 20$ nm) were initially dispersed in ethanol. The procedure consisted in adding a mixture of DMF/ethanol at RT and let them to age for 20 h under gentle stirring. The experiments were performed in similar conditions in 1.5-mL Eppendorf® tubes with a total liquid amount of 1 mL and a particle concentration of $5.3 \cdot 10^{14}$ part/L. DMF and ethanol are known to be a good and bad solvent for PS, respectively. It means that DMF molecules are prone to develop interactions with the PS macromolecules to the extent that they can swell the latex particles, even dissolve them in the situation of a large amount of solvent.

Fig. 10 summarised the self-assembly results when the DMF fraction in the mixture was progressively increased every 10 vol. %. We performed statistical analyses of the TEM images over more than 250 species in order to assign an aggregation number to each of them: $N = 1$ for unassembled one-patch silica NPs, $N = 2$ for clusters made of two NPs, *i.e.* bipods, $N = 3$ for tripods, *etc.* On the graph (Fig. 10f), the prevalence of a cluster type is quantified through the fraction of initial silica/PS dumbbells used to get it. The blue disks whose surface is proportional to this fraction were considered. Three main situations as a function of the DMF amount might be observed:

i) in the 0-20 vol. % range, the amount of DMF was too low to swell the PS lobes efficiently and make them sticky. Therefore, this is a “non-solvent regime”, and the silica/PS dumbbells remain intact and unassembled ($N = 1$);

ii) in the 30-50 vol. % range, the DMF fraction made the solvent quality better and better and clusters with aggregation number N up to 4, *i.e.* tetrapods, were systematically observed (Fig. 10b). This “sticky regime” allowed at least 70% of the dumbbells to be spontaneously changed into clusters. The higher the value of N , the lower the prevalence of the clusters and the bipods were often the majority population;

iii) in the 60-90 vol. % range, the PS chains were readily solvated and quite efficiently extracted from the dumbbells leading to silica half-shells at the internal surface of which the PS segments that had been crosslinked with MMS remained covalently bonded (“solvent regime”). Therefore, the PS lobes disappeared, and the as-obtained silica half-shells remained essentially unassembled.

Initially, the TEM samples were prepared by dropping the NPs dispersion on the grid directly, but in the “solvent regime” and “sticky regime” the image quality was often bad because of the grid pollution by the extracted PS macromolecules. In order to overcome this issue, we decided to perform a centrifugation step (12,000 g for 10 min) to remove the potentially extracted PS macromolecules and transfer the NPs in ethanol to prepare the TEM grids. Unexpectedly, this increased quite strongly the average aggregation number \bar{N} and therefore disturbed the spontaneous prevalence of the clusters (orange circles to be compared to the blue disks on Fig. 10f). It was indeed possible to observe not only new clusters with N from 5 to 8 but also large raspberry-shaped clusters with N higher than 10 up to more than 30. In the “sticky regime”, for instance for DMF fraction of 30 vol. %, the extra consumption of the dumbbells seems to be beneficial to the appearance of new clusters with N from 5 to 8 without changing the distribution within the clusters with N from 2 to 4 (Fig. 10a). Moreover, the centrifugation allows to extend the “sticky regime” to the 10-60 vol. % range of DMF fraction (Fig. 10e). For higher DMF fractions, the centrifugation stage had no effect on the absence of self-assembly.

The large raspberry-like clusters were exclusively prevalent when the DMF fraction was 40 and especially 50 vol. % (Fig. 10c vs Fig. 10b). From a morphological viewpoint, the formation of the latter could result from the full entrapment of some dumbbells within the largest clusters thanks to an excessive sticky behaviour of the PS protrusion and/or the pre-adsorption of free PS macromolecules onto the silica surface lowering its surface energy. Unfortunately, it was not possible to check unambiguously the presence of silica nodules within these largest clusters. Despite that, this assumption is supported by the fact that such raspberries were not obtained when the DMF fraction was lower, *i.e.* when the stickiness of the PS lobe and the amount of free PS macromolecules are expected to be lower.

The role of the centrifugation stage remains unclear. Nevertheless, this can shift the system in a non-equilibrium state, enhance the frequency and energy of the collisions between the silica NPs and provide areas – especially in the pellet – where the NPs concentration tends to be maximum.

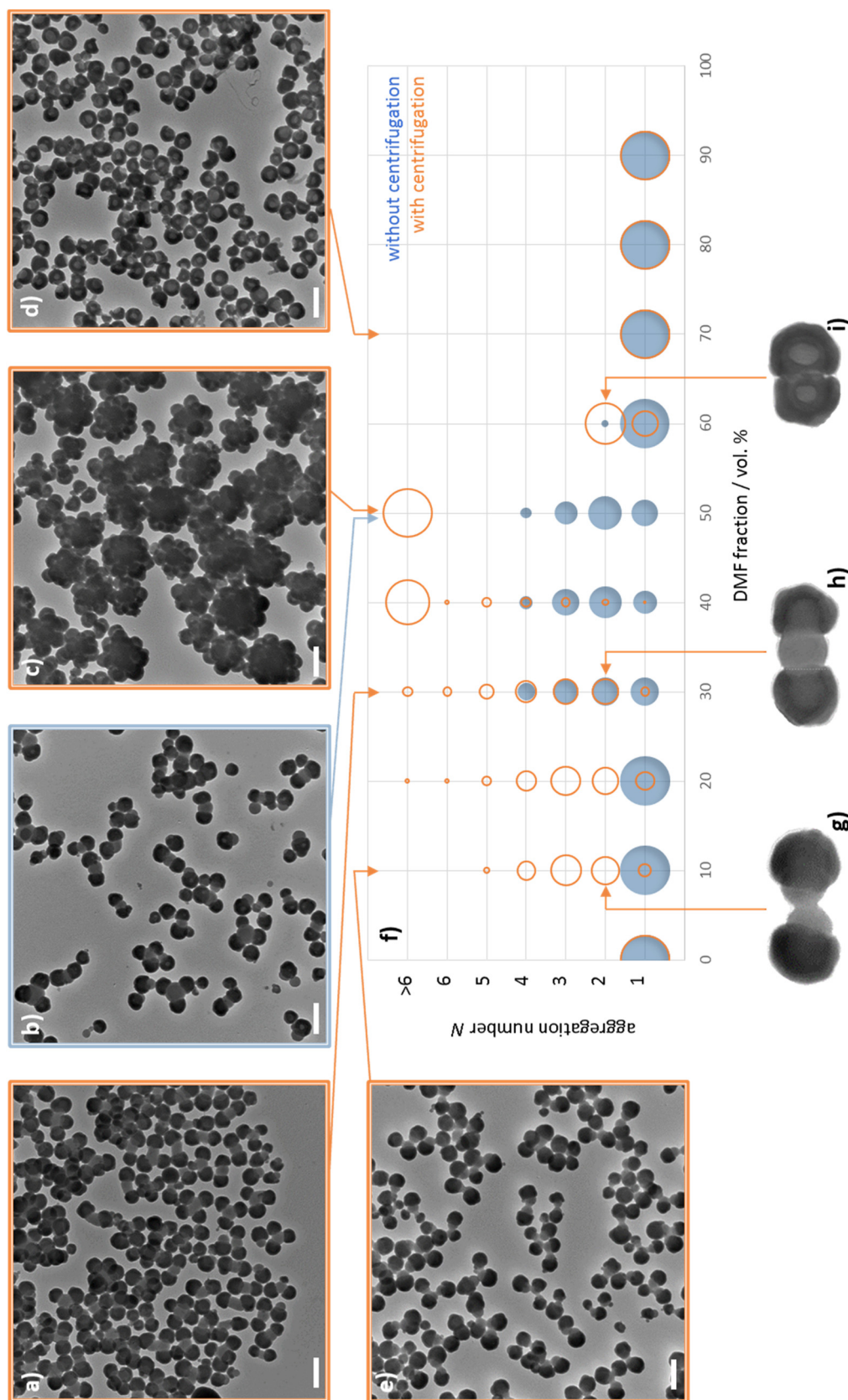


Fig. 10 a) to e) representative TEM images of the assembly mixtures of the one-patch silica NPs as a function of the composition of the liquid medium (scale bars: 200 nm); f) distribution of the one-patch silica within the clusters of aggregation number N as determined by statistical analysis of the TEM images (the surface of the disks and circles is proportional to the fraction of one-patch silica assembled within clusters of similar aggregation number); g) to i) enlarged TEM profiles of bipods ($N = 2$) showing the different types of bonding through the PS phase. Assembly experiments were performed with the silica/PS dumbbells

Lastly, the high-magnification TEM profiles of the bipods, *i.e.* clusters made of two silica half-shells attached face-to-face, was also very informative (Fig. 10g, 10h and 10i observed after the centrifugation stage). The higher the DMF fraction, the closer both half-shells. At low SDS fraction (10 vol. %; Fig. 10g), both PS lobes share only a small contact area. This means they were poorly sticky and probably the low amount of DMF allowed swelling just an external shell of the PS lobes. For 30 vol. % (Fig. 10h), both lobes readily fused in a single PS nodule making the bipod bonding particularly robust after DMF removal. For 60 vol. % (Fig. 10i), the contact between both silica half-shells is particularly close and the volume of the PS sticking point is minimal. For evident steric reasons, only bipods can be obtained. Moreover, this demonstrates that a non-negligible amount of the non-crosslinked PS macromolecules remaining physically entangled with the covalently bonded ones is mandatory to ensure the assembly. Indeed, since in the “solvent regime”, *i.e.* for higher DMF fractions, the assembly does not occur when all the non-crosslinked macromolecules are supposed to have been extracted. This means that the macromolecules which are covalently bonded at the bottom of the silica half-shells are too short or not numerous enough to stick efficiently to those of another half-shells, whatever the overcrowding provided by the centrifugation stage. This conclusion was supported by a verification experiment which consisted in incubating again the silica half-shells obtained at 90 vol. % of DMF this time in “sticky conditions”, *i.e.* 30 vol. % of DMF. We observed no cluster, meaning that the presence of a minimal amount of just-entangled PS chains is mandatory to achieve the self-assembly.

Because they allowed achieving clusters not only within the targeted aggregation number range with N from 2 to 8 but also the more robust ones, the experimental conditions for the rest of the study were set to a DMF fraction of 30 vol. % followed by a centrifugation stage.

2.3.2.2 Effect of the particle concentration

The concentration of $5.3 \cdot 10^{14}$ part/L used in the last section was defined as the reference (1x concentration). This corresponded to a DMF-to-PS lobe volume ratio of 4500/1 when the DMF fraction was 30 vol. % and considering that the average volume of the PS lobes in Batch #3 was equal to $127,000 \text{ nm}^3$. Here, we varied the concentration up to 5 times, other parameters being equal (Fig. 11). We observed a slight increase of \bar{N} with the concentration from 2.65 to 3.19.[§] This means that either the concentration range that we investigated was not large enough, or

[§] the clusters with $N > 6$ could not be integrated into the calculation of \bar{N} .

the final centrifugation stage reduced an effect that would have been more significant without it.

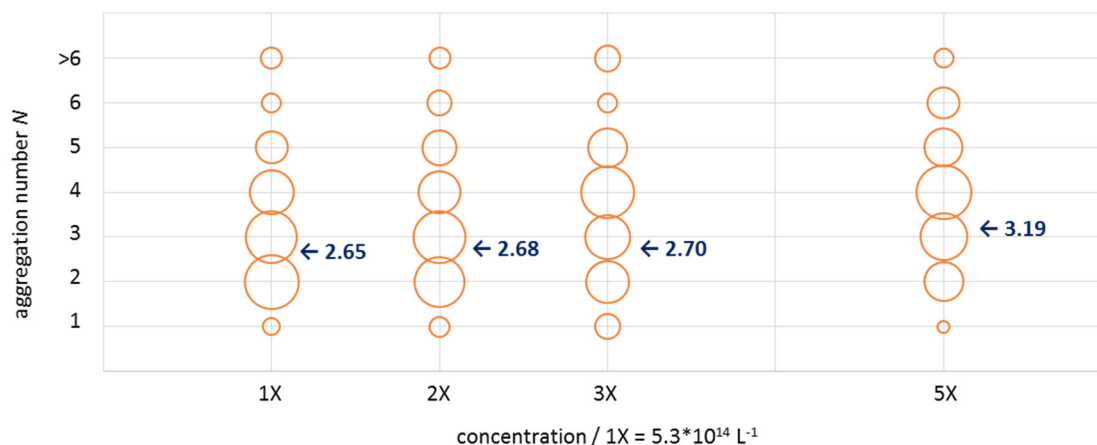


Fig. 11 Distribution of the one-patch silica NPs within the clusters of aggregation number N as a function of NPs concentration determined by statistical analysis of the TEM images (the surface of the circles is proportional to the fraction of one-patch silica assembled within clusters of similar aggregation number). The blue arrows indicate the average aggregation number \bar{N} calculated without taking into account the clusters with $N > 6$. Assembly experiments were performed with the silica/PS dumbbells of Batch #3 ($S = 2$; $E = 20$ nm) in a DMF/mixture with DMF fraction of 30 vol. % at 20°C for 20 h with a final centrifugation stage (12,000 g for 10 min).

2.3.2.3 Effect of the incubation time

We varied the incubation time from 5 min to 20 h (reference experiment), other parameters being equal (Fig. 12). We observed that the entire panel of clusters was systematically obtained even at the shortest incubation time. However, their prevalence evolved with time and \bar{N} increased from 2.09 to 2.65.** At the short time, 42% of the NPs were found in bipods, but this fell to 30% after 20 h, while the fraction of larger clusters increased progressively especially those with $N > 4$. During this time, the one-patch silica fraction decreased from 13 to 4% and this could be consistent with the enlargement by single particle unit on most of the clusters obtained in the early stages. This series of experiments shows that \bar{N} did not fully reach a plateau even after 20 h. Moreover, we wondered what the effect of the final centrifugation stage is on this evolution. That is why we checked the cluster composition before centrifugation especially at the shortest times. We observed that, after 5 and 20 min of incubation, \bar{N} was equal to 1.10 and 1.37, against 2.09 and 2.10 after centrifugation, respectively (Fig. 12). This means that the contribution of the centrifugation stage to the \bar{N} increase is significant, but not to the point where it would mask the effect of the incubation time.

** the clusters with $N > 6$ could not be integrated into the calculation of \bar{N} .

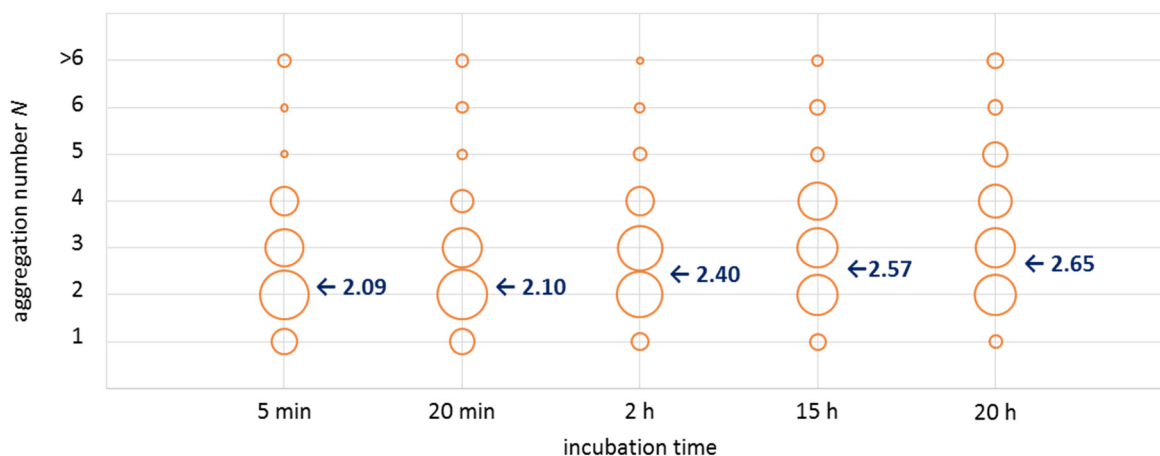


Fig.12 Distribution of the one-patch silica NPs within the clusters of aggregation number N as a function of the incubation time as determined by statistical analysis of the TEM images (the surface of the circles is proportional to the fraction of one-patch silica assembled within clusters of similar aggregation number). The blue arrows indicate the average aggregation number \bar{N} calculated without taking into account the clusters with $N > 6$. Assembly experiments were performed with the silica/PS dumbbells of Batch #3 ($S = 2$; $E = 20$ nm) in a DMF/mixture with DMF fraction of 30 vol. % at 20°C at the concentration of $5.3 \cdot 10^{14}$ part/L with a final centrifugation stage (12,000 g for 10 min).

From now, the “reference experiment” describes a solvent-induced assembly performed in the following conditions: concentration of the one-patch silica of $5.3 \cdot 10^{14}$ part/L in a DMF/mixture with DMF fraction of 30 vol. % at 20°C for 20 h with a final centrifugation stage (12,000 g for 10 min).

2.3.2.4 Effect of the patch-to-particle size ratio

The one-patch silica NPs with different patch-to-particle size ratios (*cf.* Table 1) were assembled in the conditions of the “reference experiments” and representative TEM images are shown in Fig. 13.

As expected, we observed that the lower the relative size of the patch, the lower the average aggregation number. When it was 0.32 (Batch #1), only a few number of bipods were indeed obtained ($\bar{N} = 1.10$). The exclusive bipod morphology results from the steric hindrance of the silica lobes with regard to the PS sticking point making the cluster unable to catch a third NP. The low prevalence of the bipods may be explained by the small patch size, which decreases their probability of collision, *i.e.* the first stage of the assembly process. As far as the patch-to-particle size ratio was increased, \bar{N} increased and reached the value of 2.65 (Batch #3, *i.e.* patch-to-particle size ratio of 0.62).

The results for higher patch-to-particle size ratios turned out to be unexpected because they showed a dramatic decrease of \bar{N} down to 1.24 for Batch #6, *i.e.* patch-to-particle size ratio of 1.00. Moreover, the shape of clusters was not well defined and it was quite tricky to provide solid statistics data especially for Batch #5. Nevertheless, we observed that for Batch #6, the average diameter of the PS lobes of the unassembled dumbbells was decreased from 110 to 105 nm. This value fell to 102 nm and 96 nm when the solvent-induced assembly experiment was repeated using the same NP dispersion once and twice, respectively (after recovery by centrifugation and redispersion in ethanol). This means that, for the larger size of the PS protrusion, the amount of DMF was enough to extract a fraction of the PS chains, but not enough to make them sticky. We also tried to find again a better “sticky regime” by increasing the DMF fraction up to 50 vol. % with Batch #6 (Fig. 14). However, unexpectedly, the “solvent regime” appeared from 45 vol. % with the appearance of a significant fraction of silica half-shells.

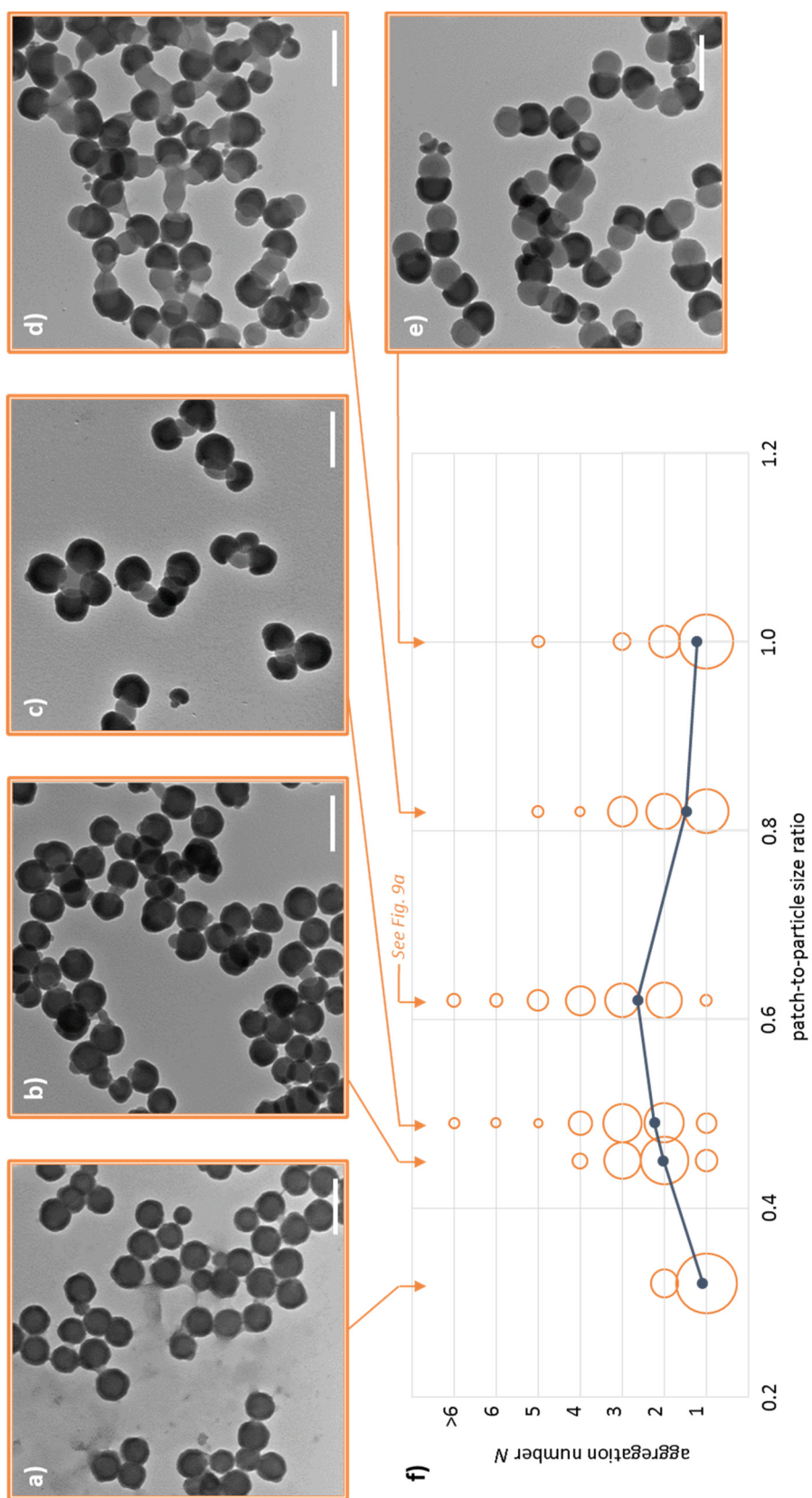


Fig. 13 a) to e) representative TEM images of the assembly mixtures of the one-patch silica NPs as a function of the patch-to-particle size ratio corresponding to Batch #1, #2, #4, #5 and #6, respectively (scale bars: 200 nm); f) distribution of the one-patch silica within the clusters of aggregation number N as determined by statistical analysis of the TEM images (the surface of the circles is proportional to the fraction of one-patch silica assembled within clusters of similar aggregation number). The blue curve shows the evolution of the average aggregation number \bar{N} . Assembly experiments were performed with a SDS fraction of 30 vol. % at the concentration of $5.3 \cdot 10^{-4}$ part/L at 20°C for 20 h with a final centrifugation stage (12,000 g for 10 min).

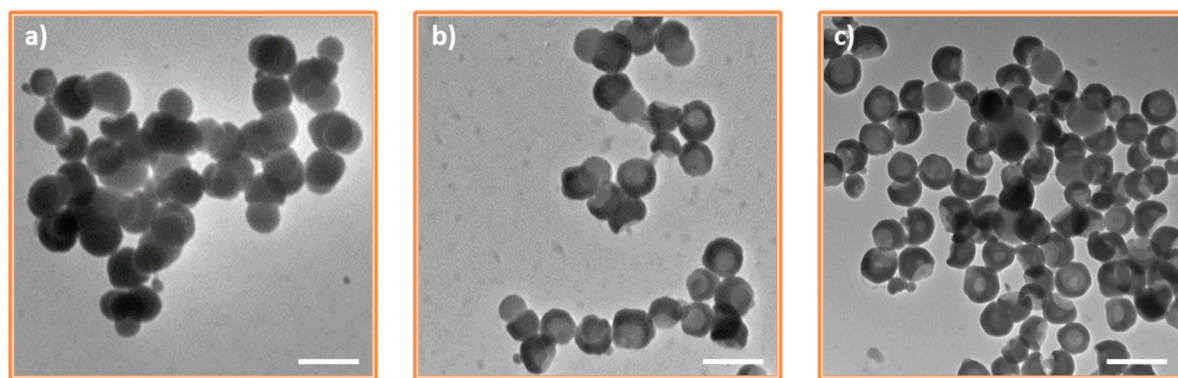


Fig. 14 Representative TEM images of the assembly mixtures of the one-patch silica from Batch #6 as a function of the DMF fraction: a) 40 vol. %, b) 45 vol. % and c) 50 vol. % (scale bars: 200 nm). Assembly experiments were performed at the concentration of $5.3 \cdot 10^{14}$ part/L at 20°C for 20 h with a final centrifugation stage (12,000 g for 10 min).

It could be concluded that quite unexpectedly the stickiness of the patch varies with the patch-to-particle size ratio, *i.e.* with the size of the PS lobe. Two assumptions could explain this phenomenon:

- i) the PS chains in the smallest patches would make the latter stickier, for instance, more easily swellable if they are particularly shorter and therefore less physically entangled;
- ii) the PS chains in the smallest patches would be more efficient for ensuring the mechanical stability of the clusters and thereby making the assembly more irreversible.

Therefore, to go further in the interpretation, we attempted to determine the molecular weight distribution of the PS chains after extraction, *i.e.* the just-entangled macromolecules. This was performed in pure THF at RT for 2 h. After removal of the silica residue by centrifugation (12,000 g, 10 min), the samples were filtered and analysed by size exclusion chromatography in DMF (Fig. 15). We observed that the molar mass distribution was made of three different macromolecular populations whatever the batch (Batch #1, #3, #5 and #6). The highest molecular weights ($M_{\text{peak}} \sim 2,000,000$) correspond to the MMS-crosslinked PS macromolecules that had never been covalently bond to the silica shell and the 2nd population ($\sim 450,000$ g/mol) matches with the PS macromolecules of the initial PS seeds. These large values are consistent with an emulsion polymerisation process using a water-soluble initiator. The 3rd population ($M_{\text{peak}} \sim 200,000$) results from the polymerisation of the swollen styrene at the time of the symmetry breaking stage. These molecular weights are lower because the process is closer to bulk polymerisation because AIBN is an organophilic initiator. The several free radicals

simultaneously decomposed from AIBN generate the high reaction-termination probability and the moderate molecular weight accordingly. We also observed logically that the higher the patch-to-particle size ratio, *i.e.* the larger the PS lobe, the higher the prevalence of this 3rd population. This result supports more readily the 2nd assumption: the largest PS lobes would be less efficient to maintain the cluster after coalescence because they would be softer than the smallest ones and the assembly would be more reversible making \bar{N} smaller. This could explain why with Batch #6 on Fig. 14b and c we observe the coexistence of apparently intact one-patch silica NPs and silica half-shells. They could result indeed simply from the dissymmetric dislocation of clusters.

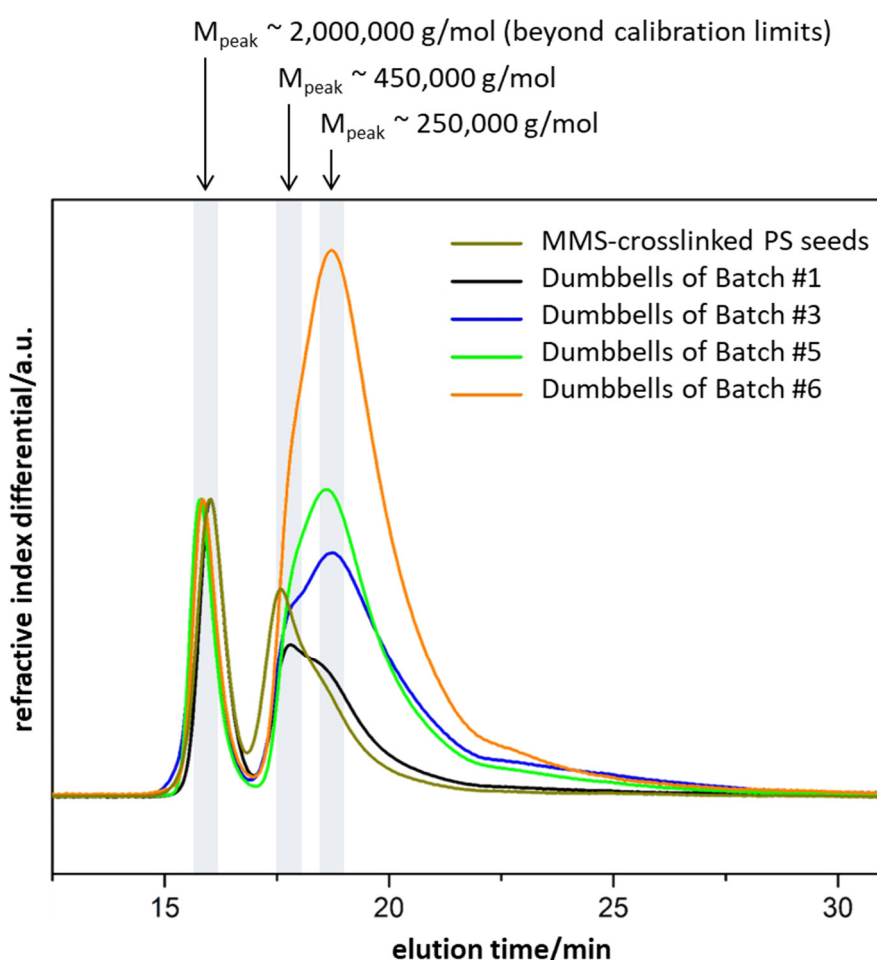


Fig. 15 Molar mass distribution of the PS macromolecules within the different NPs synthesized for this study as determined by size-exclusion chromatography (SEC).

2.3.2.5 Tentative sorting of clusters through density gradient centrifugation

As we failed to obtain pure batches of a given cluster morphology by playing with the experimental settings, we verified that it is possible to purify the as-obtained batches by density gradient centrifugation that already used in several reported works,^{9,24–26}. The purer batches

containing monopods (85%), bipods (52%), tripods (48%) or therapods (53%) were collected from the cluster mixture^{††} after the centrifugation (8,000 g; 20 min) in a linear gradient of sucrose (5-20 wt./vol. %) in water (Fig. 16).

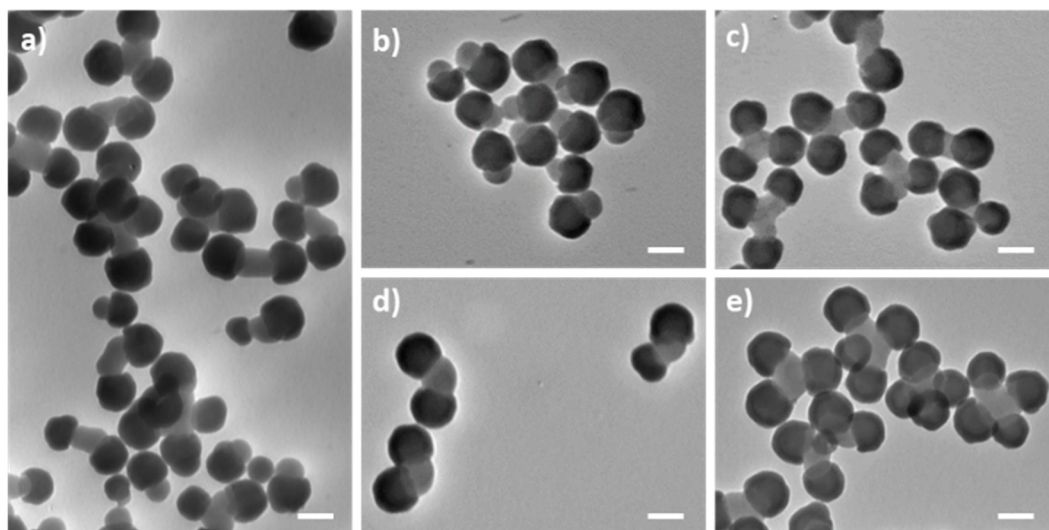


Fig. 16 Representative TEM images of a) the cluster mixture from PS/silica dumbbell-like NPs (Batch #3) as obtained after solvent-induced assembly and b-e) after sampling in the centrifugation tube in different bands (scale bars: 100 nm). Assembly experiments were performed with a SDS fraction of 30 vol. % at the concentration of $5.3 \cdot 10^{14}$ part/L at 20°C for 20 h with a final centrifugation stage (12,000 g for 10 min). Sorting by centrifugation experiment was performed once at 8,000 g for 20 min in a sucrose gradient (5-20 wt./vol. %) in water.

2.3.3 Spread of the strategy to gold-coated clusters

We extended the synthetic pathway to more complex building blocks, such as silica/PS dumbbells whose silica lobe was previously decorated with tiny gold NPs for envisaging later their regrowth. We explored two pathways (Fig. 17): Route #1 consisted in the solvent-induced assembly prior to the gold seed-growth and in Route #2 the gold seed-growth step preceded the solvent-induced assembly step.

^{††} This cluster mixture consists of 10% monopod, 41% bipod, 25% tripod, 14% tetrapod and 10% of cluster with aggregation number higher than 4.

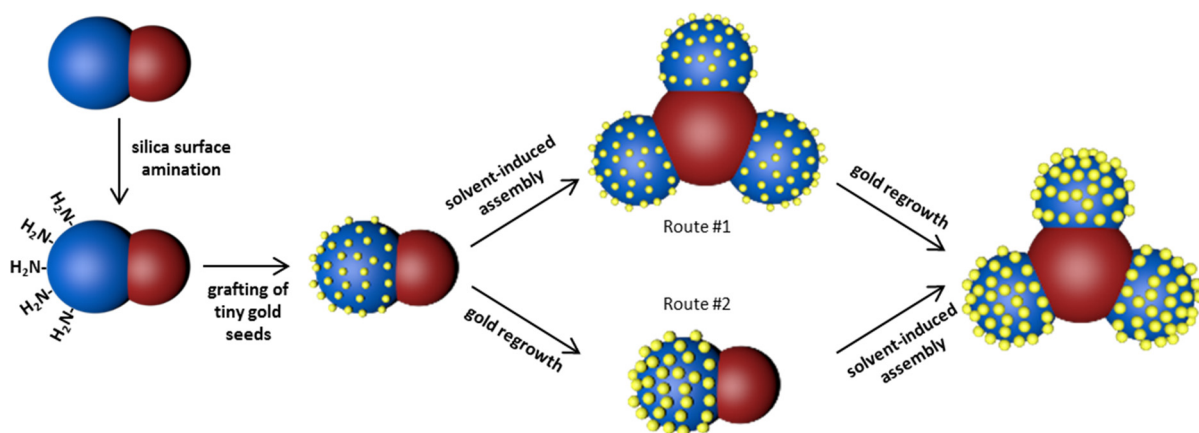


Fig. 17 Scheme summarising the two pathways to obtain the gold-coated silica clusters.

2.3.3.1 Decoration of the silica lobe of the silica/PS dumbbells with tiny gold particles

In order to make the surface of the silica lobes reactive with regard to gold NPs, we modified it with (3-aminopropyl)triethoxysilane (APTES) in ethanol. The used concentration was 50 molecules/nm² of the silica surface area. It may be mentioned here that our first experiments were performed at 50°C, as usual with conventional silica NPs. However, we observed that the combination of this temperature and the presence of APTES triggered the self-assembly (Fig. 18a). This was made possible because APTES - probably prior to the hydrolysis of its ethoxy groups - is a good solvent for PS. A significant part of APTES probably swelled the PS, decreased its glass transition temperature below 50°C and therefore made the PS patch sticky. This was confirmed by a control experiment carried out at 50°C without APTES and showing no self-assembly (Fig. 18b). Alternatively, we performed the APTES grafting at RT without observing the self-assembly phenomenon. We checked the success of this surface modification by incubating the APTES-modified silica/PS dumbbells with gold NPs (average size 1-3 nm) stabilised with tetrakis(hydroxymethyl)phosphonium chloride (THPC) and prepared according to an already-reported protocol.²¹ We indeed observed the regioselective adsorption of the gold NPs on the silica lobes through the electrostatic interaction between the positively charged silica lobes and the negatively charged gold NPs (Fig. 18c).

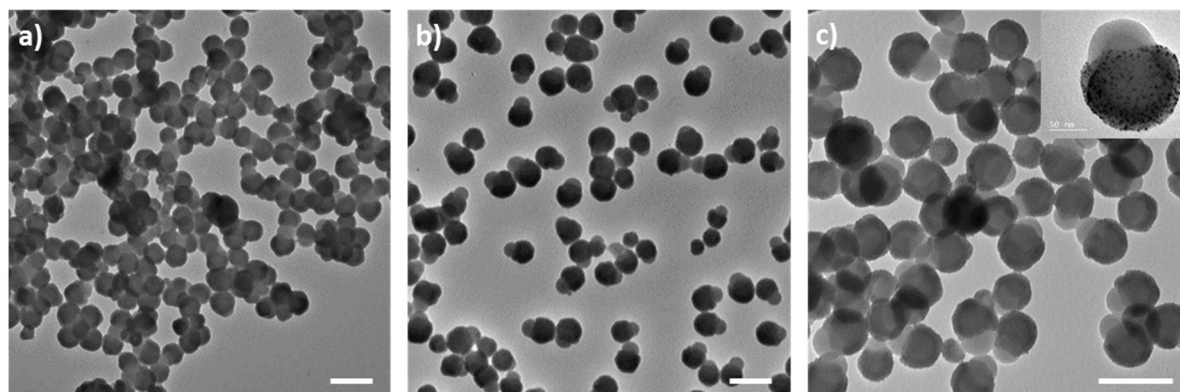


Fig. 18 Representative TEM images of the one-patch silica NPs (Batch #3) after ageing overnight in ethanol at 50°C a) with and b) without APTES (50 molecules/nm²), and c) after successful APTES grafting at RT and adsorption of THPC-stabilised gold NPs. Scale bars: 200 nm (50 nm for the inset).

2.3.3.2 Investigation of Route #1

The as-obtained gold-decorated one-patch silica NPs were successfully assembled in DMF/ethanol mixtures in the conditions of the “reference experiment” (Fig. 19a-b). We observed the formation of clusters bearing 2 to 5 silica lobes with an average aggregation number of 2.29 which is slightly lower than for bare one-patch silica NPs in similar conditions ($\bar{N} = 2.65$). The seed-growth of a gold shell specifically on the silica lobes was performed according to a recipe already published using a gold plating solution.²² The protocol was repeated three times. TEM images show that the gold coating was indeed site-specific because only silica lobes were covered by gold (Fig. 19c). However, the gold thickness was quite high, and this induced that the silica lobes of the clusters were henceforth stuck together through the gold shell. To verify this point, the PS phase was removed by dissolution in THF (3 cycles of centrifugation/redispersion at 12,000 g for 10 min) and the TEM image of the resulting clusters shows that the silica lobes remained indeed joined together (Fig. 19d).

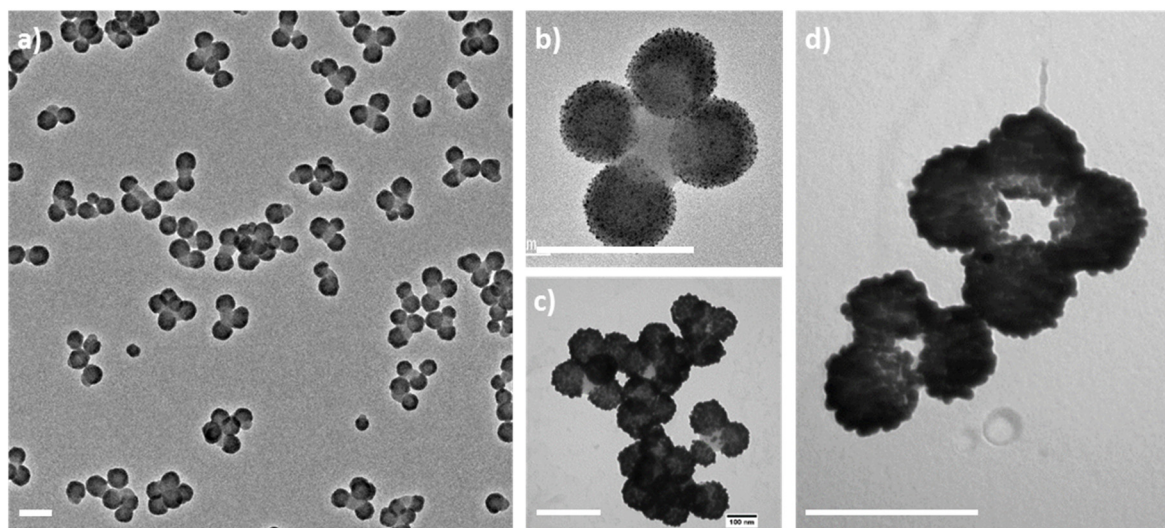


Fig. 19 Representative TEM images of a) and b) the clusters fabricated from gold-decorated one-patch silica NPs in low and high magnification, c) the cluster after gold regrowth (3 iterations), and d) the clusters after gold regrowth and dissolution of the PS phase (scale bars: 200 nm). Assembly experiments were performed at the concentration of $5.3 \cdot 10^{14}$ part/L in a DMF/mixture with DMF fraction of 30 vol. % at 20°C for 20 h with a final centrifugation stage (12,000 g for 10 min).

2.3.3.3 Investigation of Route #2

In order to avoid the sticking of the silica lobes together when the growth of the gold shell was performed after the solvent-induced assembly, we investigated the reverse pathway (Route#2, Fig. 17). The regrowth of the gold NPs was carried out on the gold-decorated one-patch silica NPs with 3 iterations of the experimental protocol (Fig. 20a). We observed the regrowth of each gold seed to an average diameter of 17 nm, but not a continuous gold coating. Then we studied their solvent-induced assembly in the conditions of the “reference experiment” for which the incubation time was reduced to 20 min to shorten the experimental process. Even if we did not perform extensive statistics, it seems that the lower the centrifugation speed, the higher would be the aggregation number (Fig. 20b,c). This could be due to the higher apparent density of these NPs that would precipitate faster compared to the bare or gold-decorated one-patch silica NPs. We performed another series of experiments by increasing the DMF fraction to 50 vol. % and varying the centrifugation speed from 12,000 g to 2,000 g (Fig. 20d-f). We also observed clusters (from $N = 2$ to $N = 5$) and again it seems that high centrifugation speed is not necessary for assembly.

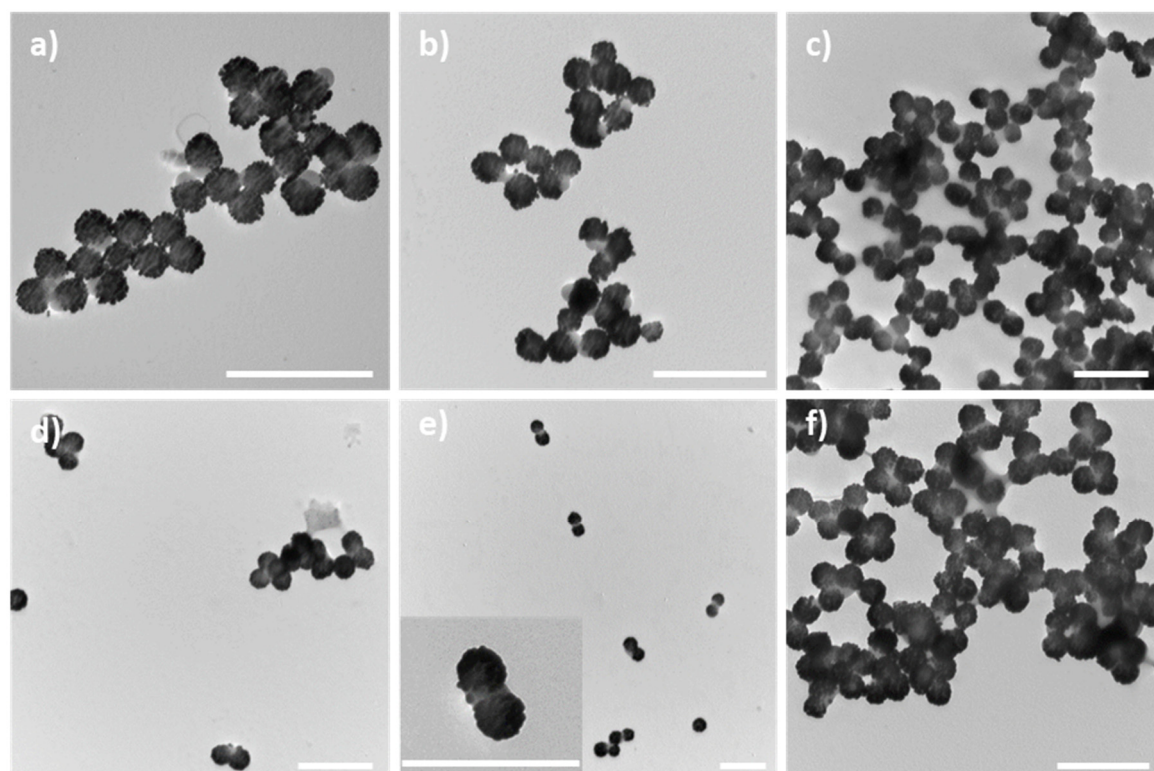


Fig. 20 a) Representative TEM images of one-patch silica NPs a) after regrowth of the gold seeds and then after solvent-induced self-assembly and a final centrifugation at b) 12,000 g and c) 6,000 g with a DMF fraction of 30 vol. %, or with a DMF fraction of 50 vol. % and a centrifugation speed of d) 12,000 g, e) 6,000 g and f) 2,000 g. Scale bars: 500 nm.

2.4 Conclusion

We showed that solvent-induced assembly of one-patch silica nanoparticles is efficient to prepare robust clusters made of a PS core and silica satellites. The dumbbells made of one silica lobe and one PS lobe were prepared successfully according to the recipe of Guignard and Lattuada. The ethanol/DMF mixture is a good medium to make the PS lobes sticky enough to coalesce with others at room temperature. The “sticky regime” corresponds to DMF fractions in the 30-50 vol. % range, which can be enlarged to 10-60 vol. % if the incubation process is completed with a centrifugation stage. The maximum aggregation numbers without and with centrifugation are 4 and more than 30, respectively. The role of the centrifugation remains poorly understood, and the effects of the NPs concentration and incubation time are quite moderate. The patch-to-particle size ratio was varied from 0.32 to 1.00 and its influence on the average aggregation number turned out to be partially unexpected. From 0.32 to 0.62, the larger the PS lobe, the higher the average aggregation number in agreement with the widespread idea that the latter is mainly controlled by the steric hindrance of the nanoparticles. However, for the higher values of the patch-to-particle size ratio, the average aggregation number decreases

probably because the assembly would be more reversible, *i.e.* the bonding within the clusters would be less strong, owing to the larger fraction of shorter PS chains. This strategy can be extended to gold-coated clusters with subject to a slight optimisation of the experimental conditions.

The morphology of the as-obtained clusters is quite regular (Fig. 21) and corresponds to the reverse morphology of the silica/PS multipods that we investigated this last decade.^{16,17} Nevertheless, they could be optimised via two strategies:

- i) as the cluster is built around a soft PS nodule, the conditions of its solidification determine the final geometry. For obtaining regular clusters, a slow solidification process combined with efficient repulsive forces between the silica satellites should be managed. This could be achieved by shifting slowly from the “sticky regime” to the “non-solvent regime” and by engineering the surface of the silica lobe to generate steric, electrostatic or electrosteric repulsion forces;
- ii) because any of the investigated experimental parameters cannot allow promoting the formation of a specific cluster with a targeted aggregation number and the tentative sorting experiment proves that the density gradient centrifugation was a promising way to purify the clusters. Iterative purification experiments should be performed and/or the centrifugation parameters should be optimised to achieve our target.

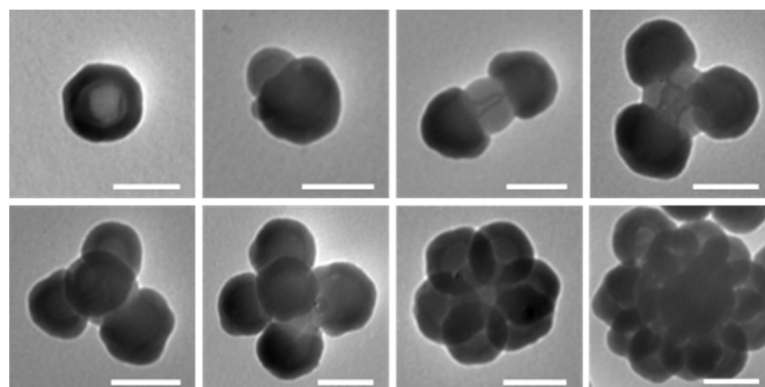


Fig. 21 TEM images of PS/silica clusters obtained from one-patch silica by the solvent-induced assembly. Note: these samples were possibly collected from different batches and therefore obtained in different experimental conditions. Scale bars: 100 nm.

2.5 References

1. Lattuada, M. & Hatton, T. A. Synthesis, properties and applications of Janus nanoparticles. *Nano Today* **6**, 286–308 (2011).

2. Walther, A. & Müller, A. H. E. Janus particles: synthesis, self-assembly, physical properties, and applications. *Chem. Rev.* **113**, 5194–5261 (2013).
3. Zhang, J., Grzybowski, B. A. & Granick, S. Janus particle synthesis, assembly, and application. *Langmuir* **33**, 6964–6977 (2017).
4. Bianchi, E., Blaak, R. & Likos, C. N. Patchy colloids: state of the art and perspectives. *Phys. Chem. Chem. Phys.* **13**, 6397–6410 (2011).
5. Yi, G.-R., Pine, D. J. & Sacanna, S. Recent progress on patchy colloids and their self-assembly. *J. Phys. Condens. Matter* **25**, 193101–193112 (2013).
6. Ravaine, S. & Duguet, E. Synthesis and assembly of patchy particles: recent progress and future prospects. *Curr. Opin. Colloid Interface Sci.* **30**, 45–53 (2017).
7. Hu, H., Ji, F., Xu, Y., Yu, J., Liu, Q., Chen, L., Chen, Q., Wen, P., Lifshitz, Y., Wang, Y., Zhang, Q. & Lee, S. T. Reversible and precise self-assembly of Janus metal-organosilica nanoparticles through a linker-free approach. *ACS Nano* **10**, 7323–7330 (2016).
8. Castro, N., Constantin, D., Davidson, P. & Abécassis, B. Solution self-assembly of plasmonic Janus nanoparticles. *Soft Matter* **12**, 9666–9673 (2016).
9. Kraft, D. J., Vlug, W. S., van Kats, C. M., van Blaaderen, A., Imhof, A. & Kegel, W. K. Self-assembly of colloids with liquid protrusions. *J. Am. Chem. Soc.* **131**, 1182–1186 (2009).
10. Liang, H., Cacciuto, A., Luijter, E. & Granick, S. Clusters of charged Janus spheres. *Nano Lett.* **6**, 2510–2514 (2006).
11. Hong, L., Cacciuto, A., Luijten, E. & Granick, S. Clusters of amphiphilic colloidal spheres. *Langmuir* **24**, 621–625 (2008).
12. Chen, Q., Whitmer, J. K., Jiang, S., Bae, S. C., Luijten, E. & Granick, S. Supracolloidal reaction kinetics of Janus spheres. *Science*. **331**, 199–202 (2011).
13. Kraft, D. J., Ni, R., Smallenburg, F., Hermes, M., Yoon, K., Weitz, D. A., van Blaaderen, A., Groenewold, J., Dijkstra, M. & Kegel, W. K. From the cover: surface roughness directed self-assembly of patchy particles into colloidal micelles. *Proc. Natl. Acad. Sci.* **109**, 10787–10792 (2012).
14. Bharti, B., Rutkowski, D., Han, K., Kumar, A. U., Hall, C. K. & Velev, O. D. Capillary bridging as a tool for assembling discrete clusters of patchy particles. *J. Am. Chem. Soc.* **138**, 14948–14953 (2016).
15. Ge, X.-H., Geng, Y.-H., Chen, J. & Xu, J.-H. Smart amphiphilic Janus microparticles: one-step synthesis and self-assembly. *ChemPhysChem* **19**, 2009–2013 (2018).
16. Perro, A., Duguet, E., Lambert, O., Taveau, J.-C., Bourgeat-Lami, E. & Ravaine, S. A chemical synthetic route towards “colloidal molecules”. *Angew. Chemie Int. Ed.* **48**, 361–365 (2009).
17. Désert, A., Morele, J., Taveau, J.-C., Lambert, O., Lansalot, M., Bourgeat-Lami, E., Thill, A., Spalla, O., Belloni, L., Ravaine, S. & Duguet, E. Multipod-like silica/polystyrene clusters. *Nanoscale* **8**, 5454–5469 (2016).
18. Hubert, C., Chomette, C., Désert, A., Sun, M., Treguer-Delapierre, M., Mornet, S., Perro, A., Duguet, E. & Ravaine, S. Synthesis of multivalent silica nanoparticles combining

- both enthalpic and entropic patchiness. *Faraday Discuss.* **181**, 139–46 (2015).
19. Guignard, F. & Lattuada, M. Template-assisted synthesis of Janus silica nanobowls. *Langmuir* **31**, 4635–4643 (2015).
 20. Stöber, W., Fink, A. & Bohn, E. Controlled growth of monodisperse silica spheres in the micron size range. *J. Colloid Interface Sci.* **26**, 62–69 (1968).
 21. Duff, D. G., Baiker, A. & Edwards, P. P. A new hydrosol of gold clusters. 1. Formation and particle size variation. *Langmuir* **9**, 2301–2309 (1993).
 22. Zhang, B. S., Ni, W., Kou, X., Yeung, M. H., Sun, L., Wang, J. & Yan, C. Formation of gold and silver nanoparticle arrays and thin shells on mesostructured silica nanofibers. *Adv. Funct. Mater.* **17**, 3258–3266 (2007).
 23. Graillat, C., Pichot, C. & Guyot, A. Preparation and characterization of low size polystyrene latex particles with various strong acid surface charges. *Colloids and Surfaces* **56**, 189–200 (1991).
 24. Manoharan, V. N. Dense packing and symmetry in small clusters of microspheres. *Science*. **301**, 483–487 (2003).
 25. Lauga, E. & Brenner, M. P. Evaporation-driven assembly of colloidal particles. *Phys. Rev. Lett.* **93**, 238301–208304 (2004).
 26. Yuan, Q., Gu, J., Zhao, Y., Yao, L., Guan, Y. & Zhang, Y. Synthesis of a colloidal molecule from soft microgel spheres. *ACS Macro Lett.* **5**, 565–568 (2016).

Chapter 3

Solvent-induced chaining of two-patch silica nanoparticles

3.1 Introduction

Chaining of particles, often described as colloidal polymerisation, is a field of intense research that was recently reviewed several times.¹⁻³ In the restricted fields of inorganic particles, Pyun and co-workers identified three main strategies based on assembly directed by dipoles, *e.g.* electrostatic or magnetic, by surface lattice fringes or by surface organic ligands providing electrostatic, covalent or non-covalent linkages, *e.g.* oligonucleotide. The state-of-the-art of Chapter 1 learned us that, in the latter scheme, few studies employing patchy particles for programming a one-direction growth were reported.³ The main investigations concerned polymer-tethered metal nanorods essentially assembled in good/bad solvent mixtures^{2,4-11} or silica-based microparticles with two concave or convex patches subjected to depletion conditions.¹² Therefore, there is sufficient room to study the assembly of silica particles in size range between the hundred nanometres and one micrometre. Beyond the academic interest of mimicking molecular systems, *i.e.* creating colloidal macromolecules, chaining metal nanoparticles (NPs) is of particular interest for developing sensors^{13,14}, SERS substrates^{15,16}, antennas,³ *etc.*

So, we reported here the fabrication of colloidal chains from two-patch silica NPs that could be envisioned as the colloidal imitation of carbyne, also known as the linear acetylenic carbon $-(C\equiv C)_n-$ and often assimilated to the polycumulene $=(C=C)_n=$. The patchy NPs were synthesised through a multistep route previously developed in our laboratory¹⁷, consisting of the fabrication of size-monodispersed silica NPs and subsequent surface modification for use as seeds in emulsion polymerisation of styrene to get silica/PS bipods, and the regrowth of the silica core (Fig. 1). Inspired by the preliminary work of Céline Hubert,¹⁷ we first attempted to form chains from the as-obtained patchy NPs in ethanol/DMF mixtures as in Chapter 2, but it appeared that this strategy was not successful as only short chains were observed in equilibrium with a large number of unassembled NPs in the solution. We thus dissolved the PS nodules and the new building blocks obtained were further called “slim two-patch silica (S2PS) NPs”, and carried out their assembly in THF/water mixture, triggered by the salt addition. We varied several experimental parameters for optimising the assembly process, studied its kinetics for understanding the growth mechanism, and mixed different types of S2PS NPs to mimic random or block copolymers.

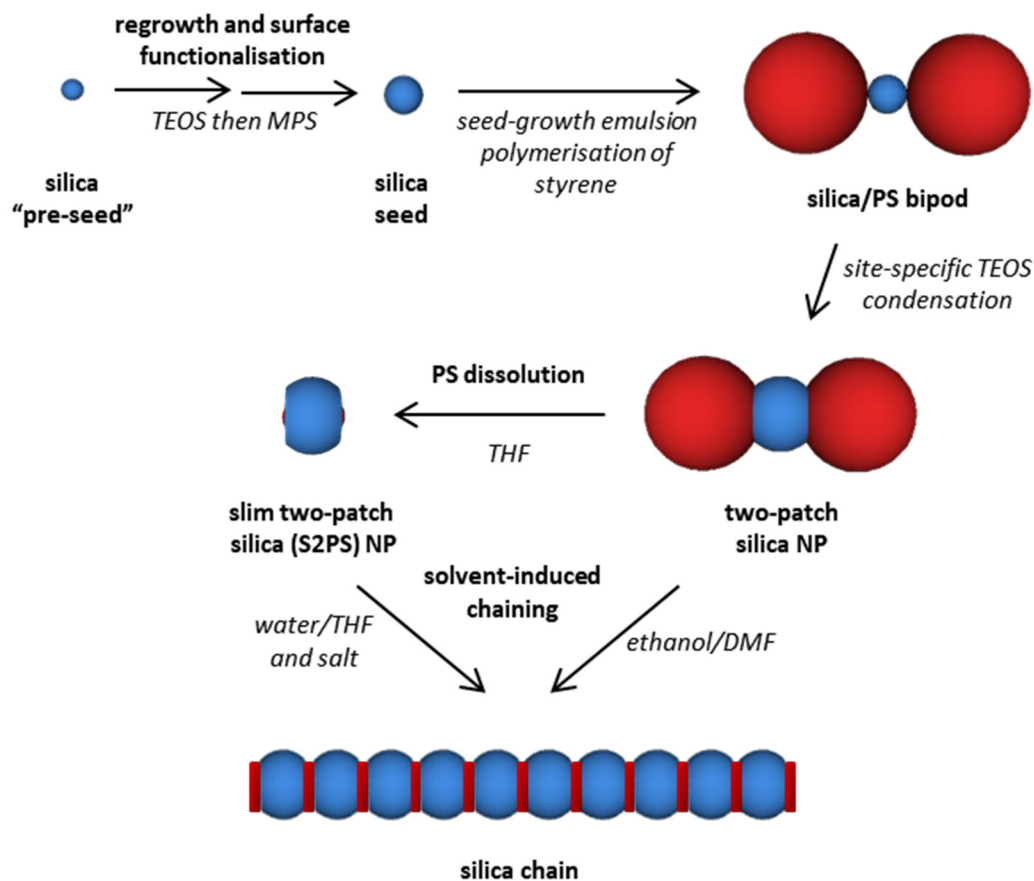


Fig. 1 Scheme summarising the patchy silica NPs preparation and their assembly into chains.

3.2 Materials and methods

3.2.1 Materials

Styrene (99.5%, with c.a. 50 ppm 4-tert-butyl catechol as stabiliser), sodium dodecyl sulphate (SDS, 99%), L-arginine (99%), sodium persulphate ($\text{Na}_2\text{S}_2\text{O}_8$, $\geq 99\%$), tetraethoxysilane (TEOS, $\geq 99\%$), (3-aminopropyl)triethoxysilane (APTES, 99%), (3-mercaptopropyl)trimethoxysilane (MPTMS, 95%), hydroxylamine hydrochloride ($\text{NH}_2\text{OH}\cdot\text{HCl}$, 98%), gold chloride hydrate (HAuCl_4 , 99.999%), potassium carbonate (K_2CO_3) and tetrakis(hydroxymethyl)phosphonium chloride solution (THPC, 80% in water), sodium hydroxide ($\geq 98.5\%$, microprills), dimethylformamide (DMF, $\geq 99\%$), and tetrahydrofuran (THF, contains 250 ppm BHT as an inhibitor) were purchased from Sigma-Aldrich. Methacryloxypropyltrimethoxysilane (MPS, 98%) was purchased from ABCR, ammonia (28-30%) and sodium chloride (NaCl) from JT. Baker, ethanol (99%) from Atlantic Labo and Synperonic[®] NP 30 from Fluka. Deionised water with a resistivity of $18.2 \text{ M}\Omega\cdot\text{cm}$ at 25°C was obtained from a Milli-Q system (Millipore). All chemicals were used without further purification.

3.2.2 Silica seed synthesis by sol-gel chemistry and surface functionalisation

Silica “pre-seeds” were first obtained according to a previously published recipe where TEOS was slowly hydrolysed at the surface of an L-arginine aqueous solution.¹⁸ Typically, 100 mL of an L-arginine aqueous solution (6 mM) were added in a 150-mL vial thermostated with hot water circulation at 60°C and equipped with a reflux condenser and a 3-cm Teflon[®]-coated stirring bar (Fig. 2). Then, 10 mL TEOS were gently added in order to create a top organic phase. The stirring rate was adjusted to maintain the organic phase undisturbed and the aqueous phase efficiently mixed (~150 rpm). The reaction was stopped 2 h after the organic phase had completely disappeared (typically after 3 or 4 days). Silica pre-seeds concentration was determined by gravimetric analysis from dried extracts. In a given volume, the number of silica pre-seeds N_{silica} was calculated from the silica concentration and the average particle diameter, assuming that the particles were spherical and their density was 2.2 g/cm³.

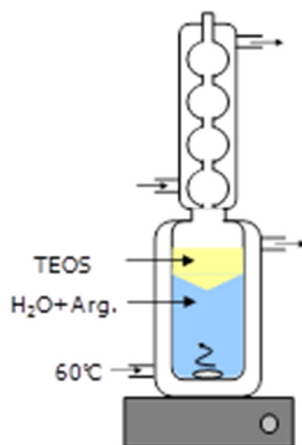


Fig. 2 Scheme of the setup used for the synthesis of the silica pre-seeds.¹⁹

The regrowth stage was performed in conventional Stöber’s conditions²⁰ at RT in a conventional 1-L glass flask where 455 mL ethanol, 35 mL of the ammonia solution and 10 mL of the aqueous dispersion of silica “pre-seeds” were successively introduced. The proper volume of TEOS, as calculated according to the following equation, was added afterwards using a syringe pump at the rate of 0.5 mL/h.

$$V_{TEOS} = \frac{M_{TEOS} \cdot \rho_{silica}}{M_{silica} \cdot \rho_{TEOS}} \cdot N_{silica} \cdot \frac{\pi}{6} \cdot (D_t^3 - D_i^3)$$

where D_i and D_t are the initial and targeted diameter of the silica NPs, respectively; M and ρ mean the molecular weight and density, respectively. The mixture was stirred till the completion of the TEOS addition.

After checking of the seed size and concentration, the reacting mixture was transferred into a three-neck round flask equipped with a reflux condenser and the coupling agent MPS was injected in one shot. This amount was previously calculated from the following equation to get a nominal surface density d_{MPS} expressed in molecule/nm².

$$V_{MPS} = \frac{6 \cdot d_{MPS} \cdot M_{MPS} \cdot V_{silica\ dispersion} \cdot C_{silica\ dispersion}}{N_A \cdot \rho_{MPS} \cdot \rho_{silica} \cdot D_{silica}}$$

where M , ρ , C and D represent the molecular weight, density, concentration and diameter, respectively, and N_A is the Avogadro number.

The reacting medium was let to age for 3 h at RT and 1 h under the reflux of ethanol. We concentrated the dispersion with the rotary evaporator to remove ethanol and ammonia and redispersed the NPs in water. The final concentration of silica seeds in water was determined by measuring the mass of a dried extract.

3.2.3 Synthesis of silica/polystyrene bipods by seed-growth emulsion polymerisation

The silica/PS bipod-like NPs were synthesised according to a seed-growth emulsion polymerisation recipe previously optimised by our group.^{17,21} Typically, in a 250-mL three-neck round flask equipped with a condenser, we prepared 50 mL of an aqueous dispersion of silica seeds ($1.8 \cdot 10^{16}$ part/L) including 3 g of the surfactant mixture made of Synperonic[®] NP30 (99 wt. %) and SDS (1 wt. %). We thoroughly deaerated the dispersion by bubbling nitrogen under stirring (170 rpm). Subsequently, 5.5 mL styrene was added and the medium was emulsified for 20 min at 250 rpm stirring at RT. The temperature was increased to 75 °C and 1.3 mL Na₂S₂O₈ solution (0.1 g dissolved in 4 mL water) was introduced to initiate the polymerisation. After 6 h, the monomer-to-polymer conversion was determined by the dried extract method. We characterised the multipods by TEM and determined statistically their morphological distribution and the average size of their PS nodules.

3.2.4 Derivatisation into S2PS NPs

To regrow the silica core from 55 to 155 nm, we mixed 1 mL of the as-obtained silica/PS bipods dispersion with 45.5 mL ethanol and 3.2 mL ammonia in a 100-mL round flask equipped with a magnetic stirrer. Then we added 1.6 mL of a TEOS solution (10 vol. % in ethanol) at the rate of 0.5 mL/h. One hour after the completion of TEOS addition, the silica/PS bipods were washed

by two centrifugation/redispersion cycles in ethanol (12,000 g; 10 min; 25 mL). Their concentration was finally adjusted to $3.6 \cdot 10^{14}$ part/L concerning the silica core number.

To regrow the silica core from 55 to 190 nm, we gave up the previous regrowth technique with the addition of TEOS in one shot, because of the increasing risk of a secondary, *i.e.* homogeneous, silica nucleation. We preferred to use an iterative method during which the volume of TEOS was added in two shots, *e.g.* 0.2 mL then 0.3 mL, including an intermediary washing stage. Their concentration was finally adjusted to $3.6 \cdot 10^{14}$ part/L based on the silica core number.

For some experiments, the surface of the freshly regrown silica core was functionalised by aminopropyl or mercaptopropyl groups, which was carried out by direct injection of the APTES or MPTMS, respectively, at a nominal surface density of 50 molecules/nm². The dispersion was aged at RT overnight and the two-patch silica NPs were washed by two centrifugation/redispersion cycles in ethanol (12,000 g; 10 min; 25 mL).

S2PS NPs were obtained by the dissolution of the PS nodules. All the macromolecules that were just physically entangled were washed away thanks to three centrifugation/redispersion cycles (12,000 g; 10 min; 20 mL) with THF. The concentration of the S2PS NPs was finally adjusted to $3.6 \cdot 10^{14}$ part/L.

3.2.5 Assembly of two-patch silica nanoparticles into chains

For two-patch silica NPs, the solvent-induced assembly experiments were performed into 1.5 mL Eppendorf® tubes using an ethanol/DMF mixture with a different volume fraction of DMF. The sum of the DMF and ethanol volumes were systematically equal to 1 mL. Typically, a known volume of the ethanol dispersion of NPs was collected and mixed with absolute ethanol, and then DMF was injected prior to vortexing for 30 s. The Eppendorf® tubes were put on a roller-mixer at 60 rpm for 10 min at RT. The dispersion might be centrifuged at a specified speed for 10 min and the pellet was redispersed into ethanol after removal of the supernatant prior to the TEM grid preparation.

For S2PS NPs, the solvent-induced assembly experiments were performed into 25-mL glass bottles equipped with polypropylene caps using a saline/THF mixture. The sum of the liquid volumes was systematically equal to 5 mL. First, the THF dispersion of NPs was extended with the right volume of THF and gently stirred. Then, the 20-mM NaCl aqueous solution was added dropwise. The mixture was let to age at RT under gentle magnetic stirring. Lastly, 40 mL

ethanol was used to freeze the assemblies, which were subsequently recovered through centrifugation (12,000 g; 10 min) prior to storage in ethanol.

3.2.6 Formation of gold-modified chains

To enrich the diversity of chains, we tried to prepare gold-modified chains through below two routes, where the synthesis of Duff gold seeds, solution #1 and #2 for enlarging gold NPs was described in sections 2.2.6 and 2.2.8 of Chapter 2.

Route #1: Chains were fabricated from 155-nm S2PS NPs following the reference protocol (*i.e.* THF/water 7/3, S2PS NPs 0.5 mL, NaCl 6 mM and an incubation time of 19 h). The surface of the silica NPs was thus functionalised with APTES with a nominal density of 50 molecules/nm² at RT overnight. The modified chains were recovered by centrifugation (12,000 g; 10 min; twice) and redispersed in 5 mL ethanol by sonication for gold decoration.

Route #2: The 155-nm two-patch silica NPs were modified with APTES (50 molecules/nm²) before dissolving the PS nodules. Chains made of amino-S2PS NPs were obtained from the reference protocol and redispersed in 5 mL ethanol for gold decoration.

Then, 0.5 mL of the chain dispersion in ethanol from Route #1 or #2 was mixed with 2.5 mL Duff gold NPs solution overnight under roller mixing (60 rpm) and the excess amount of gold seed was removed by twice centrifugation at 5000 g for 20 min. The gold-seed decorated chains were subsequently redispersed in 5 mL water; 3 mL of solution #2 and 1.5 mL of solution #1 were added at the speed of 1.5 mL/h to regrow the gold NPs. The gold decorated chains were recovered by centrifugation (12,000 g; 10 min) and redispersed in 0.5 mL ethanol prior to TEM grid preparation.

3.2.7 Characterisation

All samples were dropped on carbon-coated copper film (300 mesh) with/without ethanol dilution with a pipette and dried at RT. We let the liquid evaporate in the open air at RT and placed the grids in a box away from dust. TEM images were obtained on Hitachi H600 or JEOL JEM 1400 plus, operating at an acceleration voltage of 75 kV or 120 kV, respectively. Statistics from image analysis were performed over at least 500 items for the silica pre-seeds, 55-nm silica seeds and silica/PS bipods, and 200 items for the silica chains.

3.3 Results and discussion

3.3.1 Synthesis of the patchy silica nanoparticles

The two-patch silica NPs were prepared according to the multistep pathway summarised in Fig. 1.

1. The formulae of the main chemicals are represented in Fig. 3.

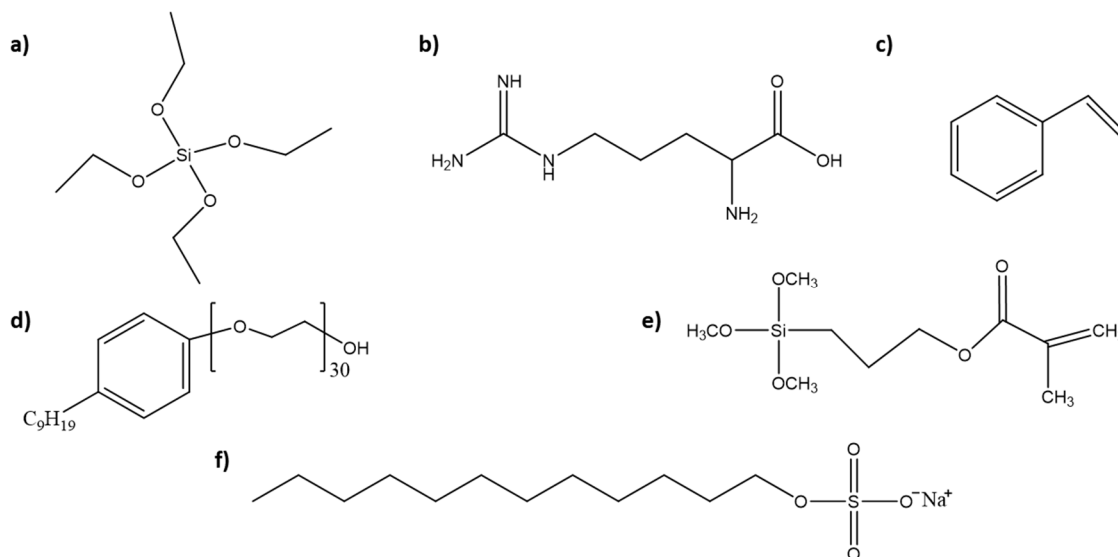


Fig. 3 Chemical formulae of the main reagents used to prepare the silica/PS bipods through a seed-growth emulsion polymerisation: a) TEOS, b) L-arginine, c) styrene, d) Synperonic[®] NP 30, e) MPS and f) SDS.

3.3.1.1 Synthesis of the 55-nm silica seeds

The batch of surface-modified silica NPs used later as seeds for the emulsion polymerisation of styrene shall be as size-monodisperse as possible. Moreover, it was previously shown that silica/PS bipods are readily obtained with a good morphology yield from seeds with a diameter of 55 nm.¹⁷

Among the numerous recipes deriving from the Stöber's process²⁰, which aimed to control the nucleation/growth mechanisms for widening the accessible size range and narrowing the size distribution for a given batch, we preferred the two-stage Hartlen's procedure.¹⁸ For a better control of the rate-determining TEOS hydrolysis step, Hartlen and co-workers used L-arginine as a catalyst making the reacting medium less alkaline (pH = 9-10 against pH = 11-12 with ammonia) and therefore slowing down the hydrolysis stage, especially as the surface area of the interface between the non-hydrolysed TEOS and the alkaline solution is weak. Moreover, the moderate pH value limits the silica solubility and hence promotes the condensation stages, *i.e.* the growth process. Lastly, it was suggested that L-arginine could stabilise the silica NPs avoiding the aggregation phenomena sometimes reported in hydro-alcoholic media. We used

the Hartlen's recipe to prepare silica "pre-seeds" typically with an average diameter of 26 nm and a polydispersity index $PDI = 1.02$ (Fig. 4a). For reaching the targeted size of 55 nm, we used the conventional Stöber's conditions, *i.e.* hydro-ethanolic medium and ammonia. The extra amount of TEOS was calculated and slowly added using a syringe pump to avoid secondary nucleation. Fig. 4b shows a representative TEM image of the as-obtained silica NPs. Their average diameter was 54.8 nm with a polydispersity index $PDI = 1.009$.

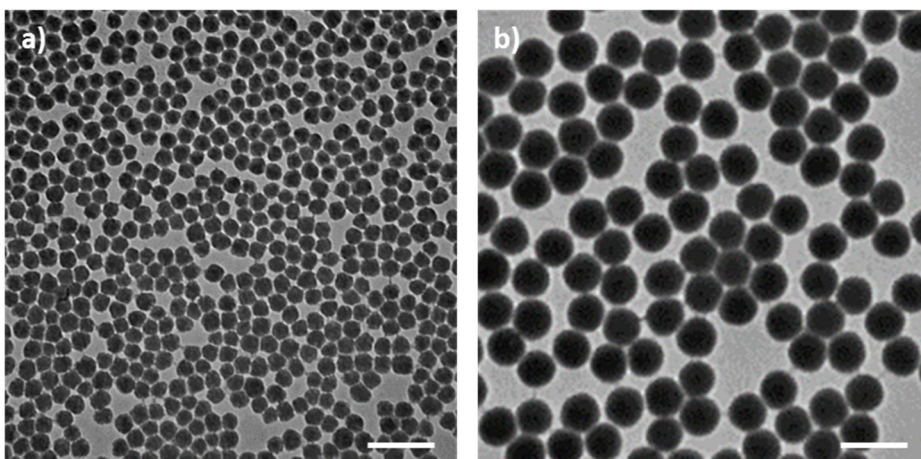


Fig. 4 Representative TEM images of a) the silica "pre-seeds" and b) the 55-nm silica NPs after regrowth of the "pre-seeds". Scale bars: 100 nm.

Lastly, the surface of the silica NPs was treated with the methacryloxypropyltrimethoxysilane (MPS) coupling agent in order to create reactive polymerisable loci promoting the surface capture of the growing macromolecules and therefore the nucleation/growth of the PS nodules. Typically, the nominal surface grafting density of MPS was fixed at 0.35 molecule per nm^2 , where we assumed that the MPS grafting is quantitative. We know qualitatively that higher values lead to core-shell morphologies, as the more organophilic the seed surface, the more wetting the PS phase.²² Conversely, when the nominal surface density is too low, the PS nodules are too weakly bonded to the silica surface and leave it easily. As a conclusion, the success of this MPS surface modification is only validated through the success of the next emulsion polymerisation stage.

3.3.1.2 Synthesis of silica/polystyrene bipods by seed-growth emulsion polymerisation

The voluntary synthesis of silica/PS bipods was infrequently reported even by our group.^{17,21,23} Obtaining two co-existing PS nodules positioned in a linear arrangement with the silica core results mainly from their steric repulsion during their growth. At the early stage, the number of growing PS nodules is probably higher than two, but it decreases as far as the nodules are

growing and the silica surface is becoming too crowded, either by the expulsion of nodules or by their coalescence. The prevalence of this last event leads to larger size distribution of the PS nodules. The experimental conditions can be varied but the parameters are interdependent: the styrene concentration, the seed concentration, the surfactant concentration and the fraction of SDS in the surfactant mixture essentially made of Synperonic[®] NP30. In particular, the higher the SDS fraction, the higher the stability of the growing PS nodules, resulting in the more numerous and hence the smaller the PS nodules.

After several polymerisation trials, the optimal conditions were set as follows:

- seed concentration: $1.8 \cdot 10^{16}$ part/L
- mass fraction of SDS: 1 wt. %
- styrene concentration: 0.96 mol/L
- temperature: 75 °C
- total concentration of surfactant: 3 g/L
- duration: 6 h

The batch synthesised following the optimal conditions contained 97% of bipods, 1.8% of monopods and 1.2% of tripods as side-products (Fig. 5) and the monomer-to-polymer conversion ratio was 65-70%. These conditions are quite robust because this experiment was repeated several times and the bipod yield was never lower than 83%. The average diameter of the PS satellites was 197 nm (PDI = 1.005), and they appeared to be mainly positioned linearly with regard to the central silica seed.

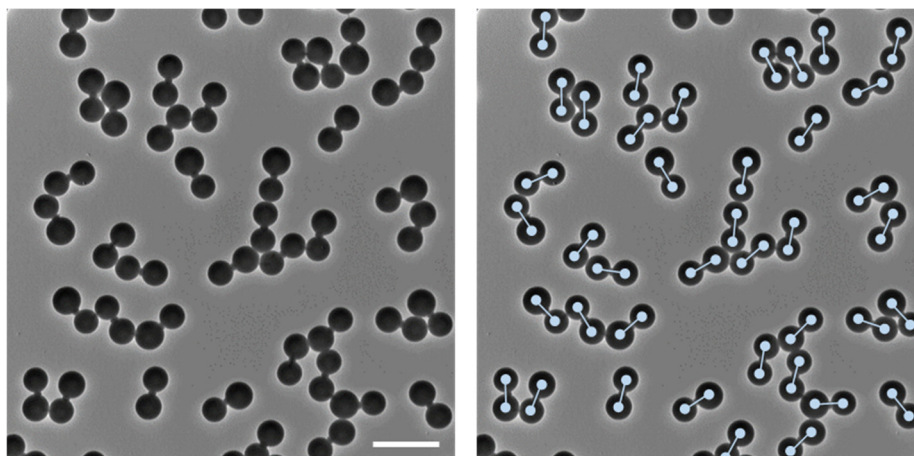


Fig. 5 Representative TEM image of the batch of silica/PS bipods whose purity at 97% is evidenced on the right image by specific blue labels showing 41 bipods and no side-product. The seed-growth emulsion polymerisation experiment was performed with the 55-nm silica seeds surface modified by MPS (0.35 molecule/nm²) in the following conditions: $[silica] = 1.8 \cdot 10^{16}$ part/L, $[styrene]_0 = 0.96$ mol/L, $[Na_2S_2O_8]_0 = 0.58$ g/L, $[surfactant] = 3$ g/L, SDS fraction = 1 wt. %, $T = 75$ °C and duration = 6 h. Scale bar: 500 nm.

3.3.1.3 Derivatization into patchy silica nanoparticles

As already demonstrated by Cyril Chomette who derivatised the grafted PS macromolecules for covalent attachment with other colloids,¹⁹ the dissolution of the PS nodules leads to uncontrolled aggregation of the silica NPs and this issue can overcome by entrapping the PS chains at the bottom of dimples. These dimples are easily created by performing a new regrowth of the silica core by site-specific condensation of TEOS. Therefore, we performed again the Stöber's conditions expecting that the newly formed silica layer fits tightly while not coating the PS nodules surface. Indeed, Fig. 6 shows that the silica core of the bipods was effectively regrown and finally exhibited a disk-like morphology with a 155-nm diameter due to the presence of both PS nodules.

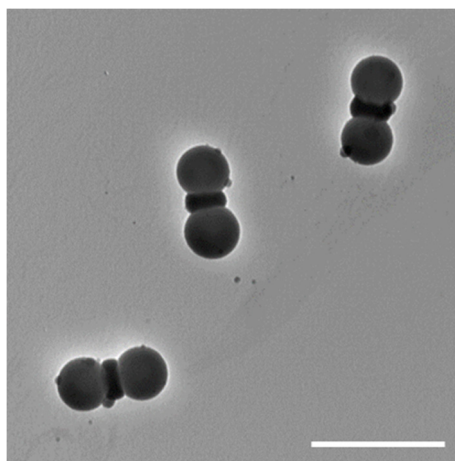
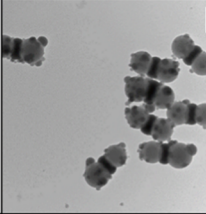
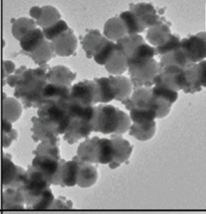
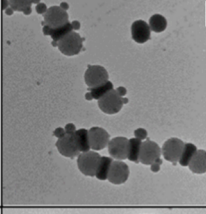
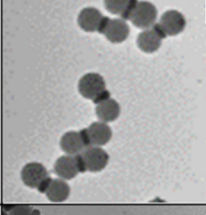
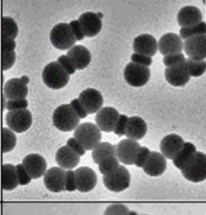
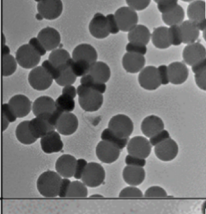
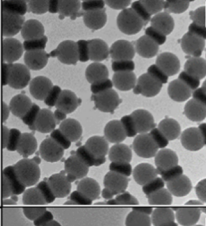


Fig. 6 Representative TEM images of the silica/PS bipods after regrowth of the silica core up to 155 nm. Scale bars: 500 nm.

As shown in Table 1, the enlargement up to 190 nm turned out to be much trickier because of the appearance of small independent silica NPs resulting from a secondary nucleation process. We failed in solving this issue by changing the experimental parameters, *e.g.* TEOS concentration, TEOS amount or TEOS addition rate. Nevertheless, we almost overcame it by performing the regrowth by iterations, *i.e.* by fragmenting the TEOS amount in smaller volumes and performing a washing stage by centrifugation/redispersion in ethanol between the fragment additions.

Table 1 Experimental conditions for the regrowth of the silica core of silica/PS bipods and representative TEM images of the obtained objects. Scale bars: 200 nm.

reacting medium		continuous regrowth		step regrowth				
0.5 mL bipod dispersion + 22.5 mL EtOH + 1.6 mL ammonia		0.125 mL bipod dispersion + 11.25 mL EtOH + 0.8 mL ammonia + 0.125 mL water						
TEOS solution in ethanol	conc. (vol.%)	10	5	10	10			
	volume (mL)	2	4	0.5	0.2 (1 st)	0.2 (2 nd)	0.1 (3 rd)	0.3 (2 nd)
	addition rate (mL/h)	1	1	0.5	0.5			
incub. time (h)	1	1	1	1	1			
size range (nm)	185-190	185-190	180-190	140-150	165-175	180-185	185-195	
TEM image								

3.3.2 Tentative chaining of the patchy silica nanoparticles in ethanol/DMF mixtures

Our first experiments were based on the assembly conditions optimised in Chapter 2 for the asymmetric silica/PS dumbbells, *i.e.* one-patch silica NPs.

We screened the influence of several parameters using the 155-nm two-patch silica NPs initially dispersed in ethanol and setting the incubation time to 10 min. We first considered the DMF fraction of 30 vol. % which corresponds to the threshold for cluster formation with the one-patch silica NPs (Fig. 9, Chapter 2). Even if the coalescence of PS nodules occurred (pointed by red arrows in Fig. 7a), no chain was formed. We thus increased the DMF fraction to 70 vol. % and then observed both the increased coalescence of PS nodules and the formation of short chains with random orientation (Fig. 7b). This result is in agreement by those obtained by Hubert¹⁷ and is due to the sphericity of the PS nodules, which can then stick together without preferential direction.

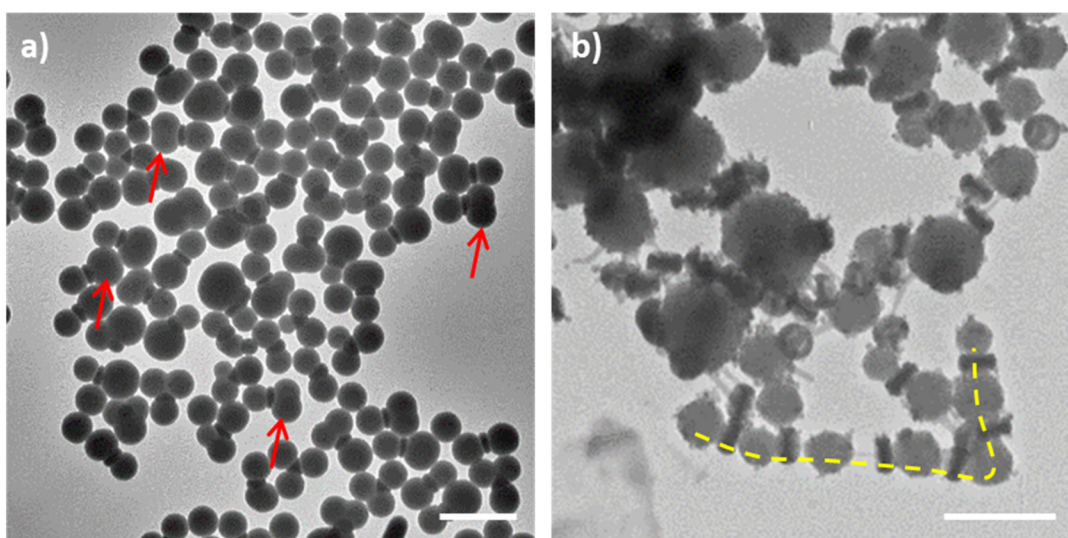


Fig. 7 Representative TEM images of the assembly mixtures of 155-nm two-patch silica NPs depending on the experimental conditions. The NPs concentration and incubation time were $1.08 \cdot 10^{13}$ part/L and 10 min, respectively. The DMF vol. % and centrifugation speed were: a) 30%, 12,000 g, b) 70%, 4,000 g. Scale bars: 500 nm.

3.3.3 Derivatisation into slim two-patch silica nanoparticles

Shrinking the PS nodules of two-patch silica NPs can theoretically increase the linear directionality of the formed chains. In this way, the PS nodules were dissolved in THF in order to remove the macromolecules that were just physically entangled. As shown on the TEM image of Fig. 8, the resulting disk-like patchy silica NPs are so slim that they are lying on one

of their sides onto the TEM grid. The black dot in the centre of the NPs corresponds simultaneously to the protuberance of the initial silica seed and non-dissolved PS macromolecules, which are chemically grafted onto its MPS-modified silica surface. This carbon-rich area was previously evidenced by energy-dispersive X-ray spectroscopy analyses coupled with scanning transmission electron microscopy on tetravalent patchy silica NPs.²⁴ These PS “residues” can be considered as the patches that are expected to become sticky in a good/bad solvent mixture and serve as the “bridge” in the forthcoming assemblies.

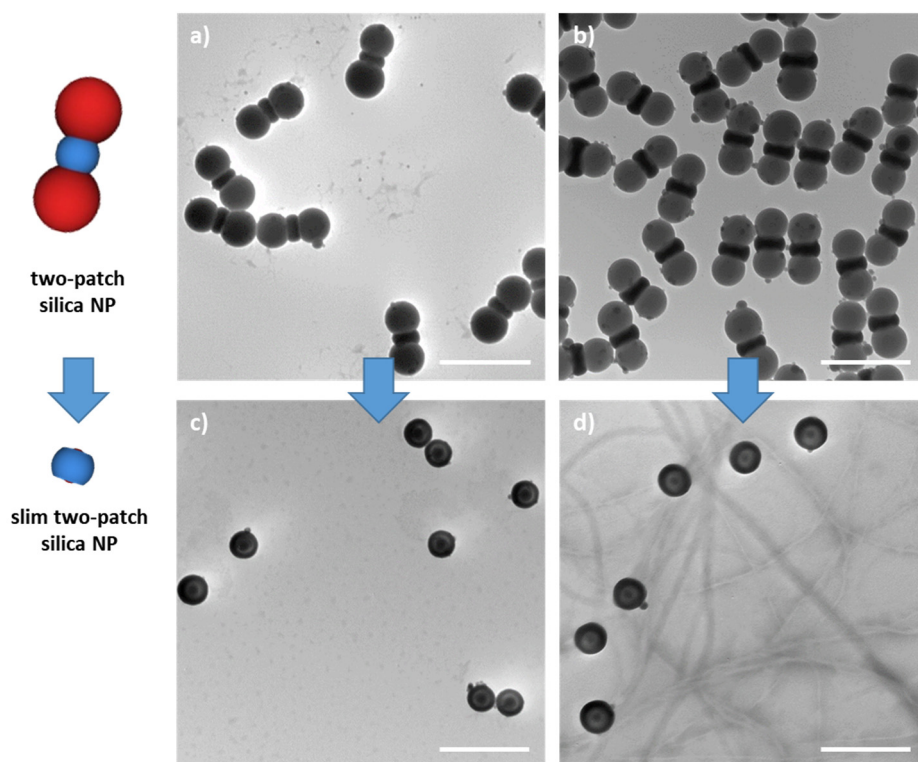


Fig. 8 Representative TEM images of a) 155-nm and b) 190-nm two-patch silica NPs; c) and d) slim two-patch silica NPs after the dissolution of the PS nodules in THF (12,000 g; 10 min). Scale bars: 500 nm.

3.3.4 Chaining of the 155-nm slim two-patch silica nanoparticles in salted water/THF mixtures

According to Kumacheva and co-workers^{25,26}, gold particles grafted with polymer brushes can be assembled to globules, chains, *etc.* through hydrophobic interaction by controlling the solvent quality and the polymer molecular weight. As mentioned above, the covalently-bonded PS chains remain grafted in the dimples after the silica core regrowth and THF dissolution/washing cycles in our system, which can be treated as the polymer brush on metallic NPs surface compared to the Kumacheva’s systems where \bar{M}_n varies from $5 \cdot 10^3$ to $5 \cdot 10^4$ g/mol. However, the average molecular weights of PS in our NPs are much higher and quite tricky to be tuned. Values of \bar{M}_n and \bar{M}_w of the free PS macromolecules on the tetrapod were previously

estimated at 540,000 g/mol and 980,000 g/mol, respectively.^{19,23} These values should be indeed similar to those of the bipods thanks to the alike polymerisation parameters. It is noteworthy that the molecular weight of the free PS chains is similar to that of the grafted ones on the silica surface.^{27,28}

The 155-nm S2PS NPs initially dispersed in THF (0.5 mL) were first incubated in THF/water (70/30 vol./vol.) mixture, where the total volume was 5 mL and the particle concentration was $3.6 \cdot 10^{13}$ part/L. The S2PS NPs remained isolated and no chain was observed after 24 h (Fig. 9a) and 65 h (Fig. 9b) incubation. The 10 times increase of the NPs concentration did not accelerate the chaining (Fig. 9c) and only short chains could be seen after 20 days of incubation (Fig. 9d). A similar result was observed when the THF/water ratio was fixed to 30/70 (vol./vol.) (Fig. 9e). This result could be due to the negatively charged silica surface (the zeta potential of S2PS NPs in water was - 42 mV at pH 5.6), that promotes electrostatic repulsions between the NPs and hinders the chain formation. We thus decided to add sodium chloride in the medium in order to screen the repulsive interactions. The influence of the salt concentration, incubation time, solvent quality, concentration of the silica NPs, *etc.* was studied.

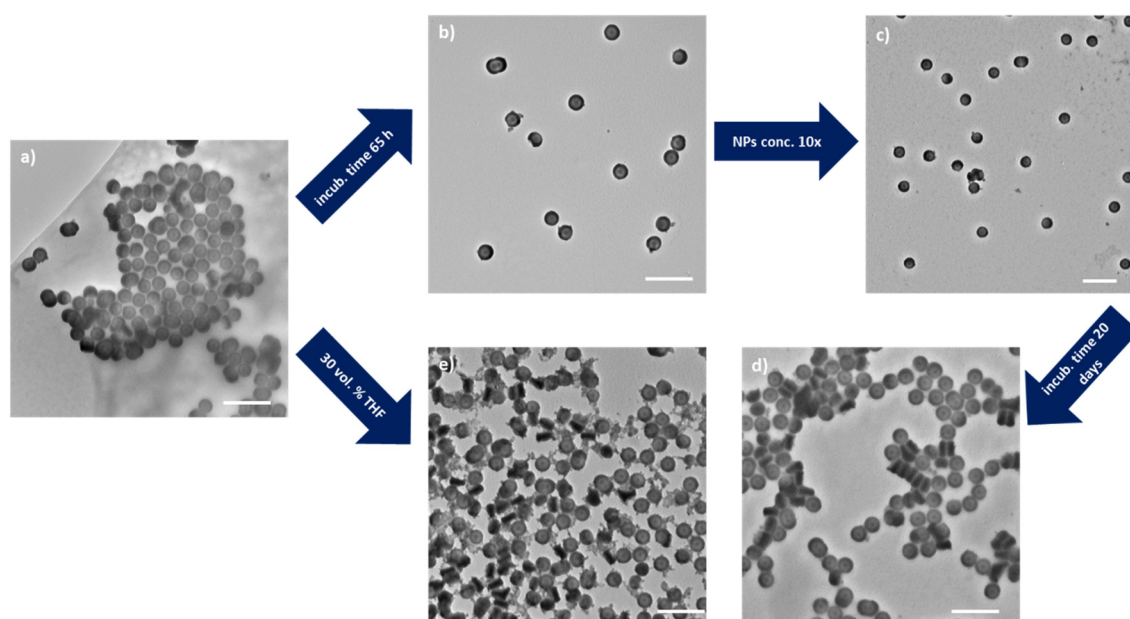


Fig. 9 TEM images of 155 nm S2PS NPs incubated in a THF/water mixture under different experimental conditions. a) $t = 24$ h, $3.6 \cdot 10^{13}$ part/L, 70 vol. % THF; b) $t = 65$ h, $3.6 \cdot 10^{13}$ part/L, 70 vol. % THF; c) $t = 65$ h, $3.6 \cdot 10^{14}$ part/L, 70 vol. % THF; d) $t = 20$ days, $3.6 \cdot 10^{14}$ part/L, 70 vol. % THF; e) $t = 24$ h, $3.6 \cdot 10^{13}$ part/L, 30 vol. % THF. Scale bars: 500 nm.

3.3.4.1 Influence of the salt concentration

The assembly medium consisted of 1.5 mL NaCl solution, 0.5 mL S2PS NPs dispersion and 3 mL THF, where the salt concentration was recalculated considering the 30% volume fraction of aqueous solution in the binary solvent mixture. The salt concentration varied from 1.5 mM to 15 mM in the following study and the incubation time was set to 43 h. It should be noticed that the TEM images in Fig. 10, 11 and 12 were obtained by using the original solution to prepare TEM grid without any purification step. The different images corresponding to the variable salt concentration are shown in Fig. 10. At low salt concentration (1.5 mM), several short chains with numerous isolated S2PS NPs can be seen, which means that 1.5 mM NaCl can incur the assembly of NPs but not with high efficiency (Fig. 10a). Relatively long chains with a maximum of 15 units can be observed when the salt concentration was increased to 3 mM despite not all the particles were chained, as in the 1.5 mM salt system (Fig. 10b). At higher salt concentrations (6 and 15 mM), the formation of long chains is observed in Fig. 10c,d with less isolated S2PS NPs. The highest salt concentration (15 mM) has no discernible effect on the chain generation in terms of their length^{‡‡} in comparison with 6 mM. The observed curvature of the chains (Fig. 11d) is possibly ascribed to the presence of asymmetric S2PS NPs resulting from bipods with two PS nodules forming an angle slightly different from 180° and/or the flexibility of the PS “bridge” between two S2PS NPs during the assembly stage. A 6 mM salt concentration was adopted for the rest of the study except explicitly mentioned.

^{‡‡} No measurement of the chain length was performed for the 155-nm silica NPs assembly process except the data in 3.3.4.5.

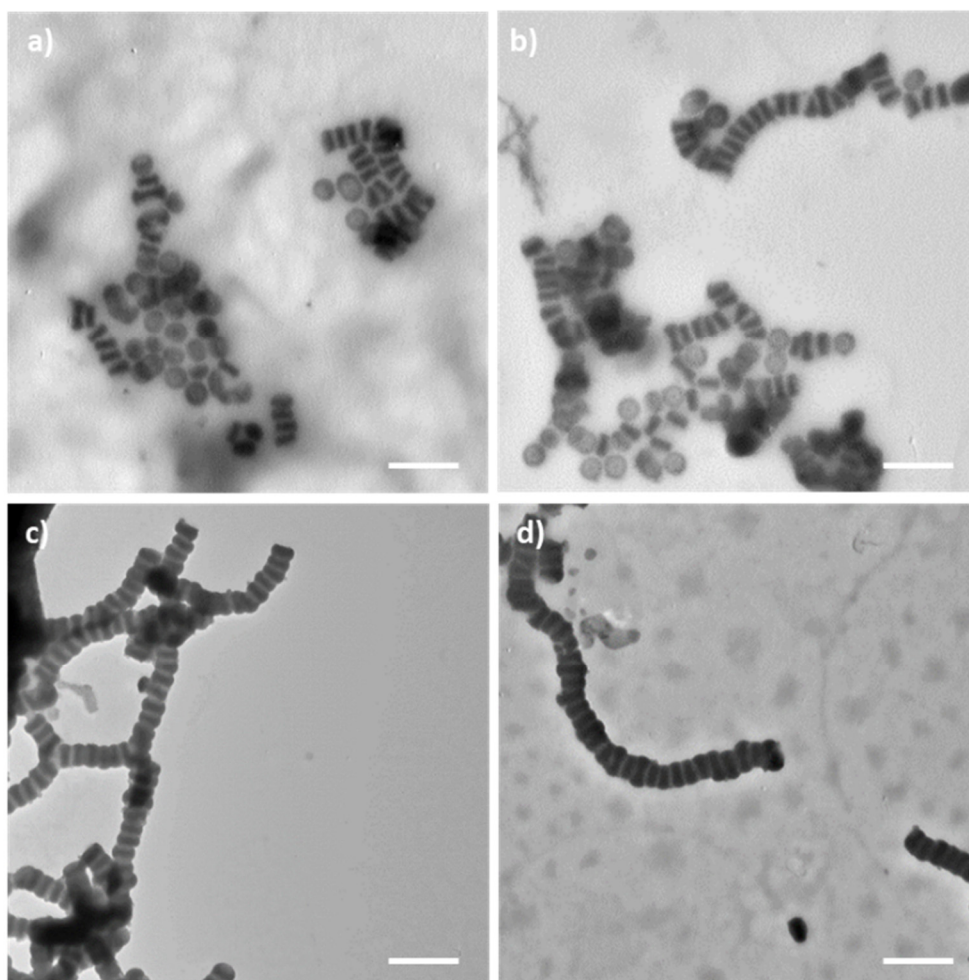


Fig. 10 Representative TEM images of the samples after incubating 155-nm S2PS NPs in a (70/30 vol./vol.) THF/salted water mixture at RT for 43 h. $[NaCl] =$ a) 1.5 mM, b) 3 mM, c) 6 mM, d) 15 mM. The particle concentration was $3.6 \cdot 10^{13}$ part/L. Scale bars: 500 nm.

3.3.4.2 Influence of the incubation time

The assembly state corresponding to different incubation times was shown in Fig. 11. The assembly was not very effective before 4 h as most of the NPs remained isolated and well dispersed in solution, with the formation of only a few short chains made of 2 to 3 particles. The chain length was increased (*i.e.* around 5-8 units on average, up to 25) when the incubation time was increased to 19 h. Almost all NPs were chained when incubated for 43 h or 70 h (Fig. 11c,d). Chain branching can be observed occasionally when three S2PS NPs stick together with an angle close to 120° due to the presence of three-patch silica NPs resulting from the silica core regrowth of few tripods present in the bipods batch (*cf.* red arrow in Fig. 11c).

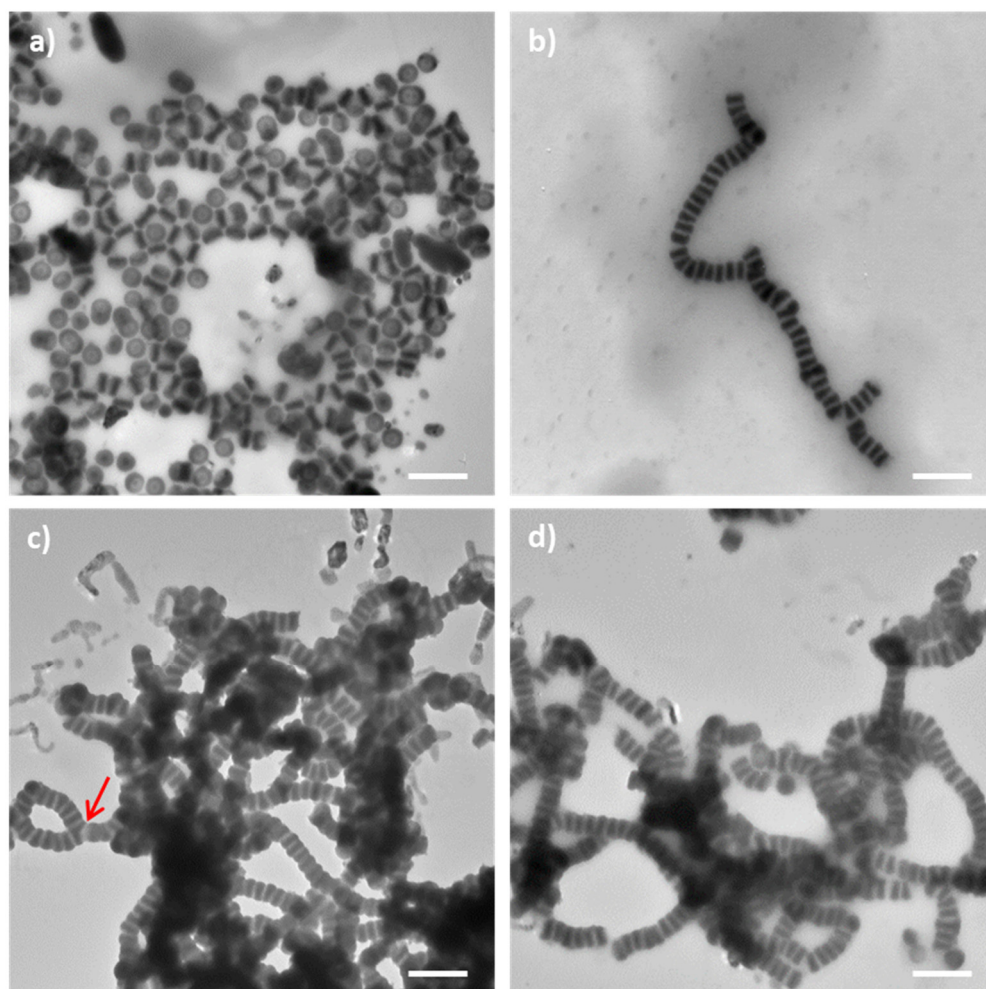


Fig. 11 Representative TEM images of the samples after incubation of 155-nm S2PS NPs for a) 4 h b) 19 h c) 43 h and d) 70 h. The assembly was performed in a (70/30 vol./vol.) THF/water mixture in the presence of 6 mM NaCl at RT. The particle concentration was $3.6 \cdot 10^{13}$ part/L. The red arrow shows a junction point resulting from the presence of a three-patch silica NP. Scale bars: 500 nm.

3.3.4.3 Influence of the solvent quality

As demonstrated by Kumacheva and co-workers,²⁵ the solvent composition strongly affects the extent of the NPs assembly. We thus varied the relative amounts of THF and salted water, while keeping the salt concentration equal to 6 mM, and studied the influence of this variation on the formation of the chains.

Decreasing the THF amount from 70% (Fig. 12c) to 50% (Fig. 12b) did not induce a noticeable variation of the chain formation, indicating that the stickiness of the PS chains remained. Further decreasing the THF volume to 30% (Fig. 12a) led to a drastic modification of the assembly process, as no long chain could be observed. Since water is a bad solvent for PS, the possible shrinkage of the PS chains within the cavities of the S2PS NPs, which thus strongly reduced the possible particular interactions, could explain this observation.

Increasing the THF volume fraction from 70 % to 90 % did not allow us to observe the formation of long chains neither (Fig. 12d). Only short ones (consisting of maximum 6 S2PS NPs) could be seen, probably due to the good quality of the solvent mixture for PS, which decreased the stickiness of the PS macromolecules.

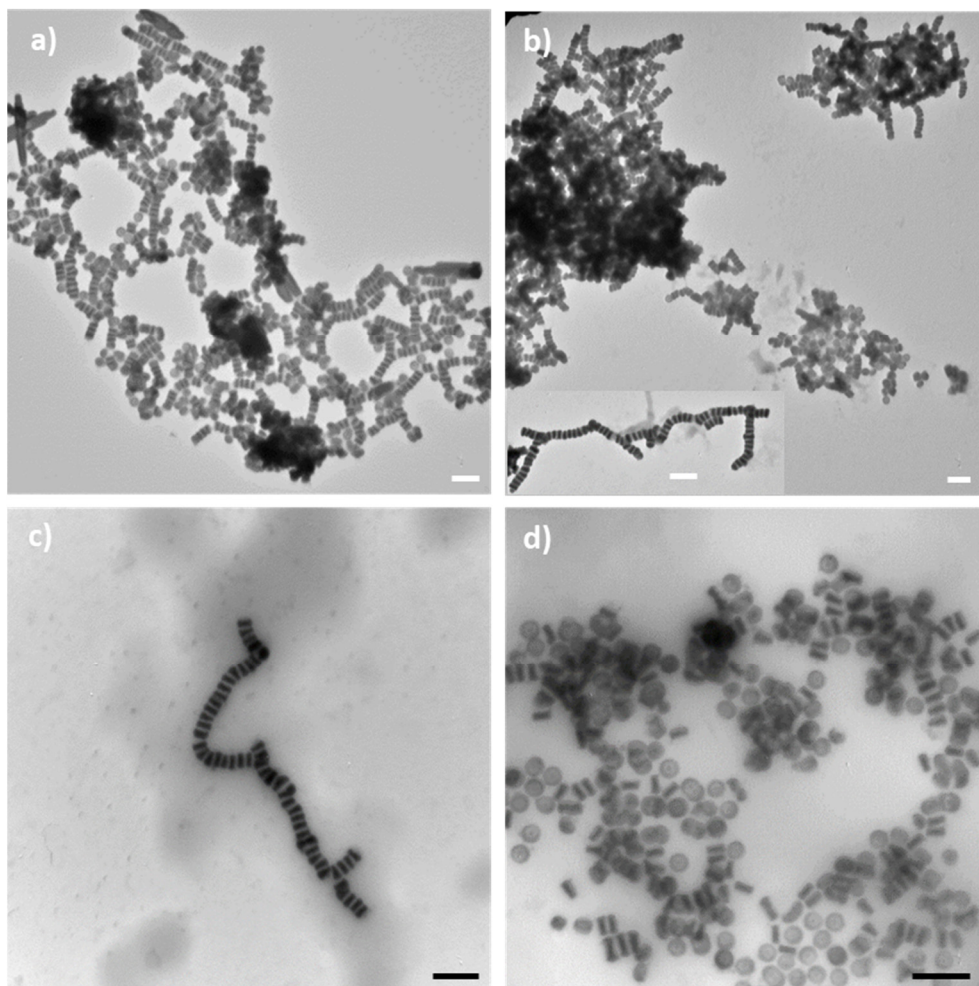


Fig. 12 Representative TEM images of the samples after incubation of 155-nm S2PS NPs in the presence of 6 mM NaCl during 19 h at RT. The particle concentration was $3.6 \cdot 10^{13}$ part/L. The (vol./vol.) THF/water ratio was a) 3/7 b) 5/5 c) 7/3 and d) 9/1. Scale bars: 500 nm

3.3.4.4 Optimising the TEM image quality

As previously mentioned, all the TEM images in Fig. 10, 11 and 12 were obtained by directly dropping the solution on the TEM grid. To improve the image quality, an excess amount of ethanol (typically 4 mL) was added into 0.5 mL of the chains solution to “freeze” them. Then, the chains were recovered by centrifugation (12,000 g; 10 min; twice). The obtained pellet was redispersed in 0.5 mL ethanol by sonication, and the solution was used to prepare the TEM grids. TEM images of chains before and after the ethanol quenching/centrifugation treatment are shown in Fig. 13. The addition of ethanol followed by centrifugation improves the quality

of the images. One also should note that the interval gap between two S2PS NPs in the chains is around 40 nm before and after the treatment, indicating that the chain structure was not loosened or destroyed during the centrifugation process. All the TEM images of chains were recorded by this method in the following sections.

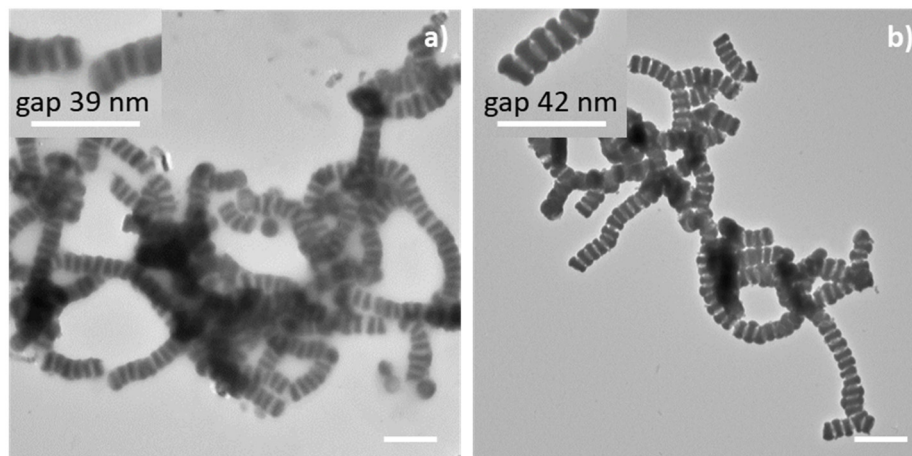


Fig. 13 Representative TEM images of the chains a) before and b) after ethanol quenching/centrifugation treatment. Scale bars: 500 nm.

3.3.4.5 Influence of the S2PS nanoparticles concentration

A series of experiments dedicated to the study of the influence of the S2PS NPs concentration was performed: a mixture of 3.5 mL of S2PS NPs in THF and 1.5 mL of NaCl aqueous solution was used, while the final salt concentration was 6 mM or 15 mM and the S2PS NPS was $2.52 \cdot 10^{14}$ part/L. The self-assembly was performed for 19 h. The formation of chains was effective when $[\text{NaCl}] = 6$ mM but many isolated particles were still visible (Fig. 14a), which was not the case when only 0.5 mL of S2PS NPs dispersion was used (Fig. 11). This could be attributed to the lower salt density relative to the NPs surface area, thereby affecting the NPs charge screening efficiency. This hypothesis was confirmed by the experiment carried out with 15 mM of salt, where long chains with 14 units on average were produced (Fig. 14b). The successful chains formation when working at higher concentration of S2PS NPs means the protocol could be scaled up by slightly tuning the salt concentration.

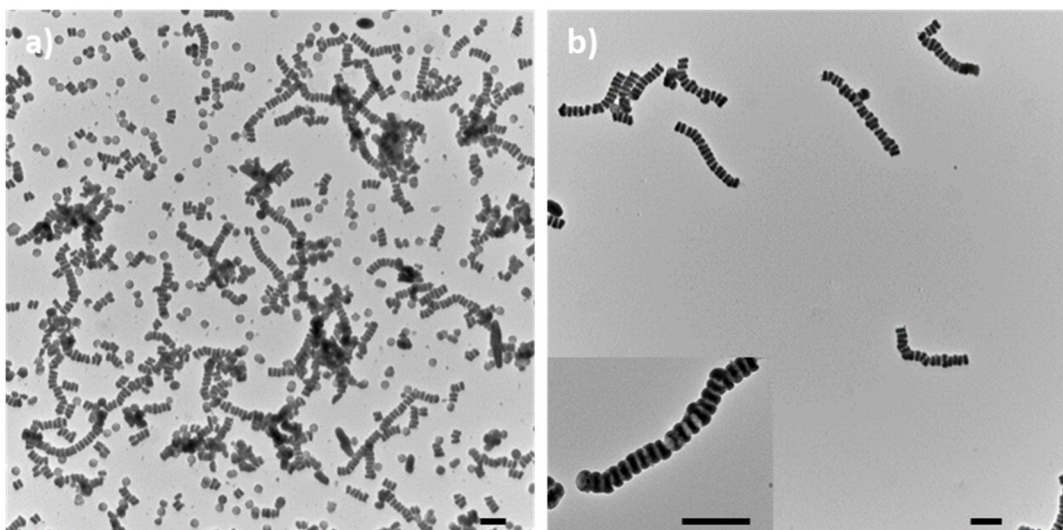


Fig. 14 Representative TEM images of the chains after incubation of 155-nm S2PS NPs in the presence of a) 6 mM and b) 15 mM NaCl during 19 h at RT. The particle concentration was $2.52 \cdot 10^{14}$ part/L. The (vol./vol.) THF/water ratio was 7/3. Scale bars: 500 nm.

3.3.4.6 Towards gold-modified chains

Gold-modified chains were fabricated according to two routes, whose difference consists in the order of the surface amination step using (3-aminopropyl)triethoxysilane (APTES) and the self-assembly step (Fig. 15).

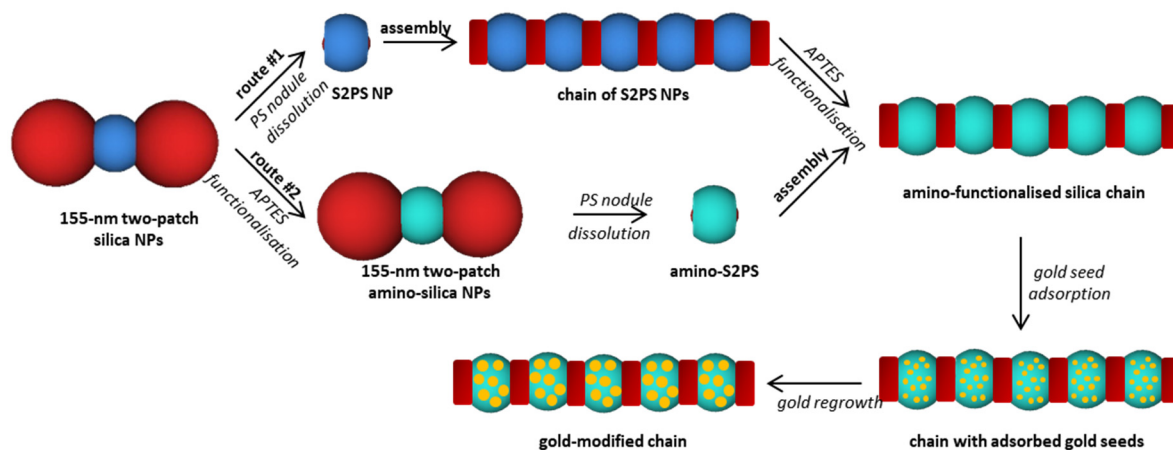


Fig. 15 Scheme of the two investigated routes to obtain gold-modified silica chains.

In the route #1, the chains assembled from S2PS were modified with APTES (Fig. 16a) and the gold seeds grafted on the silica surface were regrown to form chains whose surface was utterly coated by gold NPs (Fig. 16b). Nevertheless, gold NPs adsorption on the PS chains was also observed, probably due to the diffusion of APTES molecules into the later ones during the surface modification stage. To avoid this undesired adsorption, we developed the route #2, which should prevent the PS residues in the dimples to be exposed to APTES molecules.

The silica surface of the two-patch silica NPs was functionalised by APTES and amino-S2PS NPs were obtained after dissolving the PS nodules. The amino-S2PS NPs were assembled into chains, as shown in Fig. 16c, then gold seeds were adsorbed and regrown to give the gold-modified chains (Fig. 16d).

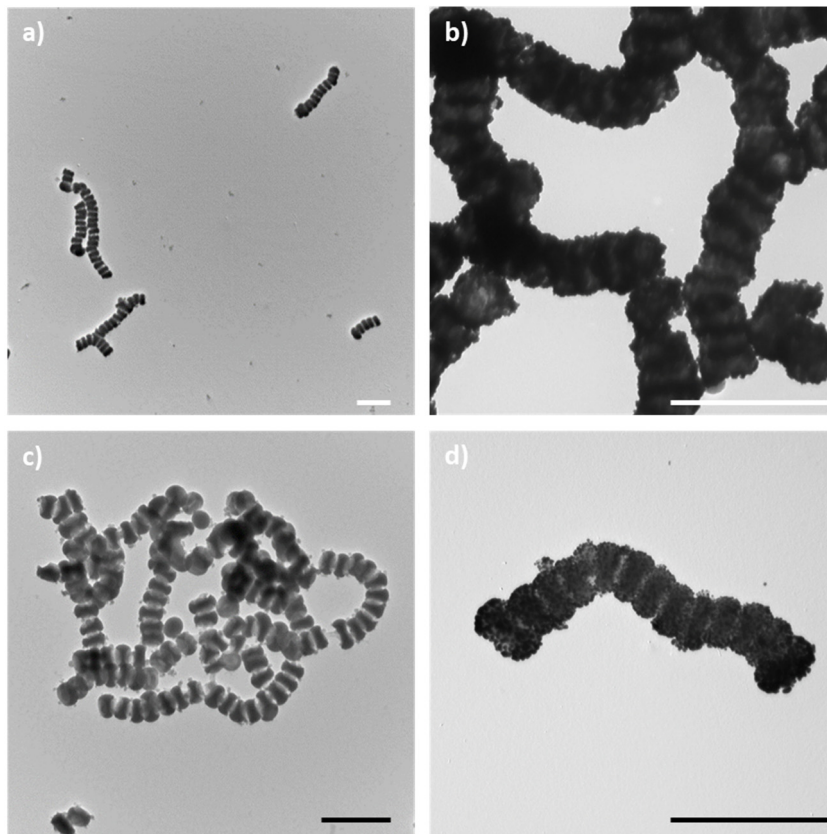


Fig. 16 TEM images of a) chains of 155-nm S2PS NPs after surface modification with APTES, b) chains decorated by gold NPs following the route #1, c) chains made of amino-S2PS NPs and d) chains decorated by gold NPs following the route #2. Scale bars: 500 nm.

3.3.5 Chaining of the 190-nm slim two-patch silica nanoparticles in salted water/THF mixtures

To extend further the range of chains that can be obtained, we studied the assembly of larger S2PS NPs, which have a 190 nm diameter. The assembly was carried out in a 7/3 (vol./vol.) THF/water mixture in the presence of 6 mM NaCl. Fig. 17a shows that chains made of 11 NPs on average were obtained after 15 h incubation. Some chains could be up to 6 μm (*i.e.* consisting of around 60 NPs) as shown in Fig. 17b. This experiment can be reproduced efficiently with a slight variation of the chain length from one batch to another.

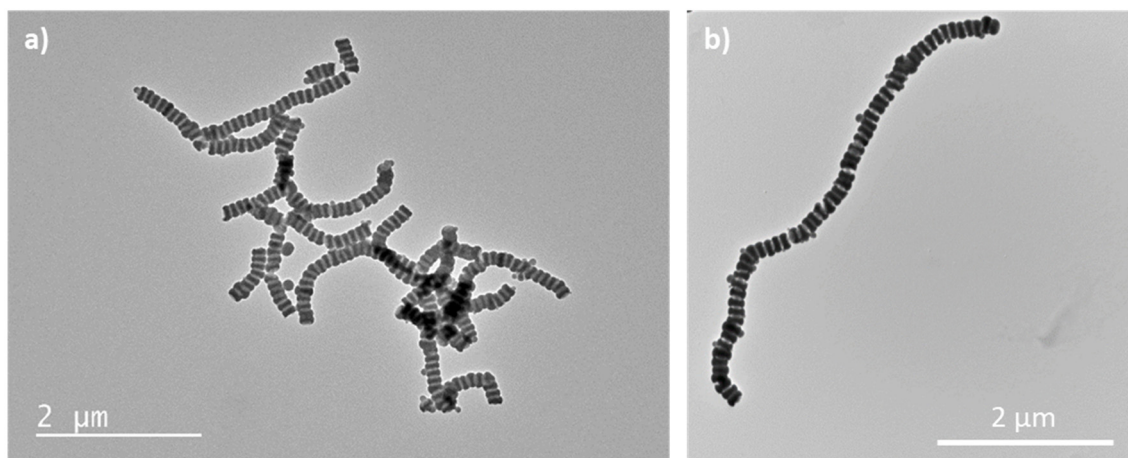


Fig. 17 Representative TEM images of the chains after incubation of 190-nm S2PS NPs in the presence of 6 mM NaCl during 15 h at RT. The (vol./vol.) THF/water ratio was 7/3.

3.3.5.1 Kinetics study

We studied the kinetics of the chains formation as a function of the incubation time and the S2PS NPs concentration, keeping the THF/water ratio constant at 7/3 and the salt concentration at 6 mM. The chain length evolution was monitored by TEM, and the average length was calculated by statistical analysis of more than 200 chains. The typical TEM images of the sample prepared with 3 mL of S2SP NPs at different incubation times are shown in Fig. 18, while Fig. 19a shows a shift of the distribution of chains with different lengths toward larger value with time, indicating the continuous growth of chains. For example, the average chain length increases from ~2.5 particles at 0.5 h to ~10.5 particles after 9 h for the sample prepared with 3 mL of S2PS NPs.

The number-average polymerisation degree (\bar{X}_n), weight-average polymerisation degree (\bar{X}_w) and polydispersity index (PDI) were calculated through the following equations to characterise the kinetics of the S2PS NPs assembly:

$$\bar{X}_n = \frac{\sum n_x x}{\sum n_x} \quad \bar{X}_w = \frac{\sum n_x x^2}{\sum n_x x} \quad PDI = \frac{\bar{X}_w}{\bar{X}_n}$$

where x is the number of S2PS NPs in the chain and n_x is the number of chains containing x S2PS NPs. The individual S2PS NPs were not counted in the statistics.

Fig. 19b shows the evolution of \bar{X}_n with time for three different volumes of S2SP NPs (ca. 0.5 mL, 2 mL and 3 mL). A linear relationship can be observed at the initial stage ($t < 2$ h), which is a characteristic of reaction-controlled step-growth polymerisation in a molecular system, in which the reactivity of the NPs is independent of the chain length.^{7,29} According to

the relation $\bar{X}_n = 2[M]_0 kt + 1$, where $[M]_0$, k and t are the initial concentration of S2SP NPs, rate constant and incubation time, respectively, which is characteristic of the kinetics of the polymerisation of bifunctional monomers with identical functional end groups,³⁰ we derived the polymerisation rate constant k of the linear fitting of $\bar{X}_n \sim t$ curves. We found that $k = 6.08 \cdot 10^5 \text{ L}\cdot\text{mol}^{-1}\cdot\text{s}^{-1}$, $k = 1.27 \cdot 10^6 \text{ L}\cdot\text{mol}^{-1}\cdot\text{s}^{-1}$ and $k = 2.32 \cdot 10^6 \text{ L}\cdot\text{mol}^{-1}\cdot\text{s}^{-1}$, for samples prepared with 3, 2, and 0.5 mL of S2SP NPs, respectively. These values are similar to that found for the copolymerisation of inorganic NPs³¹ and are two orders of magnitude larger than the value found by Kumacheva and co-workers.^{8,7} We presume that the specific shape of the S2PS NPs, which facilitates their mutual orientation, increases the polymerisation rate.

At the longer time ($t > \sim 2 \text{ h}$), a nonlinear relationship between \bar{X}_n and t started appearing (Fig. 19b), suggesting that equal reactivity of end groups is not fully held. The polymerisation of S2SP NPs seems to follow a different pathway, that is, a “diffusion-controlled” stage, which can be possibly attributed to the fact that the orientation of the chains or even their sedimentation becomes the rate-limiting factor when they become relatively long. To verify this hypothesis, we added 3 mL of S2PS NPs in a batch of chains that have been already incubated for 15 h. No longer chains were observed after 20 extra hours, indicating that new short chains preferentially formed and confirming the assumption.

Fig. 19c shows the variation of the PDI with \bar{X}_n . For all values of $[M]_0$, the PDI of growing chains is much smaller than the value predicted by Flory’s model (*i.e.* $\text{PDI} = 2 - 1/\bar{X}_n$). For example, the PDI was measured to be ~ 1.34 for $\bar{X}_n = 6$, which is much smaller than the theoretic prediction of 1.83 based on the Flory’s model. This difference is probably due to the “diffusion-controlled” polymerisation.³¹

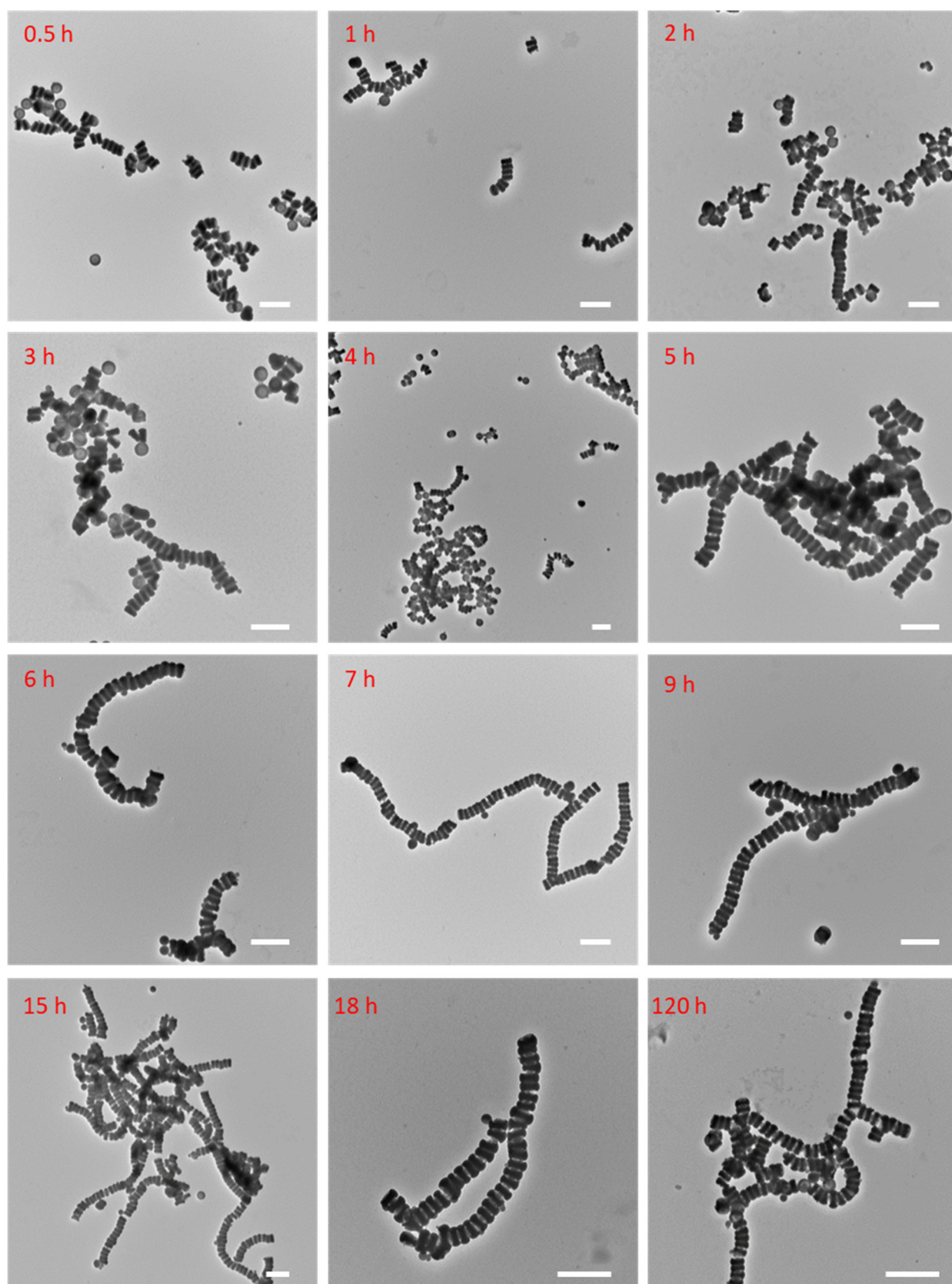


Fig. 18 Representative TEM images of the sample after incubating 3 mL of 190-nm S2PS NPs in a (70/30 vol./vol.) THF/salted water mixture at RT for different times. $[NaCl] = 6$ mM. Scale bars: 500 nm.

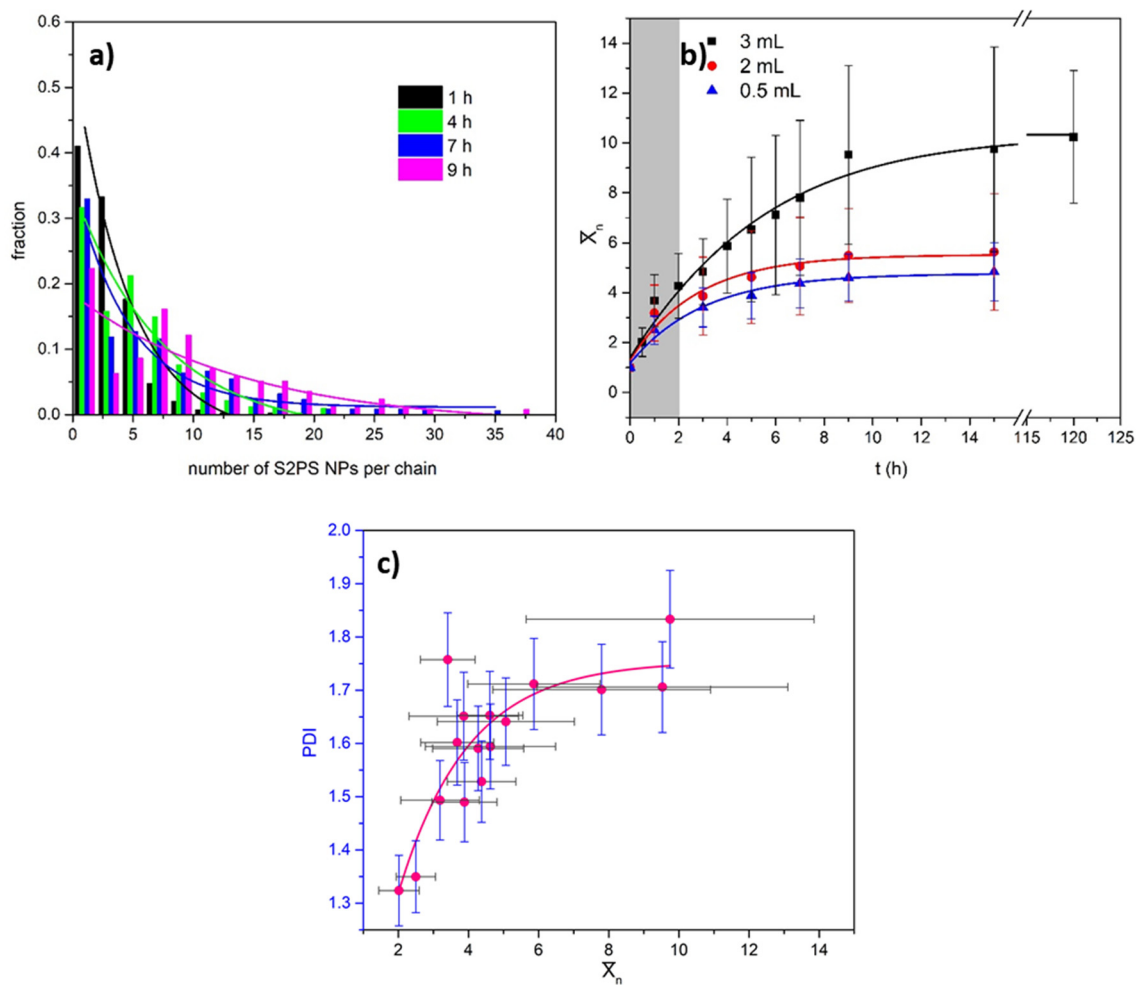


Fig. 19 a) Distribution of the chain lengths at different times, b) dependency of \bar{X}_n on time for different volumes of S2PS NPs dispersion and c) dependency of PDI on \bar{X}_n for 3 mL of S2PS NPs dispersion.

Considering the good reproducibility of chain formation from the S2PS NPs, we envisaged combining different types of particles to fabricate random copolymer-like, block copolymer-like and branched chains (Fig. 20).

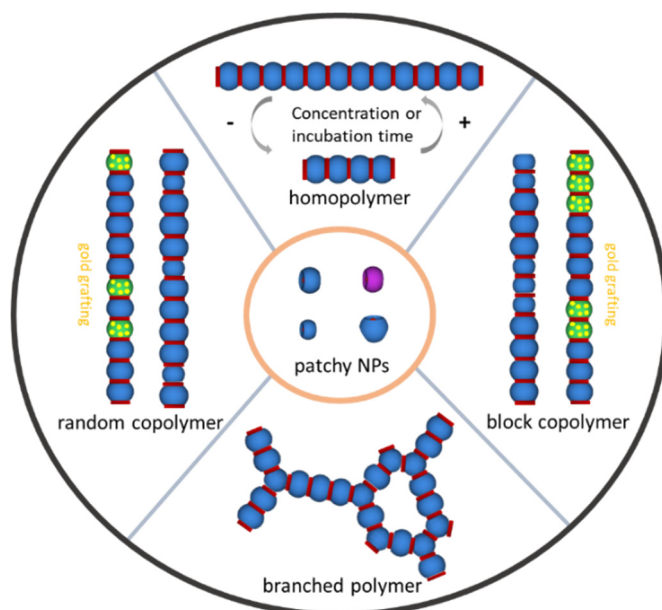


Fig. 20 Schematic representation of the different types of targeted colloidal macromolecules.

3.3.5.2 Mimicking the formation of colloidal random copolymers

The linear chains made of 150-nm or 190-nm S2PS NPs can be considered as analogues of organic homopolymers. The assembly of S2PS NPs with two different sizes or chemical properties can thus lead to the formation of random copolymer-like silica chains, as illustrated in Fig. 21.

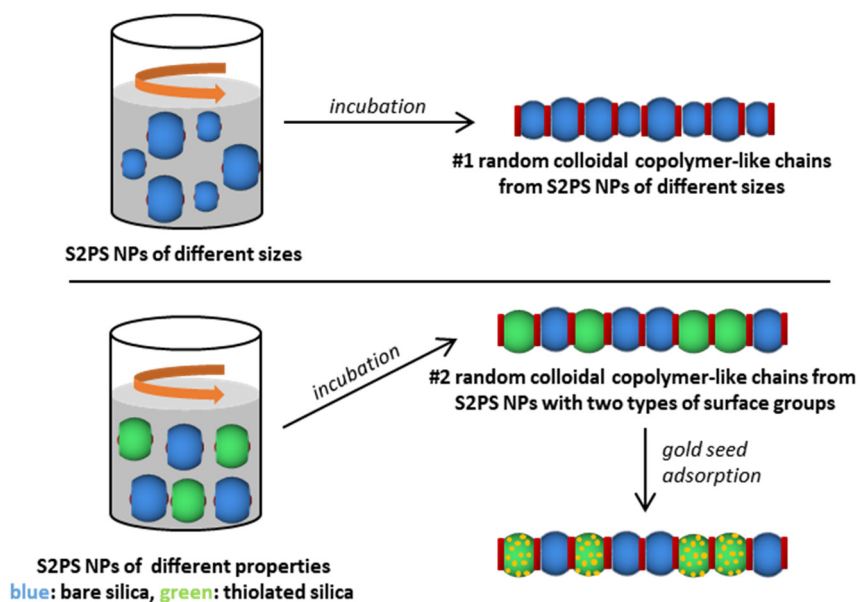


Fig. 21 Scheme illustrating the two routes investigated to prepare random copolymer-like silica chains.

Route #1 using S2PS NPs of different sizes

The protocol followed here is similar as before except replacing the 190-nm S2PS NPs by a mixture of 190-nm and 155-nm NPs at a proper volume ratio, adjusted at: 9/1, 4/1, 1/4 and 1/9. The two different types of particles tend to assemble without any selectivity in all cases, thereby forming random copolymer-like chains, as shown in Fig. 22. The chain branching shown in Fig. 22c was due to the bonding of PS chains of three S2PS NPs, which thus formed an angle close to 120°. This phenomenon was more frequent for smaller S2PS NPs and this is consistent with the comment already mentioned in Chapter 1: when the patch-to-particle size ratio is large enough, one patch can interact with more than one another. This is not possible at the atomic level where the valence is dictated by the number of available orbitals, and this is the main concession made to the extension of valence at the colloidal scale.

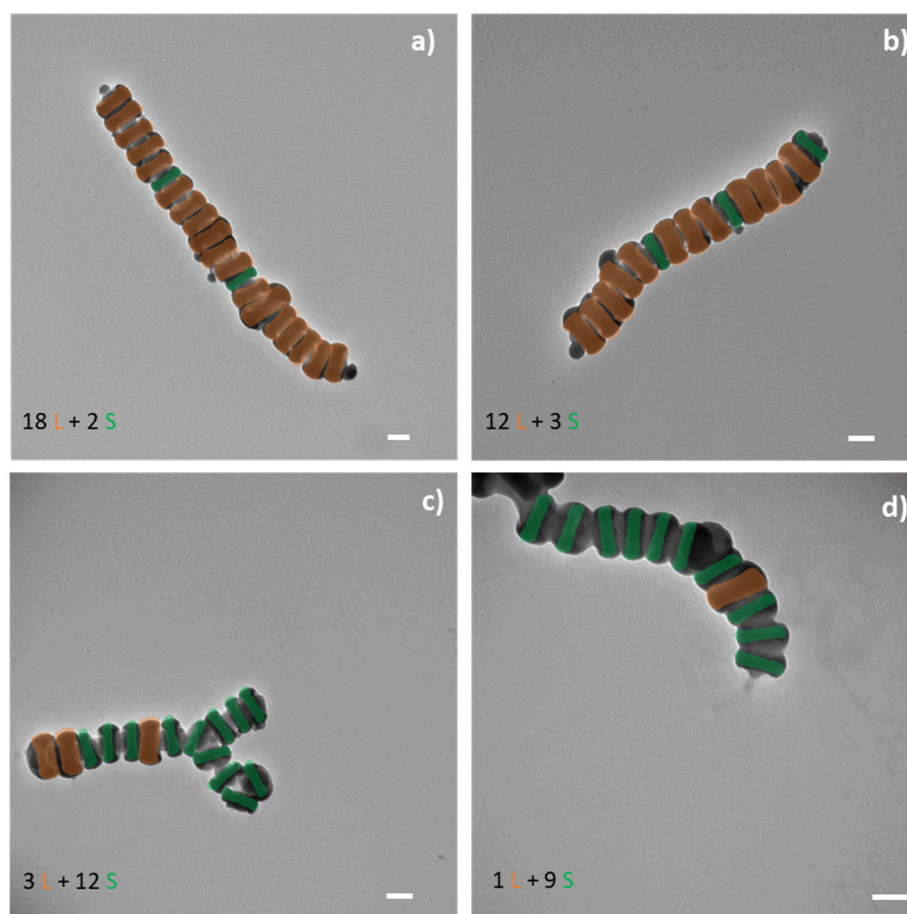


Fig. 22 TEM images of random copolymer-like chains prepared from 190-nm (orange) and 155-nm (green) S2PS NPs at different vol./vol. ratios: a) 9/1, b) 4/1, c) 1/4, and d) 1/9. Scale bars: 100 nm.

Route #2 using S2PS NPs with different surface functions

Besides the physical difference (different size) of S2PS NPs, NPs with various chemical properties can be used to prepare the random copolymer-like chains as well. The same size

S2PS NPs (190 nm) with or without thiol group functionalisation were successfully assembled. In order to discriminate both types of NPs within the chains by TEM, Duff gold NPs were adsorbed onto the thiol-modified NPs^{§§}. The gold-coated NPs are marked in yellow in Fig. 23. The analysis of the TEM pictures revealed that the ratio between thiolated- and bare-silica NPs in the chains was 1/12, 4/16, 2/8 and 11/1 when the proportions of both types of NPs introduced in the medium were 1/9, 1/4, 4/1 and 9/1, respectively. Even if this would deserve a more extensive statistical analysis, these results show that the assumption of equal reactivity of the patches is valid whatever the surface chemistry of the silica NPs probably thanks to the screening effect of the salt ions.

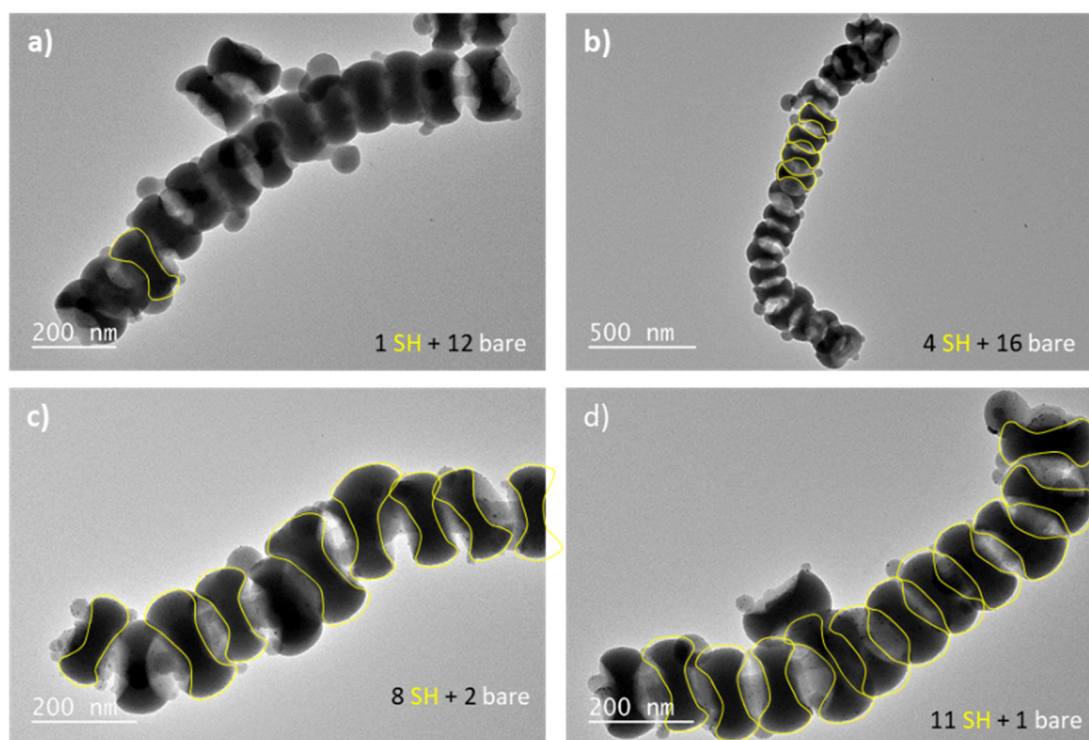


Fig. 23 TEM images of random copolymer-like chains after gold seed adsorption on thiol-modified S2PS NPs. The number ratio of thiol-modified and bare S2PS NPs was 1/9, 4/1, 1/4 and 9/1 in a), b), c) and d), respectively.

3.3.5.3 Mimicking the formation of block copolymers

The fabrication of chains with different segments mimicking block copolymers was envisaged via the assembly of pre-formed short “oligomers”, as shown in Fig. 24. As previously, two routes based on S2PS NPs of different sizes or surface chemistries were explored.

^{§§} 5 mL Duff seed was added to 1 mL of chain solution in ethanol and incubated overnight under 60 rpm roller mixing. The chains were recovered by two centrifugation/redispersion cycles (5,000 g; 10 min) before TEM characterization.

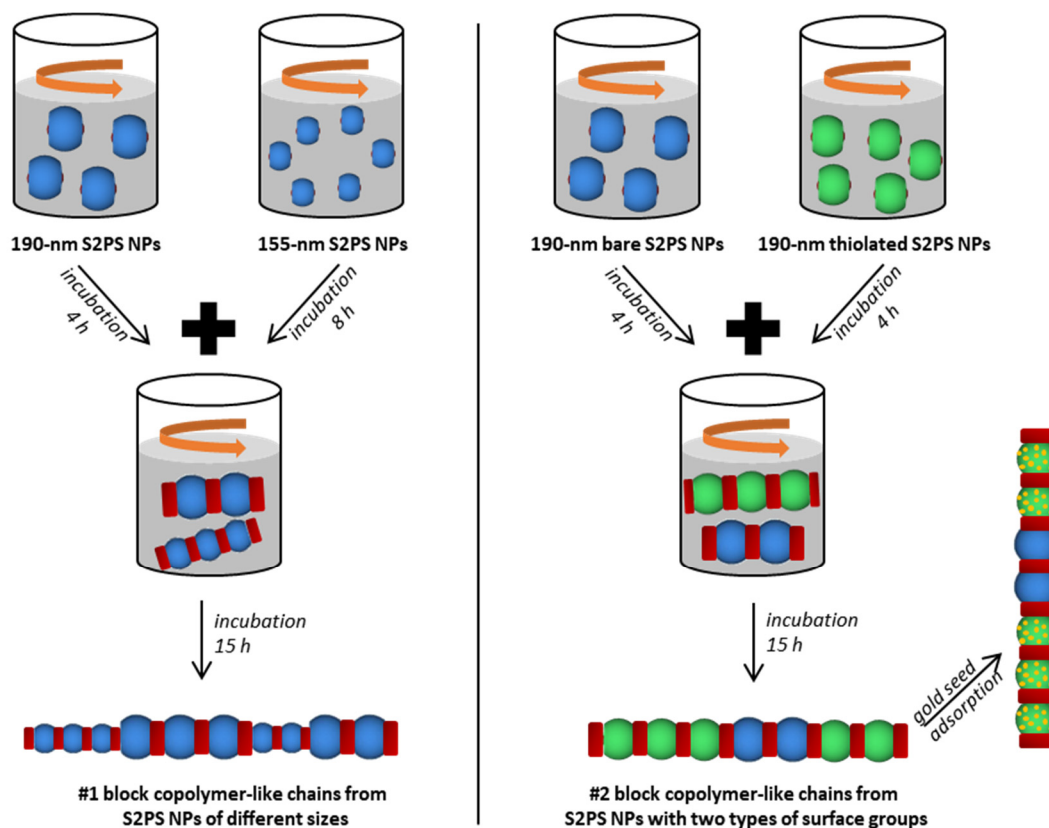


Fig. 24 Scheme illustrating the two routes investigated to prepare block copolymer-like silica chains.

Route #1 using S2PS NPs of different sizes

The 190-nm and 155-nm S2PS NPs were firstly incubated for 4 h and 8 h^{***} independently to form “oligomers”, which were then mixed in a 1/1 volume ratio and left to incubate for 15 h. Fig. 25 shows that block copolymer-like chains consisting of segments of large and small S2PS NPs are obtained.

^{***} 4 h are not sufficient for the 155-nm silica NPs to be assembled into chains as discussed before and 8 h became the adequate value based on previous experiments.

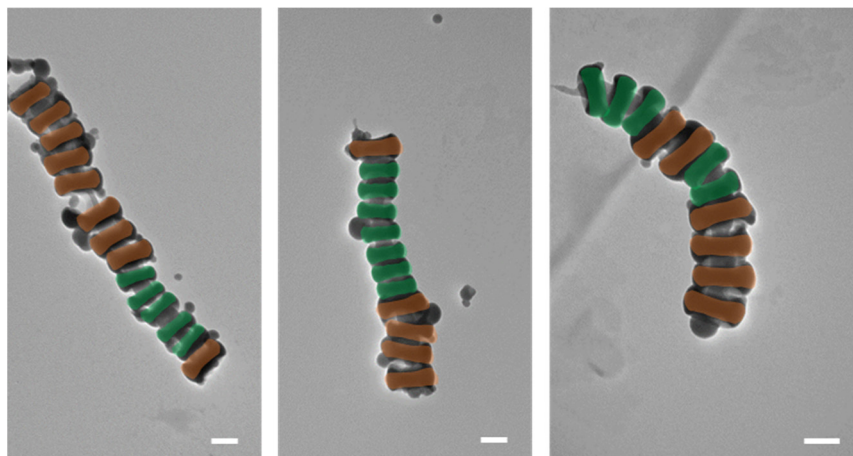


Fig. 25 TEM images of block copolymer-like chains made of 190 nm (orange) and 155 nm (green) S2PS NPs. Scale bars: 100 nm.

Route #2 using S2PS NPs with different surface functions

Similarly, thiol-modified and bare S2PS NPs were separately incubated for 4 h to form short “oligomers”. Then, the two dispersions were mixed and incubated for 15 h before the adsorption of gold NPs on the functionalised silica NPs surface. Fig. 26 demonstrates the successful formation of block copolymer-like chains with yellow frame labelling the gold seed adsorption.

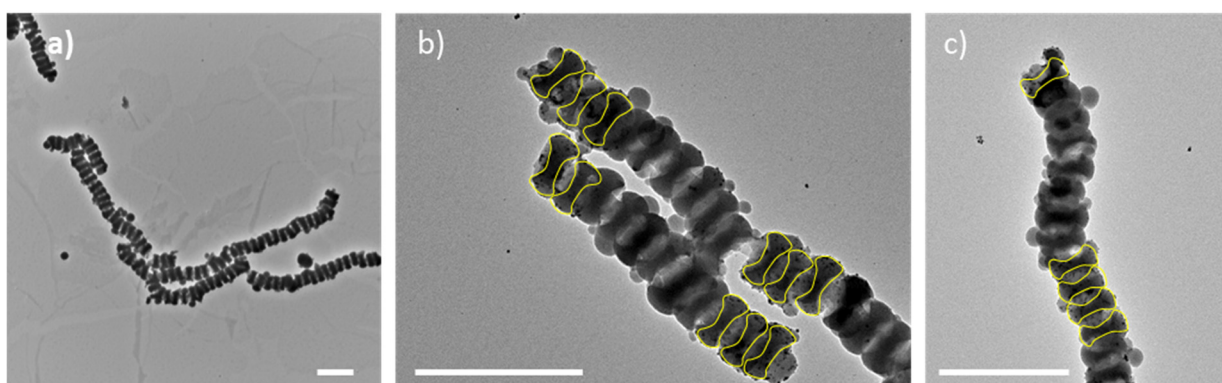


Fig. 26 TEM images of block copolymer-like chains made of thiol-modified and bare S2PS NPs a) before and b, c) after gold NPs adsorption (marked in yellow). Scale bars: 500 nm.

3.3.5.4 Using one-patch silica nanoparticles as chain stoppers

Similarly, to the synthesis of organic polymers, the growing progress of colloidal chains can be terminated by the incorporation of stoppers, *i.e.* monovalent monomers. The one-patch silica NPs prepared in Chapter 2 were thus mixed with 190 nm S2PS NPs to play this role (Fig. 27a). TEM images of Fig. 27b show that the PS moiety of the one-patch NPs effectively physically bonded with the PS chains of the S2PS NPs, which stopped the chain growth. This demonstrates that the principle of equal reactivity of functional groups, *i.e.* patches, is also true between one-

and two-patch silica NPs. Therefore, an extension of this experiment would be to study the influence of the presence of these one-patch silica NPs on the step-growth kinetics and how it could allow controlling the \bar{X}_n value.

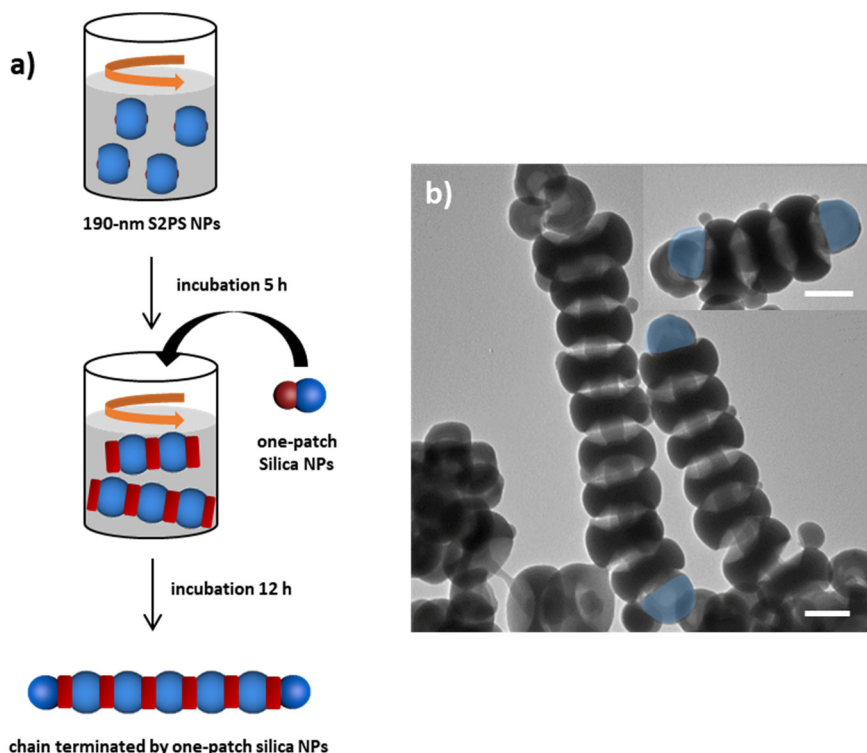


Fig. 27 a) Scheme illustrating the route investigated to prepare silica chains terminated by chain stoppers. b) TEM images of chains terminated by one-patch silica NPs as stoppers (coloured in blue). 0.3 mL of 190-nm S2PS NPs was incubated with 0.05 mL THF and 0.15 mL NaCl (20 mM) for 5 h before adding the one-patch silica particles solution as stoppers, containing 0.35 mL THF, 0.09 mL NPs and 0.06 mL NaCl (50 mM). A 12 h was used to induce the assembly between short chains and the stoppers. Scale bars: 100 nm.

3.3.5.5 Using three-patch silica nanoparticles to induce the formation of branched polymers

It has already been noticed that a small fraction (1.8%) of tripods is present in the silica/PS bipod batch and the three-patch NPs obtained after the silica core regrowth/PS dissolution from these by-products induce random chain branching as shown in Fig. 28. We thus synthesised three-patch NPs (see the detailed protocol in Chapter 4) with a different size (100 nm) from that of the by-products (150-160 nm) present in the S2PS NPs batch in order to be able to distinguish both types by TEM. We mixed them with the S2PS NPs in a 6/1 vol./vol. ratio. It can be seen in Fig. 29 that branched structures were obtained, as expected.

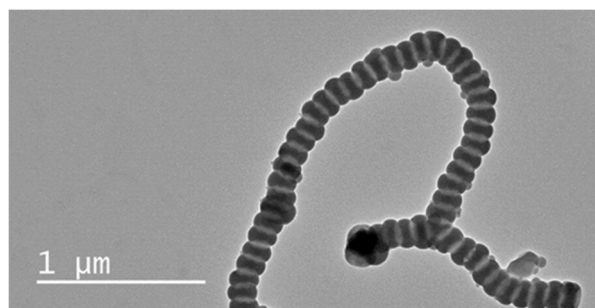


Fig. 28 TEM image of chain branching induced by one three-patch NP.

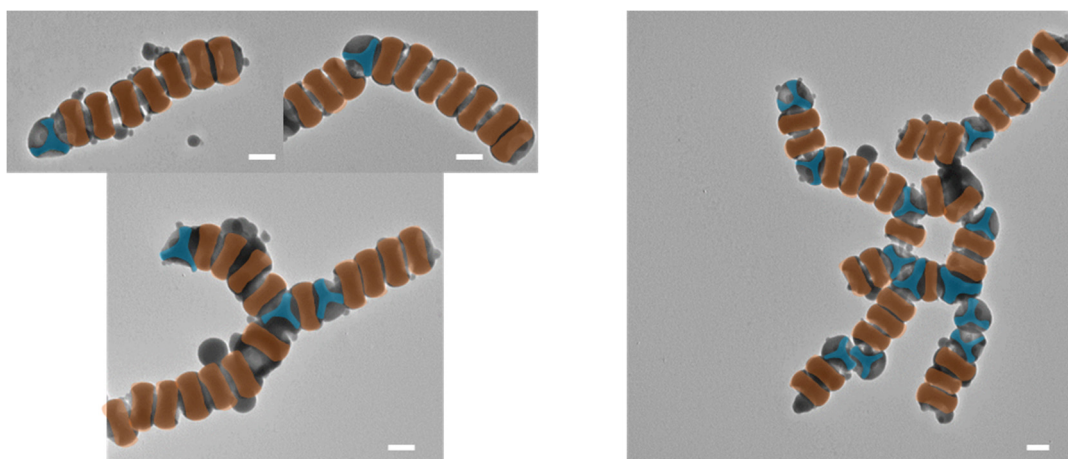


Fig. 29 TEM images of branched chains from the mixture of three-patch NPs (coloured in blue) and S2PS NPs. Scale bars: 100 nm.

3.4 Conclusion

We showed that solvent-induced assembly of two-patch silica nanoparticles is efficient to prepare robust chains made of silica NPs connected through physically entangled PS macromolecules. We first carried out the fabrication of silica/PS by seed-growth emulsion polymerisation of styrene and achieved a record morphology yield of 97%. After regrowth of the silica core and dissolution of the PS nodules, we obtained slim two-patch silica (S2PS) NPs with tuned diameters that can be roughly described as silica nanodisks with PS macromolecules grafted at the centre of both faces. S2PS NPs were successfully used as building blocks to form colloidal macromolecules when subjected to a mixture of THF/salted water. By adjusting the incubation time, NaCl concentration, solvent polarity and NPs amount, colloidal chains mimicking homopolymers were obtained. The regioselective surface functionalisation of the silica NPs with amino groups allowed the preparation of gold decorated chains. The model of the step-growth polymerisation was validated for the system with 190-nm S2PS NPs for the first 2-hour incubation, but it would evolve to a diffusion-controlled mechanism for longer incubation times. Chains mimicking random copolymers were synthesised through the

assembly of two types of S2PS NPs, while block copolymer-like chains were formed from the assembly of previously synthesised oligomers. We also showed that one- and three-patch silica NPs could serve as chain stoppers and branching junctions, respectively. Immediate perspectives would consist in studying to what extent the chain-stoppers would allow controlling finely the length and the length polydispersity of the silica chains.

3.5 References

1. Velev, O. D. & Gupta, S. Materials fabricated by micro- and nanoparticle assembly - the challenging path from science to engineering. *Adv. Mater.* **21**, 1897–1905 (2009).
2. Liu, K., Zhao, N. & Kumacheva, E. Self-assembly of inorganic nanorods. *Chem. Soc. Rev.* **40**, 656–671 (2011).
3. Hill, L. J., Pinna, N., Char, K. & Pyun, J. Colloidal polymers from inorganic nanoparticle monomers. *Prog. Polym. Sci.* **40**, 85–120 (2015).
4. Nikoobakht, B. & El-Sayed, M. A. Preparation and growth mechanism of gold nanorods (NRs) using seed-mediated growth method. *Chem. Mater.* **15**, 1957–1962 (2003).
5. Nie, Z., Fava, D., Rubinstein, M. & Kumacheva, E. “Supramolecular” assembly of gold nanorods end-terminated with polymer “pom-poms”: effect of pom-pom structure on the association modes. *J. Am. Chem. Soc.* **130**, 3683–3689 (2008).
6. Fava, D., Winnik, M. A. & Kumacheva, E. Photothermally-triggered self-assembly of gold nanorods. *Chem. Commun.* 2571–2573 (2009).
7. Liu, K., Nie, Z., Zhao, N., Li, W., Rubinstein, M. & Kumacheva, E. Step-growth polymerization of inorganic nanoparticles. *Science*. **329**, 197–200 (2010).
8. Lukach, A., Liu, K., Therien-Aubin, H. & Kumacheva, E. Controlling the degree of polymerization, bond lengths, and bond angles of plasmonic polymers. *J. Am. Chem. Soc.* **134**, 18853–18859 (2012).
9. Liu, K., Resetco, C. & Kumacheva, E. Salt-mediated kinetics of the self-assembly of gold nanorods end-tethered with polymer ligands. *Nanoscale* **4**, 6574–6580 (2012).
10. Klinkova, A., Therien-Aubin, H., Choueiri, R. M., Rubinstein, M. & Kumacheva, E. Colloidal analogs of molecular chain stoppers. *Proc. Natl. Acad. Sci.* **110**, 18775–18779 (2013).
11. Liu, K., Lukach, A., Sugikawa, K., Chung, S., Vickery, J., Therien-Aubin, H., Yang, B., Rubinstein, M. & Kumacheva, E. Copolymerization of metal nanoparticles: a route to colloidal plasmonic copolymers. *Angew. Chemie Int. Ed.* **53**, 2648–2653 (2014).
12. Sacanna, S., Irvine, W. T. M., Chaikin, P. M. & Pine, D. J. Lock and key colloids. *Nature* **464**, 575–578 (2010).
13. Tang, Y., Su, B., Liu, M., Feng, Y., Jiang, X., Jiang, L. & Yu, A. Superwettability strategy: 1D assembly of binary nanoparticles as gas sensors. *Small* **13**, 1–7 (2017).
14. Lukowiak, A., Vaccari, A., Chiappini, A., Zur, L., Armellini, C., Speranza, G., Maniglio, D., Carpentiero, A., Minati, L. & Ferrari, M. Gold nanoparticles 1D array as mechanochromic strain sensor. *Mater. Chem. Phys.* **192**, 94–99 (2017).

15. Bekana, D., Liu, R., Amde, M. & Liu, J. F. Use of polycrystalline ice for assembly of large area Au nanoparticle superstructures as SERS substrates. *ACS Appl. Mater. Interfaces* **9**, 513–520 (2017).
16. Zhang, H., Zhang, Y., Zhao, H., Ding, Q., Zhou, H. & Wang, G. 3D Fe₃O₄@Au@Ag nanoflowers assembled magnetoplasmonic chains for in situ SERS monitoring of plasmon-assisted catalytic reactions. *J. Mater. Chem. A* **4**, 8866–8874 (2016).
17. Hubert, C. PhD thesis Univ. Bordeaux. (2016).
18. Hartlen, K. D., Athanasopoulos, A. P. T. & Kitaev, V. Facile preparation of highly monodisperse small silica spheres (15 to >200 nm) suitable for colloidal templating and formation of ordered arrays. *Langmuir* **24**, 1714–1720 (2008).
19. Chomette, C. PhD thesis Univ. Bordeaux. (2015).
20. Stöber, W., Fink, A. & Bohn, E. Controlled growth of monodisperse silica spheres in the micron size range. *J. Colloid Interface Sci.* **26**, 62–69 (1968).
21. Perro, A., Duguet, E., Lambert, O., Taveau, J.-C., Bourgeat-Lami, E. & Ravaine, S. A chemical synthetic route towards “colloidal molecules”. *Angew. Chemie Int. Ed.* **48**, 361–365 (2009).
22. Anthony Desert. PhD thesis Univ. Bordeaux. (2011).
23. Hubert, C., Chomette, C., Désert, A., Sun, M., Treguer-Delapierre, M., Mornet, S., Perro, A., Duguet, E. & Ravaine, S. Synthesis of multivalent silica nanoparticles combining both enthalpic and entropic patchiness. *Faraday Discuss.* **181**, 139–46 (2015).
24. Désert, A., Hubert, C., Fu, Z., Moulet, L., Majimel, J., Barboteau, P., Thill, A., Lansalot, M., Bourgeat-Lami, E., Duguet, E. & Ravaine, S. Synthesis and site-specific functionalization of tetravalent, hexavalent, and dodecavalent silica particles. *Angew. Chemie Int. Ed.* **52**, 11068–11072 (2013).
25. Choueiri, R. M., Klinkova, A., Thérien-Aubin, H., Rubinstein, M. & Kumacheva, E. Structural transitions in nanoparticle assemblies governed by competing nanoscale forces. *J. Am. Chem. Soc.* **135**, 10262–10265 (2013).
26. Nie, Z., Fava, D., Kumacheva, E., Zou, S., Walker, G. C. & Rubinstein, M. Self-assembly of metal-polymer analogues of amphiphilic triblock copolymers. *Nat. Mater.* **6**, 609–614 (2007).
27. Yin, D., Zhang, Q., Zhang, H. & Yin, C. Fabrication of covalently-bonded polystyrene/SiO₂ composites by pickering emulsion polymerization. *J. Polym. Res.* **17**, 689–696 (2010).
28. Espiard, P. & Guyot, A. poly(ethyl acrylate) latexes encapsulating nanoparticles of silica: 2. grafting process onto silica. *Polymer.* **36**, 4391–4395 (1995).
29. Luo, B., Smith, J. W., Wu, Z., Kim, J., Ou, Z. & Chen, Q. Polymerization-like co-assembly of silver nanoplates and patchy spheres. *ACS Nano* **11**, 7626–7633 (2017).
30. Paul Flory. *Principles of polymer chemistry*. Cornell University Press Ed. (1953).
31. Yi, C., Yang, Y. & Nie, Z. Alternating copolymerization of inorganic nanoparticles. *J. Am. Chem. Soc.* **141**, 7917–7925 (2019).

Chapter 4

Tentative assembly of three-patch silica nanoparticles into honeycomb sheets

4.1. Introduction

Nanostructuring two-dimension arrays is of particular interest for a wide range of applications, going from the fabrication of photonic crystals to plasmonic devices or biomimetic surfaces with specific wettability or reflection properties.¹

The fabrication can be performed by a “top-down” method where externally controlled instruments are used to direct the formation of small-scale structures from larger materials. Such techniques include photolithography, micro-contact printing, electron-beam lithography, and dip-pen nanolithography.²⁻⁵ Conversely, the ‘bottom-up’ route consists in assembling nano- to microparticles on substrates with the advantages to be cheaper and easily extended to long-range (cm²) structures.⁶ This approach is generally based on Langmuir-Blodgett or evaporation techniques.

As discussed in the state-of-the-art of Chapter 1, there is no concrete example of colloidal monolayer made via the self-assembly of three-patch particles^{†††} and only Monte-Carlo simulations were reported.⁷⁻¹² In a two-dimension constrained environment, the minimum energy configuration where all patches are saturated via bonds is the honeycomb-like structure and it is obtained at low pressure. In three-dimension space, *i.e.* in bulk, three different fully bonded structures are expected at low temperature: a collection of independent honeycomb-like planes, a crystal consisting of inter-penetrating honeycomb-like planes and a fully bonded *fcc* structure if the patches are wide enough (see Fig. 27b in Chapter 1).

Herein, three-patch silica NPs were prepared according to the general pathway used in Chapter 2, except that the experimental conditions of the seed-growth emulsion polymerisation stage were adapted to extend the patch number from 2 to 3. The three-patch silica NPs were used as building blocks to fabricate tentatively honeycomb-like sheets not only in bulk but also along with the air/water interface of a Langmuir trough (Fig. 1).

^{†††} As far as we know, the most relevant example was reported by Pine and co-workers and consisted in assembling under electric fields polystyrene microparticles with three negatively-charged patches.¹⁸ This means that the patches are repulsive and this is not in accordance with our definition of patchy particles, which implies that the patches are sticky with regard to the other ones. In specific experimental conditions, they could indeed observe 2-D hexagonal domains but without orientational order of the patches.

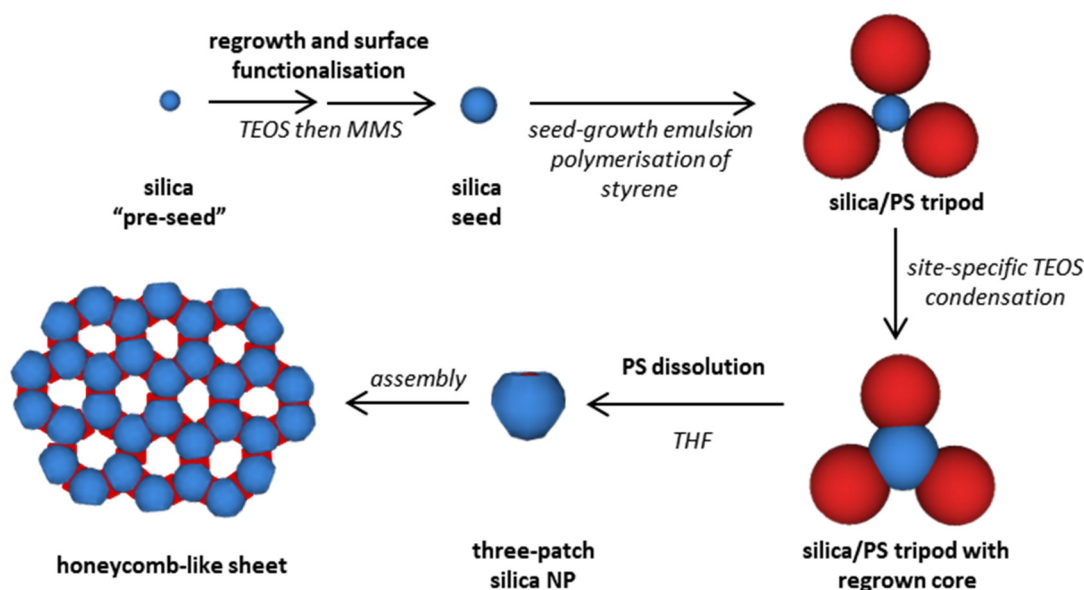


Fig. 1 Scheme summarising the synthesis of three-patch silica NPs and their assembly into honeycomb-like sheet.

4.2 Materials and methods

4.2.1 Materials

Styrene (99.5%, with c.a. 50 ppm 4-tert-butyl catechol as stabiliser), sodium dodecyl sulphate (SDS, 99%), L-arginine, sodium persulphate (NaPS, $\geq 99\%$), tetraethoxysilane (TEOS, $\geq 99\%$), tetrahydrofuran (THF, contains 250 ppm BHT as an inhibitor), chloroform (anhydrous, $\geq 99\%$, contains 0.5-1.0% ethanol as stabiliser) were supplied by Sigma-Aldrich. Methacryloxymethyltrimethoxysilane (MMS, 95%) was purchased from ABCR, Germany. Ammonia (28-30%) and sodium chloride (NaCl) were purchased from JT. Baker and ethanol (99%) were provided by Atlantic Labo. Synperonic[®] NP 30 was supplied by Fluka. Deionised water with a resistivity of $18.2 \text{ M}\Omega \cdot \text{cm}$ at 25°C was obtained from a Milli-Q system (Millipore).

4.2.2 Silica seed synthesis by sol-gel chemistry and surface functionalisation

We prepared two batches of 55-nm silica seeds surface-modified with MMS at a nominal surface density of 0.35 or 0.5 molecules/ nm^2 .

The preparation of silica pre-seeds, silica regrowth and surface modification have been reported in section 3.2.1 of Chapter 3. Briefly, the silica "pre-seeds" were synthesised from TEOS precursor in water catalysed by L-arginine and regrown to 55 nm in the conventional Stöber's conditions. The volume of TEOS was calculated from the following equation:

$$V_{TEOS} = \frac{M_{TEOS} \cdot \rho_{silica}}{M_{silica} \cdot \rho_{TEOS}} N_{silica} \cdot \frac{\pi}{6} \cdot (D_t^3 - D_i^3)$$

where D_i and D_t are the initial and targeted diameter of the silica NPs, respectively; M and ρ mean the molecular weight and density, respectively; N_{silica} is the number of silica seeds.

The obtained silica surface was functionalised with MMS whose amount was calculated from the following equation as a function of the targeted nominal surface density (d_{MMS}) and expressed in molecule/nm²:

$$V_{MMS} = \frac{6 \cdot d_{MMS} \cdot M_{MMS} \cdot V_{silica\ dispersion} \cdot C_{silica\ dispersion}}{N_A \cdot \rho_{MMS} \cdot \rho_{silica} \cdot D_{silica}}$$

where M , ρ , C and D represent the molecular weight, density, concentration and diameter, respectively, and N_A is the Avogadro number.

The reacting medium was let to age for 3 h at RT and 1 h under the reflux of ethanol. We concentrated the dispersion with the rotary evaporator to remove ethanol and ammonia and we replaced them with water. The final concentration of silica seeds in water was measured by the mass of a dried extract.

4.2.3 Synthesis of silica/polystyrene tripods by seed-growth emulsion polymerisation

In a 250-mL three-neck round flask equipped with a condenser, 50 mL of the as-prepared aqueous dispersion of silica seeds ($1.8 \cdot 10^{16}$ part/L) and the surfactant mixture (3 g/L) made of Synperonic[®] NP30 and SDS were mixed. Then, 5.5 mL of styrene was added after 20 min of nitrogen flux deaeration under moderate agitation. The polymerisation was induced by the addition of 1.3 mL Na₂S₂O₈ solution (0.1 g dissolved in 4 mL water) at 75 °C and lasted for 6 h. The monomer-to-polymer conversion was determined by the dried extract method. We characterised the multipods by TEM and determined statistically their morphological distribution and the average size of their PS nodules.

4.2.4 Derivatisation into three-patch silica nanoparticles

To regrow the silica core from 55 nm to 100 nm, 1 mL of the as-obtained silica/PS tripods dispersion was mixed with 45.5 mL ethanol and 3.2 mL ammonia in a 100-mL round flask equipped with a magnetic stirrer. Then, we added 1.18 mL of a TEOS/ethanol mixture (10 vol. % in ethanol) at the rate of 1 mL/h. One hour after the completion of the TEOS addition, the NPs were washed by two centrifugation/redispersion cycles (12,000 g; 10 min; 25 mL) with ethanol. The final concentration was adjusted to $3.6 \cdot 10^{14}$ part/L regarding the silica core

number. Smaller silica cores, *e.g.* 80 nm, were achieved by reducing the TEOS/ethanol volume to 0.8 mL and stocked with the same concentration.

The three-patch silica NPs were obtained by removing from the satellites by dissolution in THF the just physically-entangled macromolecules and they were washed by 2 to 5 centrifugation/redispersion cycles (12,000 g; 10 min; 20 mL) in THF. The obtained NPs were stored in THF and their concentration was $6 \cdot 10^{15}$ part/L.

4.2.5 Assembly of three-patch silica nanoparticles into honeycomb-like structure

Different strategies were developed to promote the assembly of three-patch silica NPs into 2D honeycomb-like structures, including the assembly in bulk solution and the assembly assisted by the Langmuir technique.

4.2.5.1 Assembly in bulk solution

These experiments were performed into 25-mL glass bottles equipped with polypropylene caps and magnetic stirrer using a saline water/THF mixture. 0.18 mL of the three-patch silica NPs dispersion was diluted with 3.32 mL THF under gentle stirring, and 1.5 mL of 20 mM NaCl aqueous solution was added dropwise. The mixture was incubated under RT with 400 rpm stirring for 19 h. The sample was diluted by adding 45 mL ethanol and the NPs assemblies were recovered by centrifugation (12,000 g; 10 min) / redispersion in 5 mL ethanol.

4.2.5.2 Assembly assisted by Langmuir technique

Compression isotherms were recorded at RT using a homemade Langmuir trough (trough dimensions: 145 mm \times 690 mm, compressible area: 1000 cm²). The surface pressure was recorded by a balance equipped with a paper Wilhelmy-plate. The NPs were dispersed in a 50/50 mixture of THF and chloroform. 0.5×0.5 cm² pieces of silicon wafer were cleaned by a 30 minutes UV-ozone treatment. The suspension of NPs was then deposited using a Hamilton syringe at the air-water interface. After a stabilisation time of \sim 15 min, the barriers were displaced symmetrically at a constant speed. When the target desired surface pressure was reached, the silicon substrate (or a TEM grid) was scooped through the interface while the trough feedback system adjusted the barrier position to maintain a constant surface pressure. A schematic view and a picture of the trough are represented in Fig. 2.

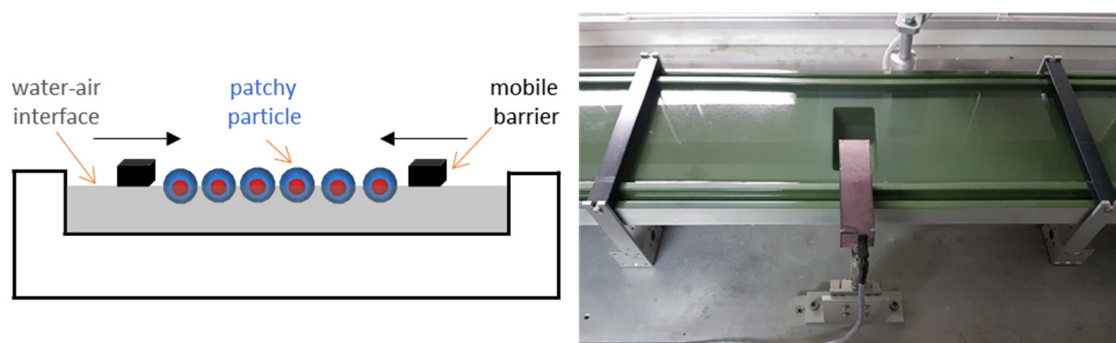


Fig.2 left) schematic representation and right) picture of the Langmuir trough.

4.2.5.3 THF solvent vapour annealing

The solvent vapour saturation was controlled by the nitrogen stream, which was passed through a bottle filled with THF and introduced into the sample chamber subsequently. The flow rate of the nitrogen stream was controlled by the electronic mass flow controllers (MKS) at 500 $\mu\text{m/s}$. The solvent reservoir and the sample chamber were kept at RT and the annealing process lasted for 2 h.

4.2.6 Characterisation

Transmission electron microscopy: TEM images were obtained on Hitachi H600 microscope or JEOL-1400 plus microscope operating at 75 kV or 120 kV, respectively. All samples were dropped directly on carbon-coated copper film (300 mesh) and dried at RT.

Scanning electron microscopy: SEM images were obtained from JSM-7800FPRIME and JEOL 6700F high-resolution microscopes. The metallisation process was obligatory for the conventional SEM apparatus (JEOL 6700F), while the characterisation can be performed directly using the gentle beam super high resolution (GBSH) model on the JSM-7800.

The packing ratio (R_p) of the 2-D structure was measured from the statistics on more than 200 NPs and computed from the following equations:

$$R_p = \frac{2 \cdot N_{cf}}{2 \cdot N_2 + 3 \cdot N_3 + 4 \cdot N_4}$$

where N_{cf} represents the number of contacts between two facets; N_2 , N_3 , and N_4 are the number of two-, three- and four-patch silica NPs, respectively, as illustrated in Fig. 3.

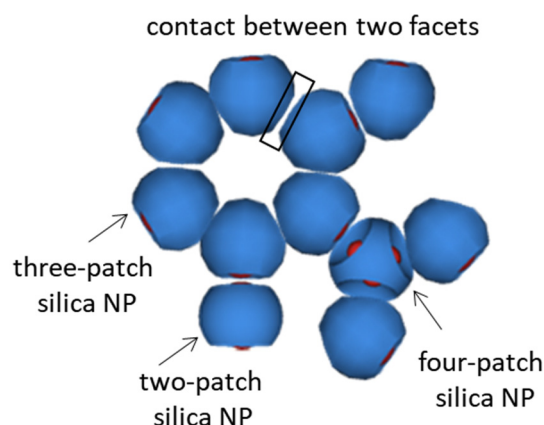


Fig. 3 Scheme illustrating the different types of NPs interactions taken into account for the calculation of the packing density. Two- and four-patch silica NPs are considered here as impurities originating from the original silica/PS tripod batch.

4.3 Results and discussion

4.3.1 Synthesis of three-patch silica nanoparticles

The three-patch silica NPs were obtained through the silica core regrowth of the silica/PS tripods followed by the PS nodules dissolution. Several silica seed batches were prepared with MMS nominal surface density of 0.35 or 0.5 molecule/nm². The critical stage is the seed-growth emulsion polymerisation of styrene whose morphology yield sets the purity level of the final batch of patchy particles. However, its success depends also on the seed modification stage with MMS. We started with a first experiment inspired by the experimental conditions reported by Céline Hubert¹³ who achieved a morphology yield of 77% from seeds with MMS surface density of 0.5 molecule/nm². Our experiment (entry #1 in Table 1) was unsuccessful because we obtained mainly bipods (75%). After having repeated this experiment several times without any success, we decided to modify the experimental conditions.

Table 1 Experimental conditions of the synthesis, morphology and geometrical parameters of several batches of silica/PS clusters ($[styrene]_0 = 0.96 \text{ mol/L}$, $[silica] = 1.8 \cdot 10^{16} \text{ part/L}$, $[Na_2S_2O_8]_0 = 0.58 \text{ g/L}$, $[surfactant] = 3 \text{ g/L}$, $T = 75 \text{ }^\circ\text{C}$ and duration = 6 h).

Entry		#1	#2	#3	#4	#5	#6	#7	
Experimental conditions	Seed batch number	I	II	III	III	IV	IV	V	
	MMS surface density (molecule/nm ²)	0.5				0.35			
	NP30/SDS weight ratio	99/1	98/2	97/3	95/5	99/1	98/2	97/3	
	Monomer-to-polymer conversion (%)	87	74	73	78	83	79	60	
Final composition	Clusters	% Bipods	75	63	24	4	52	12	2
		% Tripods	23	34	55	19	17	73	20
		% Tetrapods	-	-	17	75	25	13	75
		% Hexapods	-	-	-	-	-	-	1
		% Multi-silica clusters	2	3	4	2	6	2	2
	PS	D _{PS} (nm)	180	155	143	125	175	150	145

According to the rules demonstrated by Desert and co-workers,¹⁴ we decided to decrease the PS nodule diameter and consequently to increase their number by increasing the fraction of SDS in the surfactant mixture, as anionic surfactants are known to promote latex nucleation in comparison to non-ionic ones such as Synperonic[®] NP 30. In this way, increasing the SDS fractions to 2, 3 and 5 wt. % (entries #2 to #4 in Table 1) allowed progressively shifting the main clusters population from bipods to tetrapods in agreement with the decrease of the diameter of the PS nodules. Even if the main population was tripods for entry #3, the morphology yield was low (53%). That is why we then decreased also the MMS nominal surface density from 0.5 to 0.35 molecule/nm² (entries #5 to #7), because the lower this value, the less wetting the PS nodules and therefore the lower the probability for two neighbouring nodules to coalesce. We indeed observed the same tendency to shift from bipods to tetrapods, but this time we reached a morphology yield of 73% for tripods when the SDS fraction was 2 wt. % (entry #6).

To check the robustness of this protocol, seven batches of silica/PS clusters were prepared in the exact conditions of entry #6 (Table 2). This indeed evidenced that the main product was systematically the tripods with a morphology yield ranging from 63 to 75%. The TEM image

of entry #12 is shown in Fig. 4, and this batch was systematically used for the rest of the study despite the presence of clusters with two sometimes four silica cores and 10% multi-silica clusters. It is certainly possible to increase again the purity of the tripod batch by optimising more finely the experimental conditions.

Table 2 Experimental conditions of the synthesis, morphology and geometrical parameters of several batches of silica/PS clusters ($[styrene]_0 = 0.96 \text{ mol/L}$, $[silica] = 1.8 \cdot 10^{16} \text{ part/L}$ with $d_{MMS} = 0.35 \text{ molecule/nm}^2$, $[Na_2S_2O_8]_0 = 0.58 \text{ g/L}$, $[surfactant] = 3 \text{ g/L}$ with 2 wt. % SDS, $T = 75 \text{ }^\circ\text{C}$ and duration = 6 h).

Entry		#8	#9	#10	#11	#12	#13	#14	
Experimental conditions	Seed batch number	VI	VII	VIII	IX	X	XI	XII	
	Monomer-to-polymer conversion (%)	79	64	66	68	72	61	58	
Final composition	Clusters	% Bipods	12	8	14	5	6	11	14
		% Tripods	72	69	68	67	75	70	63
		% Tetrapods	5	20	17	26	9	17	20
		% Multi-silica clusters	11	3	2	3	10	2	3
PS	D_{PS} (nm)	154	150	151	150	152	148	145	

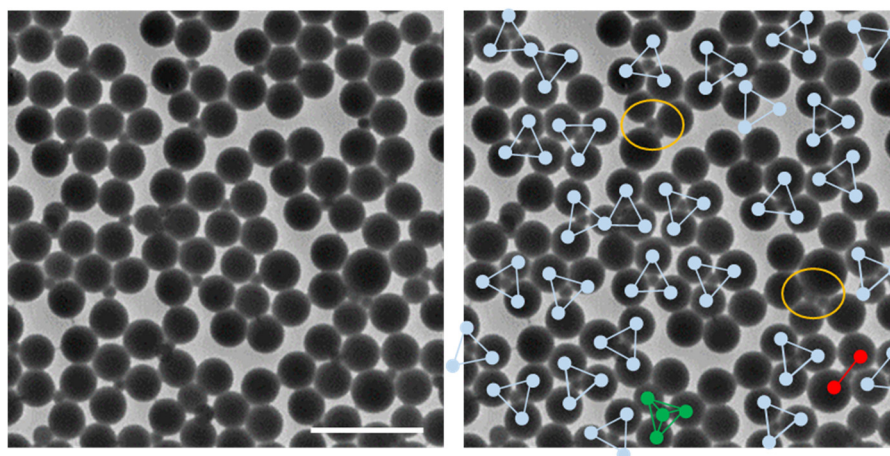


Fig. 4 Representative TEM image of the silica/PS tripods (entry#12 in Table 2), whose purity of 75% is evidenced on the right image by specific blue labels showing 28 tripods, red one showing 1 bipod, green one showing 1 tetrapod and orange ones showing 2 multi-silica clusters. Scale bar: 500 nm.

The 55-nm silica core of the tripods was regrown to 100 nm according to the Stöber's conditions (Fig. 5a). However, because of the excessive size of PS nodules, expected to serve as patches, they were successfully dissolved in THF according to the same strategy developed for the two-patch silica NPs in Chapter 3 (Fig. 5b).

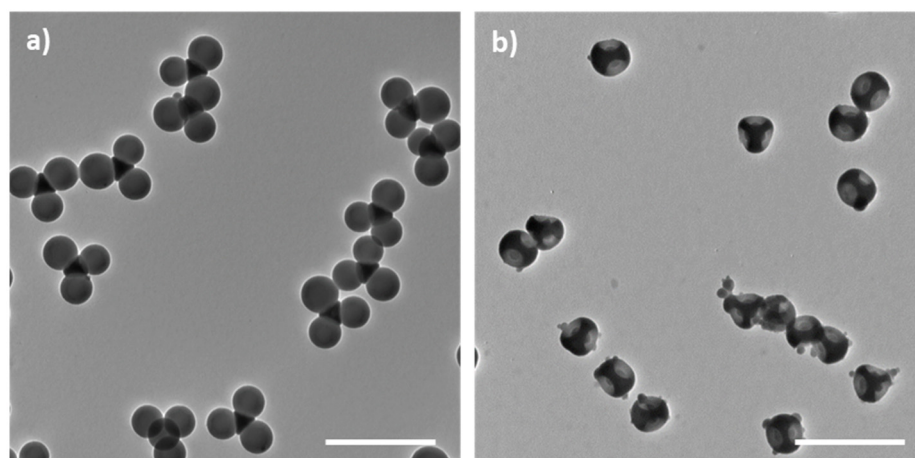


Fig. 5 TEM images of a) the silica tripods after the silica core regrowth and b) the corresponding three-patch NPs after the PS nodules dissolution in THF. Scale bars: 500 nm.

4.3.2 Assembly of three-patch silica nanoparticles in bulk solution

We incubated the three-patch NPs in a THF/saline water mixture to induce the self-assembly, according to the reference protocol given in Chapter 2. Fig. 6a and 6b show that the NPs were linked by their PS residues (indicated by red arrows) but did not form a dense packing. Some single hexagon, loop, and tetramer could be observed occasionally (Fig. 6c, 6d and 6e). Compared to the chain formation in Chapter 3, a dense 2-D structure could not be formed in the bulk solution probably due to the rotation of the NPs, which hinders their assembly in a specific plane.

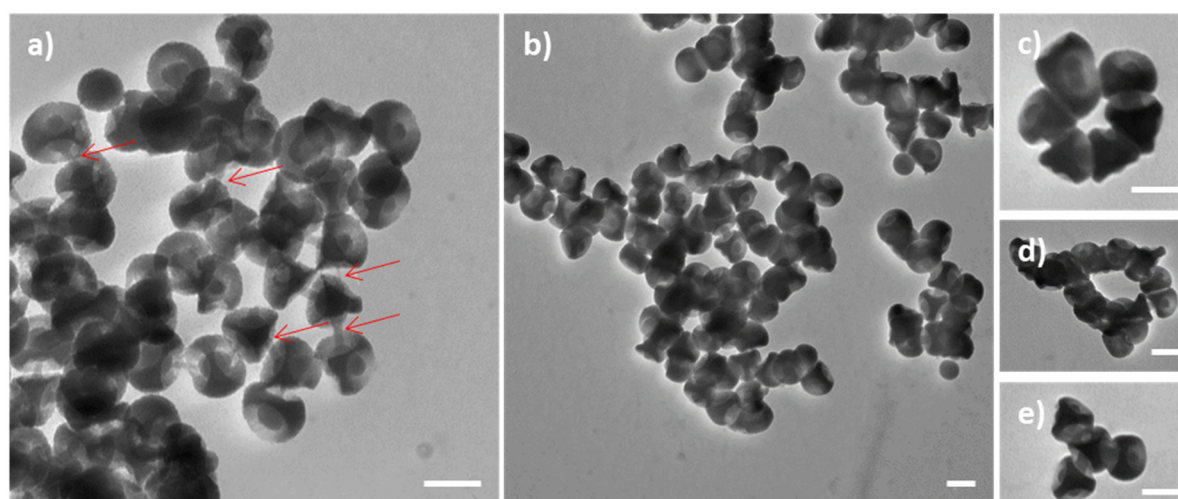


Fig. 6 TEM images of: a) and b) three-patch NPs after self-assembly in bulk solution with a specific c) hexagon, d) loop structure and e) tetramer. The assembly was carried out in a 7/3 THF/20 mM NaCl aqueous solution for 19 h under 400 rpm agitation. Scale bars: 100 nm.

4.3.3 Assembly of three-patch silica nanoparticles by the Langmuir technique

The Langmuir technique was commonly applied to form monolayers of amphiphilic molecules at a gas/water interface, which can be further transferred onto a solid substrate by the vertical lifting method invented by K. Blodgett. Nowadays, the formation of a monolayer made of nanoparticles can be fabricated and deposited onto flexible substrates by this technique.^{15,16}

A first experiment was carried out by spreading 0.8 mL of a three-patch NPs dispersion that had been purified by 2 cycles of centrifugation/redispersion (12,000 g; 10 min). The compression speed was fixed at 10 cm/min. Samples were collected at various surface pressures and characterised by TEM and SEM. Fig. 7 shows that the NPs formed dense zones, some of them being highly organised (see the red box on Fig. 7) even if the presence of impurities, *i.e.* bipods or tetrapods *etc.* limits their partial extension. These dense zones are surrounded by big “holes”, even when the surface pressure reached 30 mN/m. The packing density was estimated to $R_p = 0.261$. It is speculated that free polymer chains in the NPs dispersion could occupy the interparticle space and hinder the formation of a dense monolayer. We thus first increased the number of washing cycles to 5 to remove the maximum of free polymer chains. Fig. 8 shows that the organisation of the NPs was not drastically improved, as they were not forming a homogeneous and dense monolayer but rather interconnected dense domains ($R_p = 0.276$ at 30 mN/m).

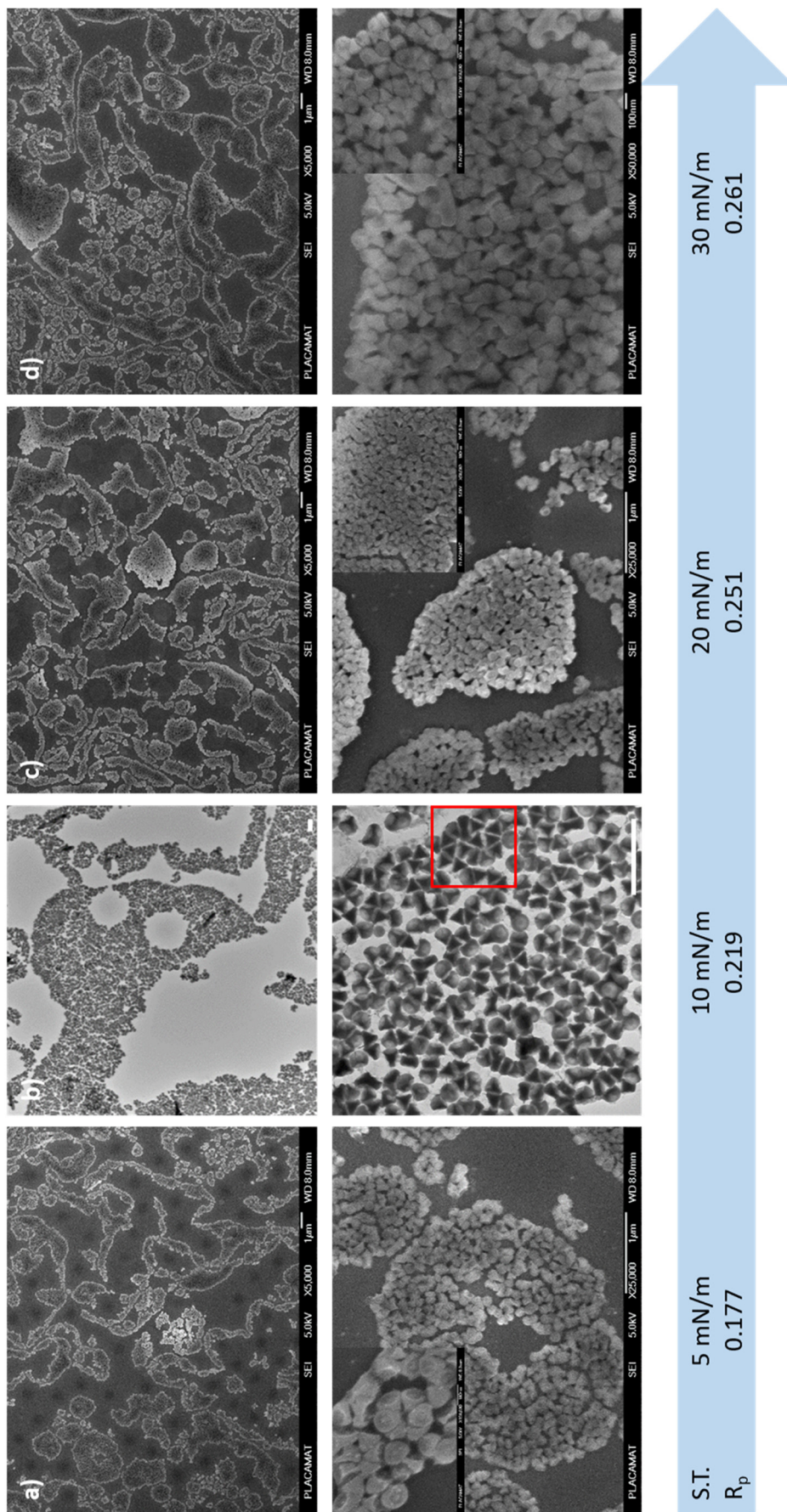


Fig. 7 Representative SEM and TEM images of the samples collected at different surface pressures. Compression rate: 10 cm/min. Dispersion volume: 0.8 mL with 2-washing cycles. Scale bars: 500 nm for the TEM images.

These domains could result from a too fast compression of the NPs at the air-water interface, which does not allow the NPs to interact in a reversible manner, but on the contrary, promotes their irreversible sticking as soon as they touch together. Therefore, we decided to study the influence of the compression rate on the organisation of the NPs.

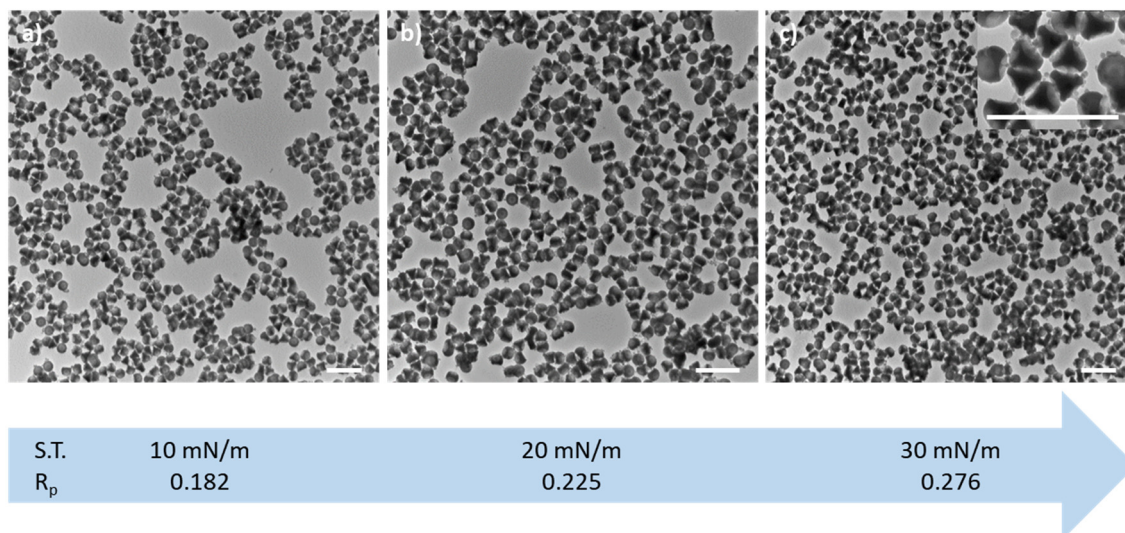


Fig. 8 Representative TEM images of the samples collected at a) 10, b) 20 and c) 30 mN/m. Inset in c) shows a hexagonal structure. Compression rate: 10 cm/min. Dispersion volume: 0.8 mL with 5-washing cycles. Scale bars: 500 nm.

We compressed the NPs at 5, 1 and 0.2 cm/min and the results shown in Fig. 9 revealed that the slower the compression rate, the higher the packing ratio.

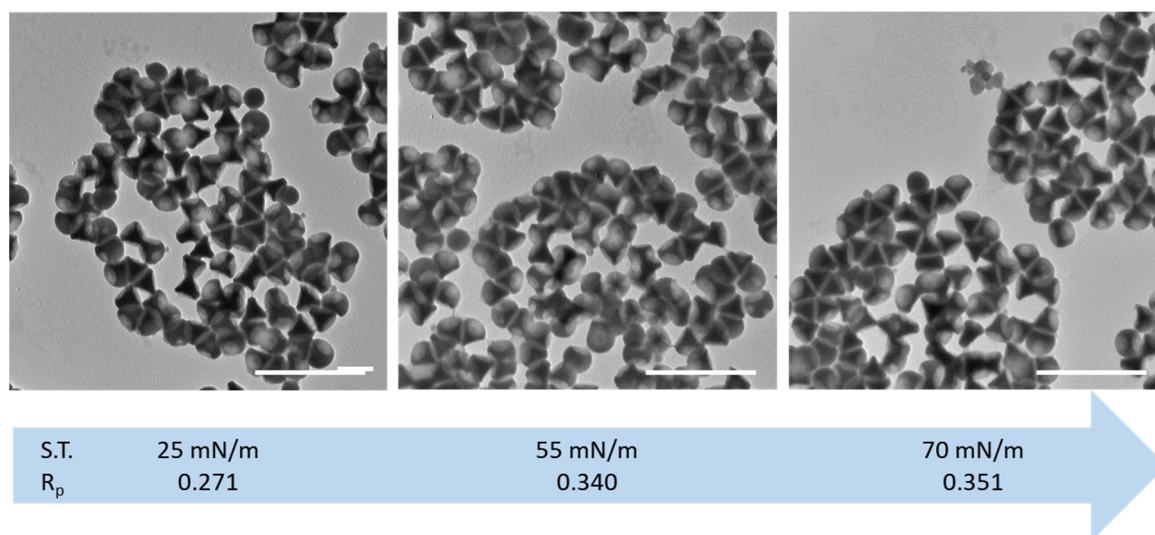


Fig. 9 Representative TEM images of the samples collected at different surface pressures. Compression rate: left: 10 cm/min. centre: 5 cm/min; right: 1 cm/min. Dispersion volume: 0.8 mL. Scale bars: 500 nm.

Keeping the compression rate at 0.2 cm/min, we studied the influence of the quantity of NPs by multiplying by 2 the volume of suspension spread at the water surface (Fig. 10). Similar R_p

values (0.297 at 55 mN/m) as before were obtained, illustrating that the increase of NPs volume did not allow us to form a close-packed monolayer. The interrelationship between R_p , particle volume, compressing speed and surface tension was summarised in Fig. 11 and a maximum R_p of 0.351 was reached when the size of particle is 100 nm.

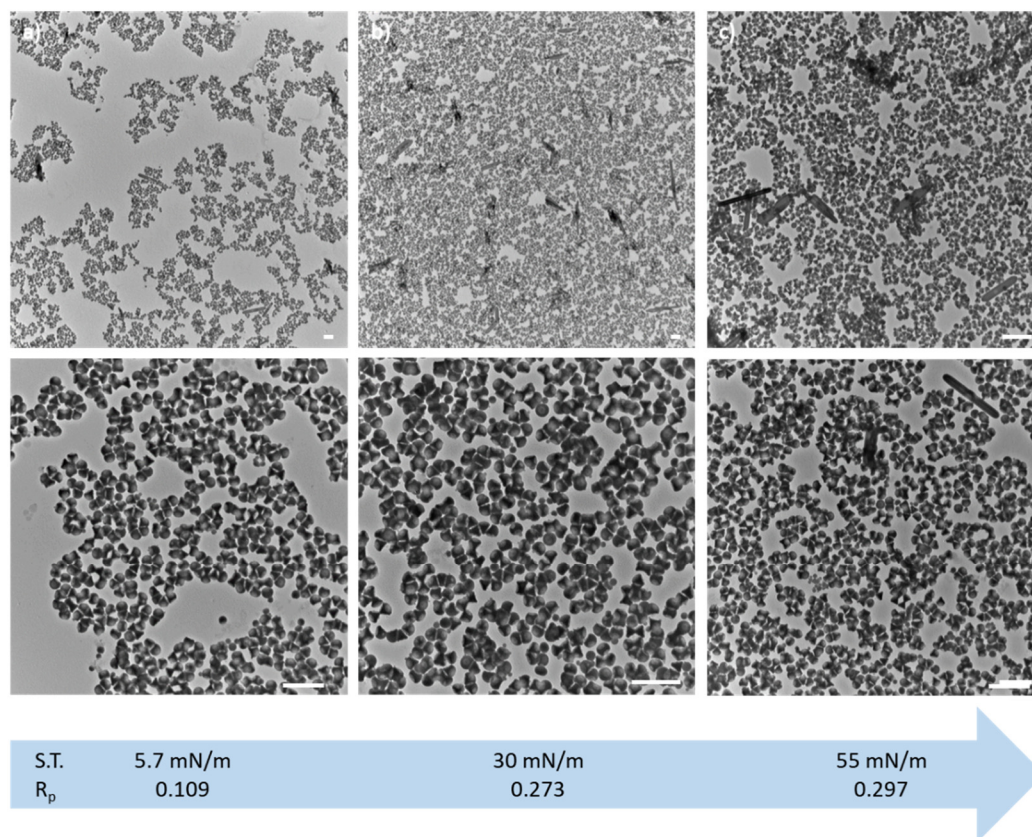


Fig. 10 Representative TEM images of the samples collected at different surface pressures. Dispersion volume: 1.6 mL. Compression rate: 0.2 cm/min. Scale bars: 500 nm.

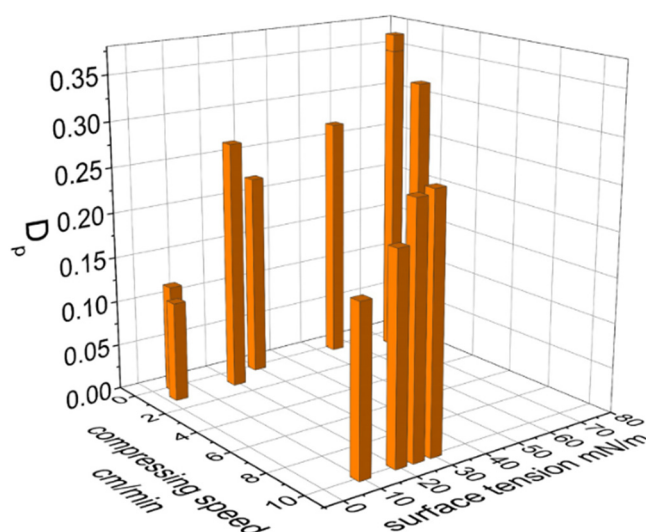


Fig. 11 Summarisation of the interrelationship between R_p , compression rate, surface tension, particle volume and particle size. a) the dispersion volume was 0.8 mL; b) the dispersion volume and the compression rate were 1.6 mL and 0.2 cm/min, respectively.

The smaller three-patch silica NPs (80 nm) are also assembled through Langmuir technique and the large-scale close-packing structure was shown in Fig. 12a, among which the local honeycomb-like structures with more than 20 particles can be found in Fig. 12b. The realistic model was presented in Fig. 12c and the R_p increased to 0.41 compared to 0.351 in the 100 nm system.

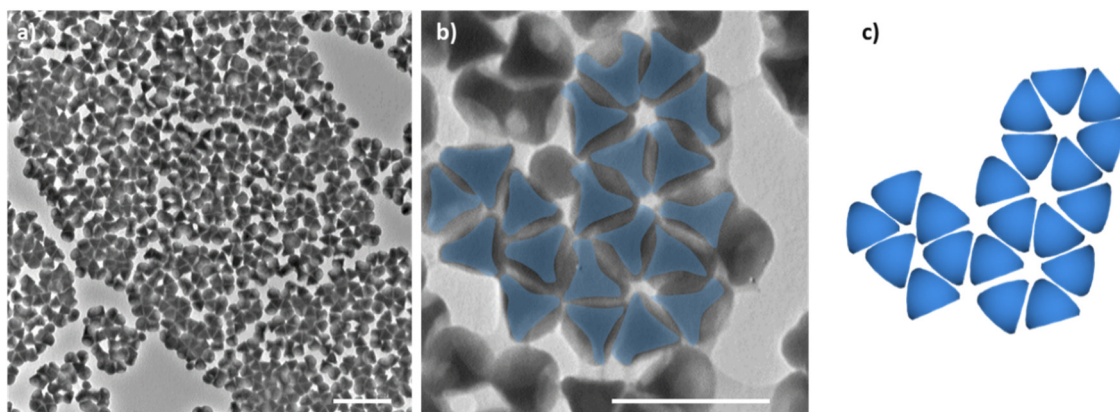


Fig. 12 Representative TEM images of the 80 nm samples collected at 55 mN/m. Dispersion volume: 1.6 mL. Compression rate: 0.2 cm/min. Scale bars: 500 nm.

4.3.4 Effect of an extra stage of solvent vapour annealing

The previous electron microscopy images show that a certain fraction of facets was in contact, but there is no clear evidence that the patches went through a sticky state and therefore that the PS junctions were cohesive. Indeed, the compression action is concomitant to the chloroform evaporation, which made the PS patches less and less sticky. The crystallisation could essentially result from the geometrical stacking of three-patch NPs that can roughly be seen as triangular prisms.

In order to promote the number of contacts between two facets and therefore the R_p value, we envisaged providing mobility to the patchy particles by plasticising the PS junctions in the presence of THF vapours. This strategy of solvent vapour annealing is well developed in polymer science to re-organize block copolymer patterns, alternatively to thermal treatments.¹⁷ We performed a few experiments in conventional conditions (2 h at RT) directly on one of the TEM grid, which was scooped through the water-air interface. The SEM images of the sample before and after the annealing process are shown in Fig. 13. No clear modification of either the global organisation of the particles or their relative orientation was observed. The only noticeable effect is perhaps a more efficient embedding of the silica NPs by the PS macromolecules making the assembly apparently more robust mechanically speaking. This

shows that the mobility of the PS macromolecules can be recovered thanks to this treatment but not the mobility of the NPs.

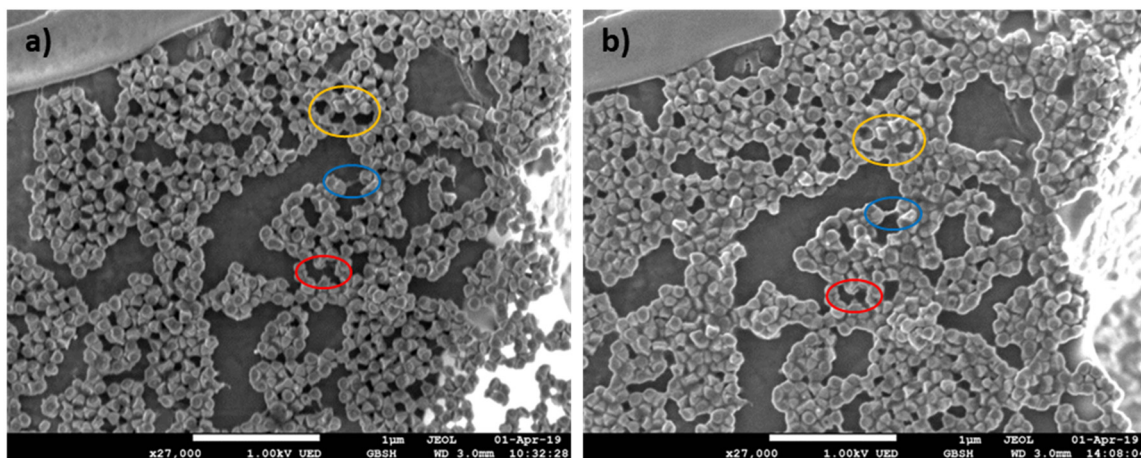


Fig. 13 SEM images of the formed 2-D sheet a) before and b) after the THF vapour annealing process. The three spots represent the same zones of the sample.

4.4 Conclusion

We demonstrated that the synthesis of silica/PS tripods by emulsion polymerisation could be considered as a robust process, even if the morphology yield seems to reach its limit at 75%. They were used as precursors of three-patch silica NPs by regrowth of the silica core followed by the dissolution of the PS nodules.

Preliminary assembly experiments showed that the three-patch silica NPs could not be efficiently assembled in honeycomb-like structures in the bulk solution probably because of the free rotation of particles and consequently the difficulty to grow in only two directions. By using the Langmuir technique, we succeeded in forming two-dimension films with a rather dense packing, *i.e.* maximum value of $R_p = 0.41$. A fine analysis of the microscopy images showed that the main limits to obtain more compact and crystalline arrays is i) the presence of free polystyrene macromolecules that generate large areas non occupied by silica NPs and ii) the too large amount of impurities within the three-patch silica NPs batch, *e.g.* two-patch and four-patch silica NPs, that increase dramatically the number of packing errors.

A subsequent solvent vapour annealing treatment with THF did not permit to further improve the ordering of the NPs within the 2-D films. However, it seems to have offered the opportunity to plasticise temporarily the PS junctions, and consequently to embed more efficiently the silica NPs making the assembly apparently more cohesive and therefore robust.

These preliminary experiments should be definitely completed by new ones with the main priority to the fabrication of three-patch silica NPs batches of much higher purity thanks to an extra refinement of the experimental parameters to get purer batches of silica/PS tripods and/or the implementation of purification stages to remove the NPs of undesirable morphology.

Other improvement solutions would necessitate complementary studies concerning:

- the interaction distance between the patches with parameters such as the patch-to-particle size ratio and the molecular weight of the grafted PS macromolecules at the bottom of the dimples. This would necessitate to fabricate new batches of three-patch silica NPs with different thicknesses of the regrown silica and changing the experimental parameters of the emulsion polymerisation, respectively;
- the reversibility of the patch-patch interactions for self-healing the packing errors. We could envision an original experiment consisting in performing the solvent vapour annealing treatment on the Langmuir trough for combining the NPs mobility at the subphase surface and the bonding reversibility of the PS junctions.

4.5 References

1. Lotito, V. & Zambelli, T. Approaches to self-assembly of colloidal monolayers: a guide for nanotechnologists. *Adv. Colloid Interface Sci.* 246, 217–274 (2017).
2. Whitesides, G. M., Ostuni, E., Takayama, S., Jiang, X. & Ingber, D. E. Soft lithography in biology and biochemistry. *Annu. Rev. Biomed. Eng.* 3, 335–373 (2001).
3. Gates, B. D., Xu, Q., Stewart, M., Ryan, D., Willson, C. G. & Whitesides, G. M. New approaches to nanofabrication: molding, printing, and other techniques. *Chem. Rev.* 105, 1171–1196 (2005).
4. Ogaki, R., Alexander, M. & Kingshott, P. Chemical patterning in biointerface science. *Mater. Today* 13, 22–35 (2010).
5. Okazaki, S. High resolution optical lithography or high throughput electron beam lithography: the technical struggle from the micro to the nano-fabrication evolution. *Microelectron. Eng.* 133, 23–35 (2015).
6. Diba, F. S., Boden, A., Thissen, H., Bhave, M., Kingshott, P. & Wang, P. Y. Binary colloidal crystals (BCCs): interactions, fabrication, and applications. *Adv. Colloid Interface Sci.* 261, 102–127 (2018).
7. Doppelbauer, G., Bianchi, E. & Kahl, G. Self-assembly scenarios of patchy colloidal particles in two dimensions. *J. Physics-Condensed Matter* 22, 104105-104116 (2010).
8. Romano, F. & Sciortino, F. Patchy from the bottom up. *Nat. Mater.* 10, 171–173 (2011).
9. Romano, F., Sanz, E., Tartaglia, P. & Sciortino, F. Phase diagram of trivalent and pentavalent patchy particles. *J. Phys. Condens. Matter* 24, 064113-064120 (2012).
10. Li, Z.-W., Zhu, Y.-L., Lu, Z.-Y. & Sun, Z.-Y. A versatile model for soft patchy particles

- with various patch arrangements. *Soft Matter* 12, 741–749 (2016).
11. Noya, E. G., Almarza, N. G. & Lomba, E. Assembly of trivalent particles under confinement: from an exotic solid phase to a liquid phase at low temperature. *Soft Matter* 13, 3221–3229 (2017).
 12. Chen, D., Zhang, G. & Torquato, S. Inverse design of colloidal crystals via optimized patchy interactions. *J. Phys. Chem. B* 122, 8462–8468 (2018)
 13. Hubert, C. PhD thesis Univ. Bordeaux. (2016).
 14. Désert, A., Morele, J., Taveau, J.-C., Lambert, O., Lansalot, M., Bourgeat-Lami, E., Thill, A., Spalla, O., Belloni, L., Ravaine, S. & Duguet, E. Multipod-like silica/polystyrene clusters. *Nanoscale* 8, 5454–5469 (2016).
 15. Li, X. & Gilchrist, J. F. Large-area nanoparticle films by continuous automated Langmuir–Blodgett assembly and deposition. *Langmuir* 32, 1220–1226 (2016).
 16. Xu, L., Tetreault, A. R., Khaligh, H. H., Goldthorpe, I. A., Wettig, S. D. & Pope, M. A. Continuous Langmuir–Blodgett deposition and transfer by controlled edge-to-edge assembly of floating 2d materials. *Langmuir* 35, 51–59 (2019).
 17. Sinturel, C., Vayer, M., Morris, M. & Hillmyer, M. A. Solvent vapor annealing of block polymer thin films. *Macromolecules* 46, 5399–5415 (2013).
 18. Song, P., Wang, Y., Wang, Y., Hollingsworth, A. D., Weck, M., Pine, D. J. & Ward, M. D. Patchy particle packing under electric fields. *J. Am. Chem. Soc.* 137, 3069–3075 (2015).

General conclusion and perspectives

With reference to the general introduction and conclusion of the state-of-the-art (Chapter 1) of this dissertation, the seminal ideas of the present work were the following ones:

- i) the most efficient way to fabricate well-defined valence-endowed patchy or dimpled CAs with valence of 1, 2, 3 and 4 consists in the deconstruction of CMs mimicking HCl, BeCl₂, BF₃ and CH₄ molecules, respectively.
- ii) the physical entanglement of PS macromolecules is an efficient way to make permanent patch-patch interactions and this phenomenon can be controlled through their swelling/deswelling in mixtures of good and bad solvents for PS;
- iii) for low values of patch-to-particle size ratio, the structures that can be obtained by full bonding (*i.e.* by authorising attraction only via the patches and maximising them) of one-, two-, three- and four-patch particles are doublets, linear chains, honeycomb-like sheets and diamond networks, respectively;
- iv) the difficulty to get defect-free assemblies increases dramatically with the patch number, *i.e.* the number of simultaneous growth directions.

1 Achievements

In this context, we repeated and sometimes optimised protocols to get copious quantities of one-patch, two-patch and three-patch silica NPs where the patches are surface PS nodules and/or grafted PS chains at the bottom of surface concavities, *i.e.* dimples. The precursor CMs were silica multipods obtained through a seed-growth emulsion polymerisation of styrene in the presence of silica NPs previously surface-modified with methacryloxyalkylsilyl groups. The PS nodule of monopods obtained through this pathway turned out to be too bulky for the assembly studies and we moved to another synthesis protocol where the silica moiety is created in the last step by the regioselective coating of dissymmetric PS dumbbells whose one lobe was both crosslinked and hydrophilic.

We then studied the possibility to assemble them through the physical entanglement of the grafted PS macromolecules. We first studied the ethanol/DMF system to assemble the one-patch NPs in clusters. The control of the fraction of DMF in the mixture allowed to define a “sticky regime” in the 30-50 vol. % range and to get clusters containing from two to four silica NPs. The poorly understood effect of a terminal centrifugation stage permitted to increase the maximum aggregation number to more than 30. It was evidenced that the NPs with a patch-to-particle size ratio of 0.62 allowed to reach the highest aggregation numbers, as the expected

rule was disturbed for higher values of the patch-to-particle size ratio by an unexpected weakening of the stickiness, probably due to a higher fraction of shorter PS chains.

For chaining the two-patch silica NPs, the ethanol/DMF mixture turned out to be quite inefficient and we moved to salted water/THF mixtures.^{†††} The advantage of this new system is the trigger behaviour of the salt and the non-necessity of a final centrifugation stage to get high aggregation numbers. We preferred making the patchy particles slim by removing the maximum of just physically entangled macromolecules from the PS nodules. The high purity of the batches (97%) allowed to get long and quasi-linear chains (up to 60 units reaching 6 μm long) and to carry out a kinetic study showing the model of the step-growth polymerisation was validated for the first 2 hours of incubation, but it would evolve to a diffusion-controlled mechanism for longer incubation times.

Getting honeycomb-like sheets from three-patch silica NPS from the same strategy turned out to be much touchier for two main reasons: the insufficient purity of the patchy NPs batches (75%) and the difficulty to maintain the structure growth in only two directions. Hence, we attempted to confine the assembly on the water/air interface of a Langmuir trough. However, the achieved structures were only partially close-packed and when quasi-crystalline zones were observed, they never concerned more than 30 NPs because of the presence of too many two- or four-patch silica NPs.

We never went to the synthesis of four-patch silica NPs and their assembly into diamond-like structures for time reasons. Nevertheless, this appears now as a much more difficult challenge concerning not only the purity of the patchy NPs batch but also the delicate experimental conditions to find for managing simultaneously sufficient attractive forces and reversibility for an efficient self-healing of every stacking fault.

2 Perspectives

We do not intend to repeat here the specific perspectives that were separately presented at the end of each chapter. The following propositions are more general and could be declined to any system from zero to three dimensions.

The purity of the batches of patchy silica NPs is a critical parameter. If the experimental conditions of their synthesis cannot be fully optimised, it is mandatory to develop purification

^{†††} Extra experiments not reported here showed that the salted water/THF system works also for clustering the one-patch silica NPs.

strategies. Density gradient centrifugation is often used to sort colloids at the micron scale but this technique is expected to be much tricky to develop for colloids with dimensions of about 100 nm.

The attraction distance between the patches plays a significant role and it would be probably rewarding to study the influence of the molecular weight and density of the PS chains grafted at the bottom of the dimples. This means considering again the experimental conditions of the seed-growth emulsion polymerisation and controlling the contact angle of the PS nodules on the silica seeds, respectively.

Even if depletion forces are probably much more difficult to implement at the scale of our systems, we could take advantage from the fact that our patches deriving from the silica/PS multipods are both entropic and enthalpic, due to the simultaneous presence of the dimples and the PS chains at the bottom of them.¹ One avenue to take advantage of this would be to insert spherical or oblong colloids to bond two patches together. These bonding particles could be considered as colloidal bond pairs mimicking the electron pairs shared in the molecular orbitals of bonded atoms.

We studied the opportunity to co-assemble differently-sized or differently-surface-modified two-patch particles in Chapter 3 to imitate copolymers. This strategy could be extended to the other systems such as the clusters obtained from one-patch NPs to get for instance chiral colloids, even if preliminary trials showed a strong tendency to self-assembly rather than cross-assembly (Fig. 1).

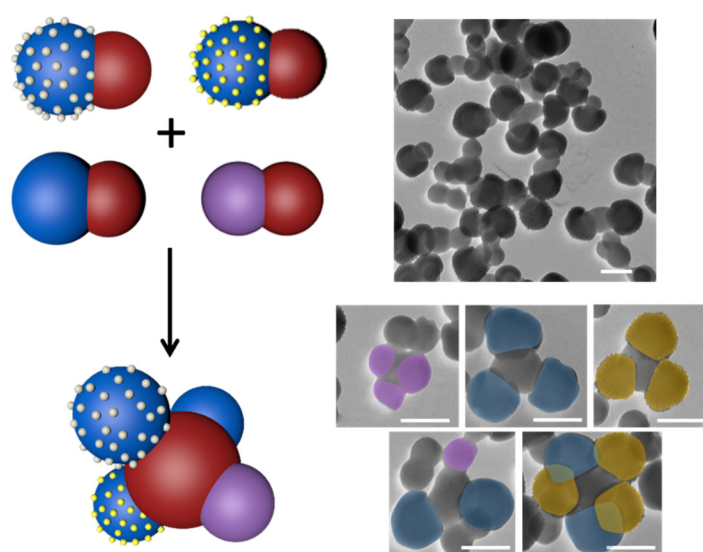


Fig 1 Principle scheme and TEM images relating the tentative synthesis of chiral clusters in the ethanol/DMF system from mixtures of one-patch silica NPs bearing different non-sticky lobes: bare silica (blue), MMS-crosslinked PS (pink), and gold-decorated silica (yellow). Scale bars: 100 nm.

Lastly, we studied the opportunity to deposit gold on our assemblies or to assemble already patchy golden NPs. It would make sense to extend this work by studying, for instance, their plasmonic properties, either conventionally on purified batches or by single-particle spectroscopy in the case of complex mixtures.

3 References

1. Hubert, C., Chomette, C., Désert, A., Sun, M., Treguer-Delapierre, M., Mornet, S., Perro, A., Duguet, E. & Ravaine, S. Synthesis of multivalent silica nanoparticles combining both enthalpic and entropic patchiness. *Faraday Discuss.* **181**, 139–146 (2015).

Titre : Assemblage induit en milieu solvant de nanoparticules de silice à patchs. Vers de nouvelles molécules colloïdales.

Résumé : Cette étude porte sur l'assemblage de particules à patchs pour obtenir de nouveaux matériaux. L'état de l'art a permis de choisir et de mettre en œuvre une stratégie originale dont la force motrice est l'assemblage induit en milieu solvant, c'est-à-dire basé sur le caractère collant des macromolécules de polystyrène (PS) lorsqu'elles sont soumises à un mélange d'un bon et d'un mauvais solvant. Nous avons étudié l'assemblage en clusters, en chaînes ou en monocouches de nanoparticules (NPs) de silice possédant respectivement un, deux ou trois patchs, constitués de macromolécules de PS greffées à des endroits spécifiques de leur surface. Les NPs de silice à un patch, présentant un rapport de taille patch/particule contrôlable, ont été synthétisées avec succès par une étape de séparation de phases induit par gonflement suivie d'un dépôt de silice régiosélectif. Leur assemblage a été réalisé dans des mélanges binaires DMF/éthanol. Les effets de la qualité du solvant, de la force de centrifugation, de la concentration en NPs, de la durée d'incubation et du rapport de taille patch/particule ont été étudiés et discutés. La stratégie a été étendue pour obtenir des clusters à base d'or. Les NPs de silice à deux patchs ont été préparées par un procédé de polymérisation en émulsion ensemencée du styrène et le rapport de taille patch/particule a été ajusté via le taux de recroissance du noyau de silice. L'assemblage en chaînes des NPs a été réalisé dans des mélanges THF/solution aqueuse de NaCl en faisant varier la concentration en NaCl, le rapport volumique THF/eau, la durée d'incubation, la concentration en NPs et le rapport de tailles patch/particule. Nous avons montré que la cinétique de croissance des chaînes est typique d'une croissance par étapes. Des stratégies pour imiter des homopolymères, des copolymères statistiques, des copolymères séquencés à blocs et des polymères ramifiés ont été mises en œuvre, en utilisant comme briques de base des NPs à un patch, des NPs à deux patchs avec des tailles ou des fonctions de surface différentes et/ou des NPs à trois patchs. Les NPs de silice à trois patchs ont été obtenues par la même voie de synthèse que celles à deux patchs. Pour les assembler dans des structures 2-D en nid d'abeille, nous avons utilisé la technique de Langmuir et nous avons étudié l'influence de différents paramètres expérimentaux. Une étape de recuit sous vapeur de THF a été mise en œuvre, ce qui a permis de renforcer mécaniquement l'assemblage, mais sans effet significatif sur la compacité.

Mots clés : particules à patchs, silice, polystyrène, assemblage, clusters, chaînes, monocouches, polymérisation en émulsion

Title : Solvent-induced assembly of patchy silica nanoparticles. Towards new colloidal molecules

Abstract : This study deals with the assembly of patchy particles to get new materials. The state-of-the-art allowed us to select and implement an original strategy whose driving force is the solvent-induced assembly, *i.e.* based on the stickiness of polystyrene (PS) macromolecules when they are subjected to a mixture of good and bad solvents. We investigated the assembly into clusters, chains or monolayers of one-patch, two-patch or three-patch silica nanoparticles (NPs), respectively, the patches being PS macromolecules grafted at specific positions on their surface. One-patch silica NPs with controllable patch-to-particle size ratio were successfully synthesised through phase separation and site-specific silica coating. Their assembly was performed in DMF/ethanol binary mixtures. The effect of the solvent quality, centrifugation force, particle concentration, incubation time and patch-to-size ratio was investigated and discussed. The strategy was spread to obtain gold-coated clusters. The two-patch silica NPs were prepared through a seed-growth emulsion polymerisation of styrene and the patch-to-particle size ratio was adjusted through the extent of the silica core regrowth. The chaining of the NPs was efficiently achieved in the THF/NaCl aqueous solution mixtures by varying the NaCl concentration, solvent quality, incubation time, NPs concentration and patch-to-particle size ratio. We showed that the kinetics of the chaining process is characteristic of a reaction-controlled step-growth polymerisation. Strategies to mimic homopolymers, random copolymers, block copolymers and branched polymers were implemented by using one-patch NPs, two-patch NPs with different sizes/surface chemical functions and/or three-patch NPs as building units. The three-patch silica NPs were obtained through the same synthetic pathway than two-patch ones. For assembling them in honeycomb-like 2-D structures, we used the Langmuir technique and we studied the influence of different experimental parameters. THF vapour annealing was implemented to reinforce mechanically the assembly but without significative effect on the packing density.

Keywords : patchy particles, silica, polystyrene, assembly, clusters, chains, monolayers, emulsion polymerisation